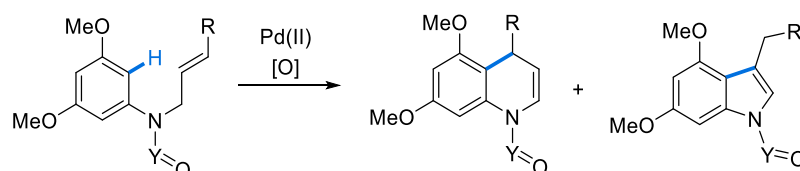


Chapter 4.

Regioselectivity of a Palladium-Catalyzed Intramolecular Fujiwara-Moritani Reaction



In this chapter, the mechanism of a palladium-catalyzed arylation is investigated, based on the experimental results provided by our collaborators in the group of Prof. Esther Lete and Prof. Nuria Sotomayor from the University of the Basque Country. They performed intramolecular Fujiwara-Moritani reactions, whose outcome depended heavily on the protecting group of the aniline substrate. Mixtures of 6-*endo* and 5-*exo* cyclization products were obtained and, through the evaluation of the possible mechanisms, the results were rationalized.

Chapter based on the publication:

Carral-Menoyo, A.; Sotorríos, L.; Ortiz-de-Elguea, V.; Diaz-Andrés, A.; Sotomayor, N.; Gómez-Bengoa, E.; Lete, E. Intramolecular Palladium(II)-Catalyzed 6-*endo* C-H Alkenylation Directed by the Remote *N*-Protecting Group. Mechanistic Insight and Application to the Synthesis of Dihydroquinolines. *J. Org. Chem.* **2020**, *85*, 2486-2503.

4.1 Context

This chapter of the thesis is based on a collaboration carried out with experimental researchers. The experimental reactions were performed in the group of Esther Lete and Nuria Sotomayor, from the University of the Basque Country (UPV/EHU). For more information, please see the full article available in the appendix.

The investigations carried out by the author of this thesis are exclusively computational and will be presented in the *results and discussion* section. The aim of this section is to provide a context for these investigations by introducing the nature of the chemistry, as well as briefly discussing the aim, procedures and results of the experimental studies.

4.1.1 Objective

The aim of the experimental study conducted by our colleagues was the synthesis of 1,4-dihydroquinolines. For this purpose, they performed intramolecular Fujiwara-Moritani reactions on *N*-protected substituted anilines. The reaction proceeds with catalytic amounts of palladium(II), which must be regenerated using an oxidant. By using a diverse set of alkenes, the synthesis of 4-substituted-1,4-dihydroquinolines is expected.

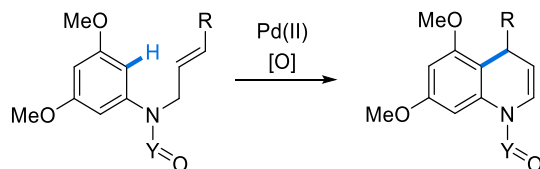


Figure 4.1. Synthesis of 1,4-dihydroquinolines by means of intramolecular Fujiwara-Moritani reaction.

4.1.1.1 1,4-dihydroquinolines

Hydroquinolines are important building blocks of several natural products, some of which have shown interesting biological activity.¹ In particular, 1,4-dihydroquinolines have attracted special attention (Figure 4.2). 4-Oxo-1,4-dihydroquinolines, also known as quinolones, show a wide range of biological activity, mainly bactericidal. They constitute family of broad-spectrum antibiotics; the second generation fluoroquinolone ciprofloxacin has been one of the most consumed antibacterial agents worldwide.² They also target several biologically interesting sites, such as cannabinoid receptor,³ STAT transcription factors (with an important role in carcinogenesis)⁴ and the CFTR protein⁵, a protein whose malfunction causes cystic fibrosis.

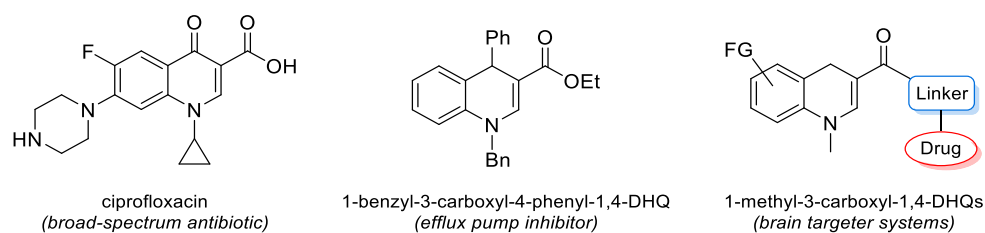


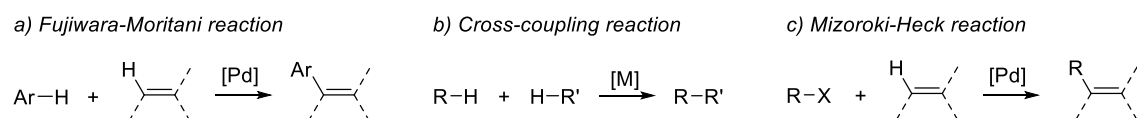
Figure 4.2. Biologically active 1,4-dihydroquinoline derivatives.

Other types of 1,4-dihydroquinolines include *N*-benzyl-4-phenyl-1,4-dihydroquinoline derivatives, which have shown efflux pump inhibition,⁶ a mechanism responsible of the multi-drug resistance present in cancerous cells. Brain-specific chemical delivery systems have been developed using a set of *N*-methyl-3-carboxyl-1,4-dihydroquinolines.^{7,8}

4.1.2 State of the art

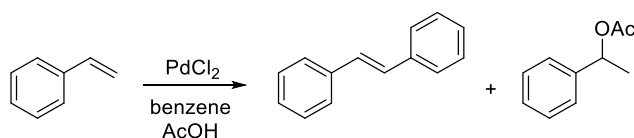
4.1.2.1 Intramolecular palladium-catalyzed arylation reactions

The reaction studied in the present work is a Fujiwara-Moritani reaction (also called dehydrogenative or oxidative Heck reaction). The reaction consists in the alkenylation of aryl groups using palladium complexes (*a*, Scheme 4.1). It is considered a cross-coupling reaction, as a new C-C bond is being formed using a metal catalyst (*b*, Scheme 4.1). It can also be classified as a variant of the Mizoroki-Heck reaction of arenes (*c*, Scheme 4.1), though it does not require the presence of a leaving group ($X = \text{halide, triflate}$).



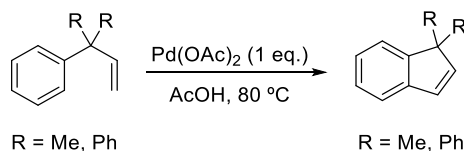
Scheme 4.1. Fujiwara-Moritani reaction and related organometallic reactions.

The reaction was first reported in 1967 by Ichiro Moritani and Yuzo Fujiwara.^{9,10} By that time, Fujiwara and Moritani were studying the stereochemistry of the substitution of olefins with nucleophiles by acetoxyating styrene with palladium chloride(II) and acetic acid. The reaction used benzene as solvent and, to their surprise, the coupling between styrene and benzene was observed, providing stilbene as one of the products (Scheme 4.2).



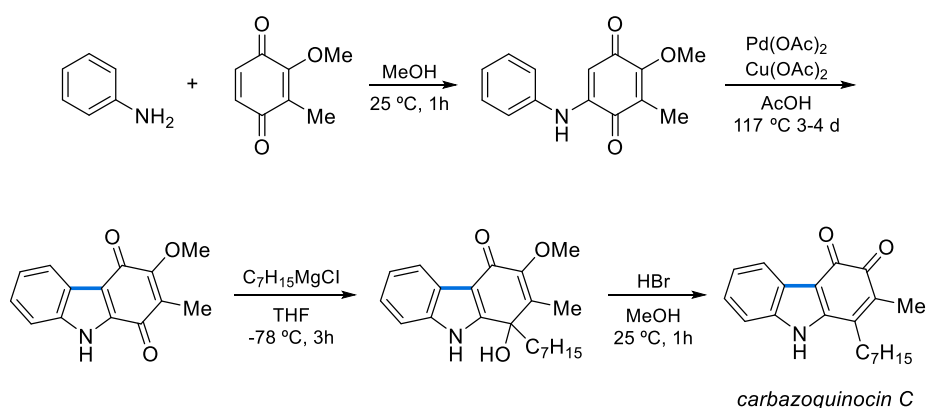
Scheme 4.2. First dehydrogenative Heck reaction reported, performed by Fujiwara and Moritani.

In later works, reaction conditions were optimized,¹¹ palladium loading was lowered using oxidants (initially, AgOAc),¹² and the scope was expanded.¹³ The reaction was established as an effective alkenylation method of arenes and heteroarenes with the use of directing groups.¹⁰ The majority of the reported Fujiwara-Moritani reactions are intermolecular, although the intramolecular variant of the reaction has also been investigated since the first example reported by Norman and coworkers (Scheme 4.3).¹⁴



Scheme 4.3. First intramolecular Fujiwara-Moritani reaction, by Norman and coworkers (ref. 14).

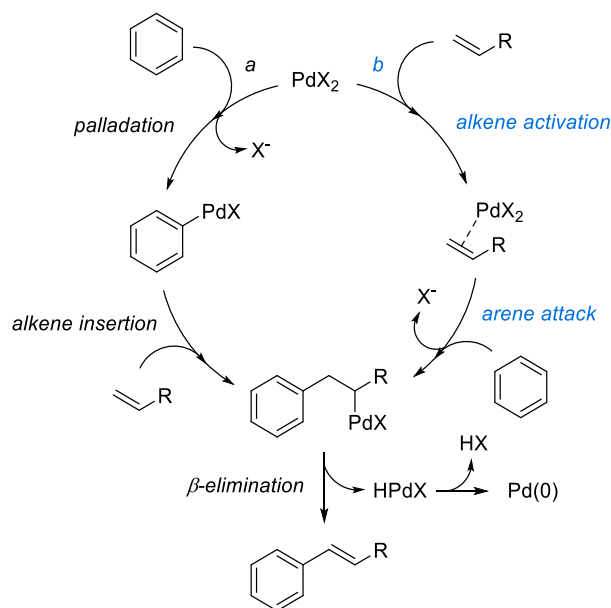
This reaction has an immense potential for the creation of complex polycyclic structures and has been broadly employed in the area of total synthesis of natural products.¹⁵ For example, the short total synthesis of carbazoquinocin C shown in Scheme 4.4 utilizes an intramolecular Fujiwara-Moritani reaction for the construction of the molecule's scaffold.^{15b}



Scheme 4.4. Total synthesis of carbazoquinocin C (ref. 15b).

4.1.2.2 Reaction mechanism

Initially, Fujiwara and Moritani¹⁶ proposed a C-H activation mechanism (*a*, Scheme 4.1) that involved the palladation of the arene, followed by the coordination and insertion of the olefin to form an arylpalladium intermediate. Then, a β -elimination takes place, forming the alkenylated arene and a palladium hydride, that later decomposes into an acid and the free metal Pd(0). Some years after their first report, phenylpalladium complexes were isolated, strengthening the hypothesis of arylpalladium intermediates.¹⁷



Scheme 4.5. Two possible mechanisms for the Fujiwara-Moritani reaction.

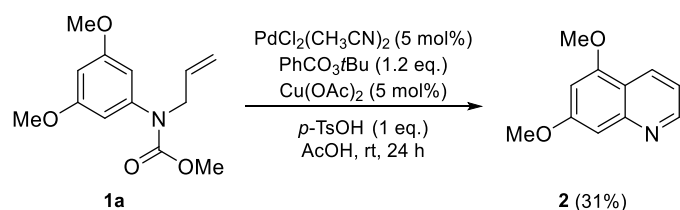
Norman and coworkers, authors of the aforementioned intramolecular Fujiwara-Moritani reaction,¹⁴ proposed a different transformation (*b*, Scheme 4.5). The proposed mechanism consisted on a Friedel-Crafts type reaction, starting with the activation of the alkene by coordination to the palladium(II) complex. Then, the attack of the arene forms the new C-C bond, delivering the same arylpalladium intermediate.

It is generally accepted that the reaction proceeds through the arene palladation and alkene insertion pathway (*a*, Scheme 4.5). Nevertheless, there is evidence of some intermolecular and intramolecular reactions proceeding through the alternative mechanism (*b*, Scheme 4.5), due to the different reactivity of the reactants^{18,19} or the stereochemistry of the products.²⁰

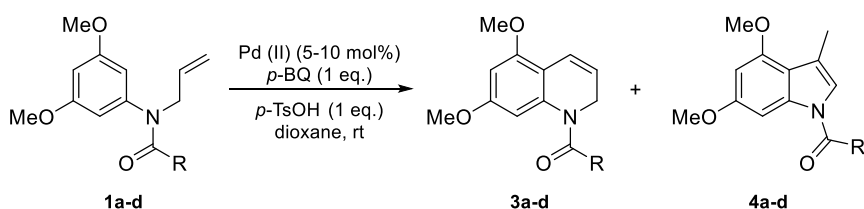
4.1.3 Experimental

Our collaborators carried out the first Fujiwara-Moritani reaction under the reaction conditions optimized for *N*-aryl-acrylamides in their previous work.²¹ The *N*-protected allyl-aniline **1a*** was chosen as model substrate as it bears an electron rich ring, which was proven to be essential to obtain good reactivity.²²

* The numbering of the molecules has been reset, as they are not related to those in previous chapters.

Scheme 4.6. Cyclization of **1a** under previously optimized conditions.

Although the reaction did take place, the nitrogen was deprotected and the molecule was fully oxidized, delivering 31% of quinoline **2** (Scheme 4.6). Therefore, milder reaction conditions were employed in order to avoid the oxidized quinoline product. The solvent was switched to dioxane and *p*-benzoquinone was used as oxidant.

Table 4.1. Optimization of the cyclization reaction of *N*-protected anilines.

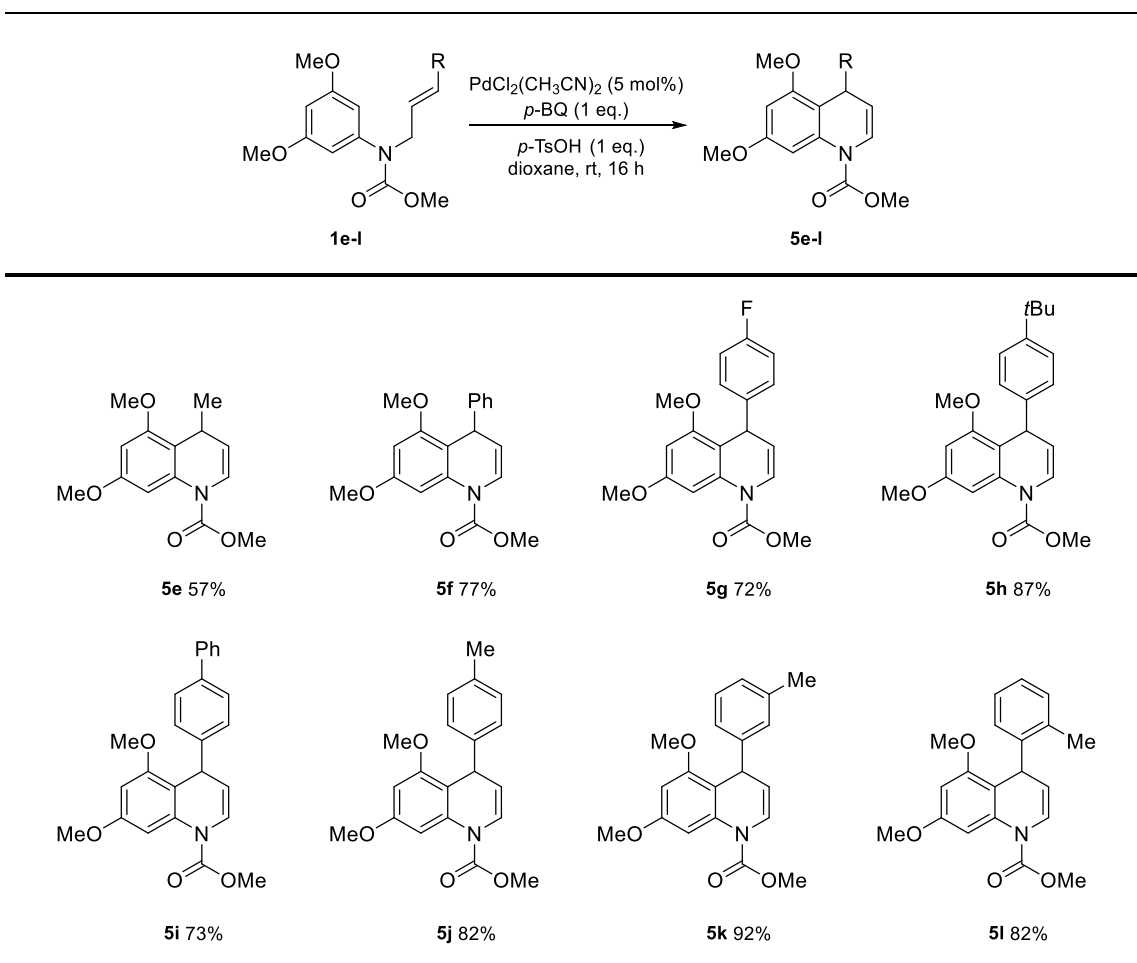
entry	1	R	[Pd (II)] (mol %)	<i>t</i> (h)	3	yield (%) ^a	4	yield (%) ^a
1	1a	OCH ₃	Pd(CH ₃ CN) ₂ Cl ₂ (5)	16	3a	85	4a	
2	1b	O <i>t</i> Bu	Pd(CH ₃ CN) ₂ Cl ₂ (5)	16	3b	38	4b	
3	1b	O <i>t</i> Bu	Pd(CH ₃ CN) ₂ Cl ₂ (10)	1.5	3b	58	4b	16
4	1b	O <i>t</i> Bu	Pd(PhCN) ₂ Cl ₂ (10)	1.5	3b	56	4b	13
5	1b	O <i>t</i> Bu	Pd(PhCN) ₂ Cl ₂ (10) ^b	2	3b	59	4b	15
6	1b	O <i>t</i> Bu	Pd(PhCN) ₂ (BF ₄) ₂ (10) ^b	3	3b	16	4b	3 ^d
7	1b	O <i>t</i> Bu	Pd(OAc) ₂ (10) ^b	6	3b	21	4b	14 ^e
8	1c	OBn	Pd(CH ₃ CN) ₂ Cl ₂ (10)	3	3c	67	4c	
9	1d	CH ₃	Pd(CH ₃ CN) ₂ Cl ₂ (5)	20	3d	^c	4d	
10	1d	CH ₃	Pd(CH ₃ CN) ₂ Cl ₂ (10)	1 ^f	3d	85	4d	10

^aYield (%) of isolated pure compound. ^bBoc-Val-OH (20 mol %) was used as ligand. ^cNo reaction. ^dYield determined by ¹H NMR using 4-dimethylaminopyridine (DMAP) as internal standard (55% conversion). ^eYield determined by ¹H NMR using DMAP as internal standard (51% conversion). ^f70 °C.

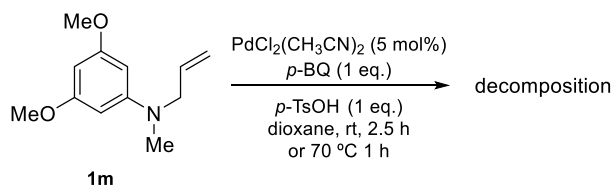
Under these milder conditions, **1a** proceeded through a 6-*endo* cyclization, but instead of the desired 1,4-dihydroquinoline, the 1,2-dihydroquinoline **3a** was obtained (entry 1, Table 4.1). The 5-*exo* process responsible for the formation of indole **4a** was not observed. The modification of the protecting group delivered the 1,2-dihydroquinoline **3b** in lower yield (entry 2) and when the catalyst load was increased (entry 3), the selectivity was lost, as a 16% of the indole product **4b** was isolated. Changing the precatalyst and ligands (entries 4-7) did not improve the selectivity. The use of benzyl carbamate as protecting group (entry 8) lead to the regioselective formation of **3c**. The amide-protected substrate **1d** did not react when subjected to the same reaction conditions as **1a**; an increase of the catalyst loading and heating were necessary for the reaction to proceed, and even then, the formation of a mixture of products was observed.

Since entry 1 delivered the best results, same conditions were applied to the reactions of allyl anilines with a substituted terminal alkene, using methyl carbamate as protecting group. Instead of the 1,2-dihydroquinolines, these reactants provided the desired 1,4-dihydroquinolines in a completely regioselective manner, in moderate to excellent yields (Table 4.2).

Table 4.2. Synthesis of 4-substituted 1,4-dihydroquinolines.



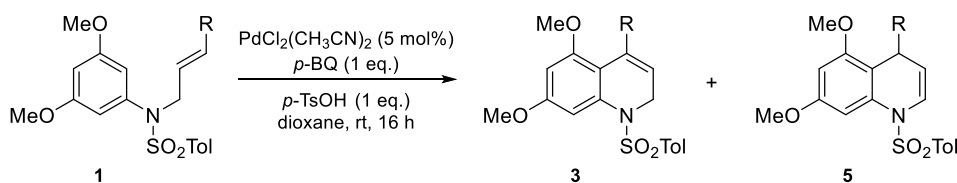
Some control experiments were carried out in order to gain some insight into the reaction mechanism. According to the results in Table 4.3, the protecting group seemed to have a significant impact in the selectivity of the reaction. When *N*-methyl aniline **1m** was used as substrate, only decomposition product was observed under standard reaction conditions, both at room temperature, and heating at 70 °C (Scheme 4.7).



Scheme 4.7. Additional experiment to assess the role of the protecting group.

The reaction was also carried out using *p*-toluenesulfonyl as protecting group. Three different substrates were employed, and the results were quite similar to those of carbamates. The unsubstituted alkene provided the 1,2-dihydroquinoline **3n**, while the phenyl substituted alkene delivered the 1,4-dihydroquinoline **5p**. However, the reaction of the methyl-substituted alkene resulted on a mixture of the two possible isomers, **3o** and **5o** (Table 4.3).

Table 4.3. Cyclization reaction with *N*-tosyl protected anilines.



entry	1	R	3	yield (%)	5	yield (%)
1	1n	H	3n	87	5n	
2	1o	Me	3o	64	5o	26
3	1p	Ph	3p		5p	42

In conclusion, a powerful method for the regioselective synthesis of 4-substituted 1,4-dihydroquinolines using a palladium(II)-catalyzed intramolecular *6-endo* cyclization was developed. The protecting group of the amine moiety seems to play a key role in the mechanism of the reaction, although the mechanism itself remained unexplored.

4.2 Computational approach

4.2.1 Objective

We believe that the mechanism of the reaction is crucial to understand the regioselectivity of this particular Fujiwara-Moritani reaction. With our DFT calculations, we should be able to compute the two possible mechanisms (*a* and *b*, Scheme 4.5) and identify which delivers the observed 5-*exo* and 6-*endo* product ratios.

We also want to explain the selectivity of the final elimination step, which seems to favour the formation of 1,2 or 1,4-dihydroquinolines depending on the substitution of the alkene (Table 4.3, products **3** and **5**).

4.2.2 General methods

For references and a more detailed description of the methodology, levels of theory and software, please see chapter 1.

All structures were optimized using density functional theory (DFT) as implemented in Gaussian with B3LYP as functional, 6-31G(d,p) as basis set for non-metals, and LANL2DZ as basis set for palladium. Unless stated otherwise, final energies were obtained performing single-point calculations on the previously optimized structures using the M06 functional and the basis set Def2TZVPP. Solvation factors were introduced with the IEF-PCM method, using 1,4-dioxane as solvent. The stationary points were characterized by frequency calculations in order to verify that they have the right number of imaginary frequencies. The 3D structures shown in this thesis were generated with the CYLview software.

At a certain point, the functional B3LYP including Grimme's dispersion with the original D3 damping function was also employed. The basis set combination of 6-311+G(d,p) for non-metals and SDD for palladium was also tested. These exceptions to the general method will be noted in the main text.

4.3 Results and discussion

4.3.1 Path a. Classic Fujiwara-Moritani mechanism

We started our computational study looking into the widely accepted mechanism, consisting on the palladation of the arene, alkene insertion (or cyclization, since the reaction is intramolecular) and β -elimination. According to the preliminary experimental data at hand, some of the reactions used palladium(II) acetate as catalyst, so we used acetates as ligands for the calculations. A conformational study was performed on the starting complex, to determine the most stable position and conformation of the palladium and the two acetate ligands. In the conformation with the lowest Gibbs free energy, one acetate is coordinated in a bidentate manner, while the second acetate is coordinated in a monodentate fashion (Figure 4.3.).

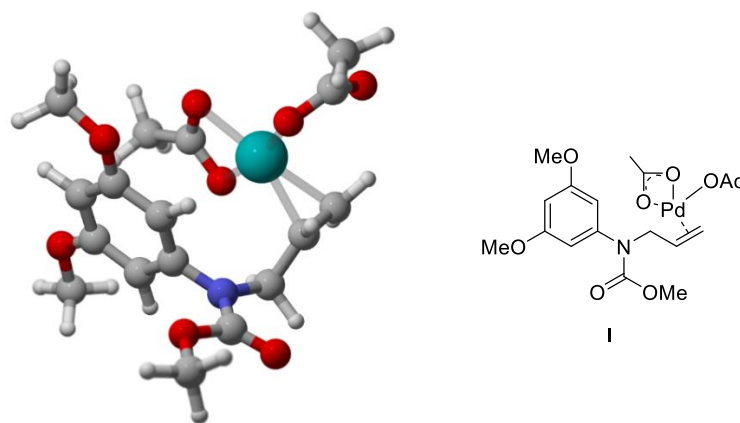
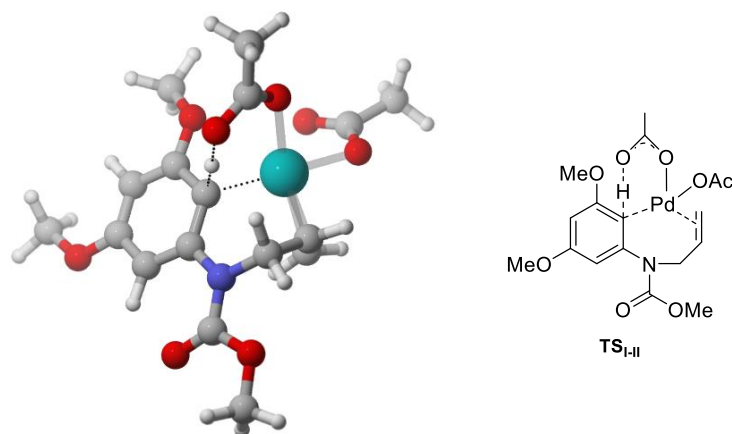
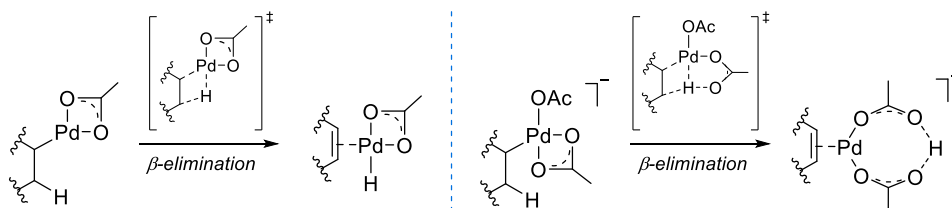


Figure 4.3. Most stable conformation for the coordinating complex I formed between Pd(OAc)₂ and allyl aniline **1a**.

Next, the transition state of the palladation was obtained (**TS_{I-II}**), whose activation energy was of 20.0 kcal/mol. As the metal is inserted in the aromatic ring, a molecule of acetic acid is generated (Figure 4.4).

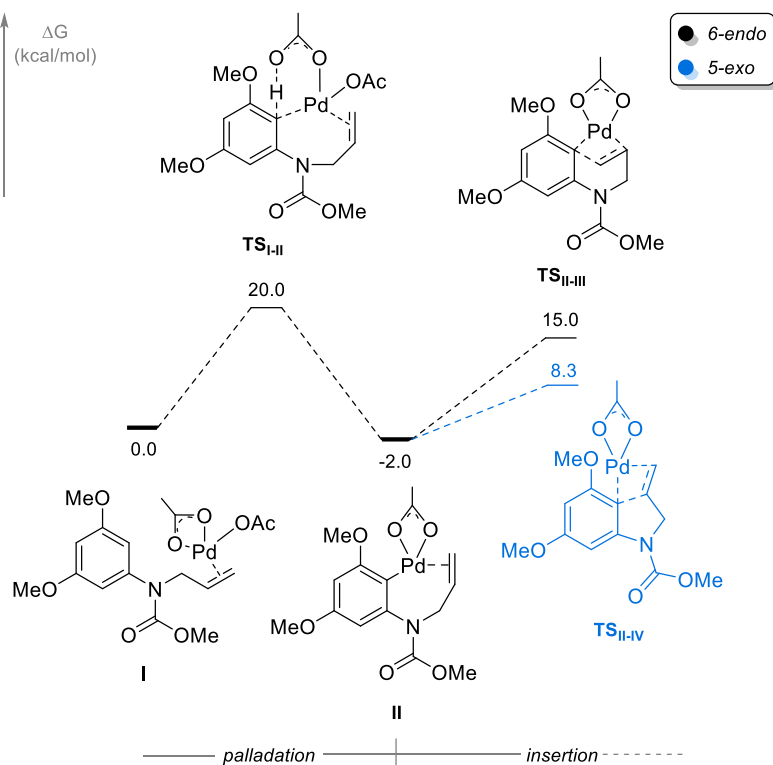
Figure 4.4. Transition state of the palladium insertion, **TS_{I-II}**.

In further steps, two different pathways were computed. In the first one, we considered that the acetic acid was removed from the coordination sphere, leaving the palladium center with a single acetate ligand coordinated on a bidentate fashion. This way, the complex has neutral charge, and the palladium has its four coordination sites occupied. During the final β -elimination, this pathway would lead to the formation of a palladium hydride (left, Scheme 4.8).

Scheme 4.8. Two possible β -eliminations, palladium hydride formation (left) and acetate assisted abstraction (right).

In the second pathway, we considered that after the detachment of the acetic acid, a new acetate ligand would enter the coordination sphere. This would lead to an intermediate bearing two monodentate acetate ligands with total negative charge. Consequently, during the β -elimination step, one of the acetates will abstract the hydrogen, as shown in Scheme 4.8 (right).

First, we followed the reaction path with the metal bearing a sole acetate ligand, starting with intermediate **II** (Scheme 4.9). Then, the key transition states were computed, both the 6-*endo* (**TS_{I-III}**) and 5-*exo* (**TS_{II-IV}**) cyclizations. The resulting Gibbs free energy profile is shown in Scheme 4.9.



Scheme 4.9. Gibbs energy profile of the palladation and insertion of **I**. Relative energy values referred to the initial complex **I**, in kcal/mol.

As previously mentioned, the mechanism of the reaction starts with a low energy barrier of 20.0 kcal/mol (**TS_{I-II}**) delivering intermediate **II**. From this intermediate, we can follow the 6-*endo* (**TS_{II-III}**, black) or 5-*exo* (**TS_{II-IV}**, blue) pathways (Figure 4.5), with relative energies of 15.0 and 8.3 kcal/mol respectively. This energy difference suggests that the reaction should proceed through the 5-*exo* pathway, as the transition state is lower in energy. Nevertheless, this would be in clear disagreement with the experiments, where only the 6-*endo* product was observed.

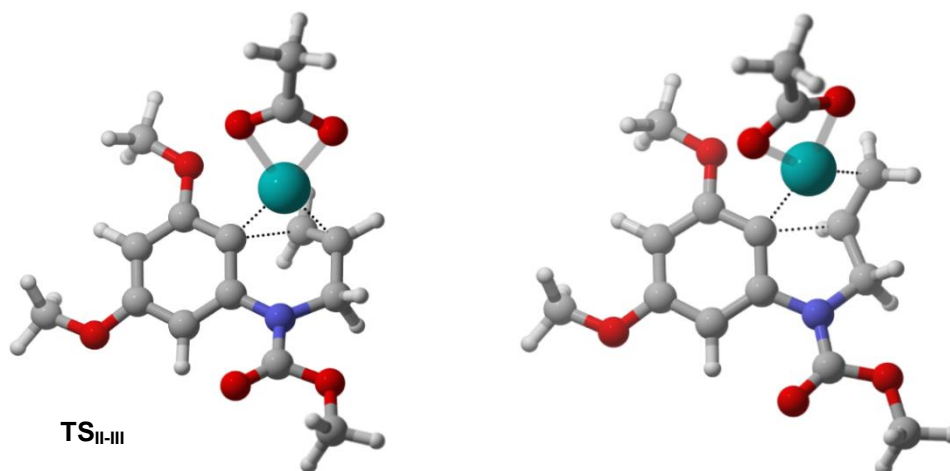


Figure 4.5. Transition states of the 6-*endo* (left, **TS_{II-III}**) and 5-*exo* (right, **TS_{II-IV}**) insertion of the olefin.

Going ahead with the pathway, we computed the products of each cyclization: intermediates **III** and **IV** (Figure 4.6). The structures obtained from the IRC calculations showed that the palladium atom does not completely detach from the aromatic carbon, as a weak interaction can still be observed in both cases. Other possible conformation of these intermediates were attempted, such as coordinating the palladium to the adjacent methoxy or the carbamate, but due to the strain of the rings, the energies of the mentioned structures were always considerably higher.

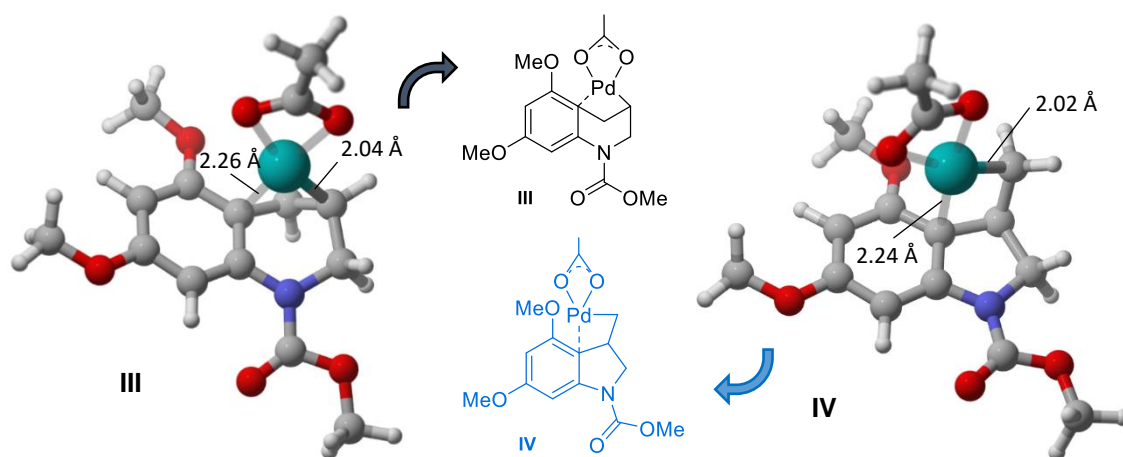


Figure 4.6. 3D representation of the coordination observed in the optimized intermediates **III** and **IV**. Bond lengths in Å.

The last step of the reaction was the β -elimination of a hydrogen atom. In the case of the 6-*endo* pathway, there are two different transition states. One leads to the desired 1,4-dihydroquinoline **5a** (**TS_{III-V}**, Figure 4.7), while the other leads to the 1,2-dihydroquinoline **3a** (**TS_{III-VI}**, Figure 4.7). The 5-*exo* pathway has only one possible transition state that provides intermediate **VIII**, which will eventually aromatize to deliver indole **4a**.

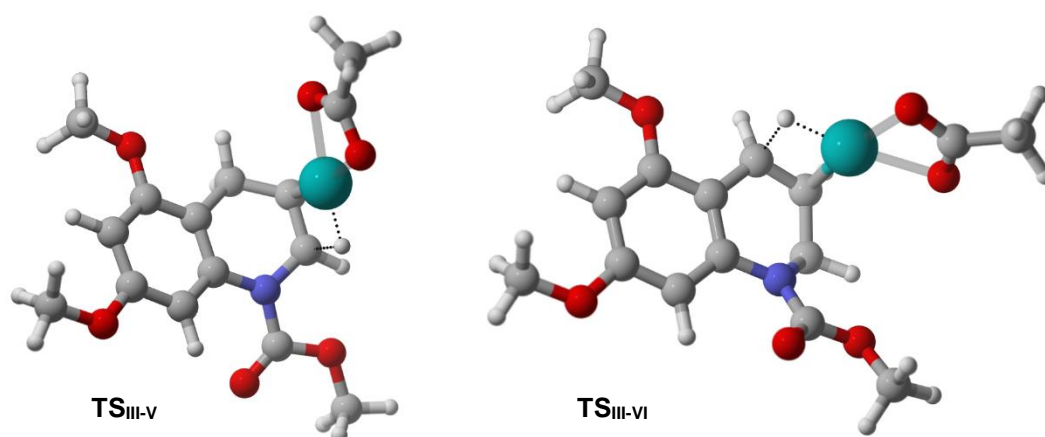
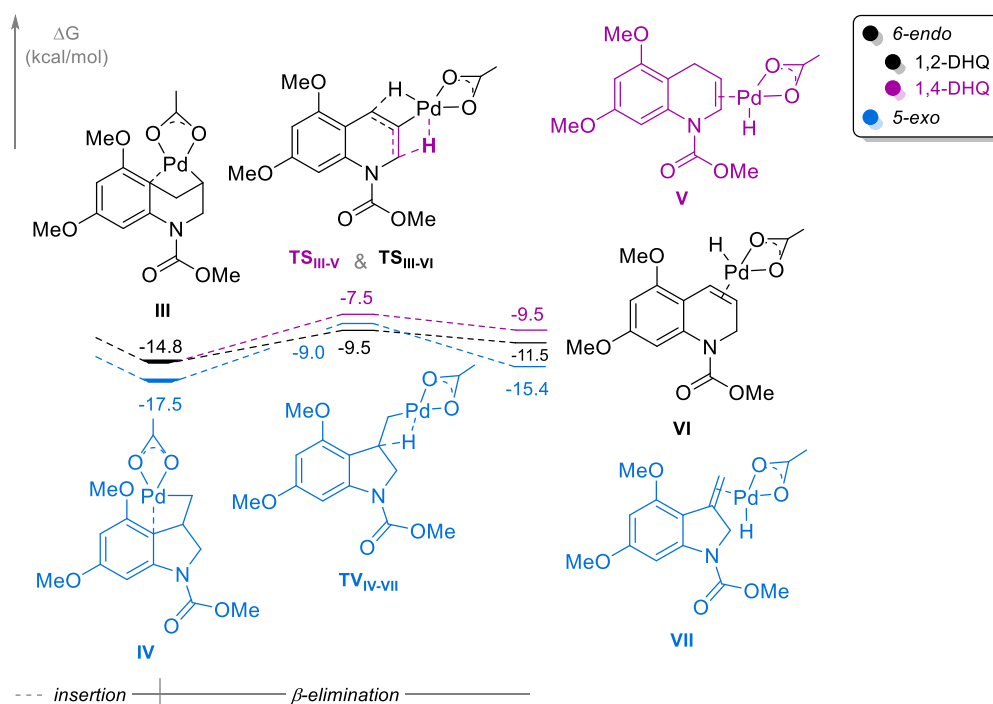


Figure 4.7. 3D representation of the β -elimination transition states.

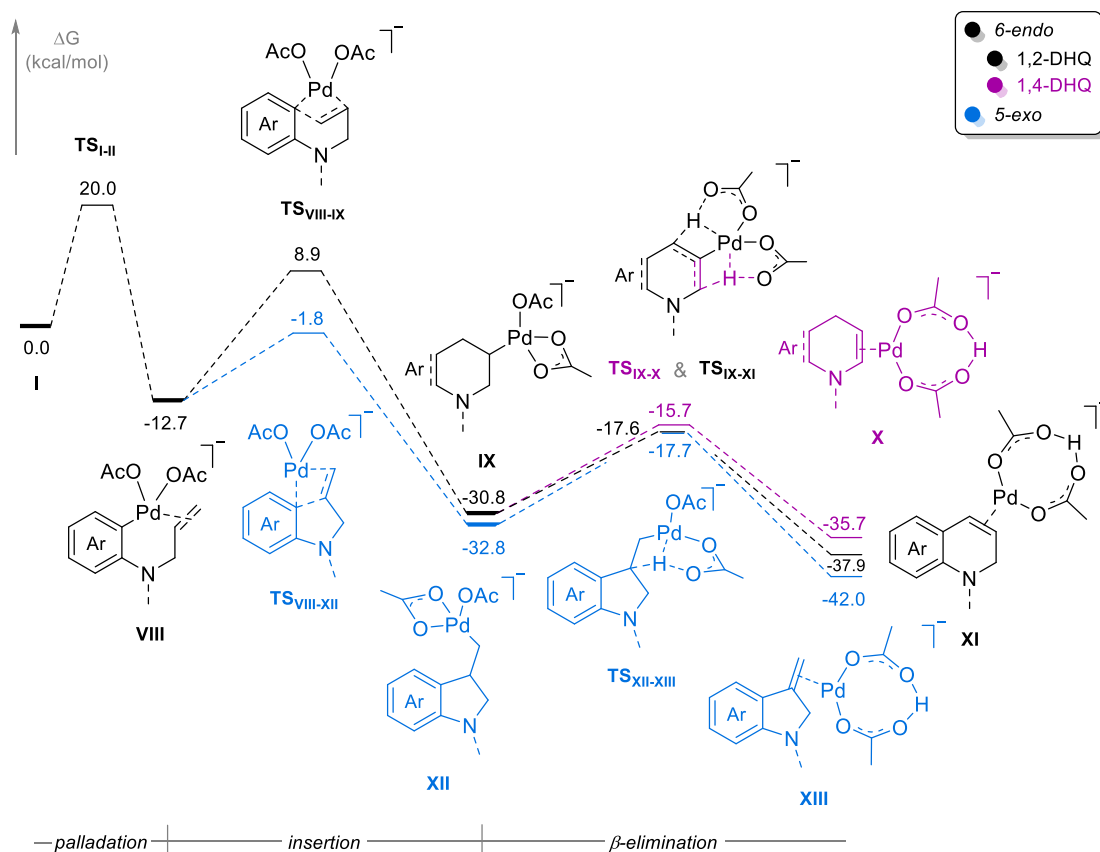
The barrier of the β -elimination step is very low for the three alternatives (Scheme 4.10). The generated hydrides are in fairly unstable, as the three of them are higher in energy than the previous intermediate.

Scheme 4.10. Gibbs energy profile of the β -elimination step, with one AcO⁻ ligand.

Since the activation barriers of the β -elimination step are very low, this step will have little impact in the 6-*endo*/5-*exo* selectivity. Nonetheless, the 1,2-DHQ/1,4-DHQ selectivity will be determined by the energy difference between **TS**_{III-V} ($\Delta G = -7.5$ kcal/mol) and **TS**_{III-VI} ($\Delta G = -9.5$ kcal/mol). The fact that the transition state leading to the 1,2-dihydroquinoline **3a** is 2.0 kcal/mol lower in energy is in agreement with the experimental results, where only product **3a** was observed.

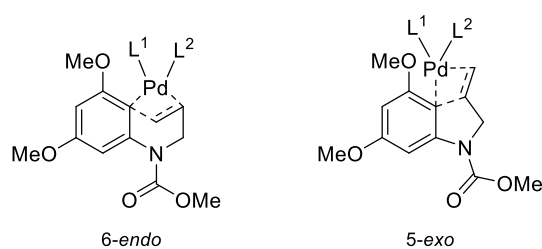
Even though the predicted 1,2-DHQ/1,4-DHQ selectivity is correct, the 5-*exo* pathway is overall lower in energy than the 6-*endo* route. The selectivity would be determined by the cyclization step (Scheme 4.9), where the 5-*exo* transition state had an activation barrier 6.7 kcal/mol lower in energy than the 6-*endo* pathway. Thus, according to this mechanism, only the indole derivative **4a** should be observed, instead of the experimentally found 1,2-dihydroquinoline **3a**.

As previously mentioned, the mechanism with two acetates coordinated to the palladium atom was also computed (Scheme 4.11). In this case, the energy of the intermediates is much lower, although the β -elimination steps present higher activation barriers. The activation energy difference between the 6-*endo* (**TS**_{VIII-IX}) and 5-*exo* (**TS**_{VIII-XII}) cyclizations is now of 10.7 kcal/mol, which is again against the experimentally observed selectivity.



Scheme 4.11. Full Gibbs free energy profile of the classic Fujiwara-Moritani mechanism with two AcO⁻ ligands. Structures have been simplified for the sake of clarity.

Because the transition state of the cyclization is crucial to determine the selectivity of the reaction, we focused on comparing the energies of the two possible transition state structures. In this last case, with two acetate ligands and total charge -1, this difference was of 10.7 kcal/mol. If we look at the previous mechanism, where we considered only one acetate ligand and the complex was neutral, the energy difference was significantly lower (6.7 kcal/mol). Therefore, we wondered if increasing the positive charge of the complex would keep on favoring the 6-*endo* transition state.

Table 4.4. Gibbs free energy differences between the 6-*endo* and 5-*exo* transition states. Energies in kcal/mol.

Entry	L ¹	L ²	Net charge	G(6- <i>endo</i>) - G(5- <i>exo</i>)
1	⁻ OAc	⁻ OAc	-1	10.7
2	⁻ OAc	none	0	6.7
3	MeCN	MeCN	+1	6.1
4	MeCN	none	+1	5.9
5	none	none	+1	3.4

The key 6-*endo* and 5-*exo* transition states were computed using different ligands and their Gibbs free energies were compared (Table 4.4). We can observe that moving from negative to positive charge and decreasing the number of ligands lowers the relative energy of the transition states. With the positively charged complex, the relative energy was lowered to 6.1 kcal/mol (entry 3), and decreasing the number of ligands reduce the difference even more, reaching a value as low as 3.4 kcal/mol (entry 5). Nevertheless, the 5-*exo* transition state is still favored, which contradicts the experimentally found regioselectivity.

In view of these results, we continued with the other possible reaction mechanism, the Friedel-Crafts type reaction, hoping that it would provide the correct experimentally observed regioselectivity.

4.3.2 Path b. Friedel-Crafts type mechanism

This mechanism consists on a direct cyclization, by electrophilic aromatic substitution of the arene to the palladium-activated alkene. We already made a conformational study on the complex formed between the palladium(II) acetate and **1a**, so we continued computing the direct cyclization transition states (Figure 4.8).

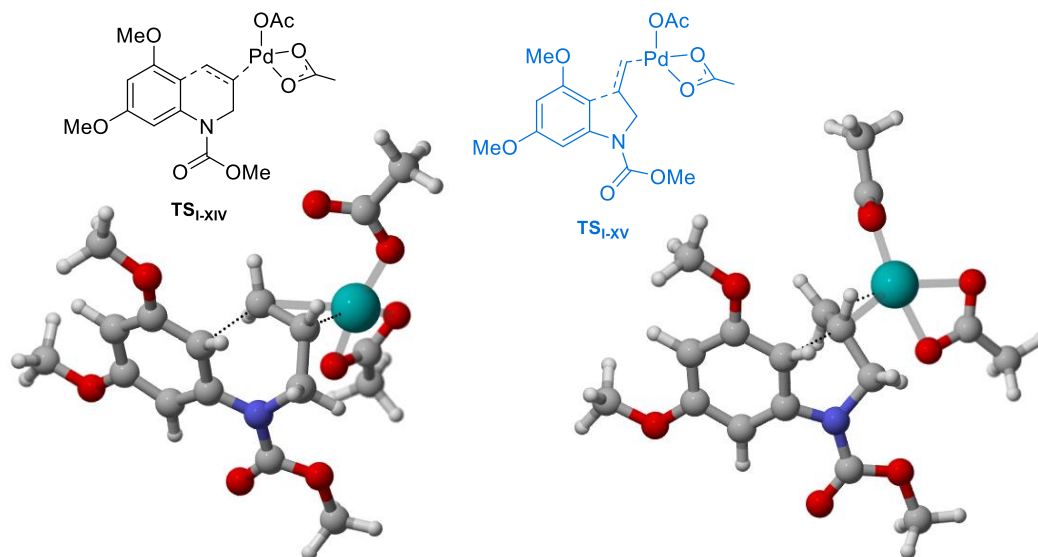
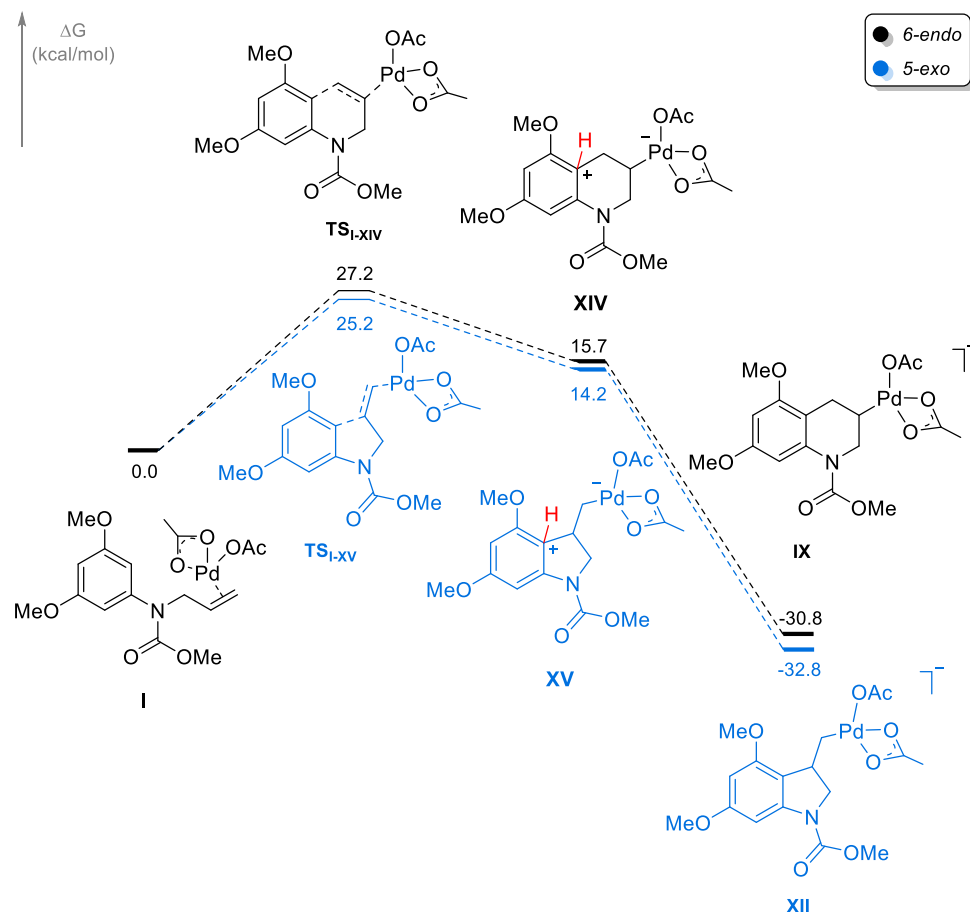


Figure 4.8. Transition states of the 6-*endo* (left, TS_{I-xiv}) and 5-*exo* (right, TS_{I-xv}) direct cyclizations.

Once the six or five-membered ring is formed, the generated intermediate will lose a hydrogen (in red, Scheme 4.12) providing the previously computed intermediates **IX** and **XII**. Unfortunately, the resulting energy profile shows a preference of the 5-*exo* pathway ($\Delta G^\ddagger = 25.2$ kcal/mol) over the 6-*endo* pathway ($\Delta G^\ddagger = 27.2$ kcal/mol), although the energy difference between both transition states is much lower than in all previous cases ($\Delta\Delta G = 2.0$ kcal/mol).



Scheme 4.12. Energy profile for the Friedel-Crafts like mechanism.

As we did for the previous mechanism, we focused on the study of the key 6-*endo* and 5-*exo* transition states to understand the effect of the ligands on the reactivity. Since the energy difference between the two transition states (TS_{I-xiv} and TS_{I-xv}) is now of only 2.0 kcal/mol, we wondered if reducing the net negative charge of the structures would decrease this energy difference and eventually, reverse it.

The removal of one of the acetates from the palladium caused an interesting phenomenon. Even if the remaining acetate was coordinated in a bidentate manner, there still was a vacant site on the palladium atom, which was occupied by the carbamate moiety. This phenomenon happened in both transition states, with a very promising effect on their relative energy.

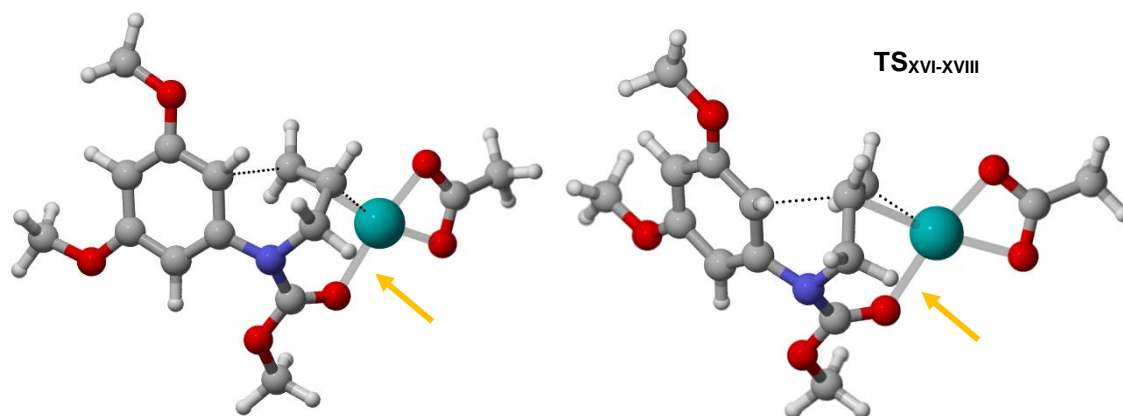


Figure 4.9. New 6-*endo* (left, $\text{TS}_{\text{xvi-xvii}}$) and 5-*exo* (right, $\text{TS}_{\text{xvi-xviii}}$) transition states for the Friedel-Crafts like direct cyclization, with only one AcO ligand. The yellow arrow marks the new coordination between the carbamate and the palladium atom.

For the first time in our computational study, the reaction is selective towards the experimentally found 6-*endo* product, as its transition state ($\text{TS}_{\text{xvi-xvii}}$) turned out to be 3.4 kcal/mol lower in energy than the 5-*exo* transition state ($\text{TS}_{\text{xvi-xviii}}$). This is likely due to the lower ring strain formed during the 6-*endo* product, as a six-membered ring is formed in opposition to the seven-membered ring formed during the 5-*exo* transition state (Figure 4.10).

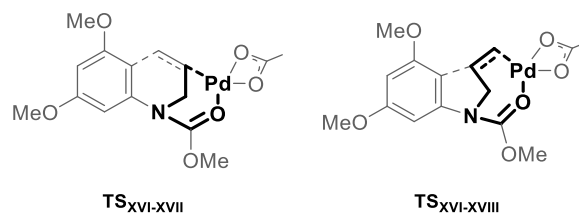


Figure 4.10. Representation of the rings formed during the transition state of the 6-*endo* and 5-*exo* reactions.

The experimental results suggested that the protecting group had a significant impact in the reaction; this hypothesis grows stronger as our calculations show the participation of the protecting group during the cyclization transition state. Thus, using bulkier carbamates like *tert*-butyl carbamate or protecting groups with different electronic properties such as amides, will have a direct impact on the outcome of the reaction.

To our surprise, the activation energy of these two transition states was very high, of 32.8 kcal/mol (6-*endo*) and 35.9 kcal/mol (5-*exo*). A reaction with such high-energy barriers would need years to proceed without heating. Thus, we focused our efforts on lowering this huge barrier, as the experiments were carried out at room temperature.

We first tried changing the functional and basis set to check whether the employed theory level is suitable for this reaction. Perhaps our theory level was underestimating the energy of the complex, or overestimating the energy of the transition states. Thus,

we performed single point calculations on the pertinent structures using a different functional and basis set (Table 4.5).

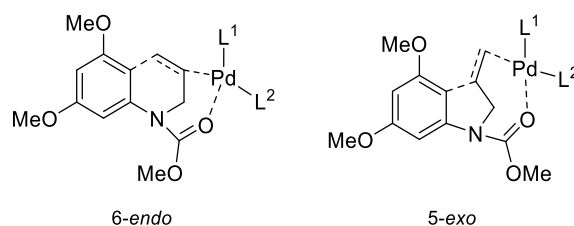
Table 4.5. Comparison of the activation energies of the 6-*endo* and 5-*exo* transition states. All structures were previously optimized in B3LYP/6-31G(d,p)/LanL2DZ.

Functional/Basis set ^a	ΔG^\ddagger 6- <i>endo</i>	ΔG^\ddagger 5- <i>exo</i>
M06/Def2TZVPP	32.8	35.9
M06/6-311+G(d,p)/SDD	30.4	33.8
B3LYP-D3/Def2TZVPP	33.7	37.6
B3LYP-D3/6-311+G(d,p),SDD	31.4	35.5

^aDioxane was used as implicit solvent.

The four tested theory levels provided similar activations barriers, suggesting that the functional and basis set we chose are not responsible the high energy barriers, although the level M06/6-311+G(d,p)/SDD did provide slightly lower values.

Since the ligands had such an influence in the case of the classic Fujiwara-Moritani mechanism, we decided to also test the effect of the ligands in the reaction. We tried different combinations of three ligands: chlorine, acetonitrile and acetate. In Table 4.6, the resulting Gibbs free energies of the 6-*endo* and 5-*exo* transition states are displayed. In all the described cases, the coordination with the carbamate was maintained, as losing it will always result in a lower activation barrier of the experimentally disfavored 5-*exo* product.

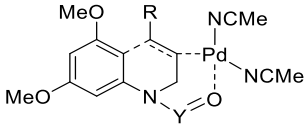
Table 4.6. Activation energies of the Friedel-Crafts type 6-*endo* and 5-*exo* cyclizations with different ligands. Energies in kcal/mol.

Entry	L ¹	L ²	Net charge	ΔG^\ddagger 6- <i>endo</i>	ΔG^\ddagger 5- <i>exo</i>
1	Bidentate	AcO ⁻	+1	32.8	35.9
2	AcO ⁻	AcO ⁻	0	40.4	43.7
3	Cl ⁻	Cl ⁻	0	40.9	44.4
4	Cl ⁻	MeCN	+1	30.5	35.1
5	AcO ⁻	MeCN	+1	30.9	36.7
6	MeCN	MeCN	+2	19.7	22.6

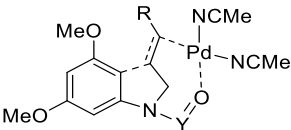
The activation energies depend greatly on the ligand, or more exactly, on the net charge of the complex. When chlorine atoms and acetates were used to stabilize the palladium (entries 2 and 3), extremely high activation barriers were observed, over 40 kcal/mol. Combinations of ligands that lead to an overall positive charge (entries 4 and 5) reduced the activation barriers to *ca.* 30-35 kcal/mol, similar to those of entry 1. Finally, when two acetonitrile ligands were employed (entry 6), feasible activation barriers of even less than 20 kcal/mol, were obtained. This is due to the positive effect of an electron deficient palladium on the activation of the double bond, making it a better electrophile and hence promoting the reaction.

We extended the study to other substrates, in order to check the consistency of our results. We calculated the activation energies of the 6-*endo* and 5-*exo* transition states of the substituted alkenes **1e** and **1f**, and the *N*-tosyl-protected anilines **1n**, **1o** and **1p**. We used two acetonitrile molecules as ligands maintaining the coordination between the protecting group and the palladium.

Table 4.7. Activation energies of different Friedel-Crafts type 6-*endo* and 5-*exo* cyclizations, with two acetonitrile ligands.



6-*endo*



5-*exo*

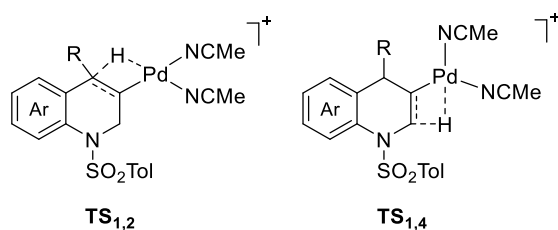
Entry	1	Y	R	ΔG^\ddagger 6- <i>endo</i>	ΔG^\ddagger 5- <i>exo</i>
1	1a	COMe	H	19.7	22.6
2	1e	COMe	Me	16.4	26.2
3	1f	COMe	Ph	11.8	25.7
4	1n	SOTol	H	14.3	18.9
5	1o	SOTol	Me	14.2	21.4
6	1p	SOTol	Ph	11.9	23.3

We can observe in Table 4.7 that the 6-*endo* transition state is always lower in energy than its 5-*exo* counterpart is. The activation barriers are feasible in all cases, never exceeding 20 kcal/mol in the case of the 6-*endo* pathway. The energy difference between both transition states is between 3-4 kcal/mol when the alkene is unsubstituted, while methyl and phenyl groups increase this difference significantly, especially in the case of phenyl substituted alkenes.

The results we obtained with this mechanistic model lead us to believe that the reaction proceeds through the Friedel-Crafts type mechanism, as the predicted selectivity is in perfect agreement with the experimentally observed ratios. Likewise, the suspected crucial role of the protecting group was confirmed, as it is actively participating during the course of the reaction.

4.3.3 Elimination step

We located the transition states of the two possible hydrogen eliminations of the 6-*endo* product under the previous conditions; this is, with the palladium atom having two acetonitrile ligands. We computed the energies of both eliminations of the tosyl-protected substrates **1n**, **1o** and **1p** and compared them with the experimental results (Table 4.8).

Table 4.8. Activation barriers for the two possible β -eliminations of *N*-tosyl protected anilines.

entry	1	R	$G_{\text{TS}2} - G_{\text{TS}1}^a$	yield 1,2-DHQ	yield 1,4-DHQ
1	1n	H	2.4	87%	
2	1o	Me	-2.1	64%	24%
3	1p	Ph	-4.5		42%

^aA positive value indicates that $\text{TS}_{1,2}$ is preferred, while a negative value indicates preference for $\text{TS}_{1,4}$.

In Table 4.8 we can observe that the results for the unsubstituted alkene **1n** (entry 1) and the aromatic alkene **1p** (entry 3) are in good agreement with the experimental results. In the case of the unsubstituted alkene, there is a 2.4 kcal/mol preference for the 1,2-DHQ, the only detected product. The reaction with the phenyl substituted alkene provided exclusively the 1,4-DHQ, which agrees with the computed 4.5 kcal/mol preference. The methyl-substituted alkene **1o** is not selective, as reaction mixtures were obtained in the experiments (64:24, entry 2). The calculations are not able to correct properly the borderline character of the methyl substituent, as an energy difference closer to zero would have been more fitting. Nevertheless, we can conclude that the experimentally observed selectivity trend can be reproduced with our computational model.

4.4 Conclusions

A comprehensive computational study on the two possible mechanisms of the intramolecular Fujiwara-Moritani reaction of allyl anilines has been conducted. The study of the Gibbs energy profiles of each mechanism was crucial to elucidate the most plausible mechanism.

Initially, both mechanisms predicted the wrong selectivity, until an unexpected coordination between the protecting group of the allyl anilines and the palladium atom was found in the Friedel-Crafts type mechanism. The newly discovered coordination favored the experimentally observed 6-*endo* product, as the activation Gibbs free energy was lower than that of the 5-*exo* transition state. This effect, caused by the higher strain formed during the 5-*exo* cyclization transition state, serves to rationalize the big influence of the protecting group of the aniline, as experimentally found by our collaborators.

The encountered Gibbs activation barriers were high and therefore the computational model was adjusted to more accurately describe the reactivity of the reaction. Appropriate activation barriers were achieved when electron deficient complexes were employed, as an increase of the electrophilicity favored the Friedel-Crafts like attack. The consistency of our model was proved, as all the tested substrates provided lower activation barriers for the 6-*endo* product. The model also proved qualitatively suitable for the prediction of the 1,2-DHQ:1,4-DHQ selectivity.

4.5 References

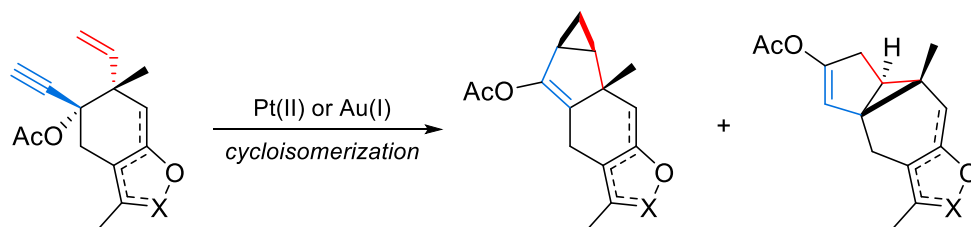
- (1) For reviews on hydroquinolines and their biological effects, please refer to: (a) Michael, J. P. Quinoline, Quinazoline and Acridonealkaloids. *Nat. Prod. Rep.* **2008**, *25*, 166–187. (b) Kumar, S.; Bawa, S.; Gupta, H. Biological Activities of Quinoline Derivatives. *Mini-Rev. Med. Chem.* **2009**, *9*, 1648–1654. (c) Kaur, K.; Jain, M.; Reddy, R. P.; Jain, R. Quinolines and Structurally Related Heterocycles as Antimalarials. *Eur. J. Med. Chem.* **2010**, *45*, 3245–3264. (d) Musiol, R.; Serda, M.; Hensel-Bielowka, S.; Polanski, J. Quinoline-Based Antifungals. *Curr. Med. Chem.* **2010**, *17*, 1960–1973. (e) Afzal, O.; Kumar, S.; Haider, M. R.; Ali, M. R.; Kumar, R.; Jaggi, M.; Bawa, S. A Review on Anticancer Potential of Bioactive Heterocycle Quinoline. *Eur. J. Med. Chem.* **2015**, *97*, 871–910.
- (2) Acar, J. F.; Goldstein, F. W. Trends in Bacterial Resistance to Fluoroquinolones. *Clin. Infect. Dis.* **1997**, *24*, S67–S73.
- (3) (a) Stern, E.; Muccioli, G. G.; Millet, R.; Goossens, J.-F.; Farce, A.; Chavatte, P.; Poupert, J. H.; Lambert, D. M.; Depreux, P.; Hénichart, J.-P. Novel 4-Oxo-1,4-dihydroquinoline-3-carboxamide Derivatives as New CB₂ Cannabinoid Receptors Agonists: Synthesis, Pharmacological Properties and Molecular Modeling. *J. Med. Chem.* **2006**, *49*, 70–79. (b) Stern, E.; Muccioli, G. G.; Bosier, B.; Hamtiaux, L.; Millet, R.; Poupert, J. H.; Hénichart, J.-P.; Depreux, P.; Goossens, J.-F.; Lambert, D. M. Pharmacomodulations around the 4-Oxo-1,4-dihydroquinoline-3-carboxamides, a Class of Potent CB₂-Selective Cannabinoid Receptor Ligands: Consequences in Receptor Affinity and Functionality. *J. Med. Chem.* **2007**, *50*, 5471–5484.
- (4) Xu, J.; Cole, D. C.; Chang, C.-P. B.; Ayyad, R.; Asselin, M.; Hao, W.; Gibbons, J.; Jelnisky, S. A.; Saraf, K. A.; Park, K. Inhibition of the Signal Transducer and Activator of Transcription-3 (STAT3) Signaling Pathway by 4-Oxo-1-phenyl-1,4-dihydroquinoline-3-carboxylic Acid Esters. *J. Med. Chem.* **2008**, *51*, 4115–4121.
- (5) Hadida, S.; Van Goor, F.; Zhou, J.; Arumugam, V.; McCartney, J.; Hazlewood, A.; Decker, C.; Negulescu, P.; Grootenhuis, P. D. J. Discovery of N-(2,4-Di-*tert*-butyl-5-hydroxyphenyl)-4-oxo-1,4-dihydroquinoline-3-carboxamide (VX-770, Ivacaftor), a Potent and Orally Bioavailable CFTR Potentiator. *J. Med. Chem.* **2014**, *57*, 9776–9795.
- (6) (a) Hemmer, M.; Krawczyk, S.; Simon, I.; Hilgeroth, A. Discovery of Substituted 1,4-Dihydroquinolines as Novel Promising Class of P-Glycoprotein Inhibitors: First Structure–Activity Relationships and Bioanalytical Studies. *Bioorg. Med. Chem. Lett.* **2015**, *25*, 3005–3008. (b) Hemmer, M.; Krawczyk, S.; Simon, I.; Lage, H.; Hilgeroth, A. Discovery of Substituted 1,4-Dihydroquinolines as Novel Class of ABCB1 Modulators. *Bioorg. Med. Chem.* **2015**, *23*, 5015–5021.
- (7) Bodor, N.; Farag, H. H.; Barros, M. D. C.; Wu, W.-M.; Buchwald, P. In Vitro and In Vivo Evaluations of Dihydroquinoline- and Dihydroisoquinoline-Based Targetor Moieties for Brain-Specific Chemical Delivery Systems. *J. Drug Target.* **2002**, *10*, 63–71.
- (8) Țințaș, M.-L.; Foucoute, L.; Petit, S.; Oudeyer, S.; Gourand, F.; Barré, L.; Papamicaël, C.; Levacher, V. New Developments in Redox Chemical Delivery Systems by Means of 1,4-Dihydroquinoline-Based Targetor: Application to Galantamine Delivery to the Brain. *Eur. J. Med. Chem.* **2014**, *81*, 218–226.
- (9) Moritani, I.; Fujiwara, Y. Aromatic Substitution of Styrene-Palladium Chloride Complex. *Tetrahedron Lett.* **1967**, *8*, 1119–1122.

- (10) Review on the reaction by Fujiwara: (a) Kitamura, T.; Fujiwara, Y. From C-H to C-C Bonds: Cross-Dehydrogenative-Coupling. In *Green Chemistry Series*; Li, C.-J., Ed.; Royal Society of Chemistry: Cambridge, 2014; pp 33-54. Other authors: (b) Ferreira, E. M.; Zhang, H.; Stoltz, B. M. Oxidative Heck-Type Reactions (Fujiwara-Moritani Reactions). In *The Mizoroki-Heck Reaction*; Oestreich, M., Ed.; Wiley: Hoboken, N.J, 2009; pp 345-382. (c) Le Bras, J.; Muzart, J. Intermolecular Dehydrogenative Heck Reactions. *Chem. Rev.* **2011**, *111*, 1170-1214. (d) Zhou, L.; Lu, W. Towards Ideal Synthesis: Alkenylation of Aryl C-H Bonds by a Fujiwara-Moritani Reaction. *Chem. Eur. J.* **2014**, *20*, 634-642.
- (11) (a) Fujiwara, Y.; Moritani, I.; Matsuda, M.; Teranishi, S. Aromatic Substitution of Styrene-Palladium Chloride Complex, II. *Tetrahedron Lett.* **1968**, *9*, 633-636. (b) Fujiwara, Y.; Moritani, I.; Matsuda, M. Aromatic Substitution of Olefin—III, Reaction of Styrene-Palladium(II) Chloride Complex. *Tetrahedron* **1968**, *24*, 4819-4824.
- (12) Fujiwara, Y.; Moritani, I.; Matsuda, M. Aromatic Substitution of Olefin. IV Reaction with Palladium Metal and Silver Acetate. *Tetrahedron Lett.* **1968**, *9*, 3863-3865.
- (13) Moritani, I.; Fujiwara, Y. Aromatic Substitution of Olefins by Palladium Salts. *Synthesis* **1973**, *9*, 524-533.
- (14) Bingham, A. J.; Dyllal, L. K.; Norman, R. O. C.; Thomas, C. B. Reactions of Palladium(II) with Organic Compounds. Part I. Oxidative Cyclisation of 3-Methyl-3-phenylbut-1-ene and 3,3,3-Triphenylpropene. *J. Chem. Soc. C* **1970**, 1879-1883.
- (15) Examples of Fujiwara-Moritani reactions in total synthesis: (a) Trost, B. M.; Godleski, S. A.; Belletire, J. L. Synthesis of (±)-Catharanthine via Organopalladium Chemistry. *J. Org. Chem.* **1979**, *44*, 2052-2054. (b) Knölker, H.-J.; Reddy, K. R.; Wagner, A. Indoloquinones, Part 5. Palladium-Catalyzed Total Synthesis of the Potent Lipid Peroxidation Inhibitor Carbazoloquinocin C. *Tetrahedron Lett.* **1998**, *39*, 8267-8270. (c) Baran, P. S.; Corey, E. J. A Short Synthetic Route to (+)-Austamide, (+)-Deoxyisoaustamide, and (+)-Hydratoaustamide from a Common Precursor by a Novel Palladium-Mediated Indole → Dihydroindoloazocine Cyclization. *J. Am. Chem. Soc.* **2002**, *124*, 7904-7905. (d) Baran, P. S.; Guerrero, C. A.; Corey, E. J. Short, Enantioselective Total Synthesis of Okaramine N. *J. Am. Chem. Soc.* **2003**, *125*, 5628-5629. (e) Williams, R. M.; Cao, J.; Tsujishima, H.; Cox, R. J. Asymmetric, Stereocontrolled Total Synthesis of Paraherquamide A. *J. Am. Chem. Soc.* **2003**, *125*, 12172-12178. (f) Garg, N. K.; Caspi, D. D.; Stoltz, B. M. The Total Synthesis of (+)-Dragmacidin F. *J. Am. Chem. Soc.* **2004**, *126*, 9552-9553.
- (16) Fujiwara, Y.; Moritani, I.; Danno, S.; Asano, R.; Teranishi, S. Aromatic Substitution of Olefins. VI. Arylation of Olefins with Palladium(II) Acetate. *J. Am. Chem. Soc.* **1969**, *91*, 7166-7169.
- (17) Fuchita, Y.; Hiraki, K.; Kamogawa, T.; Suenaga, M.; Tohgoh, K.; Fujiwara, Y. Activation of Aromatic Carbon-Hydrogen Bonds by Palladium(II) Acetate-Dialkyl Sulfide Systems. Formation and Characterization of Novel Diphenyltripalladium(II) Complexes. *Bull. Chem. Soc. Jpn.* **1989**, *62*, 1081-1085.
- (18) Dams, M.; De Vos, D. E.; Celen, S.; Jacobs, P. A. Toward Waste-Free Production of Heck Products with a Catalytic Palladium System under Oxygen. *Angew. Chem. Int. Ed.* **2003**, *42*, 3512-3515.
- (19) Schiffner, J. A.; Oestreich, M. All-Carbon-Substituted Quaternary Carbon Atoms in Oxindoles by an Aerobic Palladium(II)-Catalyzed Ring Closure onto Tri- and Tetrasubstituted Double Bonds. *Eur. J. Org. Chem.* **2011**, 1148-1154.
- (20) Liu, C.; Widenhoefer, R. A. Palladium-Catalyzed Cyclization/Carboalkoxylation of Alkenyl Indoles. *J. Am. Chem. Soc.* **2004**, *126*, 10250-10251.

- (21) (a) Carral-Menoyo, A.; Ortiz-de-Elguea, V.; Martinez-Nunes, M.; Sotomayor, N.; Lete, E. Palladium-Catalyzed Dehydrogenative Coupling: An Efficient Synthetic Strategy for the Construction of the Quinoline Core. *Mar. Drugs* **2017**, *15*, 276-290. (b) Carral-Menoyo, A.; Misol, A.; Gómez-Redondo, M.; Sotomayor, N.; Lete, E. Palladium(II)-Catalyzed Intramolecular C-H Alkenylation for the Synthesis of Chromanes. *J. Org. Chem.* **2019**, *84*, 2048-2060.
- (22) Ortiz-de-Elguea, V.; Sotomayor, N.; Lete, E. Two Consecutive Palladium(II)-Promoted C-H Alkenylation Reactions for the Synthesis of 3-Alkenylquinolones. *Adv. Synth. Catal.* **2015**, *357*, 463-473.

Chapter 5.

Platinum and Gold-Catalyzed cycloisomerization of 1,5- enynes



In the present chapter, DFT calculations have been carried out for the study of the mechanism of Pt(II) and Au(I) catalyzed cycloisomerization reactions of 1,5-enynes for the synthesis of sesquiterpenoids. Our collaborators from the Aristotle University of Thessaloniki conducted the experimental investigations, where they observed the formation of different products depending on the reaction conditions and the nature of the substrate. By means of computational tools, the divergent reactivity and observed isomeric ratios have been rationalized.

Chapter based on the publication:

Sotorríos, L.; Demertzidou, V. P.; Zografos, A. L.; Gómez-Bengoa, E. DFT Studies on Metal-Catalyzed Cycloisomerization of *Trans*-1,5-enynes to Cyclopropane Sesquiterpenoids. *Org. Biomol. Chem.* **2019**, *17*, 5112-5120.

5.1 Context

This chapter of the thesis is based on a collaboration carried out with experimental researchers. The experimental reactions were performed in the group of Prof. Alexandros Zografos from the Aristotle University of Thessaloniki. Their experimental research had been published¹ before we performed our computational investigations. The computational publication arisen from this chapter is available in the appendix.

The work carried out by the author of this thesis is entirely computational and will be presented in the *results and discussion* section. Nevertheless, in the present section we will provide a context for these investigations by introducing the nature of the chemistry, as well as briefly discussing the aim, procedures and results of the experimental studies previously carried out by our collaborators.

5.1.1 Objective

The aim of the experimental study conducted by our colleagues was the synthesis of lindenane-type sesquiterpenoids bearing a furan or a lactone ring. For this purpose, they planned to subject 1,5-enynes to cycloisomerization reactions using platinum(II) and gold(I) catalysts to construct the desired [3.1.0] bicyclic structure.

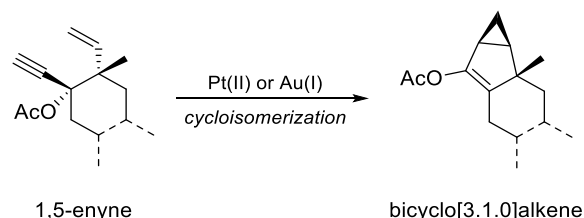
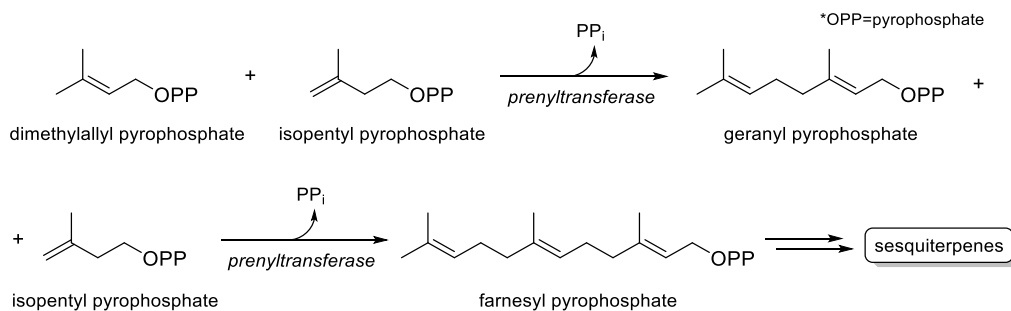


Figure 5.1. Aim of the experimental project.

5.1.1.1 Lindenane-type sesquiterpenoids

Sesquiterpenes are a class of terpenes containing three units of the basic five-carbon unit isoprene. Present in a vast number of plants, from conifers to lilies,² they are the most diverse group of terpenes.³ They are biosynthesized from dimethylallyl pyrophosphate and its isomer isopentyl pyrophosphate⁴ as illustrated in Scheme 5.1.



Scheme 5.1. Biosynthesis of farnesyl pyrophosphate, precursor of sesquiterpenes.

The core structure of lindenane is a tricyclic, as shown in Figure 5.2. Structures deriving from this framework are isolated from the *Chloranthus* species⁵, which have been extensively used in traditional Chinese medicine.⁶

Figure 5.2. *Chloranthus japonicus* and core structure of the lindenane sesquiterpene.

Several assessments of the biological activity of lindenane-type sesquiterpenoids have been carried out, with especial focus on sesquiterpenoids bearing a lactone moiety. For example, chlojaponilactone B and structurally related sesquiterpenoids can regulate the expression of inflammatory mediators and therefore, their anti-inflammatory potential has been assessed.⁷ Closely related sesquiterpenes such as onoseriolide have shown cytotoxicity against parasites from the genus *Leishmania*.⁸

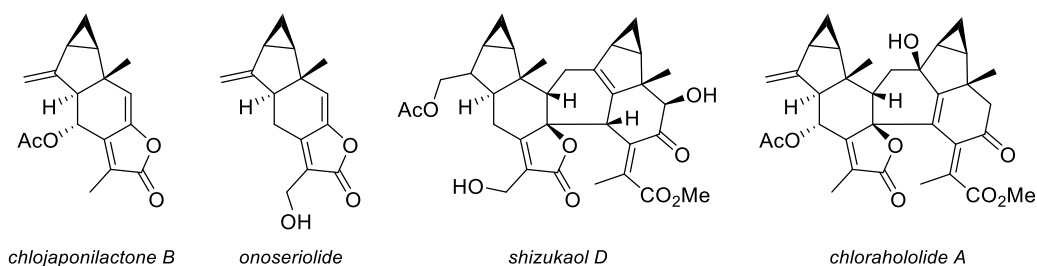


Figure 5.3. Examples of natural lindenane-type sesquiterpenoids displaying biological activity.

Although interesting monomeric lindenane-type sesquiterpenoids like the aforementioned exist, most of the isolated structures are encountered as dimers. Several dimers

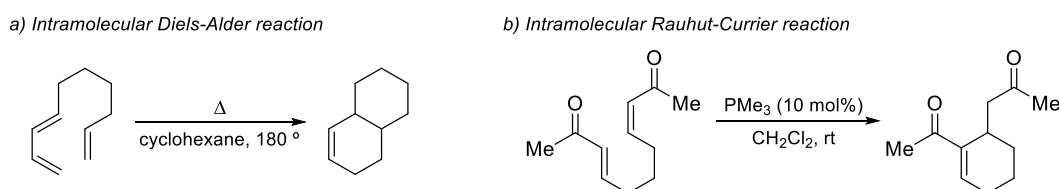
isolated from *Chloranthus Japonicus*, such as shizukaol D, have shown inhibition of the expression of nitrogen oxide, mediator in inflammatory processes.⁹ Chlorahololides A and B can act as selective blockers of the potassium ion channel, implicated in diseases such as epilepsy and Alzheimer's.¹⁰

5.1.2 State of the art

5.1.2.1 Cycloisomerizations

Cycloisomerization reactions are rearrangements of polyunsaturated substrates that form cyclic products while losing at least one degree of unsaturation. Since no formal loss or gain of atom occurs, cycloisomerizations have emerged as atom-economic approaches to cyclic and polycyclic compounds.^{11a}

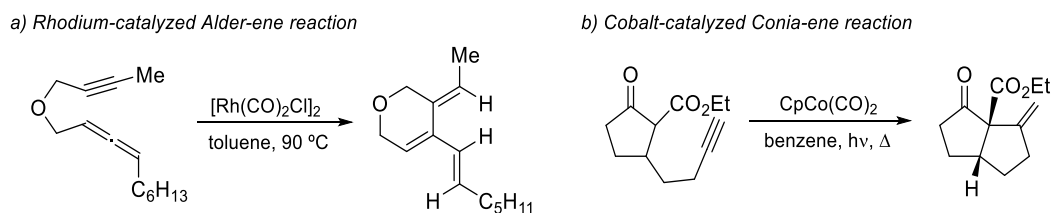
A myriad of different reactions can be categorized as cycloisomerizations.¹² Although most of them involve the use of metals for the activation of the polyunsaturated substrates, some cycloisomerizations can be carried out by using exclusively organic substrates and reactants. For example, intramolecular pericyclic reactions performed exclusively in thermal conditions would fall under this category, such as the simple intramolecular Diels-Alder reaction showed in Scheme 5.2, *a*.¹³ In the same way, intramolecular variants of the Rauhut-Currier reaction can generate cyclic products employing organophosphines (*b*, Scheme 5.2).¹⁴



Scheme 5.2. Examples of thermal (left) and organocatalyzed (right) cycloisomerizations.

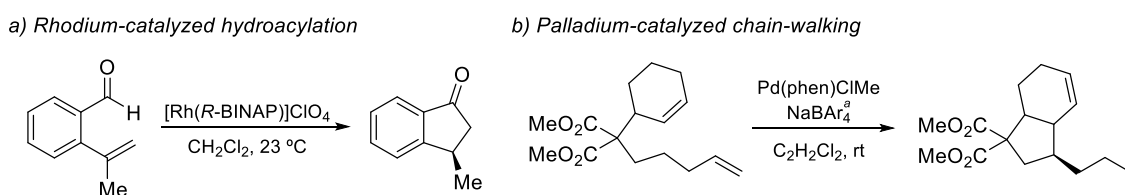
Metal-catalyzed cycloisomerization reactions have been extensively studied. Many different metals can be used for this purpose and, although most cycloisomerizations are based on the reaction of enynes, different substrates can also be subjected to these reactions.^{11,12} A few relevant examples will be highlighted in the next lines.

Several ene-type reactions can be performed using transition metal catalysts. Allenynes can be subjected to rhodium catalyzed Alder-ene reactions as shown in Scheme 5.3, *a*, to synthesize cross-conjugated trienes.¹⁵ Conia-ene cycloisomerizations can be performed in cyclic β -ketoesters to form bicyclic structures using cobalt catalysts (*b*, Scheme 5.3).¹⁶

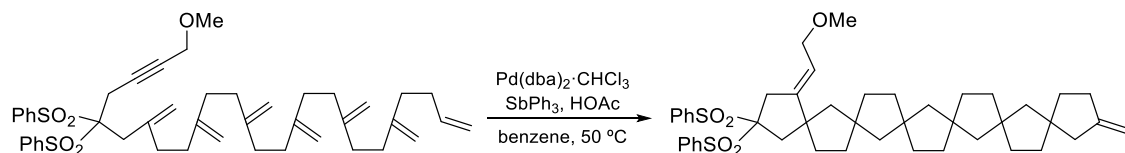


Scheme 5.3. Examples of metal-catalyzed ene-type cycloisomerizations.

Other type of reactions can be categorized as cycloisomerizations as well. For example, a rhodium-catalyzed hydroacylation is used for the synthesis of chiral 3-substituted indanones from 2-vinyl benzaldehyde systems (*a*, Scheme 5.4).¹⁷ In a different manner, an interesting palladium-catalyzed 1,*n*-diene cycloisomerization can be performed via chain-walking reaction (*b*, Scheme 5.4).¹⁸

Scheme 5.4. Further examples of metal-catalyzed cycloisomerizations. ^aAr = 3,5-(CF₃)₂C₆H₃

As will be highlighted in the next section, enynes are excellent substrates of cycloisomerizations, especially employing gold and platinum catalysts. Nevertheless, reactions using alternative metals can be found,¹⁹ as is the case of the beautiful domino Alder-ene reaction developed by Trost, the so-called palladium zipper (Scheme 5.5).²⁰



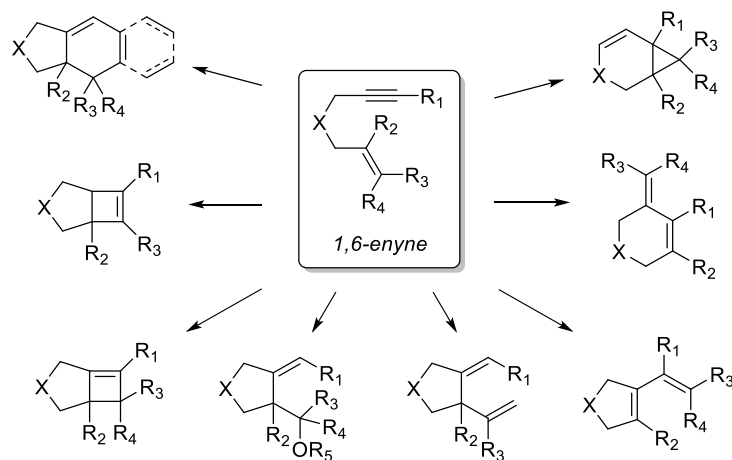
Scheme 5.5. Palladium catalyzed cycloisomerization of a polyenyne.

5.1.2.2 Platinum and gold-catalyzed cycloisomerizations of enynes

The cycloisomerizations of enynes are among the most powerful strategies for the synthesis of functionalized cycles, thanks to the level of complexity that can be obtained from relatively simple enynes. Among the metals capable of catalyzing these reactions, gold and platinum emerge as excellent alternatives, as they are capable of working under mild conditions while providing great chemoselectivity and high efficiency. In this regard, several authors have reviewed this topic thoroughly.²²

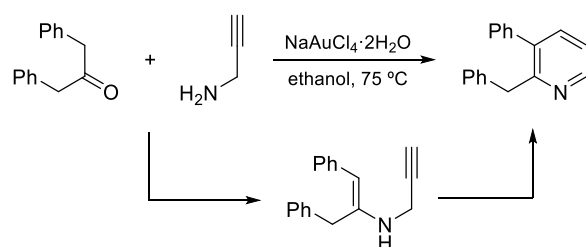
Depending on the relative position of the alkene and alkyne motifs, different skeletal rearrangements are possible. As an example, the reaction topologies observed in the cycloisomerization of 1,6-enynes are displayed in Scheme 5.6. The nature of the selected

catalyst and the substitution pattern of the substrate are crucial for the outcome of the reaction.^{22a}



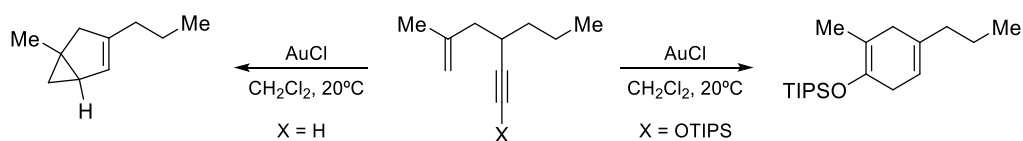
Scheme 5.6. Observed reaction topologies in platinum and gold cycloisomerizations of 1,6-enynes (adapted from ref. 22a).

A similar number of skeletal rearrangements can be conducted on 1,5-enynes. One of the first reported examples was the cycloisomerization of substituted propargyl enamines for the synthesis of pyridine rings, which was highly efficient when $\text{NaAuCl}_4 \cdot \text{H}_2\text{O}$ was used as catalyst (Scheme 5.7).²³



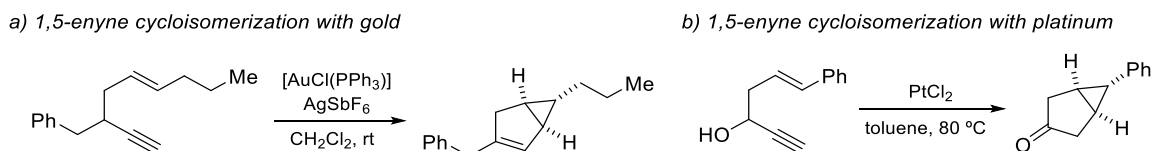
Scheme 5.7. Gold-catalyzed amination/annulation/aromatization sequence for the synthesis of substituted pyridines, with propargyl enamines as key intermediates.

Other type of rearrangements can be carried out, such as the formation of cyclohexadienes. Kozmin et al. used 1,5-enynes bearing a triisopropylsilylether (OTIPS) group to synthesize cyclohexadienes using gold(I) chloride (Scheme 5.8).²⁴ As mentioned earlier, the functionalities present in the substrate can greatly affect the outcome of the reaction. In this particular case, removing the triisopropylsilylether group (OTIPS) caused a different type of rearrangement to occur, as the formation of a bicyclo[3.1.0]alkene was observed under the same reaction conditions.



Scheme 5.8. Cycloisomerization of two similar 1,5-enynes with gold(I) chloride.

The formation of bicyclo[3.1.0]alkenes is actually the most common outcome of 1,5-enyne cycloisomerizations and it is also the aim of the synthesis described in this chapter of the thesis. In the examples presented in Scheme 5.9, [3.1.0] bicyclic systems were constructed, using gold complexes (*a*, Toste et al.)²⁵ or platinum(II) chloride (*b*, Malacria et al.)²⁶ as catalysts. It is worth mentioning that both reactions were stereospecific, as the use of *Z*-alkenes provided the opposite diastereoisomer.

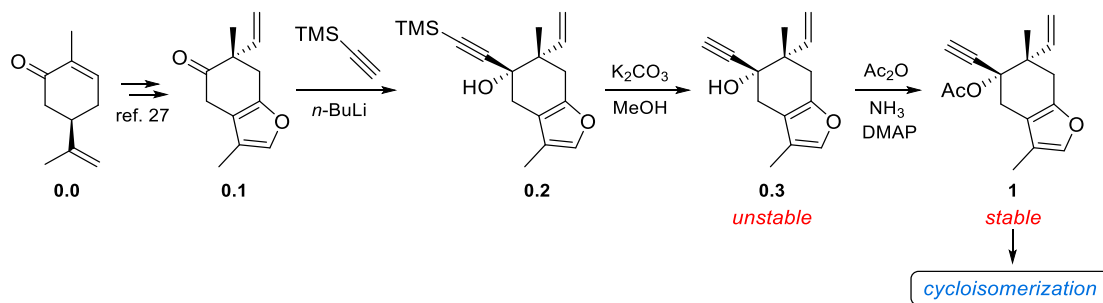


Scheme 5.9. Gold (*a*, left) and platinum (*b*, right) catalyzed cycloisomerizations for the synthesis of [3.1.0] bicyclic systems.

As proven above these lines, gold and platinum cycloisomerization of 1,5-enynes is a versatile and efficient method for the construction of complex organic molecules. Its potential on the synthesis of lindenane-type sesquiterpenoids, containing a [3.1.0] bicyclic, is very appealing.

5.1.3 Experimental

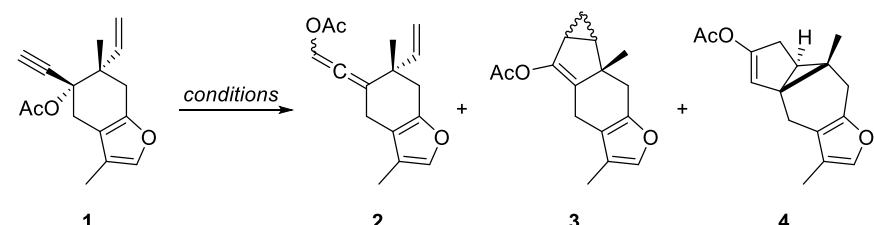
As previously mentioned, experimental reactions were performed in the group of Alexandros Zografos from the Aristotle University of Thessaloniki. Prior to the cycloisomerization reactions, they synthesized enyne **0.3*** from compound **0.1** as shown in Scheme 5.10. This was obtained from the natural terpenoid carvone (**0.0**) as previously reported.²⁷ Due to its instability, **0.3** was acetylated to generate **1**, which was a stable compound, and therefore suitable to isolation and further transformation through cycloisomerization reactions.



Scheme 5.10. Synthesis of the starting material, **1**.

* The numbering of the molecules has been reset, as they are not related to those in previous chapters.

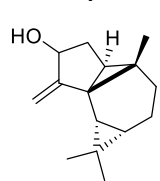
Enyne **1** was then subjected to the metal-catalyzed cycloisomerization reaction, under the conditions shown in Table 5.1. The reaction of **1** with gold(I) chloride (entry 1) lead to the formation of the allene **2** in quantitative yield. Unfortunately, compound **2**, which is the product of the 1,3-migration of the acetate, was inert to gold-catalyzed cycloisomerizations. When more harsh conditions were employed, only decomposition of the product was observed.

Table 5.1. Optimization of cycloisomerization reaction of **1**.


Entry	Metal ^a	Conditions ^b	2	3 (<i>syn:anti</i>)	4
1	AuCl	rt, 2 h	>99%	-	-
2 ^c	PtCl ₂	100 °C, o/n	-	-	65%
3	PtCl ₂	Deoxygenation; 110 °C, o/n	-	45% (2.4:1)	30%
4	PtCl ₂	Deox.; 90 °C, 1.5 h	-	48% (1.6:1)	27%
5	PtCl ₂	Deox.; 90 °C, 5 h then rt, o/n	-	42% (2.3:1)	14%
6	PtCl ₂	Deox.; 90 °C, NaHCO ₃ , o/n	-	62% (2.4:1)	8%

^a5 % mmol. ^bToluene was always used as solvent. ^c**2** was used as starting material.

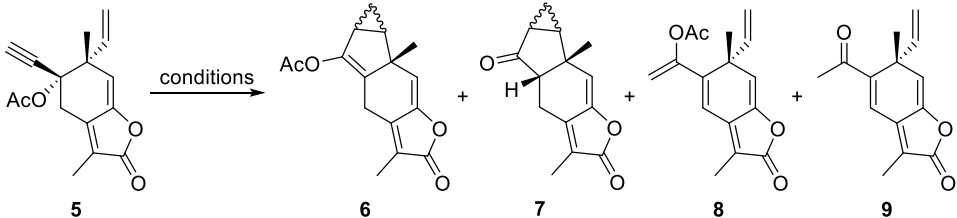
Nonetheless, allene **2** did react with platinum(II) chloride (entry 2), yielding **4** quantitatively. Although **4** is indeed the product of a cycloisomerization and a [3.1.0] bicyclic system was formed, the atom arrangement is different from the desired lindenane-type structure. After isolation of **4**, its absolute configuration was determined and the structure was found to be similar to that of a different sesquiterpenoid, myliol (see picture on the left).



Next, the catalyst was switched to platinum(II) chloride, using temperatures between 90 and 110 °C in deoxygenated toluene (entries 3-6). In these conditions, the presence of the desired lindenane-type structure **3** was observed, along with compound **4**. The reaction conditions were optimized to improve both the **3:4** ratio and the diastereomeric ratio of **3**, achieving the best results with sodium bicarbonate as additive (entry 6).

In order to obtain the lactone congener of **3**, they tried to oxidize the furan ring, but unfortunately only decomposition was observed, even under mild oxidation conditions. Therefore, they decided to synthesize the lactone congener of the starting material, **1**.

This could be achieved by treating **0.3** with pyridinium dichromate in dimethylformamide before the acetylation. The resulting lactone **5** was then subjected to similar reaction conditions, whose optimization is shown in Table 5.2.

Table 5.2. Optimization of cycloisomerization reaction of **5**.


The reaction scheme shows the conversion of lactone **5** to four products: **6**, **7**, **8**, and **9**. Product **6** is a lindenane-type structure with an acetoxy group. Product **7** is its unprotected congener. Product **8** is a lactone analogue of the myliol-type compound **4**. Product **9** is its unprotected analogue. The reaction is catalyzed by PtCl₂ in toluene.

Entry	Metal	Conditions ^a	6	7	8	9
1	PtCl ₂ (5 mmol %)	Deox.; 60 °C, o/n	traces	-	-	-
2	PtCl ₂ (5 mmol %)	Deox.; 80 °C, 3h	8%	traces	-	-
3	PtCl ₂ (10 mmol %)	Deox.; 90 °C, o/n	37%	15% ^b	19%	17%
4	PtCl ₂ (10 mmol %)	NaHCO ₃ ; 110 °C, 4 h	-	-	16%	12% ^c
5	PtCl ₂ (10 mmol %)	Deoxy.; 70 °C, o/n	40%	17% ^b	21%	11%

^aToluene was always used as solvent. ^b*syn:anti* ratio = 5:1. ^cExtended decomposition was also observed.

In contrast with furan **1**, lactone **5** delivered only the lindenane-type structure **6** (and its unprotected congener **7**); the lactone analogue of the myliol-type compound **4** was never observed. Compounds **8** and its unprotected analogue **9** were also formed, probably due to the 1,2-migration of the acetate occurring before the cycloisomerization step.

In the light of the above, it can be concluded that 1,5-enynes containing furan or lactone moieties serve as excellent substrates for platinum-catalyzed cycloisomerization reactions. The synthesized products are known intermediates of the synthesis of lindenane-type natural sesquiterpenoids, such as the furan *epi*-lindenene²⁸ and the lactone sarcandralactone A.²⁹

5.2 Computational approach

5.2.1 Objectives

In spite of the positive results of their experiments, the reasons underlying for some of the experimental results were unclear. Therefore, we intended to give an answer by means of computational chemistry to the following issues.

- Mechanism of the reactions

The exact mechanism of the two cycloisomerization reactions is far from trivial. Locating the transition states and studying the energy profile could help us comprehend this complex process.

- Divergent reactivity observed between gold and platinum catalysis

When gold was used as catalyst, only the formation of allene **2** was achieved. Comparing the reaction mechanism of the gold and platinum-catalyzed reactions should give us an answer to this question.

- Preference of product **3** over **4** in the PtCl₂ catalyzed reactions

There seems to be a preference over product **3**, although total selectivity was never achieved. An exhaustive computational study may shed some light into this matter.

- Diastereomeric ratio of **3**

Even after careful optimization of the reaction conditions, the 2.4:1 selectivity could not be improved. A comparison on the energies of the *syn* and *anti* paths would clarify this issue.

- Different reactivity of furan **1** and lactone **5**

The myliol derivative was obtained for the furan containing substrate **1**, but never for the lactone analogue **5**, although same reaction conditions were employed for both substrates. On the other hand, the diastereomeric *syn/anti* ratio of furan **3** was of 2.4:1, while in the case of the lactone **5** a ratio of 5:1 was obtained. These differences should be reflected on the energy profiles of each substrate.

5.2.2 General methods

For references and a more detailed description of the methodology, levels of theory and software, please see chapter 1.

Initially, the theory level used for the optimization of the geometries consisted of the functional B3LYP, the basis set 6-31G(d,p) for non-metals and the basis set LANL2DZ for gold and platinum (for both core and valence electrons). Final energies were obtained by performing single point calculations on the already optimized structures, with the functional M06, the basis set 6-311G(d,p) for non-metals and the basis set SDD for gold and platinum (for both core and valence electrons). Both the optimizations and single point energy calculations were carried out in a solvent model (IEFPCM, solvent = toluene).

Later, certain structures were computed on additional theory levels. The functionals used for this purpose were M11-L, ω B97X-D, B3PW91-D3 and B3LYP-D3. The basis set DefTZVPP was also tested. The cases when these methods were employed will be indicated in the text and figures.

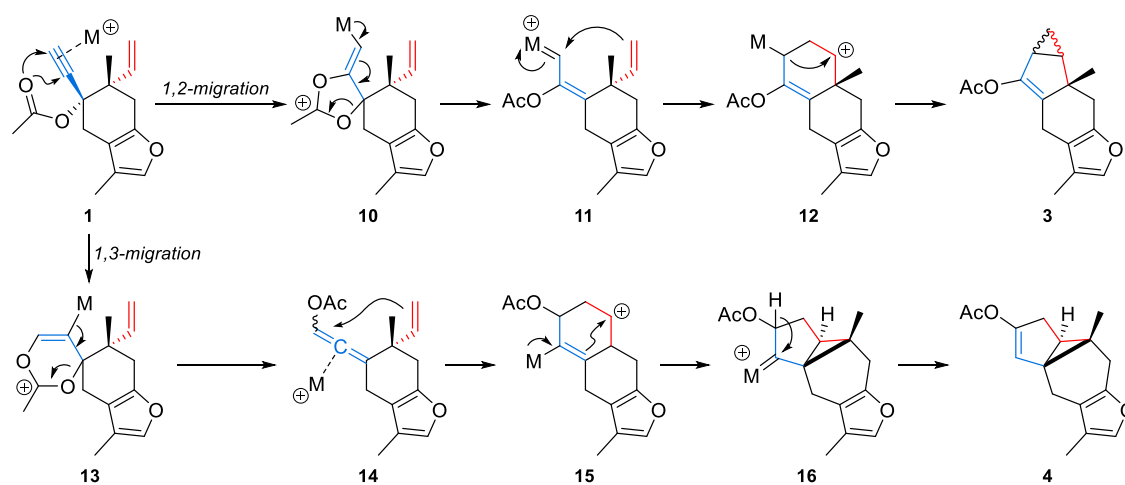
5.3 Results and discussion

5.3.1 Mechanism of the reaction

5.3.1.1 Proposal

The study of the reaction mechanism was initiated with the enyne-furan **1**. As an initial approximation, we followed the mechanism postulated by our collaborators (Scheme 5.11).

The reaction commences via 1,2 or 1,3-attack of the oxygen of the acetate to the alkyne, causing the formation of a metal-carbon bond. After the 1,2-attack, a five membered ring is formed in intermediate (**10**), which is again opened through the formation of the metal carbene **11**. Next, the terminal alkene attacks the carbene forming a six membered ring (**12**) which subsequently undergoes the final cyclization to form the lindane-type product **3**.



Scheme 5.11. Postulated mechanisms.

Following the 1,3-migration pathway, a six membered ring is generated in compound **13**. The metal-carbon bond is then broken to complete the acetate migration, forming allene **14**. Next, the terminal alkene attacks the external carbon atom of the allene, inserting the metal and forming a six membered cycle (**15**). Later, a carbene is formed causing the cyclization that assembles the myliol-type cyclic structure **16**. Finally, product **4** is generated via 1,2-hydrogen shift.

5.3.1.2 Initial complex

The reaction should start with the coordination of the metal to the alkyne. Initially, structures were calculated with neutral catalysts, AuCl and PtCl₂, and also with their cationic counterparts, Au⁺ and PtCl⁺.

It soon became clear that the cationic complexes were not feasible, since intermediates were not stable and transition state calculations did not converge. Henceforth, the neutral catalysts were used when computing all intermediates and transition states.

We found the first differences between platinum and gold when looking into the initial complexes (Figure 5.4). Gold(I) chloride is coordinated to the alkyne in a linear fashion. Platinum(II) chloride on the other hand, showed double coordination with the alkene and alkyne, acquiring a square planar conformation.

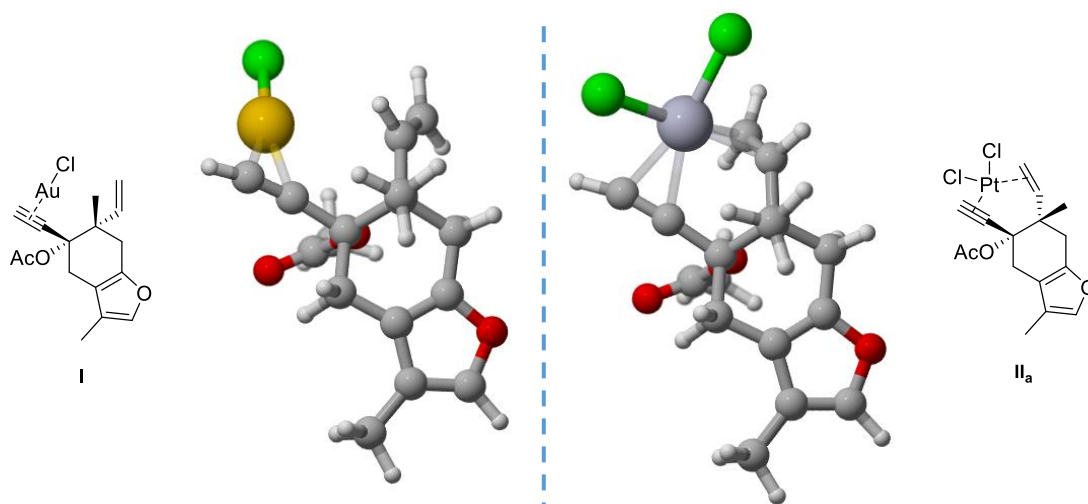
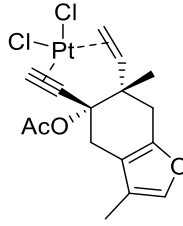
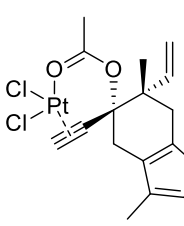
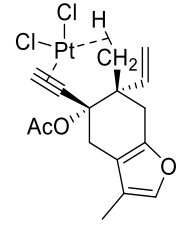
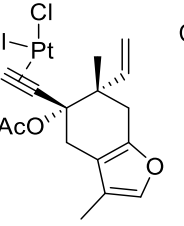
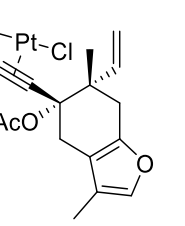


Figure 5.4. 2D and 3D structures of **I** and **II_a** (B3LYP/6-31G(d,p)/LANL2DZ).

A few different conformations of the complex **II** were taken into consideration. The platinum may be coordinated to the alkene, as displayed in Figure 5.4, but coordination with the acetate or a C-H bond is also possible. In Table 5.3, the free Gibbs energies of each conformation are displayed, related to the most stable conformer **II_a**.

Table 5.3. Different conformations of structure II. Energies referring to II_a, in kcal/mol. Calculations were performed at the M06/6-311G(d,p)/SDD(IEFPCM,toluene)//B3LYP/6-31G(d,p)/LANL2DZ theory level.

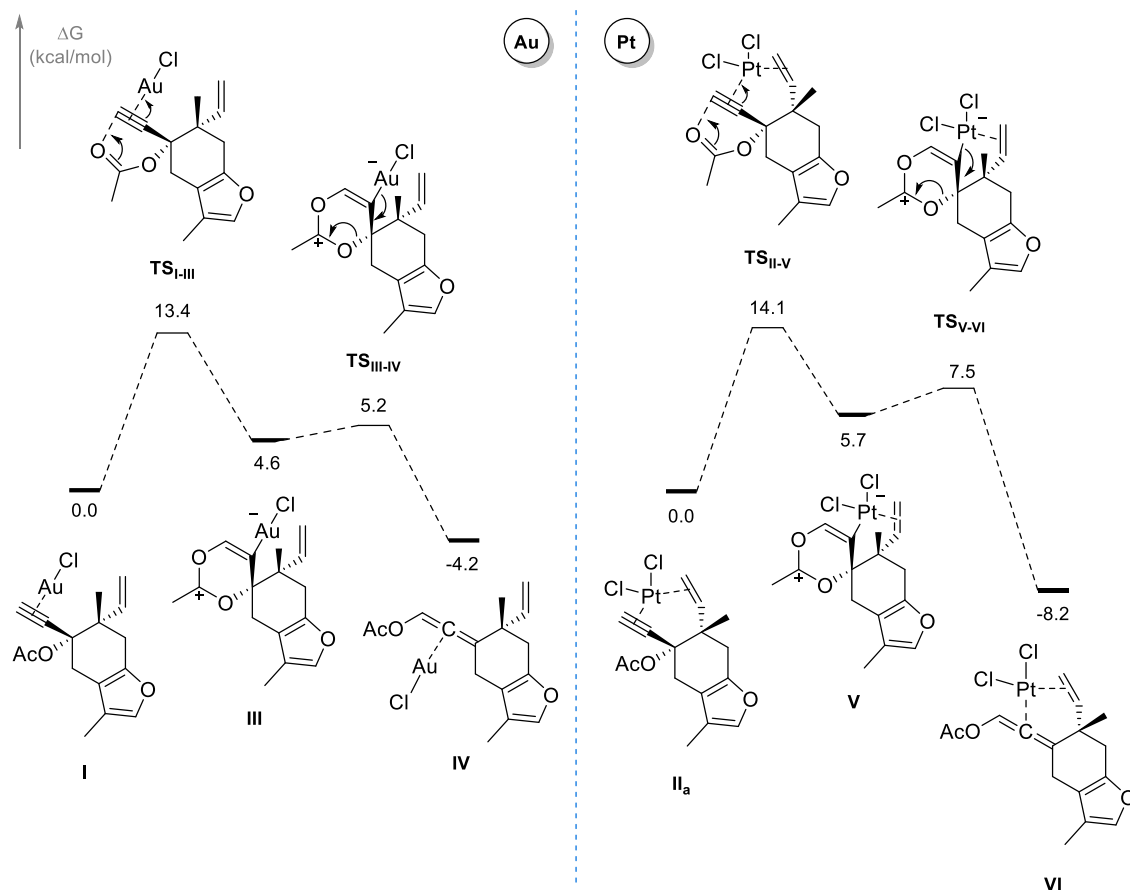
					
Conf.	II _a	II _b	II _c	II _d	II _e
ΔG	0.0	9.0	26.7	27.6	24.0

Among the computed structures where the platinum has its four coordination sites occupied (II_a, II_b and II_c), conformation II_a is clearly the most favorable; it is 9.0 kcal/mol lower in energy than II_b, and 26.7 kcal lower than II_c. Actually, the agostic interaction observed in II_c barely stabilizes the complex, as the conformation without the agostic interaction (II_d) is only 0.9 kcal/mol higher in energy. The *trans* disposition of the chlorine atoms in II_e seems slightly more stable, but it is still far from the most stable complex, II_a.

The first transition state should consist on the 1,2- and 1,3-migration of the acetate, which will eventually lead to the lindenane-type core structure and the myliol-type core structure, respectively. Both paths were studied for gold and platinum catalysis.

5.3.1.3 1,3-migration

Except for the charge of the metal, the 1,3-migration of the acetate group occurs as illustrated in the mechanism proposal. The reaction starts with the nucleophilic attack of the oxygen to the terminal carbon of the alkyne to form a zwitterionic intermediate, III. Later, intermediate III is cleaved to form an allene, which remains coordinated to the metal. The resulting energy diagrams for the computed transition states and intermediates are displayed in Scheme 5.12.



Scheme 5.12. Computed mechanism for the AuCl (left) and PtCl₂ (right) catalyzed 1,3-migration of the acetate. Free Gibbs energies in kcal/mol. Theory level: M06/6-311G(d,p)/SDD(IEFPCM,toluene)//B3LYP/6-31G(d,p)/LANL2DZ.

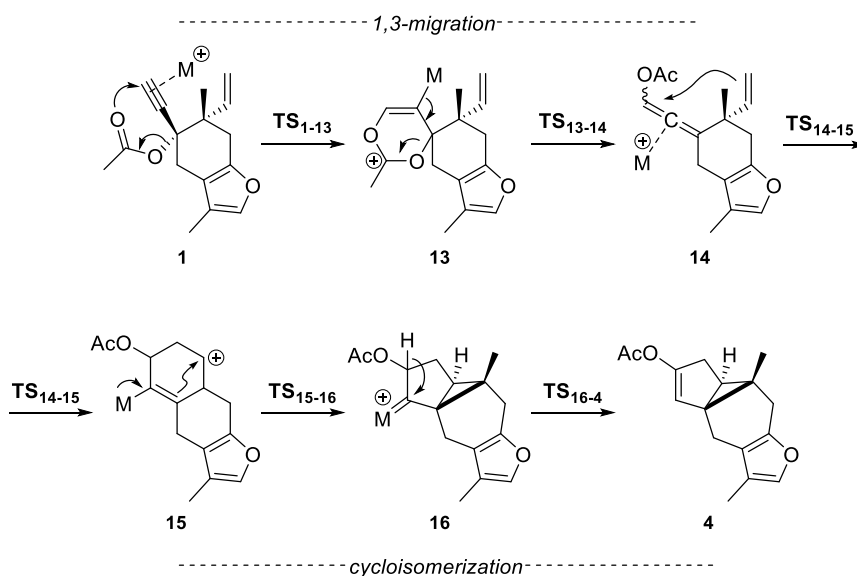
The attack of the oxygen to the gold-alkyne complex (Scheme 5.12, left) has an activation barrier of 13.4 kcal/mol and the formed zwitterionic intermediate **III** is slightly higher in energy than the starting complex **I**, by 4.6 kcal/mol. Intermediate **III** is unstable, high in energy due to the separation of the charges. Finally, complex **IV** is formed through a transition state of extremely low activation barrier (**TS_{III-IV}**, $\Delta G^\ddagger = 0.6$ kcal), which upon release of the metal would generate the experimentally observed allene **2**.

In the case of the platinum(II) chloride path, different possible conformations of the platinum complexes were computed for each transition state and intermediate (as for the starting complex **II**). Unsurprisingly, the energies were always considerably lower when the double coordination with the alkene occurred. Thus, all structures computed hereafter contained this double interaction, whenever possible.

The general profile of the platinum-catalyzed 1,3-migration seems very similar to the gold-catalyzed one. After a low barrier of 14.1 kcal/mol, the zwitterionic unstable intermediate **V** is formed. The next barrier (**TS_{II-V}**) is not as low as in the case of the gold-catalyzed reaction, but is still very low, of just 1.8 kcal/mol. This way, intermediate **VI** is generated, 8.2 kcal/mol lower in energy than the initial complex.

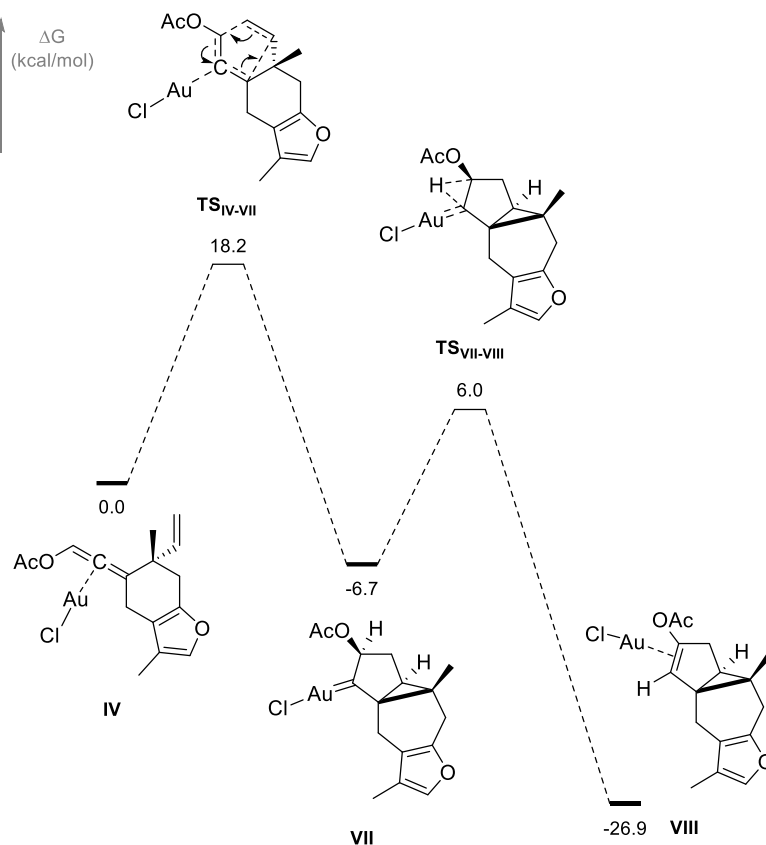
5.3.1.4 Myliol cycloisomerization

After the 1,3-migration, the cycloisomerization leading to the myliol core structure should occur. The proposed mechanism (Scheme 5.13) consisted on the attack of allene **14** by the terminal alkene, assembling a six membered ring (**15**). Then, a carbene should be formed as the final cyclization takes place, constructing the myliol core structure, **16**. Finally, the 1,2-shift of a hydrogen and release of the catalyst would provide product **4**.



Scheme 5.13. Proposed mechanism for the 1,3-pathway.

The computed mechanism differs quite a bit from the proposal. Even though the transition state **TS**₁₄₋₁₅ was found (gold, **TS**_{IV-VII}, Scheme 5.14 and platinum, **TS**_{VI-IX}, Scheme 5.15), intermediate **15** could never be isolated, as its optimization always resulted in the spontaneous cyclization and formation of **16**. IRC calculations were performed on transition states **TS**_{IV-VII} and **TS**_{VI-IX}, and although the last point of the IRC leading to product formation looked like the proposed intermediate **15**, the latter optimization of the geometry ended up providing intermediate **16** (**VII** in Scheme 5.14 and **IX** in Scheme 5.15). This suggests that the second transition state of the cycloisomerization has an extremely low activation barrier. For this very same reason, the transition state could never be located.

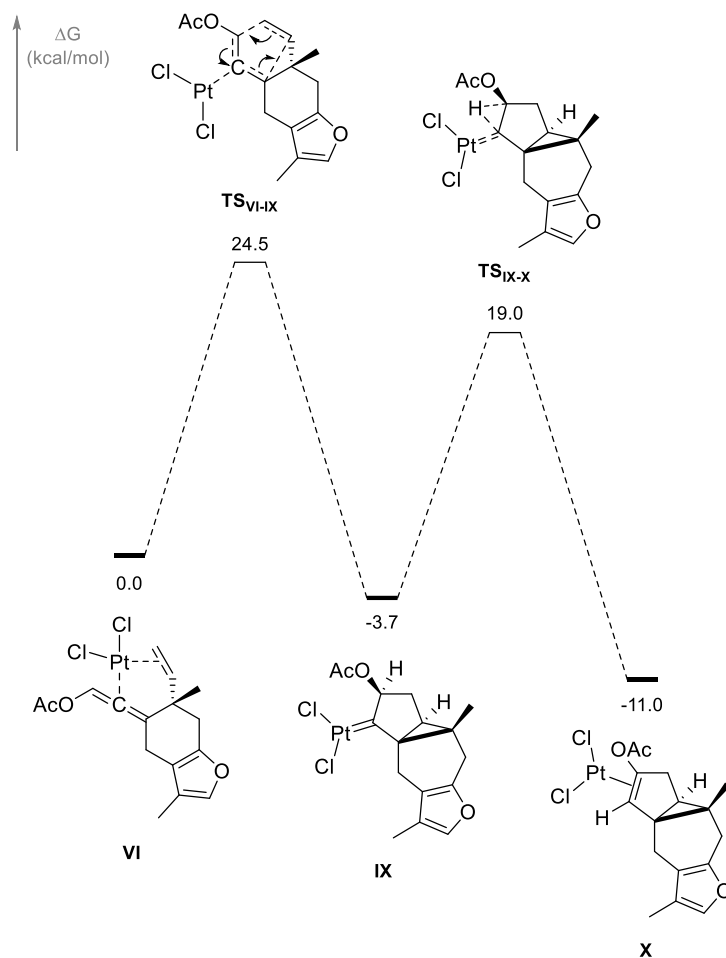


Scheme 5.14. Computed mechanism for the gold-catalyzed cycloisomerization of **IV**. Theory level: M06/6-311G(d,p)/SDD(IEFFPCM,toluene).*

The activation barriers of the cycloisomerization and the hydrogen shift are both low in energy, especially the second one, ($\Delta G^\ddagger = 12.7$ kcal/mol). The reaction is highly exergonic.

An alternative path to that displayed in Scheme 5.14 was computed. Although the absolute *R* or *S* configuration of the carbon bearing the acetate group is irrelevant for the outcome of the reaction, diastereomeric transition states and intermediates are generated during the process. Therefore, both pathways were calculated to see if there were any significant discrepancies. Energies barely changed from one path to another, with the difference never being greater than 2.0 kcal/mol. The path shown in Scheme 5.14 corresponds to the lowest energy one.

* Please note that the theoretical level of the calculations was modified during the study. This was due to a problem in the convergence of one of the transition states of the alternative mechanism regarding the formation of the lindenane-type structures. Later on, an energy diagram will be displayed with the full mechanism and all energy values computed using the same theory level.

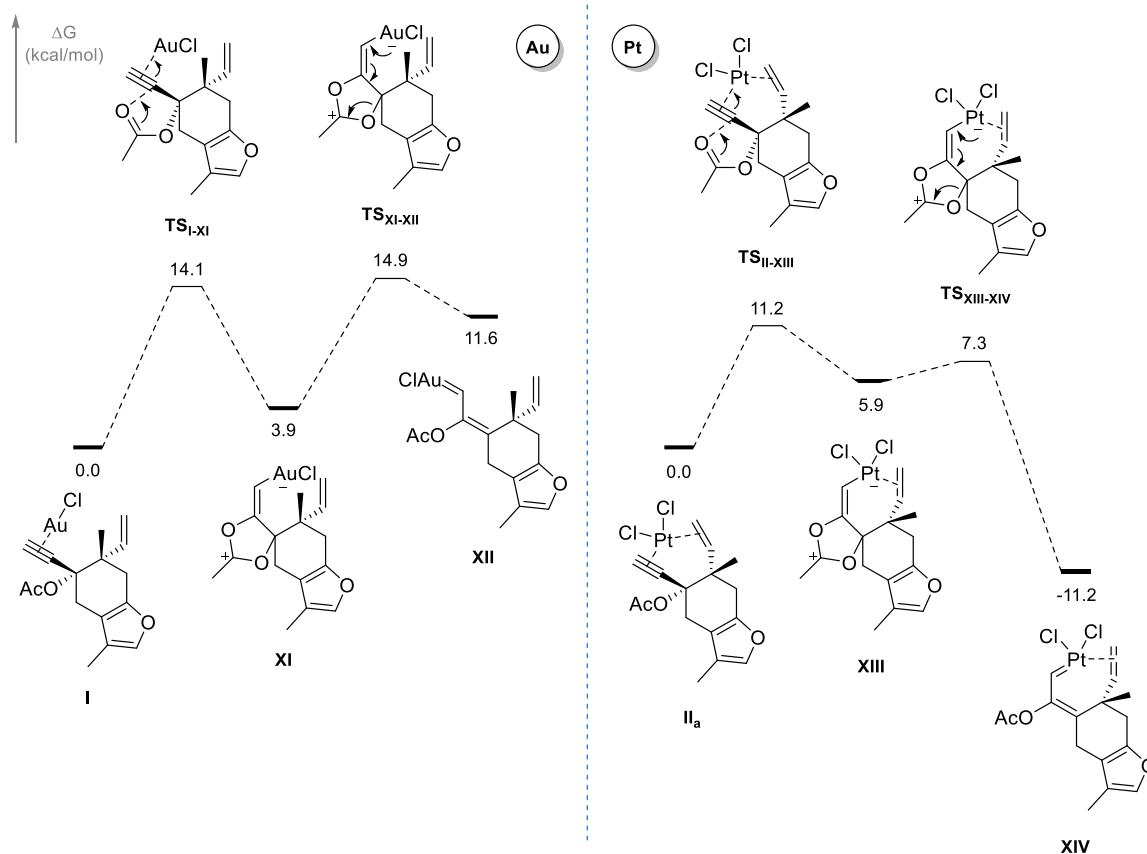


Scheme 5.15. Computed mechanism for the platinum-catalyzed cycloisomerization of **VI**. Theory level: M06/6-311G(d,p)/SDD(IEFPCM, toluene).

The mechanism of the platinum-catalyzed reaction is identical to the gold-catalyzed one, with some variations in the energies. The first transition state, **TS_{VI-IX}**, is higher in energy with the platinum catalyst (24.5 kcal/mol vs 18.2 kcal/mol with gold), probably due to the loss of the double coordination between the platinum and the alkyne and alkyne moieties. Carbene **IX** is generated and, after a 1,2-hydrogen shift with an activation barrier of 22.7 kcal/mol, the final complex **X** is formed. The reaction with platinum is less exergonic.

5.3.1.5 1,2-migration

As early proposed, the 1,2-acetate migration takes place in two steps; first, the carbonylic oxygen of the acetate attacks the alkyne, generating a zwitterionic cyclic intermediate. Then, a metal carbene is formed as the cycle is opened and the acetate migrates to its final position. The energy diagram of the reaction with each metal is shown in Scheme 5.16.



Scheme 5.16. Computed mechanism for the AuCl (left) and PtCl₂ (right) catalyzed 1,2-migration of the acetate. Theory level: M06/6-311G(d,p)/SDD(IEFPCM, toluene).

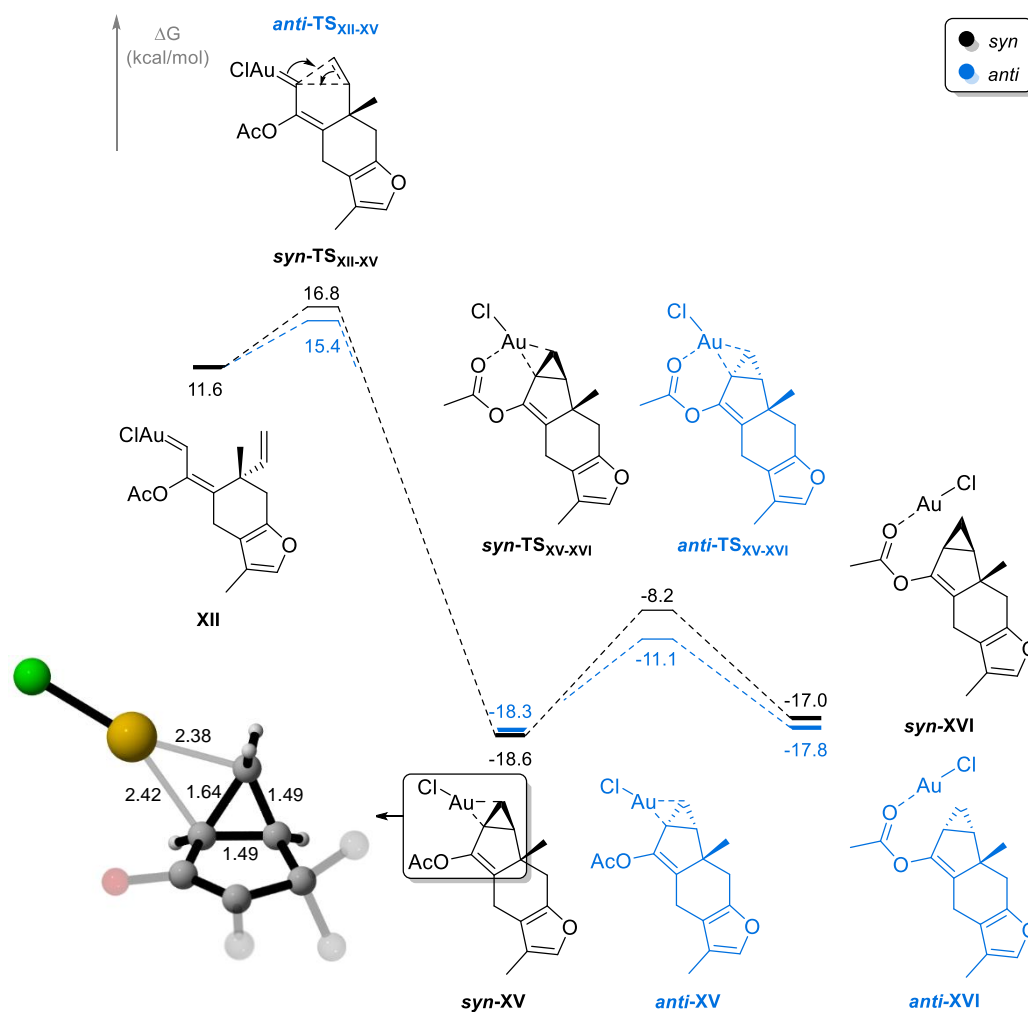
The mechanism was computed similarly for both metals, maintaining the tetracoordination with platinum and dicoordination with gold. After the first transition state, almost 3 kcal/mol lower with platinum (14.1 kcal/mol **TS_{I-XI}** vs 11.2 kcal/mol **TS_{II-XIII}**), a zwitterionic intermediate is formed. The next energy barrier is extremely low in the case of the platinum (only 1.4 kcal/mol), as happened during the 1,3-migration. Contrastively, the barrier with the gold catalyst is rather high (11.0 kcal/mol). Gold carbenes are usually found to be more unstable compared to platinum carbenes,^{22c} hence the larger activation barrier of **TS_{XI-XII}** and higher energy of intermediate **XII**.

The implications of this energy differences may be key to understand the distinct behavior of platinum and gold, and will be discussed in the next section. Now, the second part of the mechanism will be described, consisting in the cycloisomerization process to yield the desired lindenane core structure.

5.3.1.6 Lindenane cycloisomerization

We started searching for the cycloisomerization transition states using gold(I) chloride, following the proposed mechanism involving the formation of a six membered ring and the posterior annulation to form the [3.1.0] bicycle. However, the formation of the

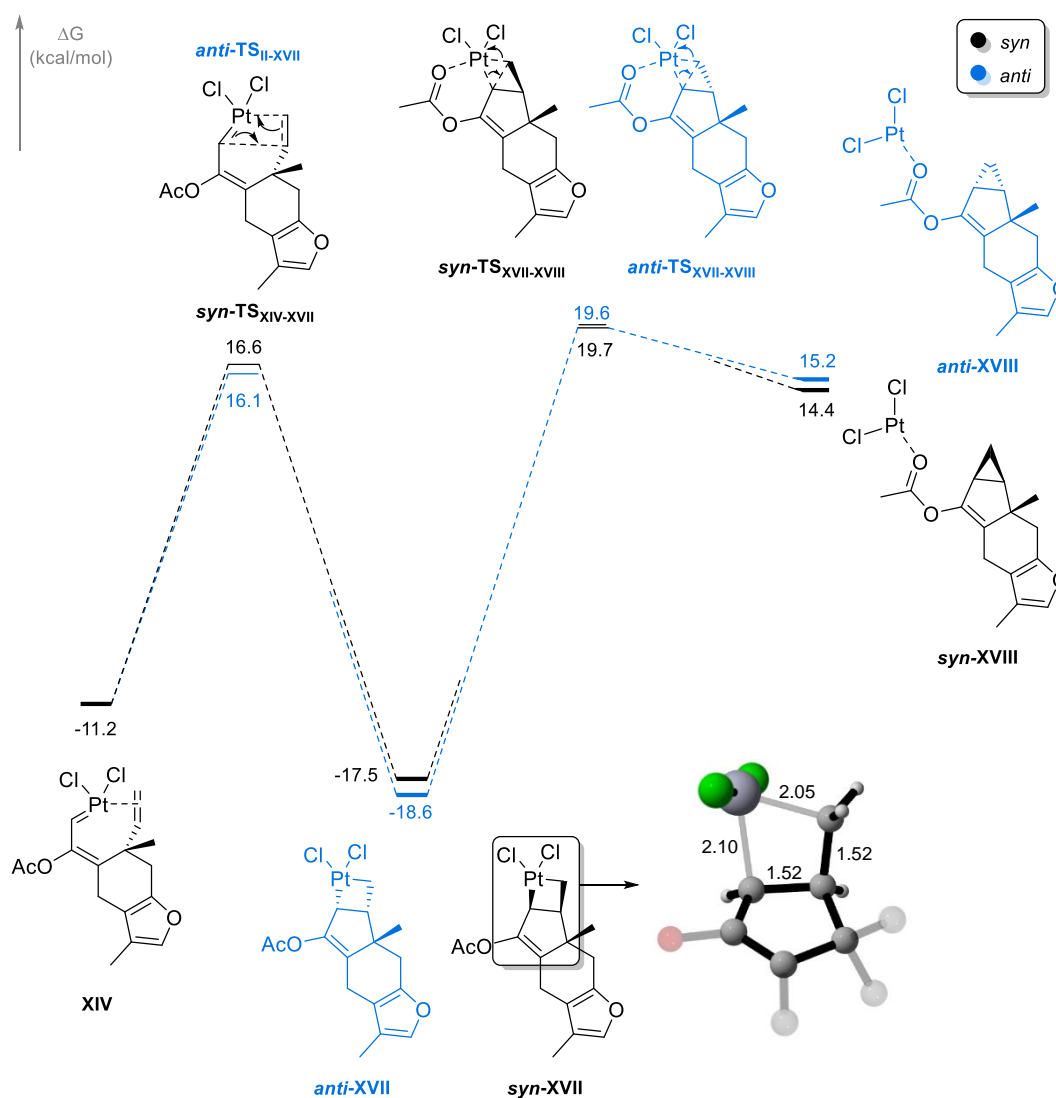
six membered ring was never observed. With the gold catalyst, the [3.1.0] system was generated with one transition state, **TS_{XII-XV}** (Scheme 5.17). Intermediates **XV** are very stable, making this step highly irreversible. In the 3D drawing displayed on the left, the interatomic distances (in Å) have been indicated. Looking at the distances we can infer that the three membered cycle is not completely formed, as one of the distances (1.64 Å) is elongated. After a final transition state of low energy barrier (**TS_{XV-XVI}**), the final product is formed, where the distances between the three carbons of the cyclopropane ring are almost identical (1.49, 1.50 and 1.51 Å).



Scheme 5.17. Formation of the lindenane core structure using gold(I) chloride. Theory level: M06/6-311G(d,p)/SDD(IEFPCM,toluene).

Since this mechanism seemed feasible, being both activation barriers low, we followed the same scheme with the platinum-catalyzed reaction. Interestingly, we found a very different profile (Scheme 5.18). The first activation barrier is very high in energy and, this time, the formed intermediates **XVII** are clearly four membered platina-cycles (Scheme 5.18, distances in Å). During the second transition state (**TS_{XVII-XVIII}**), the platina-cycle is broken to free the metal and form the final [3.1.0] bicycle. Nevertheless, the activation barrier of this step is exceedingly high, of *ca.* 37 kcal/mol. Following Eyring's

transition state theory expression, with the current heating (110 °C), the reaction would need years to overcome such a large activation barrier.

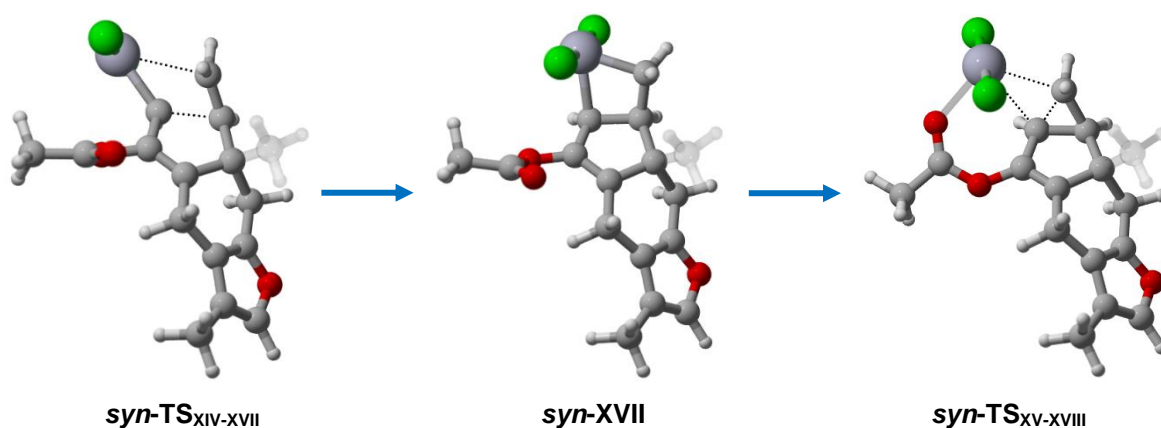


Scheme 5.18. Formation of the lindenane core structure using platinum. Theory level: M06/6-311G(d,p)/SDD(IEFPCM,toluene).

We computed the energies using a basis set that takes diffusion into account, Def2TZVPP, in order to check whether a poor description of the orbitals could be the cause for this huge barrier. The energies were almost identical, but this method was used for most upcoming calculations.

The unfeasibility of the second transition state of the cycloisomerization suggested the existence of an alternative mechanism. While the previous mechanism was a 5-*exo* cyclization, the new mechanism consists on a 6-*endo* cyclization (Scheme 5.19).

Previous 5-*exo* mechanism



New 6-*endo* mechanism

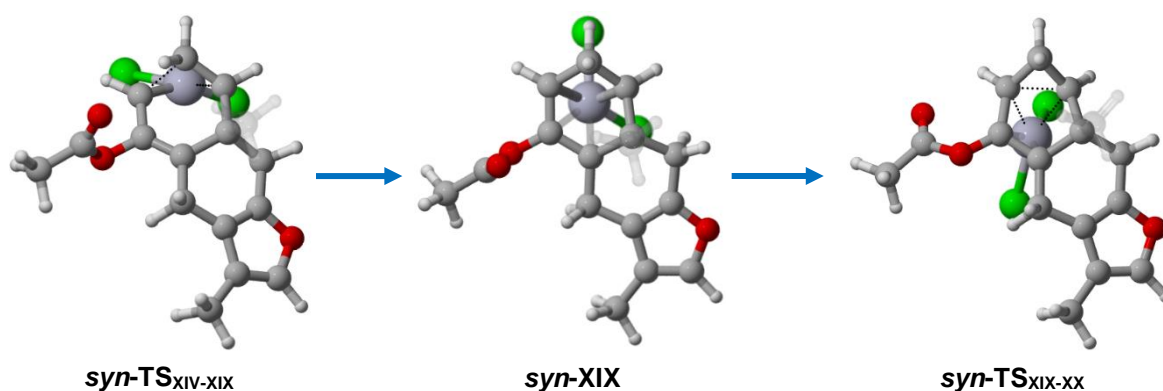
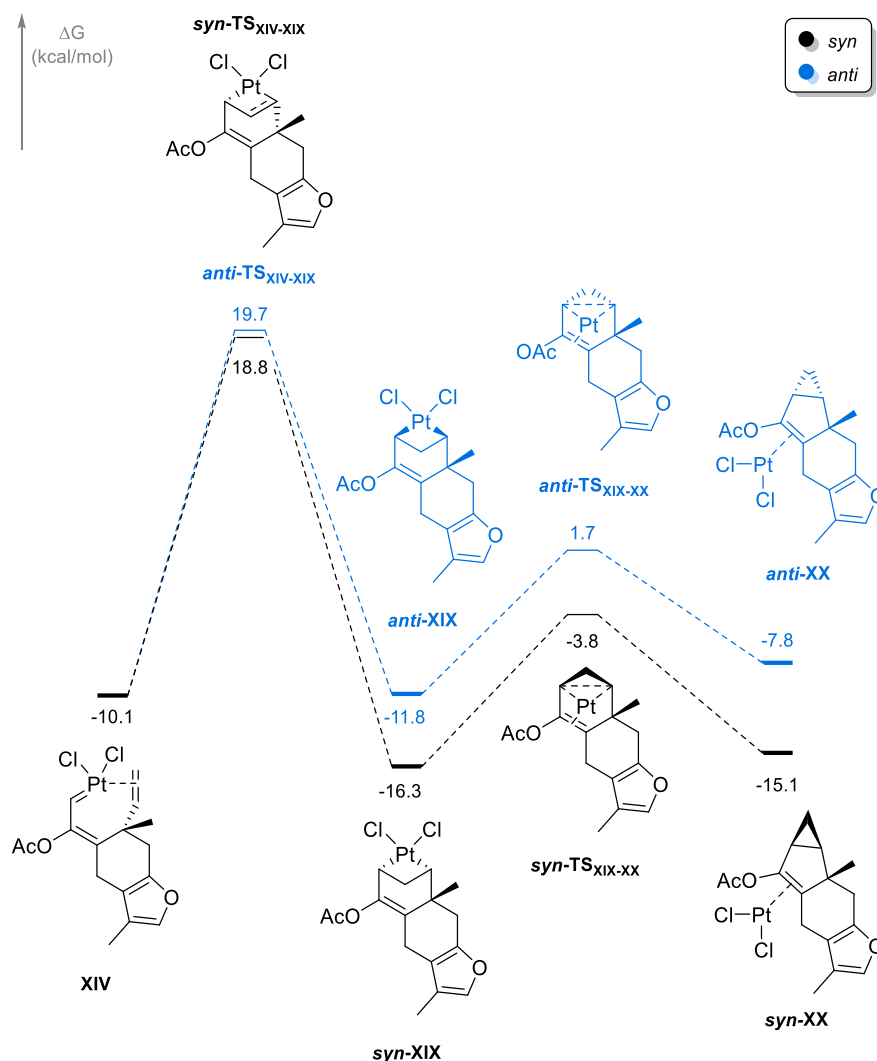


Figure 5.5. 3D structures of the cyclization transition states, intermediates and elimination transition states of the 5-*exo* mechanism (up) and 6-*endo* mechanism (down) of the platinum-catalyzed cycloisomerization. Theory level: M06/6-311G(d,p)/SDD(IEFPCM,toluene).

The results in the energy profile were very satisfactory (Scheme 5.19). While the first activation barrier is very similar to the previous mechanism (**TS_{XIV-XVII}**, $\Delta G^\ddagger = 29.4$ kcal/mol vs **TS_{XIV-XIX}**, $\Delta G^\ddagger = 28.9$ kcal/mol), the second transition state, **TS_{XIX-XX}**, has now a low activation barrier and is therefore completely reasonable.

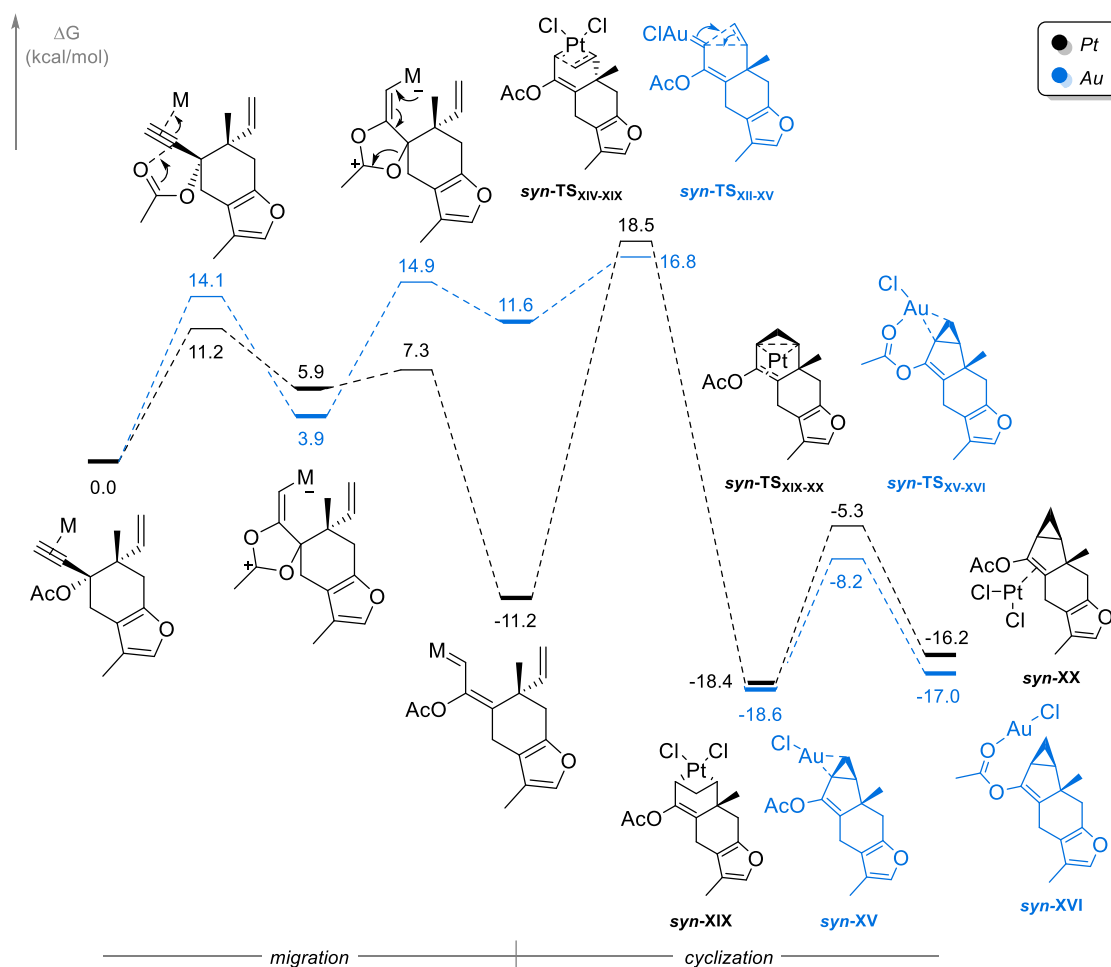


Scheme 5.19. 6-*Endo* mechanism for the cycloisomerization using platinum(II) chloride. The chlorine atoms of **TS_{XIX-XX}** were omitted for the sake of clarity. Please note that the theory level has changed from previous schemes. Theory level: M06/Def2TZVPP(IEFPCM,toluene)//M06/6-311G(d,p)/SDD(IEFPCM,toluene).

In the view of these results, we selected the 6-*endo* cyclization to be the right mechanism for the reaction with platinum, while the gold-catalyzed reaction can only proceed through the 5-*exo* mechanism.

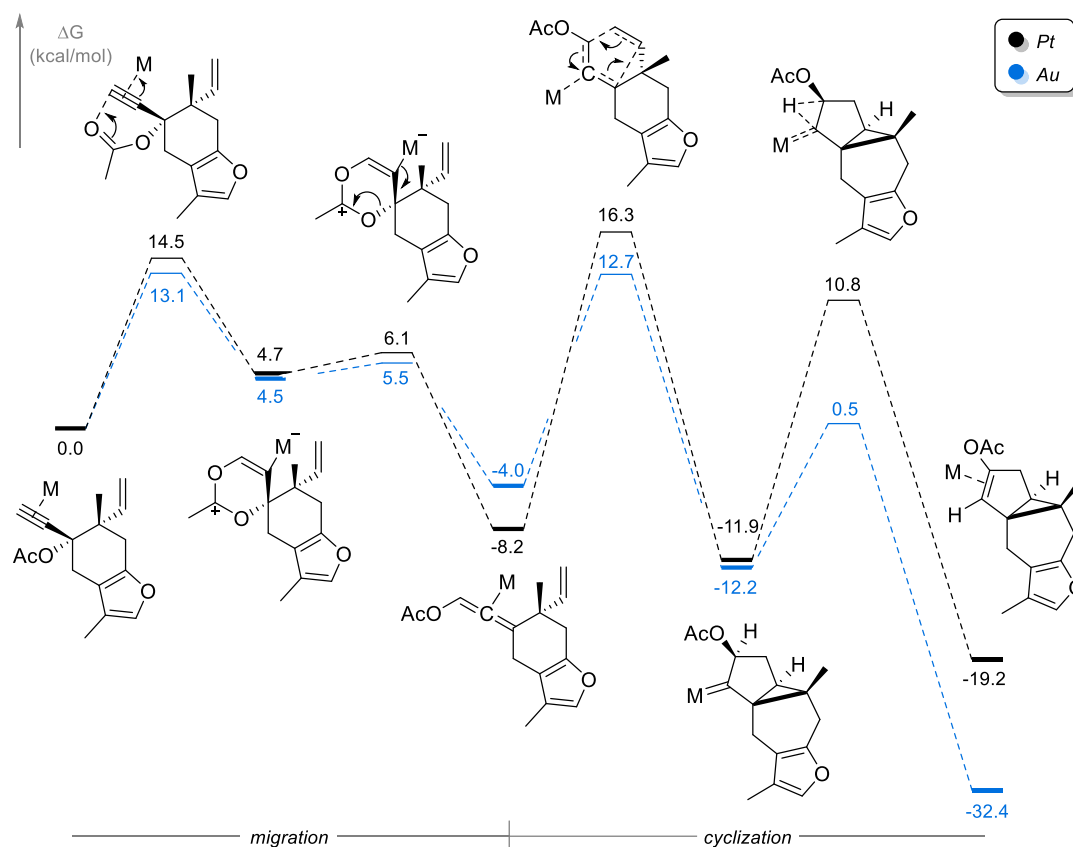
5.3.2 Difference between gold and platinum catalysis

During the experimental work of our colleagues, different reactivity was observed between gold and platinum catalysis. On the one hand, the reaction with gold provided no product or intermediate of the 1,3-migration pathway. On the other hand, only the formation of allene **2** was observed, meaning that the cycloisomerization step never occurred. In fact, when the reaction with gold was heated, only decomposition was detected. By comparing the energy profiles of the reactions with both catalysts, we hope to provide a reason for this divergent reactivity.



Scheme 5.20. Energy diagram of the 1,2-pathway of the platinum (black) and gold (blue) catalyzed synthesis of **3**. Theory level: M06/6-311G(d,p)/SDD(IEFPCM,toluene).

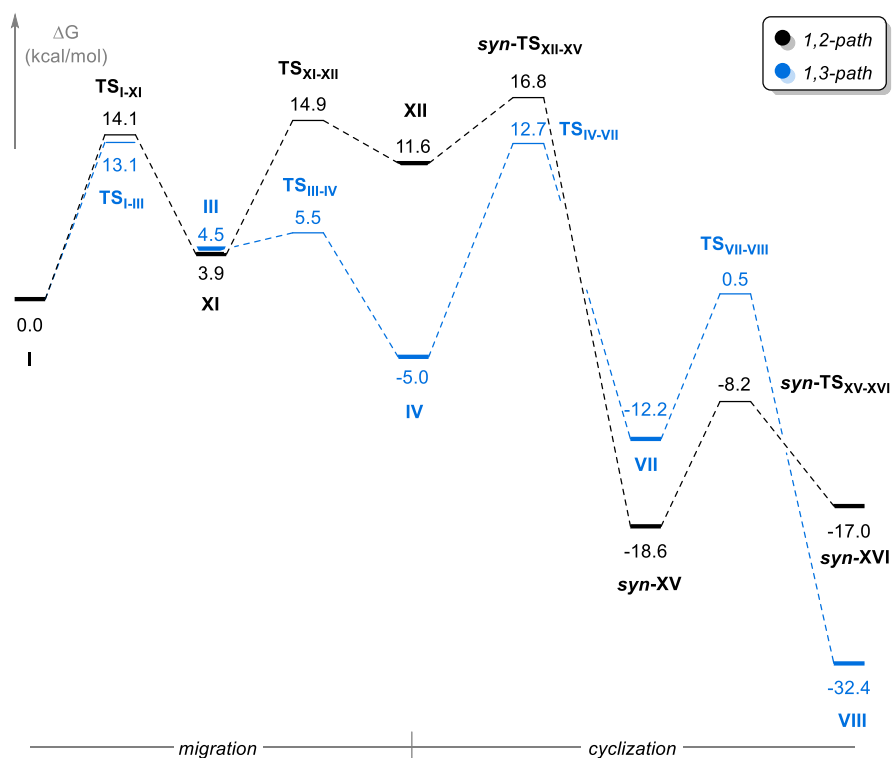
We can see a significant difference between both catalysts in the 1,2-migration reaction (Scheme 5.20). In the case of gold, the first transition state is slightly higher in energy than its platinum counterpart. Furthermore, the gold carbene and the transition state leading to it are considerably higher in energy. Although the mechanism of the cycloisomerization steps is different for each metal, the energy diagram shows two very similar profiles.



Scheme 5.21. Energy diagram of the 1,3-pathway of the platinum (black) and gold (blue) catalyzed synthesis of **4**. Theory level: M06/6-311G(d,p)/SDD(IEFPCM,toluene).

Regarding the 1,3-pathway, there are no remarkable differences among catalysts (Scheme 5.21). In fact, the path with gold is somewhat lower in energy during the whole mechanism, especially in the cyclization steps.

To fully understand the reactivity of the gold-catalyzed reaction, the comparison between both paths catalyzed by gold is shown in Scheme 5.22. The selectivity of the platinum-catalyzed reaction will be analyzed later, on its corresponding chapter.



Scheme 5.22. Energy diagram of the gold-catalyzed cycloisomerization reactions of **1**. Theory level: M06/6-311G(d,p)/SDD(IEFPCM, toluene).

The most remarkable difference between pathways is the much higher stability of the 1,3-path intermediate **IV**. Since in both pathways the migration step is reversible while the cyclization is not, we can apply the Curtin-Hammett principle (see chapter 1) and compare the energies of the two highest transition states of each pathway. These would be **TS**_{I-III} in the 1,3-route ($\Delta G = 13.1$ kcal/mol) and **TS**_{XII-XV} in the 1,2-route ($\Delta G = 16.8$ kcal/mol), meaning that $\Delta\Delta G = 3.7$ kcal/mol, favoring the 1,3-pathway. This energy difference suffices to justify the lack of intermediates and products originated from the 1,2-pathway.

The explanation to why the reaction catalyzed with gold stops at the allene is not trivial. When looking at the 1,3-pathway for both metals, we found a similar profile, with slightly lower energy barriers for gold.

We tried to look for a different coordination in **IV** that was lower in energy and could perhaps trap the gold chloride and prevent the reaction from proceeding. Nine different structures were computed, from which only the coordination to the terminal alkene moiety resulted in a lower energy intermediate (1.8 kcal/mol lower than **IV**).

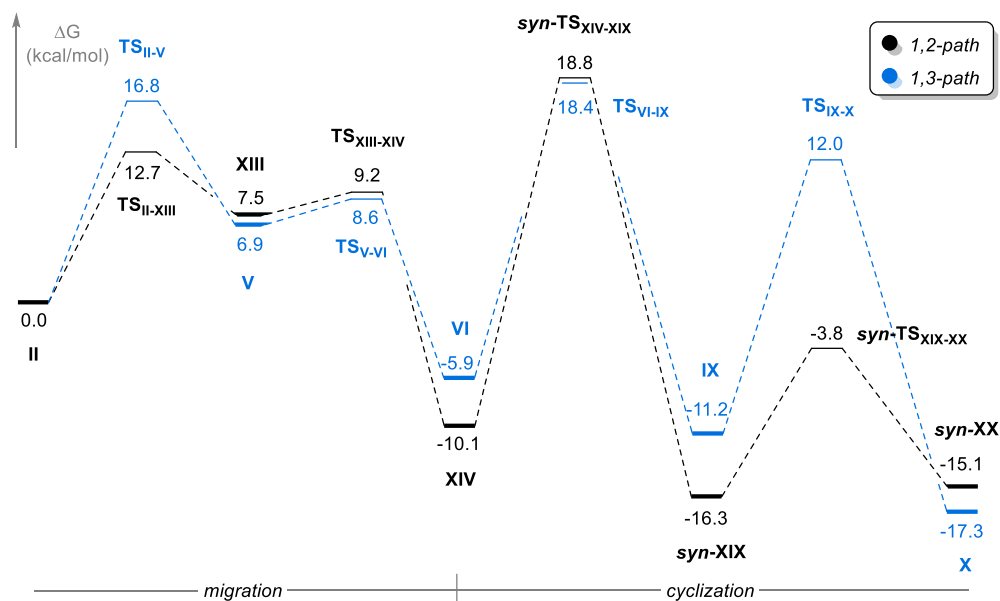
Although this could be one of the factors for the termination of the reaction, it does not suffice to completely discard the gold-catalyzed reaction. The reaction may have succeeded under different experimental conditions, but since the experiments carried out with gold were scarce, we decided not to focus excessively on the gold catalysis. Some possible side reactions were tested, aiming to explain the decomposition observed

whilst heating, but none of them succeeded. Thus, we decided to focus on the reactivity and selectivity of the platinum-catalyzed cycloisomerizations.

5.3.3 Path selectivity with platinum

As introduced in the experimental section, our colleagues observed a preference over the 1,2-migration path, with isomer ratios ranging from 65:35 to 85:15, depending on the conditions. It is important to remark that this selectivity, although crucial in an experimental context, cannot be unequivocally determined by means of DFT calculations. These two ratios would correspond to a theoretical energy difference of only 0.4 to 0.9 kcal/mol, and given the current level of accuracy of DFT calculations, such small differences can be considered negligible. Nonetheless, we tried our best to computationally simulate the experimentally observed selectivities.

We began comparing the energy profiles of both routes using the same theory level (Scheme 5.23).



Scheme 5.23. Energy profile for the 1,2 (black) and 1,3 (blue) pathways of the reaction with the platinum catalyst. Theory level: M06/Def2TZVPP(IEFPCM,toluene)//M06/6-311G(d,p)/SDD(IEFPCM,toluene).

As the migration is reversible, we can apply the Curtin-Hammett principle and consider that the isomer ratio of this reaction will depend on the relative energy between the two highest transition states ($\Delta\Delta G = \text{TS}_{\text{XIV-XIX}} - \text{TS}_{\text{VI-IX}} = 0.4$ kcal/mol). In that case, the predicted isomeric ratio of **3:4** would be approximately 35:65, in favor of the minor experimentally observed isomer.

We decided to use the software COPASI to better understand how the reaction proceeds. We calculated the constant rates according to Eyring's equation using the Gibbs

free energies obtained in the M06/Def2TZVPP(IEFPCM,toluene)//M06/6-311G(d,p)/SDD(IEFPCM,toluene) theory level. The simulation was carried out in two different ways: considering all the intermediates and transition states and neglecting the second (**TS_{XIII-XIV}** and **TS_{XV-XVI}**) and fourth (**syn-**TS_{XIX-XX}**** and **TS_{IX-X}**) transition states. Seeing that the outcome did not differ, all the following simulations were carried out omitting those transition states.

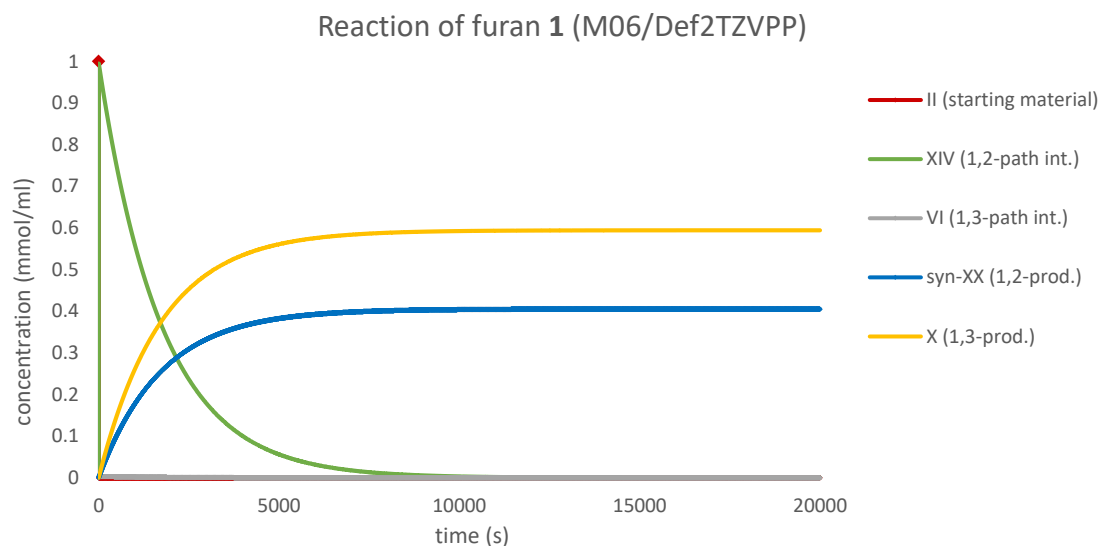


Figure 5.6. Graph based on the results provided by the COPASI simulation. Reaction of the furan substrate **1**. Theory level: M06/Def2TZVPP(IEFPCM,toluene)//M06/6-311G(d,p)/SDD(IEFPCM,toluene).

As shown in Figure 5.6, the formation of the 1,2-intermediate (**XIV**, green) occurs immediately, overlapping the curve of the starting material (**II**, a red diamond marks time = 0 s). In spite of this and due to the reversibility of this first step, the mayor product is the 1,3-migration and later cycloisomerization product (**X**, yellow), with a lower cyclization barrier.

The final **3:4** ratio is 40:60, which is in disagreement with the experimental results and highlights the difficulties of refining the energies to tenths of kcal/mol, as needed in this case. In order to properly explain the experimental selectivity, further calculations were performed. These will be discussed later, after studying the lactone containing substrate.

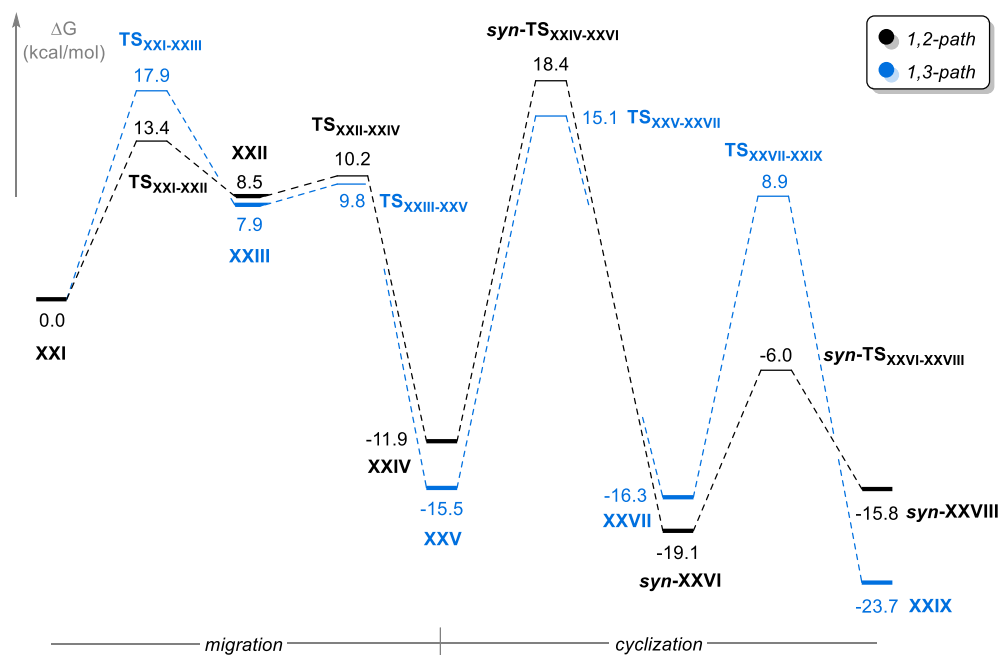
5.3.4 Difference between furan and lactone

During their experimental work, our colleagues observed a couple of differences between the reactivity of the substrate containing a furan ring, **1**, and the substrate containing a lactone moiety, **5**. The most significant is the absence of the myliol-type product in the case of the lactone. Although they obtained several byproducts, all were

derived from the 1,2-migration of the acetate, meaning that the 1,3-migration never occurs in the case of lactone **5**.

As starting point, we computed the lactone analogues of the intermediates and transition states we previously studied. This would allow us to compare their energy profiles and detect the differences that demonstrate the aforementioned divergent reactivity.

The obtained Gibbs free energy profile is presented in Scheme 5.24. Since no significant structural differences were found, only the references of each structure are displayed.



Scheme 5.24. Both pathways for the reaction of lactone **5** with the platinum catalyst. Theory level: M06/Def2TZVPP(IEFPCM, toluene)//M06/6-311G(d,p)/SDD(IEFPCM, toluene).

The resulting profile is similar to that of the furan analogue. Even so, there is a remarkable difference in the energy of the cycloisomerization transition state (TS_{XXIV-XXVI}, black and TS_{XXV-XXVII}, blue). Now, the energy of the 1,3-cyclization transition state is 3.3 kcal/mol lower in energy than the 1,2-cyclization transition state. Actually, in the case of the lactone, the highest energy transition state of the 1,3-path is not the cyclization ($\Delta G = 15.1$ kcal/mol), but the initial migration of the acetate (TS_{XXI-XXIII}, $\Delta G = 17.9$ kcal/mol). According to this, since the selectivity is determined by the relative energy between the highest energy transition state of each path, the 1,3-pathway would now be favored by 0.5 kcal/mol (TS_{XXIV-XXVI} - TS_{XXI-XXIII}). This result would contradict the experimental results, where only products derived from the 1,2-pathway were observed.

So as to predict the final ratios, we performed again a COPASI simulation to better understand the selectivity of the reaction (Figure 5.7), just as we did in the case of the furan.

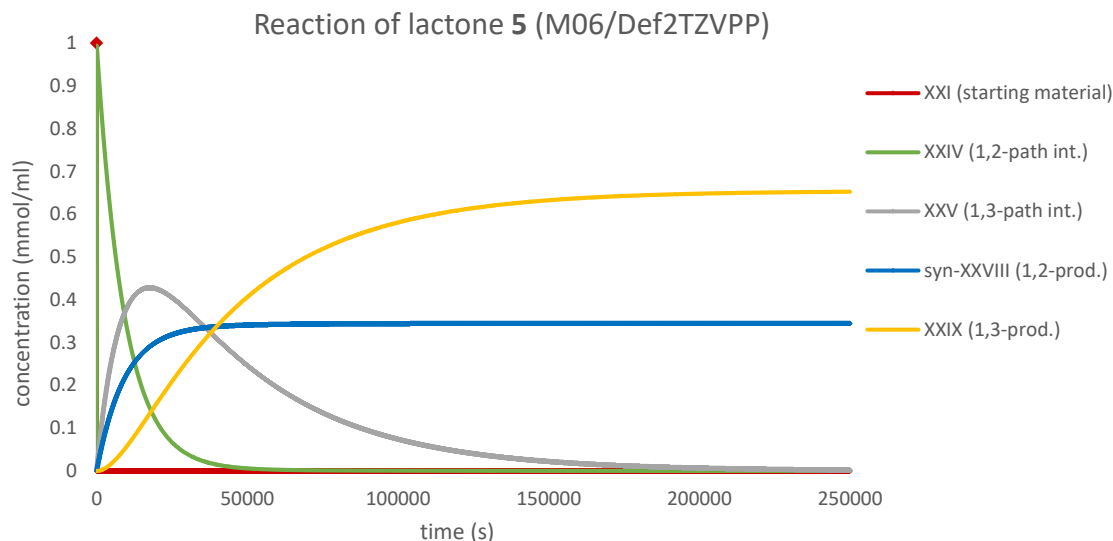
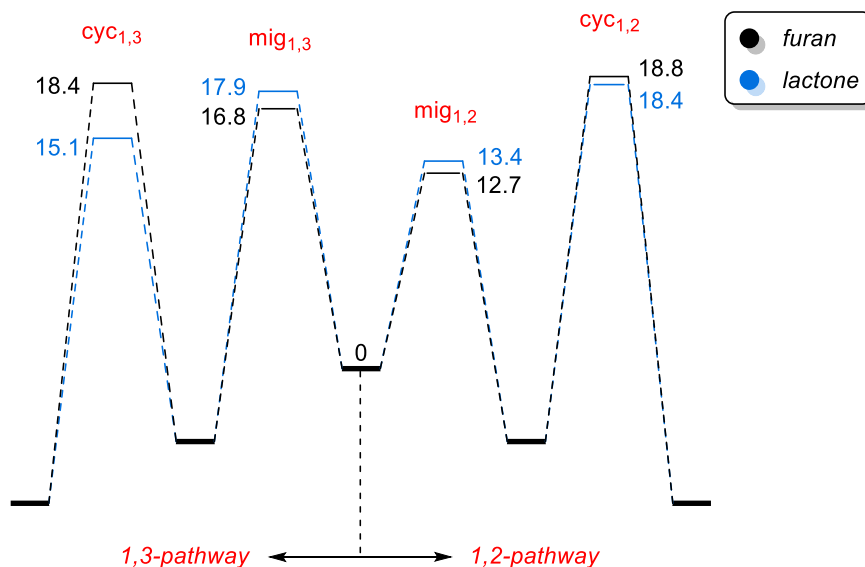


Figure 5.7. Graph based on the results provided by the COPASI simulation. Reaction of the furan lactone **5**. Theory level: M06/Def2TZVPP(IEFPCM,toluene)//M06/6-311G(d,p)/SDD(IEFPCM,toluene).

As happened with the furan, on early stages of the reaction, the intermediate of the 1,2-pathway (**XXIV**, green) accumulates due to the lower migration barrier. Shortly thereafter, this intermediate disappears to give place to the product of that path (**syn-XXVIII**, blue). At the same time, the formation of the 1,3-intermediate (**XXV**, grey) can be detected, meaning that the reaction is reversible, just as the furan reaction was. The reason why we observe the accumulation of this intermediate is that the barrier of the cyclization is quite large ($\Delta G^\ddagger = 30.6$ kcal/mol). Nevertheless, this barrier is ultimately overcome to provide the 1,3-product (**XXIX**, yellow). As we feared, the final **3:4** ratio is of 35:65, instead of the experimentally observed total selectivity towards the 1,2-path.

In the next figure, a simplified scheme of reactivity of the furan and lactone substrates has been illustrated. Only the key migration and cyclization transition state of each pathway have been represented.



Scheme 5.25. Simplified scheme of key transition states of the reaction of furan **1** and lactone **5**. Theory level: M06/Def2TZVPP(IEFPCM,toluene)//M06/6-311G(d,p)/SDD(IEFPCM,toluene).

Looking at Scheme 5.25, we see that the 1,2-pathway (right) is almost identical for both substrates, whereas the 1,3-pathway (left) has a noticeable difference. This difference is, as we saw earlier, the lower energy of the cyclization in the case of the lactone (15.1 kcal/mol). Because of this, the selectivity of the lactone will not be determined by the 1,3-cyclization, but by the 1,3-migration (17.9 kcal/mol).

5.3.5 Path selectivity of **1** and **5**

The isomer ratio of the reaction depends on, as we explained earlier, the highest energy transition state for each pathway. This transition states (green circles in Figure 5.8) are very close in energy: 0.4 kcal/mol in the case of the furan, and 0.5 kcal/mol in the case of the lactone.

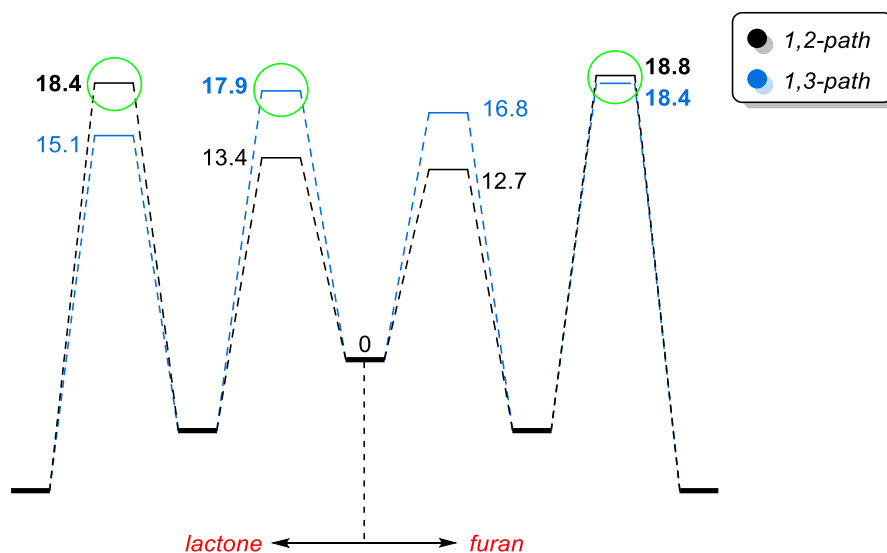


Figure 5.8. Simplified scheme of key transition states of the reaction of furan **1** and lactone **5**. Theory level: M06/Def2TZVPP(IEFPCM,toluene)//M06/6-311G(d,p)/SDD(IEFPCM,toluene).

During the publication of this work, we were suggested to run our calculations using alternative functionals and basis sets. Hopefully, this would help us find a theory level that would accurately reproduce the experimentally observed ratios.

The screening was carried out performing single point calculations of geometries computed in M06/6-311G(d,p)/SDD(IEFPCM,toluene). For this initial functional screening, only the two key transition states for each path were used. The employed functionals were B3LYP, B3PW91 (both with Grimme's 3D dispersion model), M11-L and ω B97X-D, all of them with the solvent method IEFPCM, solvent=toluene. These four functionals were combined with two different basis sets, the same as in the geometry optimizations (6-311G(d,p) for non-metals, SDD for platinum) and Def2TZVPP.

Table 5.4. Comparison between the different theory levels utilized for computing the energies of key transition states. All of them were computed using toluene as solvent. Shown values are Gibbs free energies (in kcal/mol) obtained by the addition of the potential energy obtained through single points calculations to the Gibbs free energy correction on M06/6-311G(d,p)/SDD. Green: desired result. Yellow: < 0.5 kcal/mol against desired result. Red > 0.5 kcal against desired result.

	Furan	Lactone
Theory level	cyc_{1,3} - cyc_{1,2}	cyc_{1,3} - mig_{1,2}
M06-2X/Def2TZVPP	0.4	0.5
B3LYP-D3/Def2TZVPP	5.6	1.7
B3LYP-D3/6-311G(d,p)/SDD	6.4	3.9
M11-L/Def2TZVPP	3.6	1.7
M11-L/6-311G(d,p)/SDD	4.7	2.3
ω B97X-D/Def2TZVPP	0.5	-0.2
ω B97X-D/6-311G(d,p)/SDD	2.0	2.2
B3PW91-D3/Def2TZVPP	-0.4	0.1
B3PW91-D3/6-311G(d,p)/SDD	0.7	2.5

The first column corresponds to the energy difference between the 1,2 and 1,3-cyclization transition states of the furan, while the second one corresponds to subtraction of the 1,2-migration transition state energy to the 1,3-cyclization transition state energy of the lactone. The very first row shows the numbers resulting from the theory level employed until now, while the rest of the rows correspond to the different theory levels tested.

In order to predict the right selectivity, the values would need to be closer and, ideally, of the opposite sign. Like so, the 1,2-pathways would be preferred, as found in the experimental studies. Regarding the furan, this was only the case of the B3PW91-D3/Def2TZVPP theory level. This theory level also provided a lower value for the lactone, but it was using the level ω B97X-D/Def2TZVPP when best results were obtained.

With the results of Table 5.4 in hand, we selected ω B97X-D/Def2TZVPP and B3PW91-D3/Def2TZVPP as the most suitable theory levels for our systems. The energy of starting materials, intermediates and products was also calculated in order to generate new COPASI simulations.

5.3.5.1 B3PW91-D3/Def2TZVPP

Since this theory level provided an inversion on the selectivity of the furan containing substrate, as illustrated in Table 5.4, a COPASI simulation was run to observe the course of the reaction.

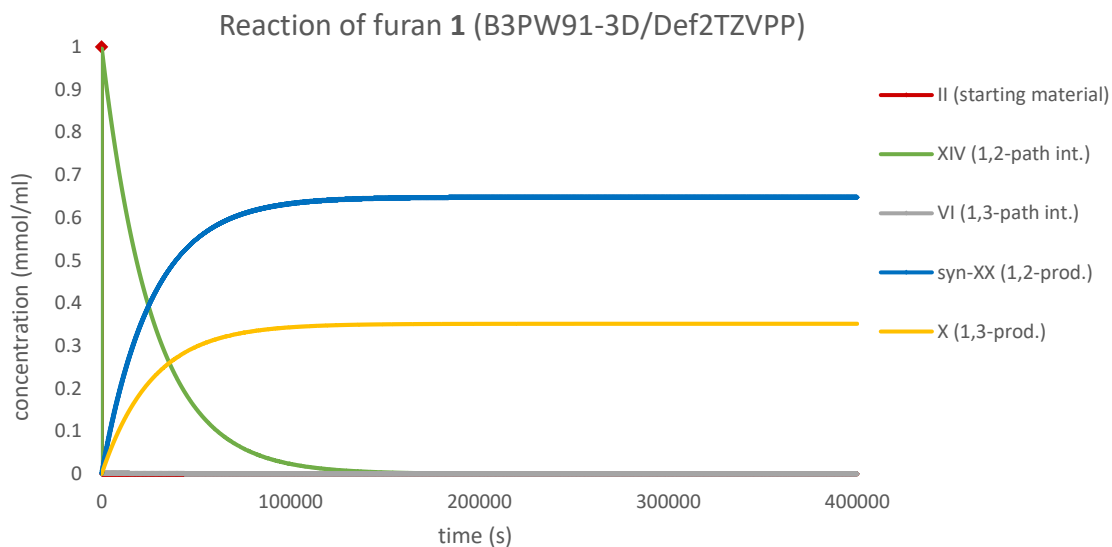


Figure 5.9. Graph based on the results provided by the simulation. Reaction of the furan substrate **1**, with single point calculations in B3PW91-3D/Def2TZVPP(IEFPCM,toluene).

The graph generated by COPASI provided excellent results. The shapes of the curves is similar to those obtained with the original theory level, but this time the selectivity is the desired one. The final **3:4** product ratio is 65:35, which is in perfect agreement with the experimental results.

5.3.5.2 ω B97X-D/Def2TZVPP

This theory level was the only one where an inversion of the selectivity of the lactone containing substrate could be observed, and therefore a COPASI simulation was carried out (Figure 5.10).

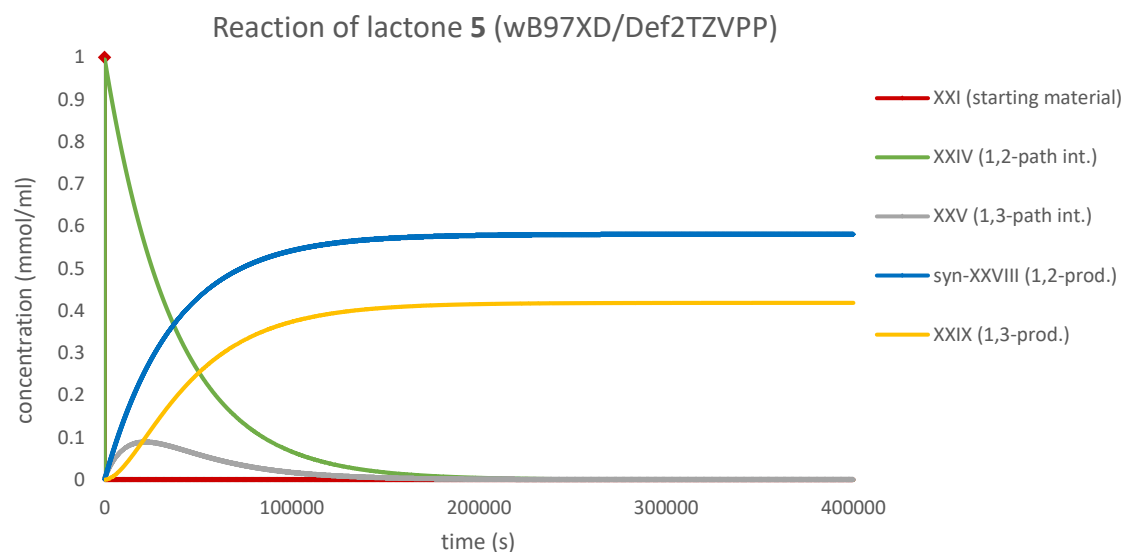


Figure 5.10. Graph based on the results provided by the simulation. Reaction of the lactone substrate **5**, with single point calculations in ω B97X-D/Def2TZVPP(IEFPCM,toluene).

The results of the COPASI simulation reflect the just 0.2 kcal preference over the 1,2-pathway. Although a bigger proportion of 1,2-product is observed, the selectivity is very poor, far from the total selectivity experimentally achieved.

5.3.5.3 Solvent influence

Our final attempt to improve our results consisted on changing the solvent of our simulations. The ability of the solvent to stabilize intermediates and transition states could have a heavy impact on the outcome of our calculations. Therefore, we tried re-running single point calculations in gas phase, but also defining the dielectric constant, ϵ , of our solvent. The values assigned to this constant were 5, 10, 25 and 50.

The changes observed when varying the solvent were similar for both theory levels; thus, only one of them is shown in the forthcoming tables: ω B97X-D/Def2TZVPP.

First, the energies of the key transition states of the reaction of lactone **5** are presented on Table 5.5, each row corresponding to a different dielectric constant. The last column shows the difference between the 1,3-cyclization and the 1,2-migration, responsible for the selectivity of the reaction.

Table 5.5. Gibbs free energy values (in kcal/mol, referred to the starting complex **XXI**) of key transition states of the reaction of lactone **5**, with different values of ϵ . Theory level: ω B97X-D/Def2TZVPP//M06/6-311G(d,p)/SDD. In bold, transition state responsible for the selectivity.

	Lactone 5				
	1,2-pathway		1,3-pathway		Cyc _{1,3} TS - Mig _{1,2} TS
	Mig. TS	Cyc. TS	Mig. TS	Cyc. TS	
Gas phase	16.1	20.8	19.4	18.4	-1.3
Original (Tol.)	12.6	16.7	16.9	12.9	0.2
$\epsilon = 5$	10.8	14.2	15.6	9.8	1.4
$\epsilon = 10$	9.8	12.7	14.8	8.1	2.1
$\epsilon = 25$	9.1	11.7	14.4	6.9	2.6
$\epsilon = 50$	8.9	11.4	14.2	6.4	2.8

In this theory level, the selectivity of the reaction was very poor, as a preference of only 0.2 kcal/mol over the 1,2-product was observed (second row, Table 5.5). Nevertheless, a clear trend can be observed; as the polarity of the solvent is increased, the difference between the highest energy transition step of each path is also increased. In fact, the final row shows a preference of 2.8 kcal/mol over the 1,2-pathway, which would result in total selectivity.

Table 5.6. Gibbs free energy values (in kcal/mol, referred to the starting complex **XXI**) of key transition states of the reaction of furan **1**, with different values of ϵ . Theory level: ω B97X-D/Def2TZVPP//M06/6-311G(d,p)/SDD. In bold, transition state responsible for the selectivity.

	Furan 1				
	1,2-pathway		1,3-pathway		Cyc _{1,3} TS - Mig _{1,2} TS
	Mig. TS	Cyc. TS	Mig. TS	Cyc. TS	
Gas phase	15.5	21.5	18.5	22.5	-3.0
Original (Tol.)	12.0	17.7	16.0	17.2	-1.7
$\epsilon = 5$	10.2	15.5	14.7	14.2	-0.8
$\epsilon = 10$	9.3	14.3	14.0	12.5	-0.3
$\epsilon = 25$	8.6	13.4	13.5	11.3	0.1
$\epsilon = 50$	8.4	13.1	13.4	10.8	0.3

Table 5.6 displays the energy of the key transition states of the furan containing substrate as well as difference between the 1,3-cyclization and the 1,2-migration. A similar trend to that of lactone **5** can be observed. With low dielectric constants, the energy difference is big, favoring the 1,3-migration product. However, as the polarity is increased, the energy gap is reduced until, at $\epsilon = 25$, the selectivity is reversed. Actually, the value of 0.3 kcal/mol (last row, $\epsilon = 50$) would produce isomeric ratios similar to those experimentally found.

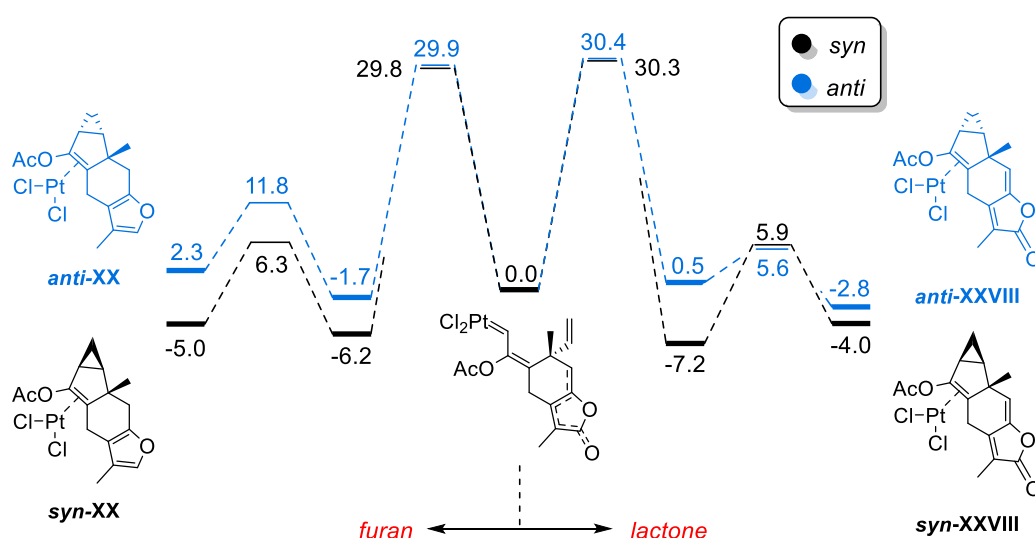
It is important to point out the change of the selectivity-inducing step in Table 5.6. At strong polarities, the highest energy transition state of the 1,3-route is, as in the lactone, the migration. Contrarily, in gas phase and with a non-polar solvent, the rate-limiting step is the cyclization. Because of this, the selectivity favoring the wrong isomer using the original solvent (second row) is of 0.5 kcal/mol instead of 1.7 kcal/mol.

In view of the results of Tables 5.5 and 5.6, we can conclude that our method is able to reproduce the experimental data when a very polar solvent is simulated. All the transition states seem to be stabilized by the polarity of solvent, since their energy goes down as the dielectric constant is increased. In the case of the furan, this causes the selectivity to reverse as the polarity is increased, while in the case of the lactone, the selectivity is increased until total selectivity is achieved with a very polar solvent.

5.3.6 *Syn/anti* selectivity

The cycloisomerization reactions performed by our collaborators produced mixtures of *syn* and *anti* isomers of the lindenane-type structure (1,2-pathway). The selectivity was poor for both the furan (**1**) and lactone (**5**) containing substrates, as the isomer ratios were of 2.6:1 and 5:1 respectively.

We computed the *syn* and *anti* cycloisomerization transition states and intermediates of the furan and lactone substrates. The results are displayed in Scheme 5.26, where the energies are related to the carbene derived from the 1,2-migration of the acetate (0.0).



Scheme 5.26. Energy profile for the *syn* and *anti* 1,2-cyclizations of furan **1** and lactone **5**. Theory level: M06/6-311G(d,p)/SDD(IEFPCM, toluene)//M06/Def2TZVPP(IEFPCM, toluene).

The energy profile of the furan and lactone containing substrates is almost identical in terms of *syn/anti* selectivity. The first activation barrier will determine the selectivity, and only a 0.1 kcal/mol energy difference was found for both substrates. The only plausible conclusion that can be reached from Scheme 5.26 is that both reactions will lead to mixtures of *syn* and *anti* isomers.

5.4 Conclusions

- Mechanism of the reactions

The mechanism of the two reactions responsible for the lindenane and myliol-type products was successfully elucidated. The transition states of the acetate migrations and later cycloisomerizations could be identified. Although the first activation barrier achieved for the lindenane-type cycloisomerization (5-*exo*) was too high, a change to a 6-*endo* transition state led to a feasible activation barrier.

- Divergent reactivity observed between gold and platinum catalysis

The mechanism of both reaction catalyzed by gold and platinum were compared. Evident differences were found between the two catalysts, both structurally and energetically. Nevertheless, the reason why the gold-catalyzed reaction stops after the 1,3-migration of the acetate is not completely clear. Probably, more experimental data would be desirable to confirm the lack of reactivity.

- Preference of product **3** over **4** in the PtCl₂ catalyzed reactions

The experimentally observed selectivity in the case of the furan was a challenge. The low experimental selectivities can only be qualitatively explained by means of computational chemistry, since the accuracy of DFT methods is not sufficient for such small differences in energy. Both pathways had similar activation barriers and, although the initial selectivity predicted the formation of the minor isomer **4**, performing a screening of theory levels and tuning the properties of the solvent improved our predictions. When the dielectric constant was low, the cyclization was the highest energy transition state of the 1,3-pathway. At higher polarities, the migration was higher in energy than the cyclization, which induced the right selectivity.

- Diastereomeric ratio of **3**

During the synthesis of **3** a preference over the *syn* product was observed, although the selectivity was poor and ranged from 1.6:1 to 2.4:1. Such low selectivity can be justified by means of DFT as long as the energy of the *syn* and *anti* leading transitions states are similar in energy, which was the case for the formation of **3**. Although the diastereoselectivity observed in the lactone analogue was slightly better (5:1), the results of the energy diagram were almost identical to those of furan **3**.

- Different reactivity of furan **1** and lactone **5**

Since the experiments showed a complete selectivity towards the lindenane-type structure in the case of the lactone, we expected to find a palpable difference between the energy diagrams of the two substrates. The only evident difference was that, in the case of the lactone, the highest energy transition state of the 1,3-pathway was not the cyclization, but the migration. Nevertheless, the difference between the two highest transition state energies was still favoring the minor isomer. After performing the screening and tuning the solvent, it was found that, under the same conditions applied to the furan, the predicted selectivity concurred with the experiments.

5.5 References

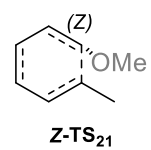
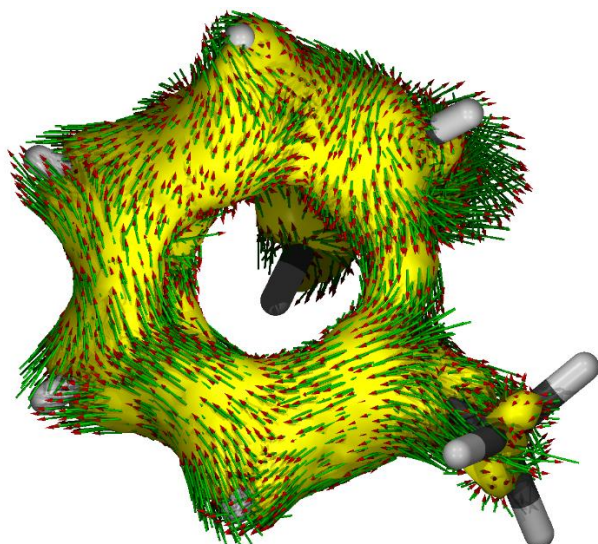
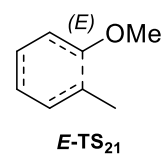
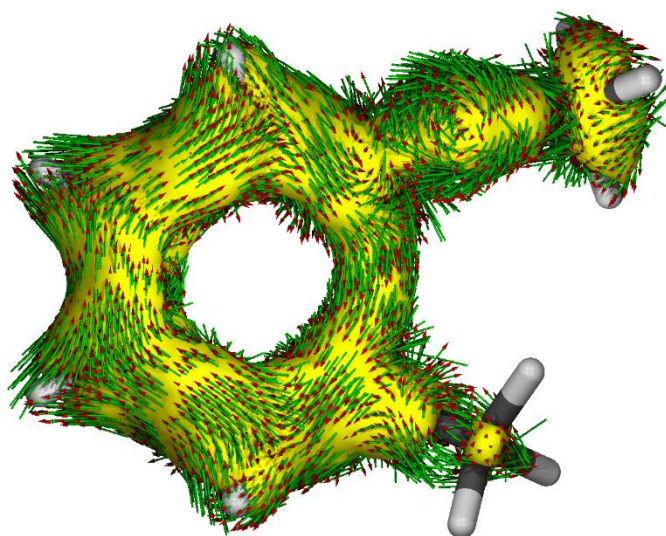
- (1) Demertzidou, V. P.; Zografos, A. L. Platinum-Catalyzed Cycloisomerizations of a Common Enyne: A Divergent Entry to Cyclopropane Sesquiterpenoids. Formal Synthesis of Sarcandalactone A. *Org. Biomol. Chem.* **2016**, *14*, 6942–6946.
- (2) Breitmaier, E. *Terpenes: Flavors, Fragrances, Pharmaca, Pheromones*; Wiley-VCH, 2006.
- (3) Ludwiczuk, A.; Skalicka-Woźniak, K.; Georgiev, M. I. Terpenoids. In *Pharmacognosy*; Elsevier, 2017; 233–266.
- (4) Garret, S. R.; Morris, R. J.; O'Maille, P. E. Steady-State Kinetic Characterization of Sesquiterpene Synthases by Gas Chromatography - Mass Spectroscopy. In *Methods in Enzymology*; Elsevier, 2012; Vol. 515, 3–19.
- (5) Kawabata, J.; Tahara, S.; Mizutani, J.; Furusaki, A.; Hashiba, N.; Matsumoto, T. Shizukanolides, Two Sesquiterpenoids from *Chloranthus Japonicus* (Chloranthaceae). *Agric. Biol. Chem.* **1979**, *43*, 885–887.
- (6) Xu, Y.-J. Phytochemical and Biological Studies of *Chloranthus* Medicinal Plants. *Chem. Biodivers.* **2013**, *10*, 1754–1773.
- (7) Zhao, J.-J.; Guo, Y.-Q.; Yang, D.-P.; Xue, X.; Liu, Q.; Zhu, L.-P.; Yin, S.; Zhao, Z.-M. Chlojaponilactone B from *Chloranthus Japonicus*: Suppression of Inflammatory Responses via Inhibition of the NF- κ B Signaling Pathway. *J. Nat. Prod.* **2016**, *79*, 2257–2263.
- (8) Acebey, L.; Jullian, V.; Sereno, D.; Chevalley, S.; Estevez, Y.; Moulis, C.; Beck, S.; Valentin, A.; Gimenez, A.; Sauvain, M. Anti-Leishmanial Lindenane Sesquiterpenes from *Hedyosmum Angustifolium*. *Planta Med.* **2010**, *76*, 365–368.
- (9) Guo, Y.-Q.; Zhao, J.-J.; Li, Z.-Z.; Tang, G.-H.; Zhao, Z.-M.; Yin, S. Natural Nitric Oxide (NO) Inhibitors from *Chloranthus Japonicus*. *Bioorg. Med. Chem. Lett.* **2016**, *26*, 3163–3166.
- (10) Yang, S.-P.; Gao, Z.-B.; Wang, F.-D.; Liao, S.-G.; Chen, H.-D.; Zhang, C.-R.; Hu, G.-Y.; Yue, J.-M. Chlorahololides A and B, Two Potent and Selective Blockers of the Potassium Channel Isolated from *Chloranthus Holostegius*. *Org. Lett.* **2007**, *9*, 903–906.
- (11) Reviews on metal-catalyzed cycloisomerization reactions: (a) Trost, B. M.; Krische, M. J. Transition Metal Catalyzed Cycloisomerizations. *Synlett* **1998**, 1–16. (b) Marinetti, A.; Jullien, H.; Voituriez, A. Enantioselective, Transition Metal Catalyzed Cycloisomerizations. *Chem. Soc. Rev.* **2012**, *41*, 4884–4908.
- (12) Knochel, P.; Molander, G. A. *Comprehensive Organic Synthesis*, 2nd ed.; Elsevier, 2014.
- (13) Lin, Y.-T.; Houk, K. N. Intramolecular Diels-Alder Reactions of Ethyl 2,4,9-Decatrienoate and 2,4,10-Undecatrienoate. *Tetrahedron Lett.* **1985**, *26*, 2517–2520.
- (14) Frank, S. A.; Mergott, D. J.; Roush, W. R. The Vinylogous Intramolecular Morita–Baylis–Hillman Reaction: Synthesis of Functionalized Cyclopentenes and Cyclohexenes with Trialkylphosphines as Nucleophilic Catalysts. *J. Am. Chem. Soc.* **2002**, *124*, 2404–2405.
- (15) Brummond, K. M.; Chen, H.; Sill, P.; You, L. A Rhodium(I)-Catalyzed Formal Allenic Alder Ene Reaction for the Rapid and Stereoselective Assembly of Cross-Conjugated Trienes. *J. Am. Chem. Soc.* **2002**, *124*, 15186–15187.

- (16) Renaud, J. L.; Petit, M.; Aubert, C.; Malacria, M. Synthetic Usefulness of the Cobalt(I)-Mediated Ene Type Reaction for the Diastereoselective Construction of Bicyclo[n.3.0]Derivatives. *Synlett* **1997**, 931–932.
- (17) Kundu, K.; McCullagh, J. V.; Morehead, A. T. Hydroacylation of 2-Vinyl Benzaldehyde Systems: An Efficient Method for the Synthesis of Chiral 3-Substituted Indanones. *J. Am. Chem. Soc.* **2005**, *127*, 16042–16043.
- (18) Kochi, T.; Hamasaki, T.; Aoyama, Y.; Kawasaki, J.; Kakiuchi, F. Chain-Walking Strategy for Organic Synthesis: Catalytic Cycloisomerization of 1,*n*-Dienes. *J. Am. Chem. Soc.* **2012**, *134*, 16544–16547.
- (19) Review on metal-catalyzed cycloisomerization of 1,*n*-enynes: (a) Lloyd-Jones, G. C. Mechanistic Aspects of Transition Metal Catalysed 1,6-Diene and 1,6-Enyne Cycloisomerisation Reactions. *Org. Biomol. Chem.* **2003**, *1*, 215–236. (b) Nieto-Oberhuber, C.; López, S.; Jiménez-Núñez, E.; Echavarren, A. M. The Mechanistic Puzzle of Transition-Metal-Catalyzed Skeletal Rearrangements of Enynes. *Chem. Eur. J.* **2006**, *12*, 5916–5923. (c) Michelet, V.; Toullec, P. Y.; Genêt, J.-P. Cycloisomerization of 1,*n*-Enynes: Challenging Metal-Catalyzed Rearrangements and Mechanistic Insights. *Angew. Chem. Int. Ed.* **2008**, *47*, 4268–4315.
- (21) Trost, B. M.; Shi, Y. Palladium-Catalyzed Cyclizations of Polyenynes. A Palladium Zipper. *J. Am. Chem. Soc.* **1993**, *115*, 9421–9438.
- (22) Reviews on gold and/or platinum-catalyzed cycloisomerization of 1,*n*-enynes: (a) Zhang, L.; Sun, J.; Kozmin, S. A. Gold and Platinum Catalysis of Enyne Cycloisomerization. *Adv. Synth. Catal.* **2006**, *348*, 2271–2296. (b) Jiménez-Núñez, E.; Echavarren, A. M. Gold-Catalyzed Cycloisomerizations of Enynes: A Mechanistic Perspective. *Chem. Rev.* **2008**, *108*, 3326–3350. (c) Soriano, E.; Marco-Contelles, J. Mechanistic Insights on the Cycloisomerization of Polyunsaturated Precursors Catalyzed by Platinum and Gold Complexes. *Acc. Chem. Res.* **2009**, *42*, 1026–1036.
- (23) Abbiati, G.; Arcadi, A.; Bianchi, G.; Di Giuseppe, S.; Marinelli, F.; Rossi, E. Sequential Amination/Annulation/Aromatization Reaction of Carbonyl Compounds and Propargylamine: A New One-Pot Approach to Functionalized Pyridines. *J. Org. Chem.* **2003**, *68*, 6959–6966.
- (24) Zhang, L.; Kozmin, S. A. Gold-Catalyzed Cycloisomerization of Siloxy Enynes to Cyclohexadienes. *J. Am. Chem. Soc.* **2004**, *126*, 11806–11807.
- (25) Luzung, M. R.; Markham, J. P.; Toste, F. D. Catalytic Isomerization of 1,5-Enynes to Bicyclo[3.1.0]hexenes. *J. Am. Chem. Soc.* **2004**, *126*, 10858–10859.
- (26) Harrak, Y.; Blaszykowski, C.; Bernard, M.; Cariou, K.; Mainetti, E.; Mouriès, V.; Dhimane, A.-L.; Fensterbank, L.; Malacria, M. PtCl₂-Catalyzed Cycloisomerizations of 5-En-1-yn-3-ol Systems. *J. Am. Chem. Soc.* **2004**, *126*, 8656–8657.
- (27) Anagnostaki, E. E.; Zografos, A. L. Non-Natural Elemene as the “Stepping Stone” for the Synthesis of Germacrane and Guaiane Sesquiterpenes. *Org. Lett.* **2013**, *15*, 152–155.
- (28) Fenlon, T.; Schwaebisch, D.; Mayweg, A.; Lee, V.; Adlington, R.; Baldwin, J. Studies towards the Synthesis of Lindenene: Unexpected Stereochemical Outcome of an Intramolecular Cyclopropanation Reaction and Synthesis of (±)-*Epi*-Lindenene and (±)-*Iso*-Lindenene. *Synlett* **2007**, *2007*, 2679–2682.
- (29) Eagan, J. M.; Hori, M.; Wu, J.; Kanyiva, K. S.; Snyder, S. A. Synthesis and Applications of Hajos-Parrish Ketone Isomers. *Angew. Chem. Int. Ed.* **2015**, *54*, 7842–7846.

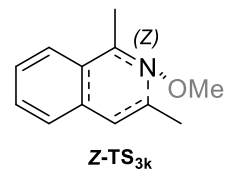
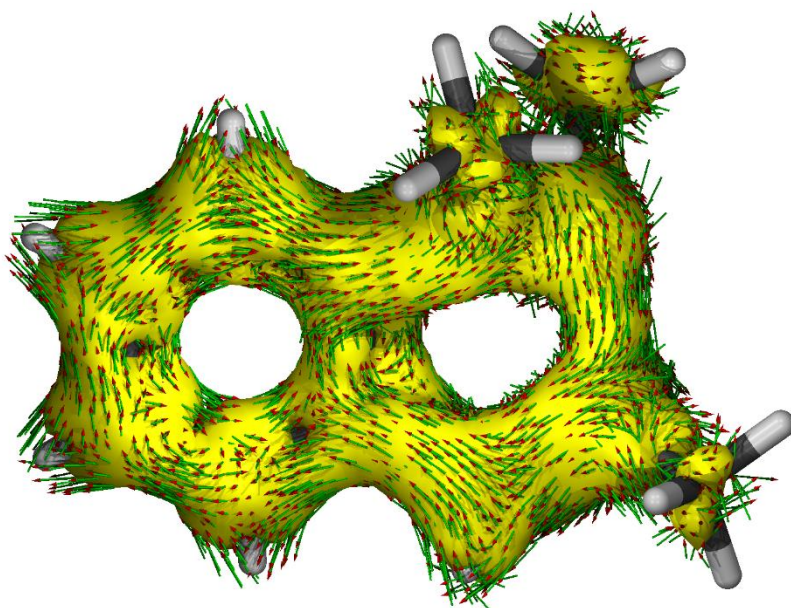
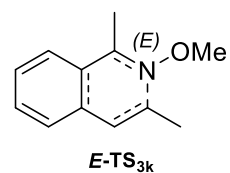
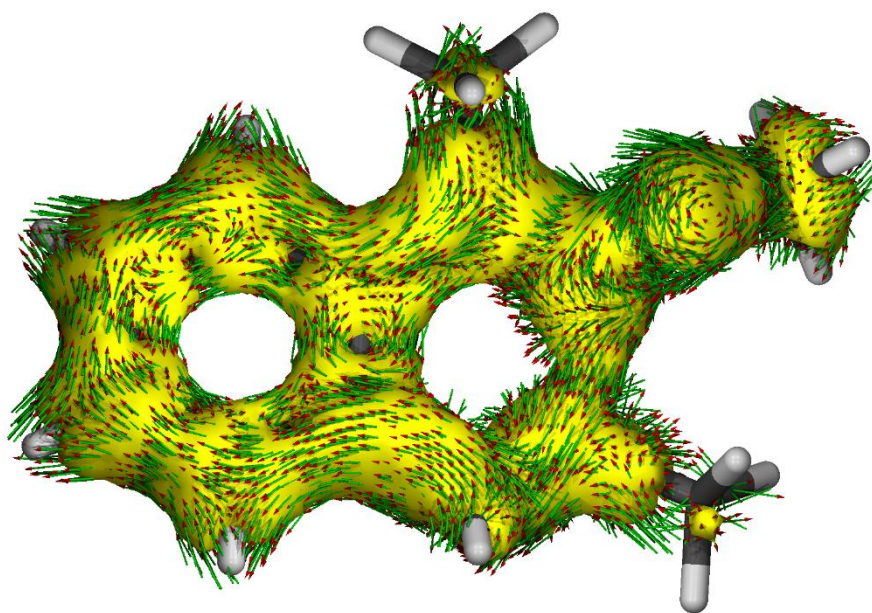
Appendix

ACID figures

- Transition states of **21**:



- Transition states of **3k**:



Publications

In the following pages, the articles chapters 2, 4 and 5 are based on will be displayed, in order.

Heterocycles

Synthetic and Mechanistic Investigation of an Oxime Ether Electrocyclization Approach to Heteroaromatic Boronic Acid Derivatives

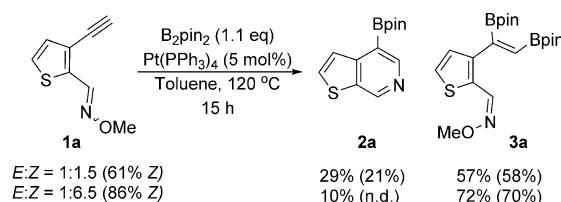
Helena Mora-Radó,^[a] Lia Sotorríos,^[b] Matthew P. Ball-Jones,^[a] Laurent Bialy,^[c] Werngard Czechtizky,^[c, d] María Méndez,^[c] Enrique Gómez-Bengoá,^{*[b]} and Joseph P. A. Harrity^{*[a]}

Abstract: A range of functionalized heteroaromatic boronic acid derivatives are readily accessed by a diboration/ 6π -electrocyclization sequence. This study revealed the surprising observation that there is a direct relationship between oxime ether stereochemistry and reactivity towards electrocyclization. Specifically, *E*-oxime ethers are found to be significantly more reactive than their *Z*-counterparts (stereochemistry relative to azatriene scaffold). In contrast, the configuration at the azatriene alkene terminus has little impact on reaction rates. Computational analysis offers a rationale for this observation; a $N_{\text{one pair}} \rightarrow C=C \pi^*$ orbital interaction lowers the energy of the transition state in the electrocyclization of *E*-oxime ethers. Finally, unreactive *Z*-oxime ethers can be converted to the corresponding heterocyclic products by a photolytically promoted *E*→*Z* isomerization and electrocyclization sequence.

Heterocycle-fused pyridines are common fragments in biologically active compounds and azole-containing analogues are particularly prominent, featuring in compounds such as nucleosides and carbolenes.^[1] These compounds are often prepared by ring-forming synthetic strategies, for which a number of catalytic methods have recently emerged.^[2] However, suitably functionalized variants of these compounds could allow them to be introduced directly using cross-coupling reactions.

In this regard, the availability of borylated azole-fused pyridine derivatives is very limited.

Recent studies in our lab have demonstrated that aromatic oxime ethers bearing an *ortho*-alkyne group can be transformed into isoquinoline boronic esters via a diboration/ 6π -electrocyclization sequence.^[3] We therefore began our studies by investigating the applicability of this transformation for the synthesis of borylated thienopyridines as this would deliver a novel class of heteroaromatic boronic ester scaffolds.^[4,5] As shown in Scheme 1, subsection of thiophene **1a** to B_2pin_2 in



Scheme 1. Synthesis of borylated thienopyridines. Estimated yields obtained by ¹H NMR spectroscopy with isolated yields in parentheses. n.d.: Not determined.

the presence of a Pt-catalyst led to a diboration–electrocyclization cascade that delivered thienopyridine boronic ester **2a** in poor yield. Interestingly however, the remaining mass balance consisted of diborylated alkene **3a**, which was found to contain exclusively the *Z*-configuration at the oxime. This result was reproduced at higher *Z*/*E*-**1a** ratios. The correlation between initial oxime ether isomer ratio and the product ratios indicated that the *Z*-minor oxime isomer of **1a** could undergo diboration, but was inert to electrocyclization.^[6]

In continuing our scoping studies, we found that the majority of heterocycles examined provided very high selectivity for *E*-oxime stereoisomers and so we were able to demonstrate that this method offers a rapid and convenient means for generating novel heteroaromatic boronic esters from readily available starting materials. As shown in Scheme 2, Boc-protected carbolenes were readily assembled by diboration of **1b,c**, although the free indole **1d** required further heating to promote cyclization. The method also allows a convenient means for accessing constitutional isomers, as exemplified by the synthesis of azaindazoles **2e,g**. Overall, this approach allows a range of

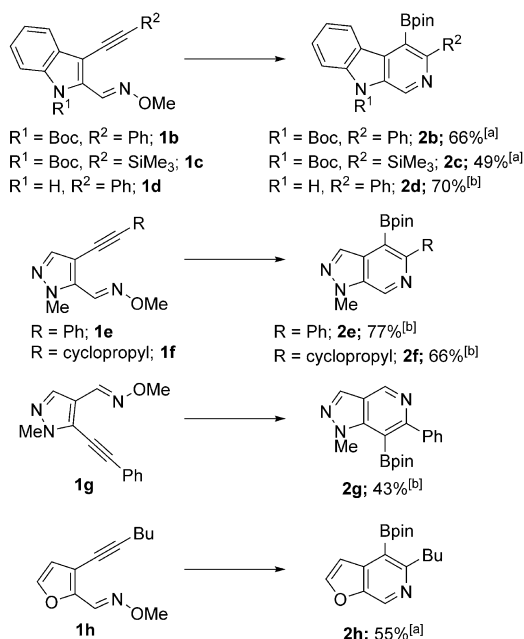
[a] H. Mora-Radó, Dr. M. P. Ball-Jones, Prof. J. P. A. Harrity
Department of Chemistry, University of Sheffield
Sheffield, S3 7HF (U.K.)
E-mail: j.harrity@sheffield.ac.uk

[b] L. Sotorríos, Prof. E. Gómez-Bengoá
Departamento de Química Orgánica I, Universidad del País Vasco
San Sebastian, 20018 (Spain)
E-mail: enrique.gomez@ehu.es

[c] Dr. L. Bialy, Dr. W. Czechtizky, Dr. M. Méndez
Integrated Drug discovery, R&D, Sanofi Aventis (Deutschland) GmbH
Industriepark Höchst, 65926 Frankfurt Am Main (Germany)

[d] Dr. W. Czechtizky
Present address: Respiratory, Inflammation, Autoimmunity IMED Biotech
Unit, AstraZeneca, Gothenburg (Sweden)

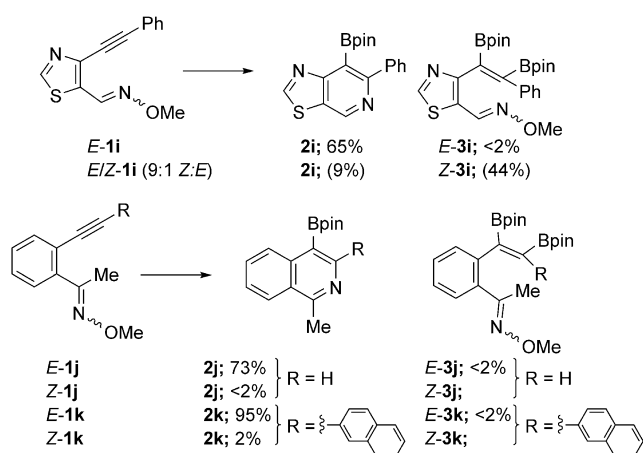
Supporting information and the ORCID number(s) for the author(s) of this article can be found under <https://doi.org/10.1002/chem.201802350>.



Scheme 2. Diboration–electrocyclization approach to heteroaromatic boronates. [a] B_2pin_2 , 10 mol% $\text{Pt}(\text{PPh}_3)_4$, toluene, 120 °C, 16 h. [b] (i) B_2pin_2 , 10 mol% $\text{Pt}(\text{PPh}_3)_4$, toluene, 120 °C, 16 h; (ii) $1,2\text{-C}_6\text{H}_4$, 200 °C, 16 h.

functionalized scaffolds to be generated in good yield over a one or two step sequence.

Returning to the issue of the dependence of the electrocyclization step on the oxime stereochemistry we explored the generality of this observation, targeting substrates that could deliver significant yields of *Z*-oxime ethers. We were able to prepare and isolate individual isomers of thiazole **1i** and ketoximes **1j–k**. The diboration–electrocyclization of these compounds reinforces the observation that the cyclization was critically dependent on oxime ether stereochemistry with *Z*-substrates inert to pyridine ring formation (Scheme 3). **E-1i** cleanly



Scheme 3. Diboration–electrocyclization efficiency in relation to oxime ether stereochemistry. (i) B_2pin_2 , 10 mol% $\text{Pt}(\text{PPh}_3)_4$, toluene, 120 °C, 16 h; (ii) $1,2\text{-C}_6\text{H}_4$, 200 °C, 16 h. Estimated yields obtained by ^1H NMR spectroscopy in parentheses.

provided 65% of pyridine **2i**, whilst a sample containing $\approx 90\%$ *Z-1i* gave $<10\%$ of the pyridine and 44% of **Z-3i**, which proved unstable with respect to protodeboronation. Similar observations were found in the synthesis of isoquinolines **2j** and **2k**.

The thermally promoted disrotatory 6π -electrocyclization of conjugated trienes to form cyclohexa-1,3-dienes is an established transformation that has attracted many theoretical and experimental studies over the years. The influence of substituent and geometrical effects in electrocyclization reactions of trienes has been studied in some detail, and it appears that the incorporation of groups in a '*cis*' configuration at the termini of the triene chain significantly retard the cyclization rate.^[7,8] This has been attributed to a reduced propensity for the substrate to adopt the reactive *s-cis*, *s-cis* conformation. In order to establish sensitivity of the reaction to the stereochemistry at the oxime ether, the alkenyl terminus, and the effect of congested boronated substrates, we computed the free activation energy of the cyclization of *Z* and *E* oxime ether isomers of a non-boronated substrate **4**, and compared this to **3k** (Figure 1).

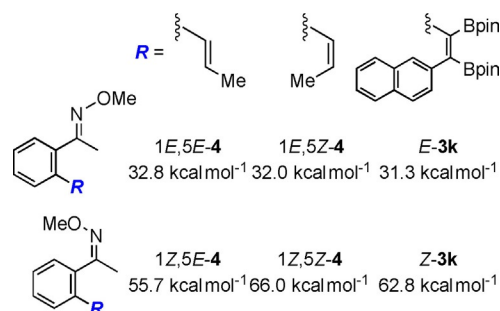


Figure 1. Calculated free activation energies for cyclizations of *E* and *Z* oxime ethers, computed at M06-2X/6-311 + G(d,p)(IEFPCM, toluene). Values in kcal mol^{-1} .

The *Z*- and *E*-isomeric forms of all initial oxime substrates show very similar relative stabilities, with differences between them of only 0–0.6 kcal mol^{-1} (see Supporting Information for details). Surprisingly however, the activation energies for the cyclization of the *Z*-oxime isomers were between 20 and 30 kcal mol^{-1} higher than those of their *E*-counterparts, which corresponds to ten or more orders of magnitude lower reaction rate. The reaction barriers for the *E*-isomers range from 31–33 kcal mol^{-1} , and these barriers are easily surmountable at the experimental temperatures typically used for the cyclization reaction. In contrast, *Z*-oximes afford activation energies over 40 kcal mol^{-1} (even as high as 63 kcal mol^{-1}), meaning that this general kind of substrate will probably never react, whatever experimental conditions are employed. In contrast to the oxime ether moiety, the computational data predict that the structural features on the alkene terminus do not exert any significant effect on the cyclizations. For example, $1E,5Z\text{-4}$ presents slightly lower activation energy than $1E,5E\text{-4}$, suggesting that *cis*-alkenes can be as good substrates (or even better) as *trans*-alkenes in this specific reaction.^[9] Furthermore, increased

substitution on the alkene seems to be well tolerated, and tetrasubstituted derivative **3i** shows comparable, slightly lower activation barrier than the simplest *E*-alkene **4**. Thus, the incorporation of boronic esters, and the substitution degree and pattern of the alkene, appear to have no significant impact on reactivity towards electrocyclozation.

To find an explanation for the above findings, we analyzed the structures of the four different transition states of compound **4** (Figure 2). As expected, all the cyclizations are disrotat-

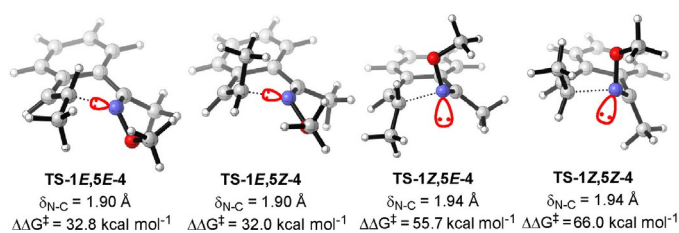


Figure 2. Structural features of the isomeric transition structures of compound **4**.

tory, and present very homogeneous C–N bond forming distances (1.90–1.94 Å). The transition states of the two *E*-oxime isomers (TS-1E,5E-4 and TS-1E,5Z-4) are structurally very similar, and differ only in the relative *cis/trans* disposition of the methyl group at the terminal alkene which does not have any effect on their relative activation barriers (32.8 and 32.0 kcal mol⁻¹). Indeed, the terminal olefinic carbon undergoes partial pyramidalization during the transition state, releasing part of the steric repulsion between the eclipsed aryl and methyl substituents in the *Z*-olefin containing substrates, providing an explanation for the good performance of hindered *Z*-alkenes in this process. Meanwhile, the geometry of the oxime moiety during the reaction is also very instructive. We hypothesize that the lone pair of the oxime-nitrogen actively participates in the electrocyclozation, and its orientation is thus crucial for the reactivity. In TS-1E,5E-4, the iminic nitrogen lone pair is point-

ing towards the terminal carbon of the double bond (see tentative disposition, Figure 2 in red), whereas in TS-1Z,5E-4, the lone pair is orthogonal to the forming C–N bond.

Evidence for donation of the nitrogen lone pair into the alkene antibonding π^* orbital at the transition state is revealed in the plotted orbital interaction diagram for TS-1E,5E-4 (**B**, Figure 3). This interaction is lacking in TS-1Z,5E-4, where the lone pair is not participating in the transition state (**C**). Also, the electronegative region (red in the ESP diagrams) of reacting oxime *Z* is large around the lone pairs of nitrogen and oxygen (**D**, Figure 3), showing that the electron density at nitrogen lies away from the forming C–N bond forming region. Meanwhile, there is an absence of negative charge around nitrogen in the *E*-oxime (**A**), since its lone pair is involved in bonding.

The fact that ketoxime ethers are commonly formed with significant proportions of *Z*-isomer present constitutes a limitation of this chemistry given that calculations suggest that *Z*-oximes are essentially inert to cyclization. This prompted us to consider the possibility of using photochemically promoted cyclization methods as a means to processing these unreactive azatrienes towards pyridine products. In principle, two pathways could be envisaged: (1) a photochemically promoted conrotatory cyclization reaction; (2) a photochemically promoted oxime ether isomerization followed by thermally promoted disrotatory cyclization. Regarding the latter pathway, photochemically promoted stereochemical isomerization of oximes has been established (Scheme 4).^[10] Moreover, Pratt and co-workers have reported that such processes can operate during electrocyclozation reactions, although they did not identify a relationship between cyclization efficiency and oxime ether stereochemistry.^[11] This approach is especially attractive in the case of oxime ethers where the rate of thermal interconversion is extremely slow.

In order to establish the potential of the photochemically promoted cyclization, we subjected substrates 1Z,5E-3a and 1Z-3k to UV irradiation in *o*-DCB. Pleasingly, these conditions successfully furnished the desired heterocyclic substrates, albeit in modest yield (Scheme 4). In the case of the reaction

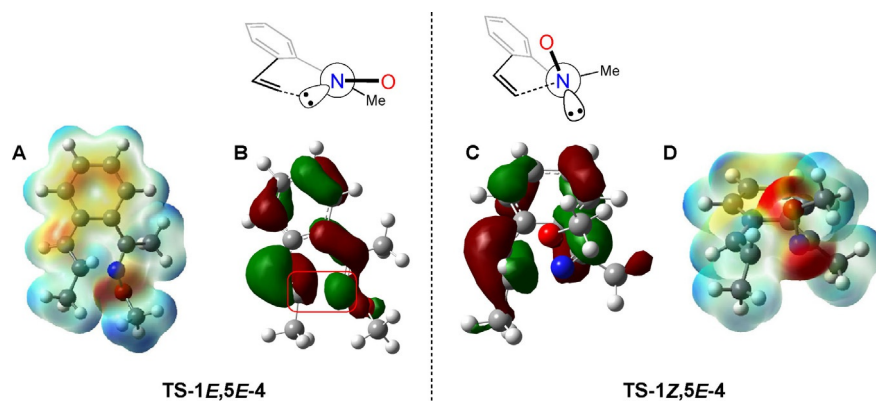
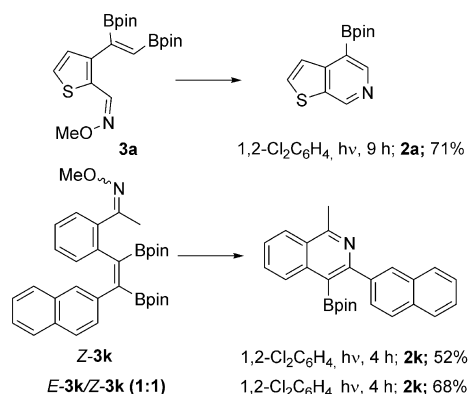


Figure 3. Orbital interaction diagrams (**B** and **C**) and Electrostatic Potential maps (**A** and **D**) for the cyclization transition states of the isomeric *E*- and *Z*-oxime ethers.



Scheme 4. Photochemically promoted electrocyclization reaction of oxime ethers.

of 1Z-3k, monitoring the reaction progress via LC-MS and ^1H NMR spectroscopic analysis showed the rapid formation of the *E*-oxime ether together with product formation. Moreover, a $\approx 1:1$ mixture of oxime ether isomers was maintained until complete consumption of starting materials (See Supporting Information). We therefore believe that, in this case, the reaction operates via a photolytically promoted oxime ether isomerization followed by a thermally promoted electrocyclization step.

In conclusion, the 6π -electrocyclization of conjugated azatrienes offers a useful method for the synthesis of heterocyclic boronic acid derivatives. Our experimental studies show that, in the case of oxime ethers, there is a direct relationship between oxime stereochemistry and reactivity towards electrocyclization. Specifically, while the configuration of the alkene at the azatriene terminus has little impact on reaction rates, *E*-oxime ethers are significantly more reactive than their *Z*-counterparts (stereochemistry relative to azatriene scaffold). Computational analysis has identified a $N_{\text{one pair}} \rightarrow \text{C}=\text{C} \pi^*$ orbital interaction that promoted the cyclization in the case of *E*-oxime isomer by lowering the energy of the transition state in the electrocyclization process. Finally, unreactive *Z*-oxime ethers can be converted to the corresponding heterocyclic products by a photolytically promoted *E* \rightarrow *Z* isomerization and electrocyclization sequence.

Experimental Section

Typical diboration-electrocyclization procedure as exemplified by the formation of 2e: A mixture of oxime 1e (1.45 g, 6.10 mmol), B_2pin_2 (1.70 g, 6.70 mmol) and $\text{Pt}(\text{PPh}_3)_4$ (759 mg, 0.61 mmol) were heated in toluene (60 mL) at reflux for 30 min in a Schlenk tube. Flash chromatography over florisil provided the diborylalkene as a yellow oil (2.50 g, 83%). ^1H NMR (400 MHz, CDCl_3): $\delta = 7.74$ (s, 1H), 7.14–7.05 (m, 3H), 7.00–6.96 (m, 3H), 3.89 (s, 3H), 3.81 (s, 3H), 1.31 (s, 12H), 1.30 (s, 12H); ^{13}C NMR (101 MHz, CDCl_3): $\delta = 141.0$, 139.7, 138.8, 130.2 (2C), 128.8, 127.8 (2C), 126.3, 123.8, 84.3 (2C), 84.1 (2C), 62.0, 40.0, 24.9 ppm (8C), two quaternary missing due to quadrupolar relaxation; ^{11}B NMR (128 MHz, CDCl_3): $\delta = 30.2$ ppm (br); FTIR: $\tilde{\nu} = 2978$, 1459, 1308, 1140, 1052 cm^{-1} ; HRMS m/z $[M+H]^+$ $\text{C}_{26}\text{H}_{38}^{11}\text{B}_2\text{N}_3\text{O}_5$ calcd 494.2998; found: 494.3021.

Diborylalkene (2.50 g, 5.0 mmol) in *o*-DCB (50 mL) was stirred at 200 $^\circ\text{C}$ for 16 h. The reaction mixture cooled to room temperature and was filtered through silica gel. The residue was purified by flash column chromatography on silica gel to give 2e as a yellow foam (1.60 g, 93%). ^1H NMR (400 MHz, CDCl_3): $\delta = 9.02$ (s, 1H), 8.23 (s, 1H), 7.68–7.63 (m, 2H), 7.45–7.36 (m, 3H), 4.21 (s, 3H), 1.32 ppm (s, 12H); ^{13}C NMR (101 MHz, CDCl_3): $\delta = 154.6$, 142.2, 134.6, 134.0, 133.9, 133.1, 129.7 (2C), 127.9 (2C), 127.8, 84.4 (2C), 36.1, 24.8 ppm (4C), one quaternary missing due to quadrupolar relaxation; ^{11}B NMR (128 MHz, CDCl_3): $\delta = 31.6$ ppm (br); FTIR: $\tilde{\nu} = 2971$, 1725, 1562, 1451, 1319, 1195, 1070 cm^{-1} ; HRMS m/z $[M+H]^+$ $\text{C}_{19}\text{H}_{22}^{11}\text{BN}_3\text{O}_2$ calcd 336.1878; found: 336.1888.

Acknowledgements

We are grateful for support from the EPSRC, the FP7 Marie Curie Actions of the European Commission (via the ITN COSSH-NET network), the Basque Government (GIC15/03, IT1033-16) and IZO/SGL SGiker of UPV/EHU. L.S. thanks MINECO (Spain, CTQ2016-78083-P) for a predoctoral contract.

Conflict of interest

The authors declare no conflict of interest.

Keywords: boronic ester · electrocyclization · heterocycles · stereochemistry

- [1] a) A. R. Sherman in *Comprehensive Heterocyclic Chemistry II*, Vol. 7 (Eds.: A. R. Katritzky, C. W. Rees, E. F. V. Scriven), Pergamon, Oxford, 1996, p. 167; b) L. B. Townsend, D. S. Wise in *Comprehensive Heterocyclic Chemistry II*, Vol. 7 (Eds.: A. R. Katritzky, C. W. Rees, E. F. V. Scriven), Pergamon, Oxford, 1996, p. 283.
- [2] a) H. Huang, S. Nakanowatari, L. Ackermann, *Org. Lett.* 2017, 19, 4620; b) C. Henrique Alves Esteves, P. D. Smith, T. J. Donohoe, *J. Org. Chem.* 2017, 82, 4435; c) X. Chen, Y. Wu, J. Xu, H. Yao, A. Lin, Y. Huang, *Org. Biomol. Chem.* 2015, 13, 9186.
- [3] H. Mora-Radó, L. Bialy, W. Czechtizky, M. Méndez, J. P. A. Harrity, *Angew. Chem. Int. Ed.* 2016, 55, 5834; *Angew. Chem.* 2016, 128, 5928.
- [4] There are no examples of 4-borylated thieno[2,3-*c*]pyridines reported in the literature, to the best of our knowledge. A single example of a 5-borylated analogue was reported by Glorius and co-workers: H. Wang, C. Grohmann, C. Nimphius, F. Glorius, *J. Am. Chem. Soc.* 2012, 134, 19592.
- [5] For alternative approaches to heteroaromatic boronic acid derivatives see: a) A. Issaian, K. N. Tu, S. A. Blum, *Acc. Chem. Res.* 2017, 50, 2598; b) A. J. Warner, J. R. Lawson, V. Fasano, M. J. Ingleson, *Angew. Chem. Int. Ed.* 2015, 54, 11245; *Angew. Chem.* 2015, 127, 11397; c) S. P. J. T. Bachollet, J. F. Vivat, D. C. Cocker, H. Adams, J. P. A. Harrity, *Chem. Eur. J.* 2014, 20, 12889.
- [6] Subjection of Z-3a to heating at 200 $^\circ\text{C}$ in 1,2-dichlorobenzene over extended periods did not lead to any detectable quantities of thienopyridine 2a.
- [7] a) E. N. Marvell, G. Caple, C. Delphey, J. Platt, N. Polston, J. Tashiro, *Tetrahedron* 1973, 29, 3797; b) C. W. Spangler, T. P. Jondahl, B. Spangler, *J. Org. Chem.* 1973, 38, 2478; c) J. D. Evanseck, B. E. Thomas IV, D. C. Spellmeyer, K. N. Houk, *J. Org. Chem.* 1995, 60, 7134; d) V. A. Guner, K. N. Houk, I. W. Davies, *J. Org. Chem.* 2004, 69, 8024; e) T.-Q. Yu, Y. Fu, L. Liu, Q.-X. Guo, *J. Org. Chem.* 2006, 71, 6157.
- [8] Although there are no reports correlating oxime ether stereochemistry with electrocyclization efficiency, a theoretical study of the corresponding reactions of pentadienimine has been documented: J. Rodríguez-Otero, *J. Org. Chem.* 1999, 64, 6842.

- [9] Heating 1*E*,5*E*-4 at 200 °C in 1,2-Cl₂C₆H₄ generated the corresponding isoquinoline in 83% yield, whereas subjecting 1*Z*,5*E*-4 resulted in <2% conversion under the same conditions.
- [10] a) A. Padwa, F. Albrecht, *J. Am. Chem. Soc.* **1972**, *94*, 1000; b) A. Padwa, F. Albrecht, *J. Am. Chem. Soc.* **1974**, *96*, 4849; c) Y. Takeda, H. Misawa, H. Sakuragi, K. Tokumaru, *Bull. Chem. Soc. Jpn.* **1989**, *62*, 2213.
- [11] M. Austin, O. J. Egan, R. Tully, A. C. Pratt, *Org. Biomol. Chem.* **2007**, *5*, 3778.

Manuscript received: May 9, 2018

Accepted manuscript online: May 11, 2018

Version of record online: June 6, 2018

Intramolecular Palladium(II)-Catalyzed 6-*endo* C–H Alkenylation Directed by the Remote *N*-Protecting Group: Mechanistic Insight and Application to the Synthesis of Dihydroquinolines

Asier Carral-Menoyo, Lia Sotorríos, Verónica Ortiz-de-Elguea, Aitor Diaz-Andrés, Nuria Sotomayor,* Enrique Gómez-Bengoa,* and Esther Lete*



Cite This: *J. Org. Chem.* 2020, 85, 2486–2503



Read Online

ACCESS |



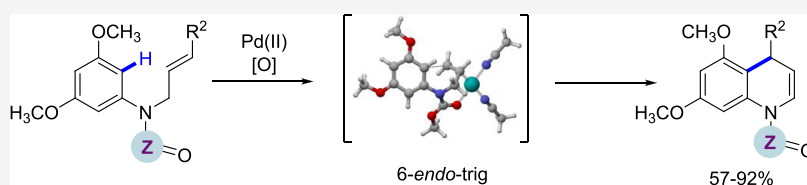
Metrics & More



Article Recommendations



Supporting Information



ABSTRACT: A protocol for the Pd(II)-catalyzed C–H alkenylation reaction of substituted *N*-allylanilines via an unusual 6-*endo* process has been developed. A density functional theory (DFT) study of the mechanistic pathway has shown that the coordination of the remote protecting group to the palladium center is determinant for the control of the regioselectivity in favor of the 6-*endo* process. The reaction would proceed via prior activation of the alkene. This procedure constitutes a mild and efficient method for the synthesis of 1,4-dihydroquinoline derivatives from simple and readily accessible substrates.

INTRODUCTION

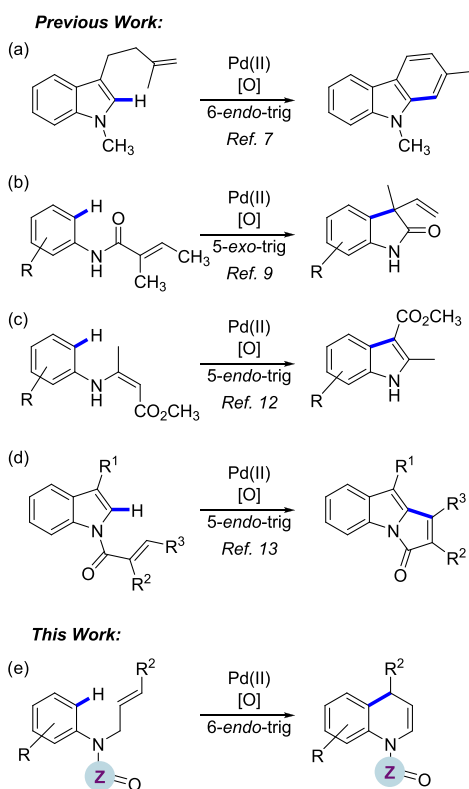
Transition-metal-catalyzed C–H functionalization reactions of (hetero)arenes have emerged as very powerful tools for the formation of carbon–carbon bonds¹ and as a good alternative to traditional cross-coupling chemistry. No prefunctionalized coupling precursors as halides or pseudohalides are required, though a stoichiometric oxidant is needed to regenerate the active catalytic species. These reactions can typically be carried out under mild conditions, even in aqueous media, avoiding the need for rigorous exclusion of oxygen. In the last years, there has been a great progress in the intermolecular dehydrogenative Heck reaction (DHR) or Fujiwara–Moritani reaction.² This reaction consists of Pd(II)-catalyzed direct coupling between a Csp²-hybridized reaction partner and an alkene followed by β -hydride elimination toward the site of initial migratory insertion, which formally provides an sp²–sp² carbon–carbon bond. The main issue of this type of reactions has been the control of site selectivity that has been addressed by using either electronically activated substrates or directing groups/ligands that are able to coordinate the metal center and facilitate the catalyst approach to the selected C–H.³ The potential of its intramolecular variant for the synthesis of carbocyclic and heterocyclic frameworks, however, remains relatively underexplored, and has been mainly applied to electron-rich heteroarenes such as indole and pyrrole. As in related Heck cyclizations, the regioselectivity is determined by the ring size and the preferential *exo* processes, which has been attributed to the strain involved in the approach of the arylpalladium intermediate. Thus, annulated indoles and

pyrroles have been prepared via 5-, 6-, and/or 7-*exo*-trig cyclizations of C-3- and/or C-2-substituted derivatives with unactivated alkenes.⁴ The procedure has also been applied to the construction of benzofurans and chromenes using electron-rich arenes.⁵ Specifically, our group has reported intramolecular dehydrogenative Heck reactions of aryl homoallyl ethers and *N*-homoallylanilines, which provide direct access to highly and diversely substituted chromenes and (dihydro)-quinolines, respectively.⁶ On the other hand, *endo*-trig cyclizations are rare and have been reported when the *exo* processes are blocked, and the palladium hydride elimination is not possible, as described by Lu in the synthesis of carbazoles⁷ (Scheme 1a).

The palladium-catalyzed cyclization/carboalkoxylation of C-2 and C-3 alkenyl indoles to give carbazoles and cyclohepta-*[b]*indoles via either 6- or 7-*exo*-trig, as well as 6-*endo*-trig processes is still an exception in dehydrogenative Heck-type cyclizations.⁸ Similarly, *exo* cyclizations are generally favored using activated alkenes (bearing an EWG). Thus, Pd(II)-catalyzed intramolecular reactions of *N*-phenylacrylamides afford oxindoles via formal 5-*exo*-trig processes, (Scheme 1b),⁹ and in some cases, even when β -hydride elimination is not possible, the Ar–Pd(II) intermediate prefers to undergo a

Received: November 26, 2019

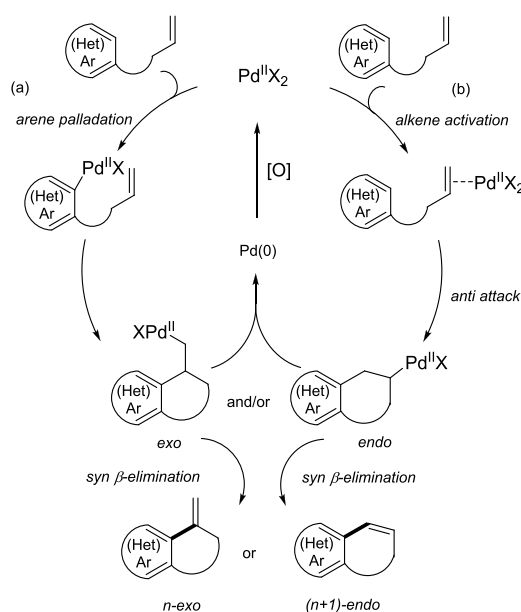
Published: December 30, 2019

Scheme 1. Intramolecular Pd(II)-Catalyzed Alkenylation Reactions through *endo* and *exo* Processes

nucleophile capture or a subsequent C–H alkylation.¹⁰ However, we have demonstrated that the intramolecular 6-*endo*-trig C–H alkenylation of related *N*-alkyl-substituted *N*-phenylacrylamides gives 4-substituted quinolin-2[1*H*]-ones,¹¹ showing that the reaction can be switched to the β -position of the acrylamide by selecting the catalyst, oxidant, and experimental conditions. On the other hand, Glorius¹² has achieved the synthesis of indoles by a formal Pd(II)-catalyzed oxidative 5-*endo* cyclization of substituted *N*-arylenamine carboxylates, although, as in the work of Oestreich,⁹ a free NH is required for the success of the reaction (Scheme 1c). The size of the formed ring can also be decisive for the regioselectivity, as in the cyclization of 1-(1*H*-indol-1-yl)prop-2-enone derivatives to give 3*H*-pyrrolo[1,2-*a*]indol-3-ones that takes place via a 5-*endo*-trig cyclization¹³ (Scheme 1d).

Two alternative mechanistic pathways have been generally proposed for the initial palladation that would be determinant for the *endo/exo* selectivity (Scheme 2). The reaction could proceed through an arene metalation–alkene insertion (Scheme 2a) or alkene activation–arene insertion (Scheme 2b). Both reaction pathways have been proposed to explain *endo* and *exo* insertions, in some cases without providing experimental or theoretical evidences in favor of any of them. However, both pathways differ in the stereochemical outcome and may lead to the formation of different diastereomers using the appropriate substrate: in pathway (a), the (hetero)aryl palladium(II) intermediate would undergo a *syn* olefin insertion, followed by *syn* β -hydride elimination. On the other hand, *anti*-nucleophilic attack of the arene to the Pd(II) complex would take place on a Pd(II)-coordinated alkene (pathway b). In both cases, reductive elimination generates the reaction product and a Pd(0) complex that can be reoxidized

Scheme 2. Schematic Mechanistic Pathways for the Intramolecular Pd(II)-Catalyzed Alkenylation Reactions



to Pd(II). Thus, there is a stereochemical support for a mechanism involving initial palladation of the (hetero)-arene^{4a,5a} or attack of the heteroarene to the palladium-complexed olefin.^{8,14} This Friedel–Crafts-type mechanism has also been proposed for the obtention of oxindoles (Scheme 1b),⁹ but also, depending on the substrate used, different mechanisms have been proposed, such as the electrophilic palladation of an electron-rich enamine, followed by deprotonation of the aromatic ring (Scheme 1c).¹² Hence, a mechanistic understanding of the reaction is required to obtain selectively the desired reaction products. In the context of our interest in this type of cyclization reactions,^{6,11} we decided to study the Pd(II)-catalyzed intramolecular alkenylation of *N*-protected allyl anilines to obtain dihydroquinolines (DHQ) through a 6-*endo* process (Scheme 1d).

Partially hydrogenated quinolines are important structural frameworks present in a myriad of bioactive natural products and pharmaceuticals, as well as building blocks in organic synthesis.¹⁵ Among them, 1,4-dihydroquinolines (1,4-DHQ) have attracted special attention, due to their important biological activities. For example, 4-aryl-1,4-dihydroquinoline derivatives have been characterized as a novel class of ABCB1 inhibitors to reverse the multidrug resistance of anticancer drugs.¹⁶ Besides 1,4-dihydroquinoline, the core of azapodophyllotoxins, known antiproliferative microtubule destabilizing agents have expressed a very pronounced antitumor activity.¹⁷ 1,4-DHQ can also be used as drug carriers for specific delivery to the central nervous system (CNS) in the treatment of Alzheimer's disease¹⁸ or cerebral ischemia/reperfusion injury,¹⁹ as well as in the targeting of positron emission tomography (PET) radioligands for brain imaging.²⁰ On the other hand, they are used as building blocks in the synthesis²¹ of pyridoacridones, a family of marine alkaloids that exhibits an array of biological activities (Figure 1).²² Therefore, the synthesis of substituted 1,4-dihydroquinolines is interesting in both synthetic and medicinal chemistry.

Although many examples of the catalytic synthesis of quinolines and tetrahydroquinolines have been reported,²³ there have been relatively few examples of the preparation of

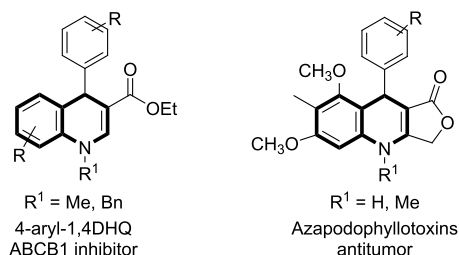


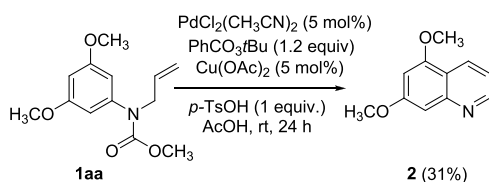
Figure 1. Selected biologically active 1,4-dihydroquinolines.

1,4-dihydroquinoline derivatives. Herein, we report a joint experimental and density functional theory (DFT) study on the 6-*endo* cyclization on *N*-protected allyl anilines that has led to an efficient method for the synthesis of 1,4-dihydroquinoline derivatives from simple and readily accessible substrates. The protecting group on nitrogen atom has been shown to be crucial to favor the *endo* cyclization process.

RESULTS AND DISCUSSION

We selected carbamate **1aa** as a model substrate (Scheme 3) using as starting point the reaction conditions that had been

Scheme 3. Cyclization of **1aa**



previously optimized for the 6-*endo* cyclization of *N*-aryl acrylamides to quinolones.¹¹ Under these conditions, quinoline **2** was obtained, although in a low yield (31%), together with decomposition products. Quinoline **2** would be obtained from a 6-*endo* cyclization followed by deprotection under the strongly acidic conditions, and further oxidation.

Consequently, to avoid the deprotection and additional oxidation, we switched to milder reaction conditions, using

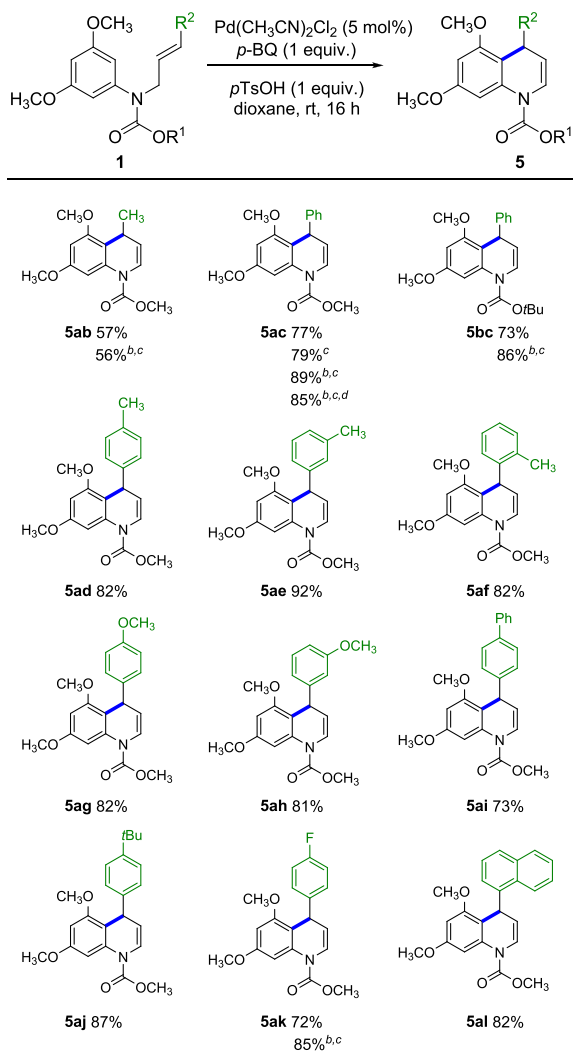
dioxane as solvent and *p*-benzoquinone as the only oxidant (Table 1). The use of *p*-toluenesulfonic acid is also important to enhance the reactivity probably through the formation of a more electrophilic Pd(II) species.⁶ Under these conditions, the 6-*endo* cyclization took place with complete regioselectivity, obtaining 1,2-dihydroquinoline **3aa** in high isolated yield (85%) after 16 h at room temperature (Table 1, entry 1). Formation of indole **4aa**, through a 5-*exo* process was not detected. Interestingly, when the protecting group is changed to a *t*-butyl carbamate (**1ba**, Table 1, entry 2), under the same reaction conditions, the reaction was sluggish, obtaining **3ba** in a much lower yield (38%), along with trace amounts of the 5-*exo* cyclization product **4ba** (not isolated) and decomposition products. An increase in the catalyst loading to 10 mol % (Table 1, entry 3) resulted in a faster reaction (1.5 h at room temperature). However, although the dihydroquinoline **3ba** was obtained in a higher yield (58%), the reaction was not selective, isolating a significant amount of indole **4ba**, through a 5-*exo* process. The change of the palladium precatalyst (Table 1, entry 4) gave a similar result. The use of a monoprotected amino acid²⁴ (Boc-Val-OH) in this case did not accelerate the reaction rate and led also to a nonselective reaction (entry 5), also when the palladium source was changed trying to obtain more electrophilic palladium intermediates (Table 1, entries 6 and 7). The use of benzyl carbamate **1ca** led also to the regioselective formation of **3ca** (Table 1, entry 8). A significant difference in reactivity was observed when the nitrogen is protected as an amide: acetyl-protected **1da** (Table 1, entry 9) did not react at all under the conditions used for **1aa** (Table 1, entry 1). It was necessary to increase the catalyst loading and to heat the reaction to 70 °C to obtain full conversion (Table 1, entry 10). Although the 6-*endo* cyclization was the major reaction pathway obtaining a good yield of **3da**, indole **4da** was also isolated from the reaction mixture. Thus, the protecting group used has a strong influence in both the reactivity and the regioselectivity of the reaction, obtaining the best results with the methyl carbamate.

Next, we extended the reaction to substrates bearing additional substituents on the alkene (**1ab-al**, Table 2). In all cases, an electron-rich aromatic ring was used, as we have previously

Table 1. Optimization of Reaction conditions: Protecting Group

entry	1	R ¹	[Pd(II)] (mol %)	t (h)	3	yield (%) ^a	4	yield (%) ^a
1	1aa	OCH ₃	Pd(CH ₃ CN) ₂ Cl ₂ (5)	16 ^b	3aa	85		
2	1ba	O <i>t</i> Bu	Pd(CH ₃ CN) ₂ Cl ₂ (5)	16 ^b	3ba,	38		
3	1ba	O <i>t</i> Bu	Pd(CH ₃ CN) ₂ Cl ₂ (10)	1.5 ^b	3ba	58	4ba	16
4	1ba	O <i>t</i> Bu	Pd(PhCN) ₂ Cl ₂ (10)	1.5 ^b	3ba	56	4ba	13
5	1ba	O <i>t</i> Bu	Pd(PhCN) ₂ Cl ₂ (10) ^c	2 ^b	3ba	59	4ba	15
6	1ba	O <i>t</i> Bu	Pd(PhCN) ₂ (BF ₄) ₂ (10) ^c	3 ^b	3ba	16 ^e	4ba	3 ^e
7	1ba	O <i>t</i> Bu	Pd(OAc) ₂ (10) ^c	6 ^b	3ba	21 ^f	4ba	14 ^f
8	1ca	OBn	Pd(CH ₃ CN) ₂ Cl ₂ (10)	3 ^b	3ca	67		
9	1da	CH ₃	Pd(CH ₃ CN) ₂ Cl ₂ (5)	20 ^b	^d			
10	1da	CH ₃	Pd(CH ₃ CN) ₂ Cl ₂ (10)	1 ^g	3da	85	4da	10

^aYield (%) of isolated pure compound. ^bRoom temperature. ^cBoc-Val-OH (20 mol %) was used as ligand. ^dNo reaction. ^eYield determined by ¹H NMR using 4-dimethylaminopyridine (DMAP) as internal standard (55% conversion). ^fYield determined by ¹H NMR using DMAP as internal standard (51% conversion). ^g70 °C.

Table 2. Synthesis of 4-Substituted Dihydroquinolines **5**^a

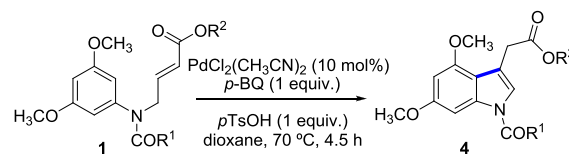
^aYield (%) of isolated pure product by column chromatography. ^bBoc-Val-OH (10 mol %) was used as ligand. ^cPd(PhCN)₂Cl₂ (5 mol %) was used as catalyst. ^d1 mmol scale.

shown in related reactions that it is required to obtain good reactivity.⁶ It is noteworthy that in the all cases, the corresponding 1,4-dihydroquinolines **5** were obtained with complete regioselectivity. No formation of the indoles, or the corresponding 1,2-dihydroquinolines, was detected by NMR. Thus, 2-butenylaniline **1ab** (R¹ = R² = CH₃) gave only a moderate yield of **5ab** (Table 2, 57%), also in the presence of Boc-Val-OH. However, the reaction is best suited for the synthesis of 4-aryl-substituted dihydroquinolines obtaining **5ac**–**5al** with high yields and complete regioselectivity under the standard conditions (Table 2).

The use of Pd(PhCN)₂Cl₂ in the reaction of **1ac** gave **5ac** in a similar yield (79%). However, the use of Boc-Val-OH as ligand improved significantly the yield (**5ac**, **5bc**, **5ak**). The yield of **5ac** was comparable when the reaction was carried out in a 1 mmol scale (85 vs 89% yield). In this case, the use of the *t*-butyl carbamate as protecting group (**1bc**) did not imply a loss of selectivity, as **5bc** was obtained in a similar yield, not detecting the formation of the indole in any case.

The regioselectivity of the reaction completely changed when electron-withdrawing groups were introduced in the

terminal position of the alkene (Table 3). Under the standard conditions, no reaction was observed for **1am**, and in this case,

Table 3. Use Electron-Deficient Alkenes: Synthesis of Indoles **4**

entry	1	R ¹	R ²	4	yield (%) ^a
1	1am	OCH ₃	CH ₃	4am	68
2	1bm	<i>t</i> Bu	CH ₃	4bm	41
3	1an	OCH ₃	Et	4an	68
4	1ao	OCH ₃	<i>n</i> Bu	4ao	63
5	1ap	OCH ₃	<i>t</i> Bu	4ap	54
6	1aq	OCH ₃	Bn	4aq	78

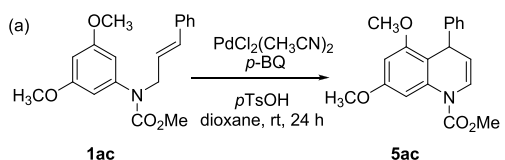
^aYield (%) of isolated pure product.

an increase of the catalyst loading to 10 mol % and heating to 70 °C was required. Under these conditions, indole **4am** was selectively obtained in a moderate yield (Table 3, entry 1). The same result was obtained with the Boc-protected substrate **1bm**, although indole **4bm** was isolated with lower yield (Table 3, entry 2), observing decomposition of the substrate. The reaction could be extended to different esters **1an**–**1aq**, obtaining selectively the indoles **4** with moderate to good yields (Table 3, entries 3–6).

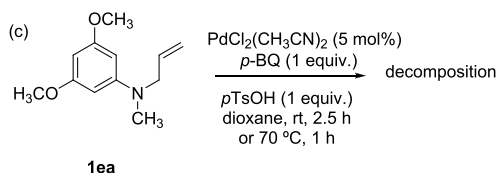
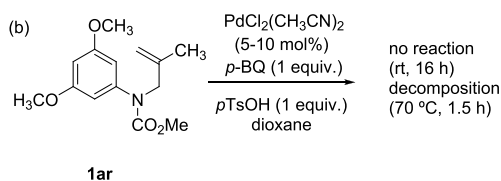
The results obtained show that the regioselectivity of the reaction is strongly influenced on the one hand by the protecting group on the nitrogen and on the other hand by the nature of the alkene, leading to 6-*endo* or 5-*exo* pathways. At this point, additional experiments were carried out to establish the scope and limitations of the reaction and provide additional information on the possible reaction pathway. First, control experiments were carried out with **1ac** (Scheme 4a). In the absence of palladium, the reaction does not take place and unreacted **1ac** is recovered after 24 h at rt. When the reaction was carried out in the absence of *p*-TsOH, decomposition products were obtained. Finally, just a minor amount of **5ac** (<5%) was observed by ¹H NMR when the reaction was performed with no oxidant. The reaction is not compatible with substitution on the internal position of the alkene. Under standard conditions, **1ar** was unreactive, whereas only decomposition products were obtained when the reaction was heated at 70 °C (Scheme 4b). The influence of the protecting group on nitrogen is clear, as only decomposition products were obtained when *N*-methyl aniline **1ea** is treated under the standard reaction conditions at rt or at 70 °C (Scheme 4c).

In view of these results, we next studied the effect of a *p*-toluenesulfonyl group under the reaction conditions. Recently, *N*-allyl-arylsulfonamides have been used as precursors of tetrahydroquinolines in a palladium-catalyzed cascade reaction with benzenesulfonyl chlorides.²⁵ The proposed mechanism involves the initial coordination of the alkene to an arylpalladium(II) intermediate formed by oxidative addition of the sulfonyl chloride to Pd(0). Although the reaction results in a formal 6-*endo* cyclization, the proposed mechanistic pathway does not involve the cyclization of a substituted alkene. Under our reaction conditions, sulfonamide **1fa** gave

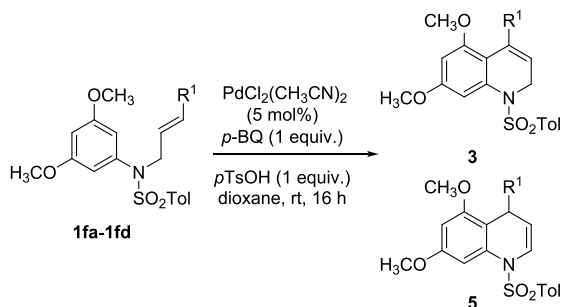
Scheme 4. Additional Experiments



- (a1) no $\text{PdCl}_2(\text{CH}_3\text{CN})_2$; BQ (1 equiv.), *p*-TsOH (1 equiv.): no reaction
 (a2) $\text{PdCl}_2(\text{CH}_3\text{CN})_2$ (5 mol%); BQ (1 equiv.), no *p*-TsOH: decomposition
 (a3) $\text{PdCl}_2(\text{CH}_3\text{CN})_2$ (5 mol%); no BQ, *p*-TsOH (1 equiv.): < 5% **5ac**



1,2-dihydroquinoline **3fa** with complete regioselectivity in an excellent yield (Table 4, entry 1), comparable to that obtained

Table 4. Use of *N*-Tosyl-Protected Anilines **1f**

entry	1	R ¹	3	yield (%) ^a	5	yield (%) ^a
1	1fa	H	3fa	87	5fa	
2	1fb	CH ₃	3fb	64	5fb	26
3	1fc	Ph	3fc		5fc	42
4	1fd	Bn	3fd		5fd	60

^aYield (%) of isolated pure product.

with carbamate **1aa** (Table 1, entry 1). However, **1fb** afforded a regioisomeric mixture of 1,2- and 1,4-dihydroisoquinolines **3fb** and **5fb**, respectively (Table 4, entry 2). In addition, **5fc** and **5fd** were selectively obtained, although with moderate yields (Table 4, entries 3 and 4).

At this point, we decided to examine this reactivity pattern computationally, to get a more precise insight into the mechanistic course of the reaction. Substrate **1aa** was considered as a useful starting point for DFT calculations,²⁶ to explore the main role of the palladium catalyst in the mechanism (alkene activation or arene palladation, Scheme 2), and the subsequent 5-*exo*/6-*endo* selectivity of the cyclization process. Three key features of the reaction ought to be explained during the study, namely, the unusual 6-*endo* selectivity, the large influence of the *N*-protecting group on

the reaction outcome, and the preference for 1,2- or 1,4-dihydroquinoline final product depending on the nature of the substituent at the alkene terminus. According to Scheme 2a, a hypothetical arene palladation would be followed by a *syn* insertion of the alkene into the Ar–Pd bond, which could occur through 5-*exo* or 6-*endo* pathways. Interestingly, the DFT-computed activation barriers for palladium complexes of very diverse electronic properties show a general high preference for 5-*exo* insertion (Figure 2) in disagreement with the experimental results.

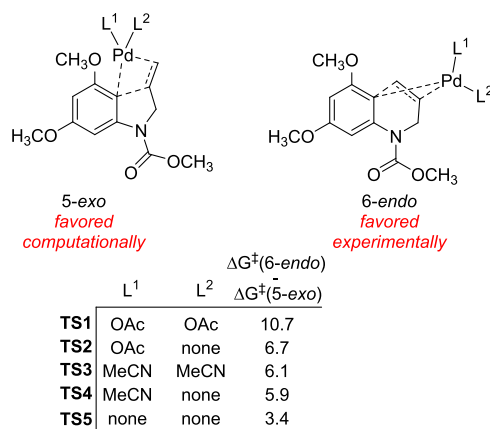


Figure 2. Computed activation energies for the alkene insertion into the Ar–Pd bond with complexes of different electronic properties.

While this phenomenon presents no exception, more electron-rich complexes like the anionic Pd(II) species in **TS1** show the largest *exo/endo* energy difference ($\Delta\Delta G^\ddagger = 10.7$ kcal/mol). Decreasing the electronic charge in the metal center reduces consistently the *exo* preference (note the trend from **TS1** to **TS5** in Figure 2), but even the dicationic Pd complex in **TS5**, which lacks L1 and L2, is still not able to explain the formation of the quinoline moiety ($\Delta\Delta G^\ddagger = 3.4$ kcal/mol). Thus, these data served to clearly discard a mechanism involving cyclization after a previous arene palladation step, as hypothesized in Scheme 2a.

Meanwhile, low activation barriers were measured when the palladium complexes are activating the alkene toward an S_EAr cyclization step (Scheme 2b). However, once again, the major product of the reaction was predicted to be the 5-*exo* derivative, by a difference of 0.8 kcal/mol when an acetate is coordinated to the metal center (**TS6**, Figure 3) and 2.2 kcal/mol for the chloride derivative. Noteworthy, if the coordination of the oxygen of the carbamate to the palladium center is considered (Figure 4),²⁷ the interesting effect of a complete

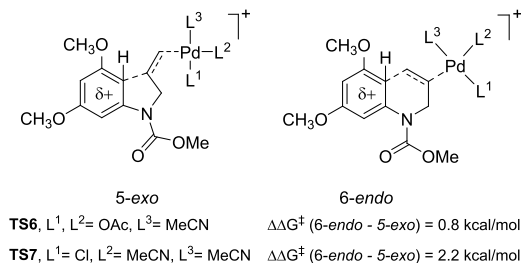


Figure 3. Predicted *endo/exo* selectivity of the S_EAr to the Pd(II) activated alkene.

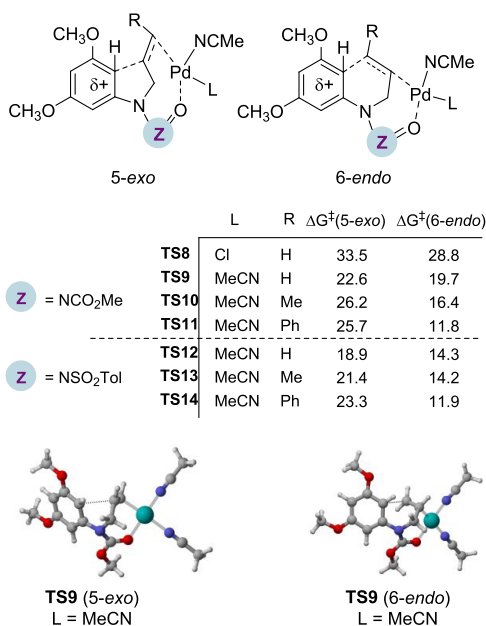


Figure 4. Computed activation energies for the cyclization after alkene activation by the Pd complexes.

inversion of the *endo/exo* selectivity is observed. In all cases, the quinoline adduct becomes the preferred adduct (TS8–TS11), as experimentally noted. If a chloride is still coordinated to palladium, as in TS8, the activation energies are high, over 28 kcal/mol. The replacement of the chloride by a second molecule of MeCN reduces the values below 20 kcal/mol, predicting a feasible reaction in the experimental conditions. The *endo* regioselectivity is general for terminal (TS9) and substituted alkenes (TS10 and TS11), and the energy difference with respect to the 5-*exo* counterparts is always high (3.0–10.0 kcal/mol), ensuring a complete regioselectivity. Even more, the tosylamide group can play a similar role, and the activation energies for the 6-*endo* approach are in the three cases (TS12–TS14) largely lower than those of the 5-*exo* transition states. The sense of regioselectivity seems logical since the coordination of the carbamate to palladium induces a larger ring strain in the *exo* structures. On the other hand, the participation of the carbamate in the reaction through intramolecular coordination to the metal can help explain the effect of the different substituents of nitrogen (Table 1). For example, increasing the steric bulkiness of the carbamate (*OtBu*, Table 1, entries 2–8) or replacing the carbamate by an amide (Table 1, entries 9–10) can reduce their coordination ability, affecting negatively the reactivity and/or selectivity of the process.

The formation of different amounts of 1,2- or 1,4-dihydroquinoline products depending on the substitution at the alkene terminus is difficult to rationalize at the first sight. Thus, we calculated the β -elimination of the H atoms at the 2 or 4 positions of the cyclized palladium complexes, to ascertain whether the adduct formation is under kinetic or thermodynamic control. Interestingly, the calculations show that the 1,2-dihydro adduct 3 is slightly (ca. 1 kcal/mol) more stable than 5 regardless of the presence of the R substituent (hydrogen, methyl, phenyl) in the benzylic position, in complete disagreement with the results in Table 4. Thus, the regioselectivity is not dictated by the relative stability of adducts 3 and 5. Gratifyingly, during the study of the kinetic

conditions, the substrate bearing a terminal alkene (R = H, TS15, Figure 5) was predicted to be deprotonated

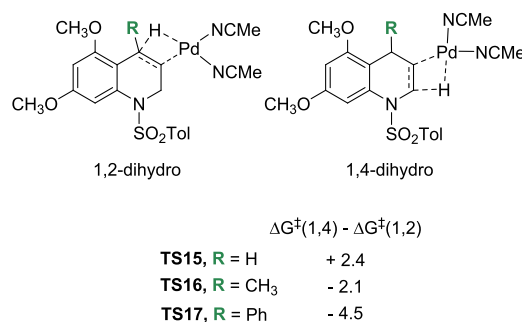
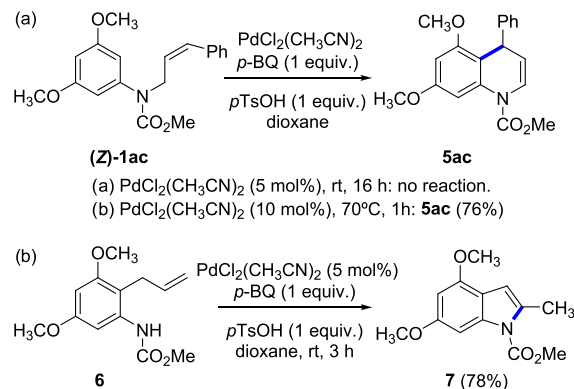


Figure 5. Computed activation energies for the β -elimination step and comparison of the 1,2- and 1,4-dihydro pathways.

preferentially ($\Delta\Delta G^\ddagger = 2.4$ kcal/mol) at the benzylic position to afford the 1,2-dihydro adduct, as in the experimental result (entry 1, Table 4). The conjugation of the forming double bond is probably responsible for this behavior. On the other hand, with phenyl as substituent (TS17), the computed and experimental selectivities also match, favoring the major 1,4-dihydro product. The steric hindrance between MeO/Ph and Ph/Pd moieties probably induces a severe increase in the activation barrier of the 1,2-dihydro transition state. The methyl group shows a mixed behavior; while TS16 is energetically in between the two other cases, the reaction is experimentally nonselective (entry 2, Table 4). Nonetheless, the calculations are not able to predict correctly the right sense of selectivity for the methyl case, probably due to its borderline character.

Along these lines, we also found that the reaction is not stereospecific, and 1,4-dihydroquinoline is formed, regardless of the geometry of the double bond in the starting material. Thus, (Z)-1ac required heating at 70 °C and 10 mol % of catalyst to react, but yielded 1,4-dihydroquinoline 5ac with good yield, not detecting the formation of the 1,2-dihydroquinoline (Scheme 5a). A mechanism involving a

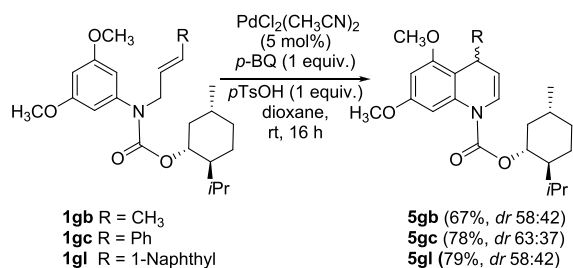
Scheme 5. Additional Experiments



palladium-catalyzed Claisen rearrangement followed by a 5-*exo* oxidative cyclization has been proposed for the obtention of benzofurans from allyl aryl ethers.^{5b} To rule out a related mechanism for the formation of the dihydroquinolines, the Claisen transposition product of 1aa (*o*-allylaniline 6) was prepared. Under the standard reaction conditions, the aza-Wacker reaction took place efficiently in only 3 h at rt, but

exclusively through a 5-*exo* pathway, leading to 2-methylindole 7 in high yield (Scheme 5b). Finally, we studied the cyclization reaction using a chiral nonracemic carbamate as protecting group on the nitrogen. For this purpose, we selected the carbamate derived from (–)-menthol as protecting group. We reasoned that the coordination of the carbonyl with palladium in transition states such as those depicted in Figure 4 could favor a closer disposition of the auxiliary to the stereocenter being formed, and thus some extent of diastereoselectivity could be obtained that would not be expected without the coordination effect. As shown in Scheme 6, the reaction took

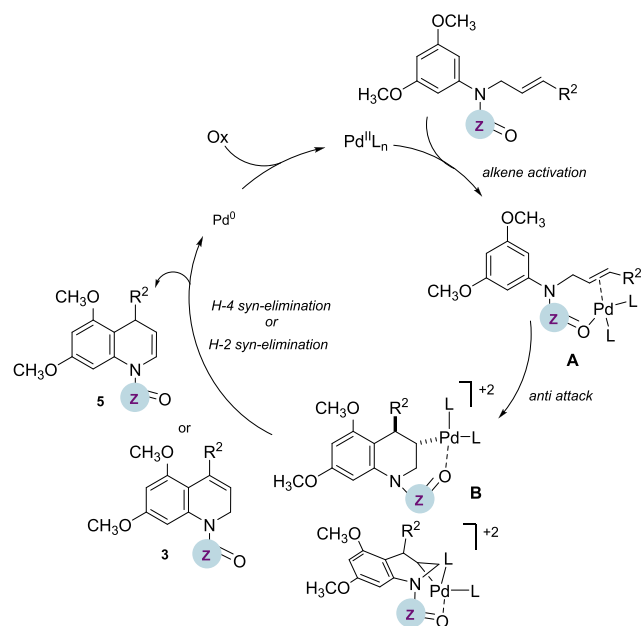
Scheme 6. Cyclization of Carbamates 1g



place in a good yield, and with modest, but appreciable, diastereoselectivity in the case of 5gc.²⁸ Thus, the possibility of a modest 1,7-induction supports the coordination of the remote protecting group with palladium in the transition state, leading to the C–C bond formation.

To sum up, a reaction pathway proposal in accordance with the computational and experimental data is shown in Scheme 7. Thus, the cyclization reaction would involve attack of the

Scheme 7. Mechanistic Proposal



electron-rich aromatic ring onto the palladium-complexed olefin of A. As discussed earlier (see Figures 3 and 4), the formation of intermediate B through a 6-*endo* process would be energetically favored by the effect of the coordination of palladium to the oxygen atom of protecting group on nitrogen. Finally, *syn* β-hydride elimination of H-2 or H-4 would account

for the formation of 1,2-dihydro- or 1,4-dihydroquinolines 3 or 5 respectively. The formation of the more stable 1,2-dihydroquinoline is favored when R² = H, whereas H-4 elimination is preferential when R² = Ar (Figure 5).

In conclusion, an efficient procedure for the synthesis of 4-substituted 1,4-dihydroquinolines via Pd(II)-catalyzed 6-*endo* intramolecular C–H alkenylation reaction of readily accessible *N*-allylanilines has been developed. The regioselectivity is controlled by the nature of the protecting group on the nitrogen atom. DFT studies have provided understanding of the factors that govern this unusual 6-*endo* process, in agreement with the observed outcome of these cyclizations. The reaction proceeds via prior activation of the alkene, being the coordination of the remote protecting group to the palladium center crucial to favor the formation of the six-membered ring.

EXPERIMENTAL SECTION

General Experimental Methods. Melting points were determined in unsealed capillary tubes and are uncorrected. IR spectra were obtained using an attenuated total reflectance (ATR). NMR spectra were recorded at 20–25 °C, at 300 MHz for ¹H and 75.5 MHz for ¹³C in CDCl₃ solutions. Assignments of individual ¹³C and ¹H resonances are supported by DEPT experiments and 2D correlation experiments (COSY, HSQCed or HMBC). Mass spectra were recorded under electron impact (EI) at 70 eV, chemical ionization (CI) at 230 eV, or with an ESI⁺ source. Exact mass was obtained using a TOF detector. TLC was carried out with 0.2 mm thick silica gel plates. Visualization was accomplished by UV light. Flash column chromatography was performed on silica gel (230–400 mesh). All solvents used in the reactions were anhydrous and purified according to standard procedures. All air- or moisture-sensitive reactions were performed under argon; the glassware was dried (130 °C) and purged with argon. Heating blocks with temperature control were used, when necessary, for the reactions that required heating. Palladium catalysts were commercially available and were used without further purification: PdCl₂(CH₃CN)₂ (99% purity), Pd(OAc)₂ (98%), and Pd(CHCN)₄(BF₄)₂ (99.9%).

Computational Methods. All structures were optimized using density functional theory (DFT) as implemented in Gaussian with B3LYP as functional, 6-31G** as basis set for nonmetallic atoms, and LANL2DZ as basis set for palladium. Final energies were obtained performing single-point calculations on the previously optimized structures using the M06 functional, 6-311 + G** as basis set for nonmetallic atoms and SDD for palladium. Solvation factors were introduced with the IEF-PCM method, using 1,4-dioxane as solvent. The stationary points were characterized by frequency calculations to verify that they have the right number of imaginary frequencies.

Synthesis of Substituted *N*-allylanilines 1. Substrates 1 were prepared following the synthetic schemes described in the Supporting Information (Schemes S1–S3).

Alkylation Reactions. Synthesis of Substituted *N*-allylanilines 1a,b,c,g. General Procedure (Scheme S1a–c). Over a solution of the corresponding *N*-protected 3,5-dimethoxyaniline (1 mmol) in dry DMF (15 mL) at 0 °C under argon atmosphere, NaH (60% in mineral oil) (1.1 mmol) was added. The reaction was stirred at 0 °C for 1 h, and afterward, the corresponding allyl chloride (1.2 mmol) was added. Then, the reaction was allowed to warm up to room temperature and stirred for 3–7.5 h. Afterward, water (20 mL) was added and the aqueous layer was extracted with AcOEt (3 × 15 mL). The organic extracts were dried (Na₂SO₄) and concentrated in vacuo. Flash column chromatography (silica gel, hexane/AcOEt) afforded the corresponding *N*-substituted *N*-allyl-3,5-dimethoxyanilines 1aa–1gc.

Methyl Allyl(3,5-dimethoxyphenyl)carbamate (1aa). Prepared from methyl (3,5-dimethoxyphenyl)carbamate (0.64 g, 3.03 mmol), NaH (60% in mineral oil) (0.13 g, 3.33 mmol), and allyl chloride (0.30 mL, 3.64 mmol). The reaction mixture was stirred at room

temperature for 3 h. After workup and purification by flash column chromatography (silica gel, hexane/AcOEt 7/3), **1aa** was obtained as an oil (0.69 g, 91%): ^1H NMR (300 MHz, CDCl_3): δ 3.64 (s, 3H), 3.69 (s, 6H), 4.15–4.21 (m, 2H), 5.05–5.17 (m, 2H), 5.86 (ddt, J = 17.0, 10.2, 5.8 Hz, 1H), 6.30 (t, J = 2.2 Hz, 1H), 6.36 (d, J = 2.2 Hz, 2H) ppm; $^{13}\text{C}\{^1\text{H}\}$ NMR (75.5 MHz, CDCl_3): δ 52.7, 53.2, 55.2, 98.5, 106.1, 116.9, 133.9, 143.7, 155.6, 160.7 ppm; IR (ATR): 1702 cm^{-1} ; MS (EI) m/z (rel intensity): 251.1 (M^+ , 93), 236.1 (100); HRMS (CI-TOF): calcd for $\text{C}_{13}\text{H}_{18}\text{NO}_4$: 252.1236 [MH^+]; found, 252.1234.

(*E*)-Methyl-but-2-en-1-yl(3,5-dimethoxyphenyl)carbamate (**1ab**). Prepared from methyl (3,5-dimethoxyphenyl)carbamate (0.46 g, 2.20 mmol), NaH (60% in mineral oil) (96.7 mg, 2.42 mmol), and (*E*)-1-chlorobut-2-ene (0.26 mL, 2.64 mmol). The reaction mixture was stirred at room temperature for 7 h. After workup and purification by flash column chromatography (silica gel, hexane/AcOEt 8/2), **1ab** was obtained as an oil and as a mixture of rotamers in a 75:25 ratio (0.51 g, 88%): ^1H NMR (300 MHz, CDCl_3): δ 1.57 (d, J = 6.0 Hz, 3H, minor rotamer), 1.64–1.68 (m, 3H, major rotamer), 3.69 (s, 3H, both rotamers), 3.76 (s, 6H, both rotamers), 4.07–4.22 (m, 2H, major rotamer), 4.27 (d, J = 6.3 Hz, minor rotamer), 5.53–5.62 (m, 2H, both rotamers), 6.33–6.40 (m, 3H, both rotamers) ppm; $^{13}\text{C}\{^1\text{H}\}$ NMR (75.5 MHz, CDCl_3): δ 12.8 (minor rotamer), 17.7 (major rotamer), 47.2 (minor rotamer), 52.6 (major rotamer), 52.8 (both rotamers), 55.3 (both rotamers), 98.6 (major rotamer), 98.7 (minor rotamer), 106.4 (both rotamers), 126.1 (minor rotamer), 126.5 (major rotamer), 127.1 (minor rotamer), 128.6 (major rotamer), 143.8 (both rotamers), 155.7 (major rotamer), 155.8 (minor rotamer), 160.7 (minor rotamer), 160.8 (major rotamer) ppm; IR (ATR): 1702 cm^{-1} ; MS (EI) m/z (rel intensity): 265.2 (M^+ , 49), 236.1 (100); HRMS (ESI-TOF): calcd for $\text{C}_{14}\text{H}_{20}\text{NO}_4$: 266.1392 [MH^+]; found, 266.1403.

Methyl Cinnamyl(3,5-dimethoxyphenyl)carbamate (**1ac**). Prepared from methyl (3,5-dimethoxyphenyl)carbamate (0.30 g, 1.43 mmol), NaH (60% in mineral oil) (62.9 mg, 1.57 mmol), and cinnamyl chloride (0.24 mL, 1.71 mmol). The reaction mixture was stirred at room temperature for 3 h. After workup and purification by flash column chromatography (silica gel, hexane/AcOEt 7/3), **1ac** was obtained as an oil (0.45 g, 70%): ^1H NMR (300 MHz, CDCl_3): δ 3.74 (s, 9H), 4.40 (d, J = 6.2 Hz, 2H), 6.07–6.60 (m, 5H), 7.12–7.41 (m, 5H) ppm; $^{13}\text{C}\{^1\text{H}\}$ NMR (75.5 MHz, CDCl_3): δ 52.9, 53.0, 55.4, 98.8, 106.5, 125.1, 126.5, 127.7, 128.6, 132.6, 136.7, 143.7, 155.9, 160.9 ppm; IR (ATR): 1702 cm^{-1} ; MS (EI) m/z (rel intensity): 327.2 (M^+ , 16), 236.1 (56), 117.1 (100); HRMS (ESI-TOF): calcd for $\text{C}_{19}\text{H}_{22}\text{NO}_4$: 328.1549 [MH^+]; found, 328.1565.

Methyl (*Z*)-(3,5-Dimethoxyphenyl)(3-phenylallyl)carbamate (**(Z)-1ac**). Prepared from methyl (3,5-dimethoxyphenyl)carbamate (0.45 g, 2.1 mmol), NaH (60% in mineral oil) (93.5 mg, 2.3 mmol), and (*Z*)-(3-chloroprop-1-en-1-yl)benzene²⁹ (0.39 g, 2.5 mmol). The reaction mixture was stirred at room temperature for 5.5 h. After workup and purification by flash column chromatography (silica gel, hexane/AcOEt 8/2), (*Z*)-**1ac** was obtained as a solid (0.54 g, 78%): mp (CH_2Cl_2) 65–67 °C; ^1H NMR (300 MHz, CDCl_3): δ 3.72 (s, 6H), 3.74 (s, 3H), 4.60 (dd, J = 6.3, 1.8 Hz, 2H), 5.84 (dt, J = 12.0, 6.3 Hz, 1H), 5.35–5.38 (m, 1H), 6.39 (d, J = 2.0 Hz, 2H), 6.58 (d, J = 12.0 Hz, 1H), 7.11–7.35 (m, 5H) ppm; $^{13}\text{C}\{^1\text{H}\}$ NMR (75.5 MHz, CDCl_3): δ 48.7, 53.0, 55.3, 98.8, 105.1, 127.1, 128.3, 128.7, 128.8, 131.1, 136.5, 143.5, 155.8, 160.8 ppm; IR (ATR): 1690 cm^{-1} ; MS (ESI) m/z (rel intensity): 328.2 (MH^+ , 60), 224.1 (100); HRMS (ESI-TOF): calcd for $\text{C}_{19}\text{H}_{22}\text{NO}_4$: 328.1549 [MH^+]; found, 328.1548.

Methyl (3,5-Dimethoxyphenyl)(2-methylallyl)carbamate (**1ar**). Prepared from methyl (3,5-dimethoxyphenyl)carbamate (0.22 g, 1.05 mmol), NaH (60% in mineral oil) (46.3 mg, 1.16 mmol), and 3-chloro-2-methylprop-1-ene (0.12 mL, 1.26 mmol). The reaction mixture was stirred at room temperature for 3 h. After workup and purification by flash column chromatography (silica gel, hexane/AcOEt 6/4), **1ar** was obtained as an oil (0.25 g, 89%): ^1H NMR (300 MHz, CDCl_3): δ 1.75 (s, 3H), 3.71 (s, 3H), 3.76 (s, 6H), 4.18 (s, 2H), 4.80–4.88 (m, 2H), 6.30–6.36 (m, 1H), 6.41 (d, J = 1.5 Hz,

2H) ppm; $^{13}\text{C}\{^1\text{H}\}$ NMR (75.5 MHz, CDCl_3): δ 20.1, 53.0, 55.4, 56.2, 98.2, 104.9, 112.0, 141.2, 143.9 (C_1), 156.0, 160.6 ppm; IR (ATR): 1706 cm^{-1} ; MS (EI) m/z (rel intensity): 265.2 (M^+ , 80), 250.2 (100); HRMS (ESI-TOF): calcd for $\text{C}_{14}\text{H}_{20}\text{NO}_4$: 266.1392 [MH^+]; found, 266.1401.

tert-Butyl Allyl(3,5-dimethoxyphenyl)carbamate (**1ba**). Prepared from *tert*-butyl (3,5-dimethoxyphenyl)carbamate (0.47 g, 1.86 mmol), NaH (60% in mineral oil) (82.0 mg, 2.05 mmol), and allyl chloride (0.18 mL, 2.24 mmol). The reaction mixture was stirred at room temperature for 4 h. After workup and purification by flash column chromatography (silica gel, hexane/AcOEt 9/1), **1ba** was obtained as an oil (0.39 g, 72%): ^1H NMR (300 MHz, CDCl_3): δ 1.46 (s, 9H), 3.76 (s, 6H), 4.20 (d, J = 5.5 Hz, 2H), 5.07–5.23 (m, 2H), 5.92 (qd, 1H, J = 10.6, 5.5 Hz), 6.31 (t, J = 2.0 Hz, 1H), 6.42 (d, J = 2.0 Hz, 2H) ppm; $^{13}\text{C}\{^1\text{H}\}$ NMR (75.5 MHz, CDCl_3): δ 28.3, 53.0, 55.3, 80.4, 97.9, 104.8, 116.3, 134.4, 144.4, 154.2, 160.5 ppm; IR (ATR): 1699 cm^{-1} ; MS (ESI) m/z (rel intensity): 294.2 (MH^+ , 6), 238.1 (100); HRMS (ESI-TOF): calcd for $\text{C}_{16}\text{H}_{24}\text{NO}_4$: 294.1705 [MH^+]; found, 294.1715.

tert-Butyl Cinnamyl(3,5-dimethoxyphenyl)carbamate (**1bc**). Prepared from *tert*-butyl (3,5-dimethoxyphenyl)carbamate (0.63 g, 2.50 mmol), NaH (60% in mineral oil) (0.11 g, 2.75 mmol), and cinnamyl chloride (0.42 mL, 3.00 mmol). The reaction mixture was stirred at room temperature for 7.5 h. After workup and purification by flash column chromatography (silica gel, hexane/AcOEt 9/1), **1bc** was obtained as a solid (0.91 g, 98%): mp (CH_2Cl_2) 63–64 °C; ^1H NMR (300 MHz, CDCl_3): δ 1.48 (s, 9H), 3.76 (s, 6H), 4.40 (d, J = 6.2 Hz, 2H), 6.22–6.38 (m, 2H), 6.39–6.57 (m, 3H), 7.18–7.42 (m, 5H) ppm; $^{13}\text{C}\{^1\text{H}\}$ NMR (75.5 MHz, CDCl_3): δ 28.3, 52.6, 55.4, 80.5, 98.1, 105.0, 125.8, 126.4, 127.5, 128.5, 131.9, 136.9, 144.6, 154.3, 160.6 ppm; IR (ATR): 1685 cm^{-1} ; MS (ESI) m/z (rel intensity): 370.2 (MH^+ , 6), 314.1 (100); HRMS (ESI-TOF): calcd for $\text{C}_{22}\text{H}_{28}\text{NO}_4$: 370.2018 [MH^+]; found, 370.2024.

Benzyl Allyl(3,5-dimethoxyphenyl)carbamate (**1ca**). Prepared from benzyl (3,5-dimethoxyphenyl)carbamate (0.40 g, 1.41 mmol), NaH (60% in mineral oil) (61.9 mg, 1.55 mmol), and allyl chloride (0.14 mL, 1.69 mmol). The reaction mixture was stirred at room temperature for 5 h. After workup and purification by flash column chromatography (silica gel, hexane/AcOEt 9/1), **1ca** was obtained as an oil (0.40 g, 86%): ^1H NMR (300 MHz, CDCl_3): δ 3.76 (s, 6H), 4.28 (dt, J = 5.8, 1.4 Hz, 2H), 5.12–5.24 (m, 4H), 5.85–6.03 (m, 1H), 6.37 (t, J = 2.2 Hz, 1H), 6.43 (d, J = 2.2 Hz, 2H), 7.25–7.41 (m, 5H) ppm; $^{13}\text{C}\{^1\text{H}\}$ NMR (75.5 MHz, CDCl_3): δ 53.3, 55.3, 67.3, 98.8, 106.1, 117.1, 127.8, 127.9, 128.4, 133.9, 136.6, 143.8, 155.1, 160.7 ppm; IR (ATR): 1702 cm^{-1} ; MS (ESI) m/z (rel intensity): 328.2 (MH^+ , 93); HRMS (ESI-TOF): calcd for $\text{C}_{19}\text{H}_{22}\text{NO}_4$: 328.1541 [MH^+]; found, 328.1558.

N-Allyl-*N*-(3,5-Dimethoxyphenyl)acetamide (**1da**). Prepared from *N*-(3,5-dimethoxyphenyl)acetamide (0.28 g, 1.43 mmol), NaH (60% in mineral oil) (62.9 mg, 1.57 mmol), and allyl chloride (0.14 mL, 1.72 mmol). The reaction mixture was stirred at room temperature for 3 h. After workup and purification by flash column chromatography (silica gel, hexane/AcOEt 5/5), **1da** was obtained as an oil (0.32 g, 97%): ^1H NMR (300 MHz, CDCl_3): δ 1.80 (s, 3H), 3.67 (s, 6H), 4.26 (d, J = 6.2 Hz, 2H), 5.02–5.20 (m, 2H), 5.87 (ddt, J = 16.8, 10.7, 6.2 Hz, 1H), 6.31 (d, J = 2.1 Hz, 2H), 6.42 (t, J = 2.1 Hz, 1H) ppm; $^{13}\text{C}\{^1\text{H}\}$ NMR (75.5 MHz, CDCl_3): δ 22.5, 51.8, 55.4, 99.5, 106.4, 117.7, 133.3, 144.7, 161.2, 169.9 ppm; IR (ATR): 1652 cm^{-1} ; MS (EI) m/z (rel intensity): 235.1 (M^+ , 84), 192.1 (100); HRMS (CI-TOF): m/z calcd for $\text{C}_{13}\text{H}_{18}\text{NO}_3$: 236.1287 [MH^+]; found, 236.1294.

(1*R*,2*S*,5*R*)-2-Isopropyl-5-methylcyclohexyl Allyl(3,5-dimethoxyphenyl)carbamate (**1ga**). Prepared from (1*R*,2*S*,5*R*)-2-isopropyl-5-methylcyclohexyl (3,5-dimethoxyphenyl)carbamate (**A**, see below) (0.45 g, 1.36 mmol), NaH (60% in mineral oil) (59.6 mg, 1.49 mmol), and allyl chloride (0.13 mL, 1.63 mmol). The reaction mixture was stirred at room temperature for 4 h. After workup and purification by flash column chromatography (silica gel, hexane/AcOEt 9/1), **1ga** was obtained as an oil (0.37 g, 72%): $[\alpha]_D^{20}$ –36.9 (c 2.75, CH_2Cl_2); ^1H NMR (300 MHz, CDCl_3): δ 0.73–0.93 (m, 10H), 0.93–1.14 (m, 2H), 1.22–1.38 (m, 1H), 1.39–1.57 (m,

1H), 1.58–1.71 (m, 2H), 1.86–1.99 (m, 1H), 2.05–2.16 (m, 1H), 3.76 (s, 6H), 4.23 (d, $J = 5.6$ Hz, 2H), 4.62 (td, $J = 10.8, 4.3$ Hz, 1H), 5.11–5.22 (m, 2H), 5.84–6.00 (m, 1H), 6.32 (t, $J = 2.2$ Hz, 1H), 6.42 (d, $J = 2.2$ Hz, 2H) ppm; $^{13}\text{C}\{^1\text{H}\}$ NMR (75.5 MHz, CDCl_3): δ 16.3, 20.8, 22.0, 23.4, 26.2, 31.4, 34.3, 41.2, 47.1, 53.1, 55.3, 75.8, 98.4, 104.9, 116.7, 134.2, 144.2, 155.0, 160.6 ppm; IR (ATR): 1700 cm^{-1} ; MS (ESI) m/z (rel intensity): 376.2 (MH^+ , 23), 238.1 (87); HRMS (ESI-TOF): calcd for $\text{C}_{22}\text{H}_{34}\text{NO}_4$: 376.2488 [MH^+]; found, 376.2491.

(1*R*,2*S*,5*R*)-2-isopropyl-5-methylcyclohexyl (3,5-dimethoxyphenyl)-carbamate (**A**): Over a solution of commercially available 3,5-dimethoxyaniline (0.67 g, 4.4 mmol) and pyridine (0.69 g, 8.8 mmol) in dry THF (20 mL) under argon atmosphere, (1*R*)-(-)-menthyl chloroformate (1.1 mL, 4.8 mmol) was added dropwise. The reaction was stirred for 16 h at room temperature, and afterward, the solvent was removed under reduced pressure. The crude reaction was dissolved in CH_2Cl_2 (30 mL) and washed with a 10% aqueous solution of HCl (2 \times 15 mL) and with water (15 mL). The combined organic extracts were dried (Na_2SO_4) and concentrated in vacuo. The resulting residue was purified by flash column chromatography (silica gel, petroleum ether/AcOEt 9/1) affording the title compound as a solid (1.1 g, 75%): mp (CH_2Cl_2) 89–91 $^\circ\text{C}$; $[\alpha]_{\text{D}}^{20} -118.4$ (c 1.15, CH_2Cl_2); ^1H NMR (300 MHz, CDCl_3): δ 0.75–0.91 (m, 10H), 0.93–1.13 (m, 2H), 1.24–1.38 (m, 1H), 1.38–1.57 (m, 1H), 1.60–1.70 (m, 2H), 1.88–2.02 (m, 1H), 2.01–2.11 (m, 1H), 3.74 (s, 6H), 4.62 (td, $J = 10.8, 4.3$ Hz, 1H), 6.16 (t, $J = 2.2$ Hz, 1H), 6.66 (d, $J = 2.2$ Hz, 2H), 6.91 (br s, 1H) ppm; $^{13}\text{C}\{^1\text{H}\}$ NMR (75.5 MHz, CDCl_3): δ 16.4, 20.8, 22.0, 23.5, 26.2, 31.4, 34.2, 41.3, 47.2, 55.3, 75.1, 95.7, 96.7, 140.2, 153.4, 161.1 ppm; IR (ATR): 3357, 1739 cm^{-1} ; MS (ESI) m/z (rel intensity): 358.2 (MNa^+ , 100), 198.1 (18); HRMS (ESI-TOF): calcd for $\text{C}_{19}\text{H}_{29}\text{NO}_4\text{Na}$: 358.1994 [MNa^+]; found, 358.1993.

(1*R*,2*S*,5*R*)-2-isopropyl-5-methylcyclohexyl [(*E*)-but-2-en-1-yl](3,5-dimethoxyphenyl)carbamate (**1gb**). Prepared from **A** (0.42 g, 1.3 mmol), NaH (60% in mineral oil) (55.4 mg, 1.4 mmol), and crotyl chloride (0.15 mL, 1.5 mmol). The reaction mixture was stirred at room temperature for 7 h. After workup and purification by flash column chromatography (silica gel, hexane/AcOEt 9/1), **1gb** was obtained as an oil (0.40 g, 82%): $[\alpha]_{\text{D}}^{20} -42.9$ (c 0.74, CH_2Cl_2); ^1H NMR (300 MHz, CDCl_3): δ 0.77–0.92 (m, 10H), 0.92–1.09 (m, 2H), 1.24–1.36 (m, 1H), 1.42–1.54 (m, 1H), 1.57–1.66 (m, 2H), 1.67 (d, $J = 4.0$ Hz, 3H), 1.86–1.96 (m, 1H), 2.07–2.15 (m, 1H), 3.77 (s, 6H), 4.09–4.34 (m, 2H), 4.61–4.72 (dt, $J = 10.8, 4.3$ Hz, 1H), 5.49–5.65 (m, 2H), 6.32 (t, $J = 2.0$ Hz, 1H), 6.40 (br s, 2H) ppm; $^{13}\text{C}\{^1\text{H}\}$ NMR (75.5 MHz, CDCl_3): δ 16.3, 17.7, 20.9, 22.1, 23.4, 26.2, 31.4, 34.3, 41.3, 47.2, 52.5, 55.4, 75.7, 98.4, 105.1, 126.8, 128.2, 144.3, 155.0, 160.5 ppm; IR (ATR): 1695 cm^{-1} ; MS (ESI) m/z (rel intensity): 412.2 (MNa^+ , 100); HRMS (ESI-TOF): calcd for $\text{C}_{23}\text{H}_{35}\text{NO}_4\text{Na}$: 412.2464 [MNa^+]; found, 412.2455.

(1*R*,2*S*,5*R*)-2-isopropyl-5-methylcyclohexyl cinnamyl(3,5-dimethoxyphenyl)carbamate (**1gc**). Prepared from **A** (0.21 g, 0.64 mmol), NaH (60% in mineral oil) (28.1 mg, 0.70 mmol), and cinnamyl chloride (0.11 mL, 0.77 mmol). The reaction mixture was stirred at room temperature for 7 h. After workup and purification by flash column chromatography (silica gel, hexane/AcOEt 9/1), **1gc** was obtained as an oil (0.21 g, 71%): $[\alpha]_{\text{D}}^{20} -95.2$ (c 1.05, CH_2Cl_2); ^1H NMR (300 MHz, CDCl_3): δ 0.77–0.94 (m, 10H), 0.94–1.15 (m, 2H), 1.26–1.39 (m, 1H), 1.41–1.58 (m, 1H), 1.60–1.75 (m, 2H), 1.88–2.06 (m, 1H), 2.10–2.20 (m, 1H), 3.75 (s, 6H), 4.31–4.49 (m, 2H), 4.61–4.72 (m, 1H), 6.25–6.37 (m, 2H), 6.43–6.54 (m, 3H), 7.19–7.38 (m, 5H) ppm; $^{13}\text{C}\{^1\text{H}\}$ NMR (75.5 MHz, CDCl_3): δ 16.3, 20.8, 22.1, 23.4, 26.3, 31.4, 34.3, 41.3, 47.2, 52.7, 55.4, 75.9, 98.6, 105.0, 125.5, 126.4, 127.6, 128.5, 132.1, 136.8, 144.2, 155.1, 160.7 ppm; IR (ATR): 1695 cm^{-1} ; MS (ESI) m/z (rel intensity): 474.3 (MNa^+ , 77), 314.1 (10); HRMS (ESI-TOF): calcd for $\text{C}_{28}\text{H}_{37}\text{NO}_4\text{Na}$: 474.2620 [MNa^+]; found, 474.2623.

N-allyl-3,5-dimethoxy-*N*-methylaniline (**1ea**) (Scheme S1c). Over a solution of 3,5-dimethoxy-*N*-methylaniline (0.20 g, 1.22 mmol) in DMSO (5 mL), powder KOH (0.14 g, 2.47 mmol) was added. After 15 min, allyl bromide (0.13 mL, 1.46 mmol) was added dropwise at

room temperature and the reaction was heated at 50 $^\circ\text{C}$ (heating block with temperature control) for 1 h. Then, water (10 mL) was added and the mixture was extracted with AcOEt (3 \times 10 mL). The combined organic extracts were dried (Na_2SO_4) and concentrated in vacuo. Flash column chromatography (silica gel, petroleum ether/AcOEt 9/1) afforded **1ea** as an oil (0.15 g, 60%): ^1H NMR (300 MHz, CDCl_3): δ 2.94 (s, 3H), 3.79 (s, 6H), 3.91 (dt, $J = 5.1, 1.6$ Hz, 2H), 5.15–5.21 (m, 2H), 5.85 (ddt, $J = 17.0, 10.2, 5.1$ Hz), 5.93 (s, 3H) ppm; $^{13}\text{C}\{^1\text{H}\}$ NMR (75.5 MHz, CDCl_3): δ 38.2, 55.2, 55.3, 88.6, 91.8, 116.2, 133.8, 151.4, 161.6 ppm; IR (ATR): 1612 cm^{-1} ; MS (CI) m/z (rel intensity): 208.1 (MH^+ , 97), 207.1 (100), 176.1 (32); HRMS (CI-TOF): calcd for $\text{C}_{12}\text{H}_{18}\text{NO}_2$: 208.1338 [MH^+]; found, 208.1320.

Alkylation Reactions. Synthesis of Tosylamides 1fa–1fd. General Procedure (Scheme S1d). Over a solution of *N*-(3,5-dimethoxyphenyl)-4-methylbenzenesulfonamide (1 mmol) in dry acetone (20 mL), K_2CO_3 (2.5 mmol) and the corresponding allyl bromide (1.5 mmol) were added under argon atmosphere. The reaction mixture was heated at reflux (heating block) for 16 h and then allowed to cool down to room temperature. Afterward, CH_2Cl_2 (20 mL) was added and the mixture was washed with water (15 mL). The aqueous phase was extracted with CH_2Cl_2 (2 \times 10 mL), and the combined organic extracts were dried (Na_2SO_4) and concentrated in vacuo. Flash column chromatography (silica gel, hexane/AcOEt 8/2) afforded the corresponding *N*-allyl-*N*-(3,5-dimethoxyphenyl)-4-methylbenzenesulfonamides **1fa–1fd**.

N-allyl-*N*-(3,5-dimethoxyphenyl)-4-methylbenzenesulfonamide (**1fa**). Prepared from *N*-(3,5-dimethoxyphenyl)-4-methylbenzenesulfonamide (0.40 g, 1.32 mmol), K_2CO_3 (0.45 g, 3.29 mmol), and allyl bromide (0.17 mL, 1.97 mmol). After workup and purification by flash column chromatography, **1fa** was obtained as a solid (0.41 g, 89%): mp (CH_2Cl_2) 82–84 $^\circ\text{C}$; ^1H NMR (300 MHz, CDCl_3): δ 2.42 (s, 3H), 3.70 (s, 6H), 4.13 (d, $J = 6.1$ Hz, 2H), 5.00–5.18 (m, 2H), 5.64–5.86 (m, 1H), 6.21 (d, $J = 1.8$ Hz, 1H), 6.37 (t, $J = 1.8$ Hz, 1H), 7.26 (d, $J = 8.0$ Hz, 2H), 7.55 (d, $J = 8.0$ Hz, 2H) ppm; $^{13}\text{C}\{^1\text{H}\}$ NMR (75.5 MHz, CDCl_3): δ 21.5, 53.6, 55.4, 100.0, 107.0, 118.7, 127.8, 129.4, 132.8, 135.5, 140.9, 143.5, 160.6 ppm; IR (ATR): 1345 cm^{-1} , 1155 cm^{-1} ; MS (ESI) m/z (rel intensity): 370.1 (MNa^+ , 100), 348.1 (MH^+ , 52), 193.1 (57); HRMS (ESI-TOF): calcd for $\text{C}_{18}\text{H}_{21}\text{NO}_4\text{SNa}$: 370.1089 [MNa^+]; found, 370.1091.

(*E*)-*N*-(but-2-en-1-yl)-*N*-(3,5-dimethoxyphenyl)-4-methylbenzenesulfonamide (**1fb**). Prepared from *N*-(3,5-dimethoxyphenyl)-4-methylbenzenesulfonamide (0.30 g, 0.98 mmol), K_2CO_3 (0.34 g, 2.45 mmol), and crotyl bromide (0.18 mL, 1.47 mmol). After workup and purification by flash column chromatography, **1fb** was obtained as a solid and as a mixture of rotamers in a 83:17 ratio (0.30 g, 83%): mp (CH_2Cl_2) 101–102 $^\circ\text{C}$; ^1H NMR (300 MHz, CDCl_3): δ 1.59–1.54 (m, 3H, minor rotamer), 1.55–1.59 (m, 3H, major rotamer), 2.41 (s, 3H, both rotamers), 3.70 (s, 6H, both rotamers), 4.02–4.09 (m, 2H, major rotamer), 4.14–4.20 (m, 2H, minor rotamer), 5.30–5.58 (m, 2H, both rotamers), 6.19 (d, $J = 2.3$ Hz, 2H, major rotamer), 6.21 (d, $J = 2.3$ Hz, 2H, minor rotamer), 6.36 (t, $J = 2.3$ Hz, 1H, both rotamers), 7.25 (d, $J = 8.3$ Hz, 2H, both rotamers), 7.54 (d, $J = 8.3$ Hz, 2H, both rotamers); $^{13}\text{C}\{^1\text{H}\}$ NMR (75.5 MHz, CDCl_3): δ 12.9 (minor rotamer), 17.7 (major rotamer), 21.5 (both rotamers), 47.4 (minor rotamer), 53.1 (major rotamer), 55.4 (both rotamers), 100.0 (both rotamers), 106.9 (minor rotamer), 107.1 (major rotamer), 124.7 (minor rotamer), 125.5 (major rotamer), 127.8 (major rotamer), 128.4 (minor rotamer), 129.3 (major rotamer), 129.4 (minor rotamer), 130.2 (both rotamers), 135.8 (both rotamers), 141.1 (both rotamers), 143.3 (both rotamers), 160.5 (both rotamers) ppm; IR (ATR): 1285, 1160 cm^{-1} ; MS (ESI) m/z (rel intensity): 384.1 (MNa^+ , 100), 362.1 (MH^+ , 78), 308.1 (24), 207.1 (59); HRMS (ESI-TOF): calcd for $\text{C}_{19}\text{H}_{23}\text{NO}_4\text{SNa}$: 384.1246 [MNa^+]; found, 384.1241.

N-Cinnamyl-*N*-(3,5-dimethoxyphenyl)-4-methylbenzenesulfonamide (**1fc**). Prepared from *N*-(3,5-dimethoxyphenyl)-4-methylbenzenesulfonamide (0.27 g, 0.87 mmol), K_2CO_3 (0.30 g, 2.16 mmol), and cinnamyl bromide (0.26 g, 1.30 mmol). After workup and purification by flash column chromatography, **1fc** was obtained as a solid (0.21 g,

58%): mp (CH₂Cl₂) 123–126 °C; ¹H NMR (300 MHz, CDCl₃): δ 2.41 (s, 3H), 3.68 (s, 6H), 4.32 (dd, *J* = 6.5, 1.0 Hz, 2H), 6.14 (dt, *J* = 15.8, 6.5 Hz, 1H), 6.28 (d, *J* = 2.2 Hz, 2H), 6.38 (t, *J* = 2.2 Hz, 1H), 6.43 (d, *J* = 15.8 Hz, 1H), 7.17–7.30 (m, 7H), 7.61 (d, *J* = 8.3 Hz, 2H); ¹³C{¹H} NMR (75.5 MHz, CDCl₃): δ 21.6, 53.4, 55.4, 100.1, 107.1, 124.2, 126.5, 127.8, 128.6, 129.5, 133.7, 135.7, 136.4, 141.1, 143.6, 160.7 ppm; IR (ATR): 1345, 1155 cm⁻¹; MS (ESI) *m/z* (rel intensity): 446.1 (MNa⁺, 53), 424.2 (MH⁺, 100), 117.1 (89); HRMS (ESI-TOF): calcd for C₂₄H₂₅NNaO₄S: 446.1402 [MNa⁺]; found, 446.1397.

(E)-N-(3,5-dimethoxyphenyl)-4-methyl-N-(4-phenylbut-2-en-1-yl) benzene sulfonamide (1fd). Prepared from *N*-(3,5-dimethoxyphenyl)-4-methylbenzenesulfonamide (0.30 g, 0.99 mmol), K₂CO₃ (0.34 g, 2.47 mmol), and (*E*)-(4-bromobut-2-en-1-yl)benzene³⁰ (0.31 g, 1.48 mmol). After workup and purification by flash column chromatography, **1fd** was obtained as an oil (0.40 g, 92%): ¹H NMR (300 MHz, CDCl₃): δ 2.41 (s, 3H), 3.26 (d, *J* = 6.6 Hz, 2H), 3.67 (s, 6H), 4.16 (d, *J* = 6.4 Hz, 2H), 5.38–5.71 (m, 2H), 6.24 (d, *J* = 2.3 Hz, 2H), 6.42 (t, *J* = 2.3 Hz, 1H), 6.84–6.99 (m, 2H), 7.10–7.30 (m, 5H), 7.58 (d, *J* = 8.3 Hz, 2H) ppm; ¹³C{¹H} NMR (75.5 MHz, CDCl₃): δ 21.6, 38.4, 53.0, 55.4, 100.2, 107.3, 126.0, 126.1, 127.8, 128.4, 128.5, 129.5, 134.1, 135.7, 139.7, 140.9, 143.5, 160.7 ppm; IR (ATR): 1360, 1170 cm⁻¹; MS (ESI) *m/z* (rel intensity): 438.2 (MH⁺, 100), 308.1 (25), 131.1 (22); HRMS (ESI-TOF): calcd for C₂₅H₂₈NO₄S: 438.1739 [MH⁺]; found, 438.1746.

Metathesis Reactions. Synthesis of Carbamates 1ad–1gl. General Procedure (Scheme S2a). Two different procedures were employed depending on the styrene used: In the case of liquid styrene, a solution of allyl(3,5-dimethoxyphenyl)carbamate **1aa** or **1ga** (1 mmol) and the corresponding styrene (5 mmol) in dry CH₂Cl₂ (2.3 mL) was added via *cannula* over a solution of second-generation Grubbs catalyst (0.05 mmol) in dry CH₂Cl₂ (1.1 mL) under argon atmosphere. In the case of solid styrene, a solution of second-generation Grubbs catalyst (0.05 mmol) in dry CH₂Cl₂ (1.1 mL) was added via *cannula* over a solution of allyl(3,5-dimethoxyphenyl)carbamate **1aa** or **1ga** (1 mmol) and the corresponding styrene (5 mmol) in dry CH₂Cl₂ (2.3 mL) under argon atmosphere. In both cases, the reaction mixture was stirred at reflux (heating block) for 24 h and the volatile compounds were evaporated in vacuo. The obtained residue was purified by flash column chromatography (silica gel, petroleum ether/AcOEt) to obtain the corresponding carbamates **1ad–1gl**.

Methyl (E)-(3,5-Dimethoxyphenyl)[3-(*p*-tolyl)allyl]carbamate (1ad). Prepared from **1aa** (0.28 g, 1.13 mmol) and 4-methylstyrene (0.74 mL, 5.65 mmol) in dry CH₂Cl₂ (2.6 mL) and second-generation Grubbs catalyst (48.0 mg, 0.056 mmol) in dry CH₂Cl₂ (1.3 mL). Purification by flash column chromatography (silica gel, petroleum ether/AcOEt 8/2) afforded **1ad** as a solid (0.27 g, 70%): mp (CH₂Cl₂) 93–95 °C; ¹H NMR (300 MHz, CDCl₃): δ 2.34 (s, 3H), 3.74 (s, 3H), 3.76 (s, 6H), 4.38 (d, *J* = 6.3 Hz, 2H), 6.26 (dt, *J* = 15.9, 6.3 Hz, 1H), 6.37 (t, *J* = 2.2 Hz, 1H), 6.40–6.50 (m, 3H), 7.11 (d, *J* = 8.0 Hz, 2H), 7.26 (d, *J* = 8.0 Hz, 2H) ppm; ¹³C{¹H} NMR (75.5 MHz, CDCl₃): δ 21.2, 53.0, 55.4, 98.8, 106.5, 124.0, 126.4, 129.2, 132.5, 133.9, 137.5, 143.7, 155.8, 160.8 ppm; IR (ATR): 1690 cm⁻¹; MS (ESI) *m/z* (rel intensity): 343.2 342.2 (MH⁺, 100), 224.1 (7); HRMS (ESI-TOF): calcd for C₂₀H₂₄NO₄: 342.1705 [MH⁺]; found, 342.1711.

Methyl (E)-(3,5-Dimethoxyphenyl)[3-(*m*-tolyl)allyl]carbamate (1ae). Prepared from **1aa** (0.37 g, 1.49 mmol) and 3-methylstyrene (0.99 mL, 7.44 mmol) in dry CH₂Cl₂ (3.4 mL) and second-generation Grubbs catalyst (63.2 mg, 0.074 mmol) in dry CH₂Cl₂ (1.7 mL). Purification by flash column chromatography (silica gel, petroleum ether/AcOEt 8/2) afforded **1ae** as an oil (0.31 g, 61%): ¹H NMR (300 MHz, CDCl₃): δ 2.36 (s, 3H), 3.75 (s, 3H), 3.76 (s, 6H), 4.39 (d, *J* = 6.1 Hz, 2H), 6.22–6.50 (m, 5H), 6.99–7.29 (m, 4H) ppm; ¹³C{¹H} NMR (75.5 MHz, CDCl₃): δ 21.4, 53.0, 55.4, 98.8, 106.4, 123.6, 124.8, 127.1, 128.4, 132.7, 136.6, 138.1, 143.7, 155.8, 160.8 ppm; IR (ATR): 1702 cm⁻¹; MS (ESI) *m/z* (rel intensity): 342.2 (MH⁺, 100), 224.1 (12); HRMS (ESI-TOF): calcd for C₂₀H₂₄NO₄: 342.1705 [MH⁺]; found, 342.1714.

Methyl (E)-(3,5-Dimethoxyphenyl)[3-(*o*-tolyl)allyl]carbamate (1af). Prepared from **1aa** (0.34 g, 1.36 mmol) and 2-methylstyrene (0.91 mL, 6.78 mmol) in dry CH₂Cl₂ (3.1 mL) and second-generation Grubbs catalyst (57.5 mg, 0.068 mmol) in dry CH₂Cl₂ (1.5 mL). Purification by flash column chromatography (silica gel, petroleum ether/AcOEt 8/2) afforded **1af** as an oil (0.35 g, 75%): ¹H NMR (300 MHz, CDCl₃): δ 2.28 (s, 3H), 3.74 (s, 3H), 3.77 (s, 6H), 4.41 (dd, *J* = 6.4, 1.4 Hz, 2H), 6.15 (dt, *J* = 15.7, 6.4 Hz, 2H), 6.38 (t, *J* = 2.3 Hz, 1H), 6.43 (d, *J* = 2.3 Hz, 2H), 6.68 (d, *J* = 15.7 Hz, 1H), 7.10–7.19 (m, 3H), 7.37–7.43 (m, 1H); ¹³C{¹H} NMR (75.5 MHz, CDCl₃): δ 19.7, 53.0, 55.4, 98.8, 106.5, 125.9, 126.1, 126.4, 127.5, 130.2, 130.8, 135.4, 136.0, 143.6, 155.8, 160.8 ppm; IR (ATR): 1702 cm⁻¹; MS (ESI) *m/z* (rel intensity): 342.2 (MH⁺, 100), 224.1 (13); HRMS (ESI-TOF): calcd for C₂₀H₂₄NO₄: 342.1705 [MH⁺]; found, 342.1712.

Methyl (E)-(3,5-Dimethoxyphenyl)[3-(3-methoxyphenyl)allyl]carbamate (1ah). Prepared from **1aa** (0.13 g, 0.50 mmol) and 3-vinylanisole (0.35 mL, 2.52 mmol) in dry CH₂Cl₂ (1.1 mL) and second-generation Grubbs catalyst (21.4 mg, 0.025 mmol) in dry CH₂Cl₂ (0.6 mL). Purification by flash column chromatography (silica gel, petroleum ether/AcOEt 8/2) afforded **1ah** as an oil (0.11 g, 61%): ¹H NMR (300 MHz, CDCl₃): δ 3.73 (s, 3H), 3.75 (s, 6H), 3.80 (s, 3H), 4.38 (d, *J* = 5.9 Hz, 2H), 6.21–6.53 (m, 5H), 6.76–6.82 (m, 1H), 6.87–6.91 (m, 1H), 6.92–6.98 (m, 1H), 7.17–7.27 (m, 1H) ppm; ¹³C{¹H} NMR (75.5 MHz, CDCl₃): δ 52.9, 53.0, 55.2, 55.4, 98.8, 106.4, 111.8, 113.3, 119.1, 125.4, 129.5, 132.5, 138.2, 143.7, 155.8, 159.8, 160.8 ppm; IR (ATR): 1706 cm⁻¹; MS (ESI) *m/z* (rel intensity): 358.2 (MH⁺, 100), 224.1 (15); HRMS (ESI-TOF): calcd for C₂₀H₂₄NO₄: 358.1654 [MH⁺]; found, 358.1664.

Methyl (E)-[3-([1,1'-Biphenyl]-4-yl)allyl](3,5-dimethoxyphenyl)carbamate (1ai). Prepared from **1aa** (0.35 g, 1.41 mmol) and 4-vinylbiphenyl (1.27 mL, 7.05 mmol) in dry CH₂Cl₂ (3.2 mL) and second-generation Grubbs catalyst (59.8 mg, 0.070 mmol) in dry CH₂Cl₂ (1.6 mL). Purification by flash column chromatography (silica gel, petroleum ether/AcOEt 8/2) afforded **1ai** as a solid (0.23 g, 40%): mp (CH₂Cl₂) 122–125 °C; ¹H NMR (300 MHz, CDCl₃): δ 3.76 (s, 3H), 3.77 (s, 6H), 4.42 (dd, *J* = 6.2, 0.9 Hz, 2H), 6.28–6.58 (m, 5H), 7.30–7.38 (m, 1H), 7.40–7.48 (m, 4H), 7.53–7.63 (m, 4H) ppm; ¹³C{¹H} NMR (75.5 MHz, CDCl₃): δ 53.0, 55.4, 98.8, 106.5, 125.2, 126.9, 127.0, 127.2, 127.3, 128.8, 132.2, 135.7, 140.4, 140.6, 143.7, 155.9, 160.8 ppm; IR (ATR): 1706 cm⁻¹; MS (ESI) *m/z* (rel intensity): 404.2 (MH⁺, 100), 193.1 (8); HRMS (ESI-TOF): calcd for C₂₅H₂₆NO₄: 404.1862 [MH⁺]; found, 404.1859.

Methyl (E)-[3-[4-(*tert*-Butyl)phenyl]allyl](3,5-dimethoxyphenyl)carbamate (1aj). Prepared from **1aa** (0.25 g, 1.01 mmol) and 4-*tert*-butylstyrene (0.92 mL, 5.03 mmol) in dry CH₂Cl₂ (2.3 mL) and second-generation Grubbs catalyst (42.6 mg, 0.050 mmol) in dry CH₂Cl₂ (1.1 mL). Purification by flash column chromatography (silica gel, petroleum ether/AcOEt 9/1) afforded **1aj** as a solid (0.26 g, 67%): mp (CH₂Cl₂) 108–111 °C; ¹H NMR (300 MHz, CDCl₃): δ 1.31 (s, 9H), 3.73 (s, 3H), 3.76 (s, 6H), 4.37 (d, *J* = 5.9 Hz, 2H), 6.15–6.57 (m, 5H), 7.20–7.39 (m, 4H) ppm; ¹³C{¹H} NMR (75.5 MHz, CDCl₃): δ 31.3, 34.4, 53.0, 55.4, 98.7, 106.4, 124.2, 125.5, 126.2, 132.4, 133.9, 143.7, 150.8, 155.8, 160.8 ppm; IR (ATR): 1706 cm⁻¹; MS (ESI) *m/z* (rel intensity): 384.2 (MH⁺, 86), 173.1 (20); HRMS (ESI-TOF): calcd for C₂₃H₃₀NO₄: 384.2175 [MH⁺]; found, 384.2183.

Methyl (E)-(3,5-Dimethoxyphenyl)[3-(4-fluorophenyl)allyl]carbamate (1ak). Prepared from **1aa** (0.31 g, 1.25 mmol) and 4-fluorostyrene (0.74 mL, 6.23 mmol) in dry CH₂Cl₂ (2.8 mL) and second-generation Grubbs catalyst (52.9 mg, 0.062 mmol) in dry CH₂Cl₂ (1.4 mL). Purification by flash column chromatography (silica gel, petroleum ether/AcOEt 8/2) afforded **1ak** as a solid (0.24 g, 56%): mp (CH₂Cl₂) 90–91 °C; ¹H NMR (300 MHz, CDCl₃): δ 3.73 (s, 3H), 3.75 (s, 6H), 4.36 (dd, *J* = 6.3, 1.1 Hz, 2H), 6.21 (dt, *J* = 15.8, 6.3 Hz, 1H), 6.37 (t, *J* = 2.2 Hz, 1H), 6.39–6.49 (m, 3H), 6.93–7.02 (m, 2H), 7.27–7.34 (m, 2H) ppm; ¹³C{¹H} NMR (75.5 MHz, CDCl₃): δ 52.9, 53.0, 55.4, 98.7, 105.5, 115.4 (d, *J* = 21.6 Hz), 124.8 (d, *J* = 2.0 Hz), 128.0 (d, *J* = 8.7 Hz), 131.4, 132.9 (d, *J* = 3.8 Hz), 143.7, 155.8, 160.8, 162.3 (d, *J* = 247.4 Hz) ppm; IR (ATR): 1695

cm⁻¹; MS (ESI) *m/z* (rel intensity): 346.1 (MH⁺, 100), 224.1 (12); HRMS (ESI-TOF): calcd for C₁₉H₂₁FNO₄: 346.1455 [MH⁺]; found: 346.1453.

Methyl (E)-(3,5-Dimethoxyphenyl)[3-(naphthalen-1-yl)allyl]carbamate (1al). Prepared from **1aa** (0.30 g, 1.21 mmol) and 1-vinylnaphthalene (0.90 mL, 6.06 mmol) in dry CH₂Cl₂ (2.8 mL) and second-generation Grubbs catalyst (51.4 mg, 0.061 mmol) in dry CH₂Cl₂ (1.4 mL). Purification by flash column chromatography (silica gel, petroleum ether/AcOEt 8/2) afforded **1al** as an oil (0.32 g, 70%): ¹H NMR (300 MHz, CDCl₃): δ 3.78 (s, 3H), 3.80 (s, 6H), 4.55 (d, *J* = 6.4 Hz, 2H), 6.35 (dt, *J* = 15.9, 6.6 Hz, 1H), 6.45 (t, *J* = 2.0 Hz, 1H), 6.54 (d, *J* = 2.0 Hz, 2H), 7.26 (d, *J* = 15.9 Hz, 1H), 7.42–7.46 (m, 1H), 7.46–7.54 (m, 2H), 7.56–7.61 (m, 1H), 7.76–7.82 (m, 1H), 7.83–7.89 (m, 1H), 7.96–8.05 (m, 1H) ppm; ¹³C{¹H} NMR (75.5 MHz, CDCl₃): δ 53.1, 55.5, 99.0, 105.7, 123.9, 124.1, 125.7, 125.9, 126.1, 128.1, 128.3, 128.6, 130.4, 131.2, 133.6, 134.6, 143.7, 155.9, 161.0 ppm; IR (ATR): 1702 cm⁻¹; MS (ESI) *m/z* (rel intensity): 400.2 (MNa⁺, 100), 378.2 (MH⁺, 94), 224.1 (70), 167.1 (65); HRMS (ESI-TOF): calcd for C₂₃H₂₄NO₄: 378.1705 [MH⁺]; found, 378.1703.

(1R,2S,5R)-2-Isopropyl-5-methylcyclohexyl (3,5-dimethoxyphenyl) [(E)-3-(naphthalene-1-yl) allyl]carbamate (1gl). Prepared from **1ga** (0.28 g, 0.74 mmol) and 1-vinylnaphthalene (0.55 mL, 3.71 mmol) in dry CH₂Cl₂ (1.7 mL) and second-generation Grubbs catalyst (31.5 mg, 0.037 mmol) in dry CH₂Cl₂ (0.84 mL). Purification by flash column chromatography (silica gel, petroleum ether/AcOEt 9/1) afforded **1gl** as an oil (0.23 g, 62%): [α]_D²⁰ = -114.2 (c 0.53, CH₂Cl₂); ¹H NMR (300 MHz, CDCl₃): δ 0.78–0.93 (m, 10H), 0.96–1.16 (m, 2H), 1.29–1.40 (m, 1H), 1.42–1.55 (m, 1H), 1.61–1.74 (m, 2H), 1.89–2.04 (m, 1H), 2.11–2.23 (m, 1H), 3.77 (s, 6H), 4.52 (dd, *J* = 6.1, 1.2 Hz, 2H), 4.69 (td, *J* = 10.8, 4.3 Hz, 1H), 6.19–6.58 (m, 4H), 7.23 (d, *J* = 15.7 Hz, 1H), 7.41–7.62 (m, 4H), 7.74–7.92 (m, 2H), 7.97–8.07 (m, 1H) ppm; ¹³C{¹H} NMR (75.5 MHz, CDCl₃): δ 16.4, 20.8, 22.1, 23.4, 26.3, 31.4, 34.3, 41.3, 47.2, 52.8, 55.4, 76.0, 98.8, 105.2, 123.9, 124.0, 125.6, 125.8, 126.0, 127.9, 128.5, 128.7, 129.8, 131.2, 133.6, 134.7, 144.1, 155.1, 161.7 ppm; IR (ATR): 1700 cm⁻¹; MS (ESI) *m/z* (rel intensity): 502.3 (MH⁺, 36), 364.2 (100); HRMS (ESI-TOF): calcd for C₃₂H₄₀NO₄: 502.2957 [MH⁺]; found, 502.2961.

Metathesis Reactions. Synthesis of Esters 1am–1bm. **General Procedure (Scheme S2b).** To a solution of the corresponding carbamate **1aa–1ba** (1 mmol) and acrylate (20 mmol) in dry CH₂Cl₂ (28.9 mL), a solution of second-generation Grubbs catalyst (0.05 mmol) in dry CH₂Cl₂ (8.1 mL) was added via cannula, under argon atmosphere. The reaction mixture was stirred at reflux (heating block) for 7 h and it was allowed to cool down to room temperature. Afterward, the solvent was evaporated in vacuo, and purification by flash column chromatography (silica gel, petroleum ether/AcOEt) afforded the corresponding esters **1am–1bm**.

Methyl (E)-4-[(3,5-dimethoxyphenyl)(methoxycarbonyl)amino]but-2-enoate (1am). Prepared from **1aa** (0.24 g, 0.95 mmol) and methyl acrylate (1.7 mL, 18.9 mmol) in dry CH₂Cl₂ (27.3 mL) and second-generation Grubbs catalyst (40.2 mg, 0.047 mmol) in dry CH₂Cl₂ (7.6 mL). After purification by flash column chromatography (silica gel, petroleum ether/AcOEt 8/2), **1am** was obtained as an oil (0.27 g, 91%): ¹H NMR (300 MHz, CDCl₃): δ 3.67 (s, 3H), 3.68 (s, 3H), 3.71 (s, 6H), 4.33 (dd, *J* = 5.5, 1.7 Hz, 2H), 5.90 (dt, *J* = 15.7, 1.7 Hz, 1H), 6.26–6.38 (m, 3H), 6.92 (dt, *J* = 15.7, 5.5 Hz, 1H) ppm; ¹³C{¹H} NMR (75.5 MHz, CDCl₃): δ 51.5, 51.6, 53.1, 55.3, 98.7, 105.0, 122.2, 143.3, 143.4, 155.5, 160.9, 166.3 ppm; IR (ATR): 1710 cm⁻¹; MS (ESI) *m/z* (rel intensity): 310.1 (MH⁺, 100), 278.1 (23); HRMS (ESI-TOF): calcd for C₁₅H₂₀NO₆: 310.1291 [MH⁺]; found, 310.1300.

Ethyl (E)-4-[(3,5-Dimethoxyphenyl)(methoxycarbonyl)amino]but-2-enoate (1an). Prepared from **1aa** (0.26 g, 1.04 mmol) and ethyl acrylate (2.3 mL, 20.8 mmol) in dry CH₂Cl₂ (30.1 mL) and second-generation Grubbs catalyst (44.2 mg, 0.052 mmol) in dry CH₂Cl₂ (8.4 mL). After purification by flash column chromatography (silica gel, petroleum ether/AcOEt 8/2), **1an** was obtained as an oil

(0.33 g, 99%): ¹H NMR (300 MHz, CDCl₃): δ 1.26 (t, *J* = 7.1 Hz, 3H), 3.70 (s, 3H), 3.75 (s, 6H), 4.16 (q, *J* = 7.1 Hz, 2H), 4.36 (dd, *J* = 5.5, 1.7 Hz, 2H), 5.92 (dt, *J* = 15.7, 1.7 Hz, 1H), 6.28–6.41 (m, 3H), 6.92 (dt, *J* = 15.7, 5.5 Hz, 1H) ppm; ¹³C{¹H} NMR (75.5 MHz, CDCl₃): δ 14.2, 51.6, 53.2, 55.4, 60.5, 98.7, 106.0, 122.6, 143.2, 143.4, 155.6, 160.9, 165.9 ppm; IR (ATR): 1710 cm⁻¹; MS (ESI) *m/z* (rel intensity): 324.1 (MH⁺, 100), 278.1 (9); HRMS (ESI-TOF): calcd for C₁₆H₂₂NO₆: 324.1447 [MH⁺]; found: 324.1454.

Butyl (E)-4-[(3,5-Dimethoxyphenyl)(methoxycarbonyl)amino]but-2-enoate (1ao). Prepared from **1aa** (0.31 g, 1.25 mmol) and *n*-butyl acrylate (3.6 mL, 24.9 mmol) in dry CH₂Cl₂ (36.0 mL) and second-generation Grubbs catalyst (52.9 mg, 0.062 mmol) in dry CH₂Cl₂ (10.0 mL). After purification by flash column chromatography (silica gel, petroleum ether/AcOEt 8/2), **1ao** was obtained as an oil (0.40 g, 91%): ¹H NMR (300 MHz, CDCl₃): δ 0.88 (t, *J* = 7.3 Hz, 3H), 1.25–1.45 (m, 2H), 1.53–1.68 (m, 2H), 3.67 (s, 3H), 3.71 (s, 6H), 4.08 (t, *J* = 6.7 Hz, 2H), 4.33 (dd, *J* = 5.4, 1.4 Hz, 2H), 5.89 (d, *J* = 15.7 Hz, 1H), 6.26–6.36 (m, 3H), 6.90 (dt, *J* = 15.7, 5.4 Hz, 1H) ppm; ¹³C{¹H} NMR (75.5 MHz, CDCl₃): δ 13.7, 19.1, 30.6, 51.6, 53.1, 55.3, 64.3, 98.7, 105.1, 122.6, 143.2 (C₁), 143.4, 155.6, 160.9, 166.0 ppm; IR (ATR): 1710 cm⁻¹; MS (ESI) *m/z* (rel intensity): 352.2 (MH⁺, 100), 278.1 (5); HRMS (ESI-TOF): calcd for C₁₈H₂₆NO₆: 352.1760 [MH⁺]; found: 352.1761.

tert-Butyl (E)-4-[(3,5-Dimethoxyphenyl)(methoxycarbonyl)amino]but-2-enoate (1ap). Prepared from **1aa** (0.23 g, 0.91 mmol) and *tert*-butyl acrylate (2.7 mL, 18.3 mmol) in dry CH₂Cl₂ (26.4 mL) and second-generation Grubbs catalyst (38.8 mg, 0.046 mmol) in dry CH₂Cl₂ (7.4 mL). After purification by flash column chromatography (silica gel, petroleum ether/AcOEt 9/1), **1ap** was obtained (0.31 g, 99%) as an oil: ¹H NMR (300 MHz, CDCl₃): δ 1.44 (s, 9H), 3.68 (s, 3H), 3.73 (s, 6H), 4.32 (dd, *J* = 5.5, 1.7 Hz, 2H), 5.82 (dt, *J* = 15.7, 1.7 Hz, 1H), 6.28–6.38 (m, 3H), 6.81 (dt, *J* = 15.7, 5.5 Hz, 1H) ppm; ¹³C{¹H} NMR (75.5 MHz, CDCl₃): δ 28.0, 51.5, 53.1, 55.3, 80.5, 98.7, 105.0, 124.3, 141.9, 143.5, 155.6, 160.8, 165.2 ppm; IR (ATR): 1702 cm⁻¹; MS (ESI) *m/z* (rel intensity): 352.2 (MH⁺, 11), 296.1 (100); HRMS (ESI-TOF): calcd for C₁₈H₂₆NO₆: 352.1760 [MH⁺]; found, 352.1760.

Benzyl (E)-4-[(3,5-Dimethoxyphenyl)(methoxycarbonyl)amino]but-2-enoate (1aq). Prepared from **1aa** (0.20 g, 0.81 mmol) and benzyl acrylate (2.4 mL, 16.2 mmol) in dry CH₂Cl₂ (23.4 mL) and second-generation Grubbs catalyst (34.4 mg, 0.041 mmol) in dry CH₂Cl₂ (6.5 mL). After purification by flash column chromatography (silica gel, petroleum ether/AcOEt 8/2), **1aq** was obtained as an oil (0.31 g, 99%): ¹H NMR (300 MHz, CDCl₃): δ 3.69 (s, 3H), 3.71 (s, 6H), 4.37 (d, *J* = 4.1 Hz, 2H), 5.15 (s, 2H), 5.99 (d, *J* = 15.7 Hz, 1H), 6.35 (br s, 1H), 6.38 (br s, 2H), 6.91–7.08 (m, 1H), 7.20–7.37 (m, 5H) ppm; ¹³C{¹H} NMR (75.5 MHz, CDCl₃): δ 51.6, 53.1, 55.3, 66.3, 98.8, 105.1, 122.3, 128.2, 128.5, 135.9, 143.4, 144.0, 155.6, 160.9, 165.7 ppm; IR (ATR): 1710 cm⁻¹; MS (ESI) *m/z* (rel intensity): 408.1 (MNa⁺, 100), 386.2 (MH⁺, 60), 354.1 (37), 3; HRMS (ESI-TOF): calcd for C₂₁H₂₃NO₆Na: 408.1423 [MNa⁺]; found, 408.1420.

Methyl (E)-4-[(tert-Butoxycarbonyl)(3,5-dimethoxyphenyl)amino]but-2-enoate (1bm). Prepared from **1ba** (0.26 g, 0.88 mmol) and methyl acrylate (1.6 mL, 17.5 mmol) in dry CH₂Cl₂ (25.3 mL) and second-generation Grubbs catalyst (37.2 mg, 0.044 mmol) in dry CH₂Cl₂ (7.1 mL). After purification by flash column chromatography (silica gel, petroleum ether/AcOEt 8/2), **1bm** was obtained as an oil (0.26 g, 86%): ¹H NMR (300 MHz, CDCl₃): δ 1.44 (s, 9H), 3.72 (s, 3H), 3.75 (s, 6H), 4.34 (dd, *J* = 5.2, 1.8 Hz, 2H), 5.93 (dt, *J* = 15.7, 1.8 Hz, 1H), 6.30 (t, *J* = 2.2 Hz, 1H), 6.36 (d, *J* = 2.2 Hz, 2H), 6.97 (dt, *J* = 15.7, 5.2 Hz, 1H) ppm; ¹³C{¹H} NMR (75.5 MHz, CDCl₃): δ 28.3, 51.3, 51.6, 55.4, 81.0, 98.1, 104.7, 121.7, 144.1, 144.4, 154.0, 160.7, 166.5 ppm; IR (ATR): 1699 cm⁻¹; MS (ESI) *m/z* (rel intensity): 374.2 (MNa⁺, 54), 352.2 (MH⁺, 2), 252.1 (100); HRMS (ESI-TOF): calcd for C₁₈H₂₅NO₆Na: 374.1580 [MNa⁺]; found, 374.1584.

Reductive Amination and Protection. Synthesis of Methyl (E)-(3,5-dimethoxyphenyl)[3-(4-methoxyphenyl)allyl]carbamate (1ag) (Scheme S3). Over a solution of commercially available 3,5-

dimethoxyaniline (0.53 g, 3.47 mmol) in dry Et₂O (17 mL), *trans-p*-methoxycinnamaldehyde (0.56 g, 3.47 mmol) and anhydrous MgSO₄ (4 g) were added under argon atmosphere. The reaction mixture was stirred at room temperature for 16 h; it was filtered and the solvent was evaporated in vacuo. The crude imine was dissolved in dry MeOH (23 mL) and NaBH₄ (0.39 g, 10.4 mmol) was added portionwise under argon atmosphere. The reaction mixture was allowed to warm up to room temperature and stirred for 3.5 h. Afterward, a 1 M NaOH aqueous solution (15 mL) was added to quench the reaction and it was diluted with water (20 mL). The mixture was extracted with AcOEt (3 × 15 mL), the combined organic extracts were dried (Na₂SO₄), and the solvent was evaporated in vacuo. Flash column chromatography (silica gel, hexane/AcOEt 7/3) afforded **1hg** as an oil (0.64 g, 62%): ¹H NMR (300 MHz, CDCl₃): δ 3.77 (s, 6H), 3.81 (s, 3H), 3.84–3.96 (m, 3H), 5.88 (d, *J* = 2.1 Hz, 2H), 5.93 (t, *J* = 2.1 Hz, 1H), 6.18 (dt, *J* = 15.8, 5.7 Hz, 1H), 6.57 (d, *J* = 15.8 Hz, 1H), 6.87 (d, *J* = 8.8 Hz, 2H), 7.32 (d, *J* = 8.8 Hz, 2H) ppm; ¹³C{¹H} NMR (75.5 MHz, CDCl₃): δ 46.3, 55.2, 55.3, 89.9, 91.9, 114.0, 124.6, 127.5, 129.7, 131.2, 150.1, 159.2, 161.8 ppm; IR (ATR): 3408 cm⁻¹; MS (ESI) *m/z* (rel intensity): 300.2 (MH⁺, 37), 298.1 (44), 148.1 (7), 147.1 (100); HRMS (ESI-TOF): calcd for C₁₈H₂₂NO₃: 300.1600 [MH⁺]; found, 300.1600. Over a solution of **1hg** (0.51 g, 1.71 mmol) and freshly distilled pyridine (0.27 mL, 3.41 mmol) in dry THF (20 mL), methyl chloroformate (0.16 mL, 2.05 mmol) was added dropwise. The reaction mixture was stirred at room temperature for 16 h, and afterward, the solvent was evaporated under reduced pressure. The crude reaction was dissolved in CH₂Cl₂ (30 mL) and washed with a 10% aqueous solution of HCl (2 × 15 mL) and with water (15 mL). The combined organic extracts were dried (Na₂SO₄) and concentrated in vacuo. Flash column chromatography (silica gel, hexane/AcOEt 7/3) afforded **1ag** as an oil (0.54 g, 89%): ¹H NMR (300 MHz, CDCl₃): δ 3.72 (s, 3H), 3.74 (s, 6H), 3.77 (s, 3H), 4.32 (d, *J* = 6.4 Hz, 2H), 6.16 (dt, *J* = 15.8, 6.4 Hz, 1H), 6.33–6.48 (m, 4H), 6.83 (d, *J* = 8.7 Hz, 2H), 7.28 (d, *J* = 8.7 Hz, 2H) ppm; ¹³C{¹H} NMR (75.5 MHz, CDCl₃): δ 52.9, 53.0, 55.2, 55.4, 98.8, 106.5, 114.0, 122.8, 127.6, 129.5, 132.1, 143.8, 155.8, 159.3, 160.8 ppm; IR (ATR): 1695 cm⁻¹; MS (ESI) *m/z* (rel intensity): 380.1 (MNa⁺, 100), 358.2 (MH⁺, 60), 224.1 (30), 147.1 (66); HRMS (ESI-TOF): calcd for C₂₀H₂₃NO₃Na: 380.1474 [MNa⁺]; found, 380.1473.

5,7-Dimethoxyquinoline (2). Over a solution of **1aa** (0.10 g, 0.41 mmol) in AcOH (1.7 mL), PhCO₃^tBu (0.10 mL, 0.49 mmol), Cu(OAc)₂ (3.8 mg, 0.021 mmol), *p*-TsOH (79.5 mg, 0.41 mmol), and PdCl₂(CH₃CN)₂ (5.4 mg, 0.021 mmol) were added. The mixture was stirred at room temperature for 24 h, and then the solvent was removed under vacuum. The residue was dissolved in AcOEt (5 mL), and it was washed with a 2 M aqueous solution of Na₂CO₃ (2 × 10 mL) and brine (2 × 10 mL). The aqueous phase was reextracted with AcOEt (10 mL), and the combined organic extracts were dried (Na₂SO₄) and concentrated in vacuo. Flash column chromatography (silica gel, hexane/AcOEt 5/5) afforded **2** as an oil (24.5 mg, 31%), whose data are coincidental to those reported:³¹ ¹H NMR (300 MHz, CDCl₃): δ 3.94 (s, 3H), 3.96 (s, 3H), 6.51 (d, *J* = 1.7 Hz, 1H), 7.02 (d, *J* = 1.7 Hz, 1H), 7.22 (dd, *J* = 8.3, 4.3 Hz, 1H), 8.43 (d, *J* = 8.3 Hz, 1H), 8.79 (d, *J* = 4.3 Hz, 1H) ppm; ¹³C{¹H} NMR (75.5 MHz, CDCl₃): δ 55.6, 55.8, 98.1, 99.6, 116.8, 118.1, 130.6, 150.4, 150.9, 155.9, 161.2 ppm; IR (ATR): 1627 cm⁻¹; MS (EI) *m/z* (rel intensity): 189.1 (M⁺, 100), 160 (17), 146 (15); HRMS (CI-TOF): calcd for C₁₁H₁₂NO₂: 190.0868 [MH⁺]; found: 190.0868.

Synthesis of 1,2-Dihydroquinolines 3. General Procedure. To a solution of the corresponding *N*-protected aniline **1** (1 mmol) in 1,4-dioxane (66.7 mL), *p*-TsOH (1 mmol), BQ (1 mmol), and PdCl₂(CH₃CN)₂ (0.05 or 0.1 mmol) were added and the reaction mixture was stirred at room temperature or 70 °C (heating block with temperature control) for 1–16 h. Afterwards, water was added to quench the reaction and it was extracted with CH₂Cl₂ (3 × 10 mL). The combined organic extracts were washed with brine (10 mL) and dried (Na₂SO₄). The solvent was evaporated in vacuo and the residue was purified by flash column chromatography (silica gel, petroleum ether/AcOEt) affording the corresponding 1,2-dihydroquinolines **3**.

Methyl 5,7-Dimethoxyquinoline-1(2H)-carboxylate (3aa) (Table 1, Entry 1). Prepared from **1aa** (0.14 g, 0.57 mmol), *p*-TsOH (0.11 g, 0.57 mmol), BQ (61.6 mg, 0.57 mmol), and PdCl₂(CH₃CN)₂ (7.4 mg, 0.028 mmol) in dioxane (38 mL). The reaction mixture was stirred for 16 h at room temperature, and after workup and purification by flash column chromatography (silica gel, petroleum ether/AcOEt 7/3), **3aa** was obtained as an oil (0.12 g, 85%): ¹H NMR (300 MHz, CDCl₃): δ 3.78 (s, 3H), 3.80 (s, 6H), 4.32 (dd, *J* = 4.3, 1.7 Hz, 2H), 5.82 (dt, *J* = 9.6, 4.3 Hz, 1H), 6.24 (d, *J* = 2.3 Hz, 1H), 6.76 (dt, *J* = 9.6, 1.7 Hz, 1H), 6.85 (br s, 1H) ppm; ¹³C{¹H} NMR (75.5 MHz, CDCl₃): δ 43.2, 53.0, 55.4, 55.6, 94.8, 101.0, 111.2, 120.7, 120.8, 138.2, 154.7, 155.6, 159.4 ppm; IR (ATR): 1702 cm⁻¹; MS (EI) *m/z* (rel intensity): 249.1 (M⁺, 79), 190.1 (100); HRMS (CI-TOF): calcd for C₁₃H₁₆NO₄: 250.1079 [MH⁺]; found, 250.1085.

tert-Butyl 5,7-Dimethoxyquinoline-1(2H)-carboxylate (3ba) (Table 1, Entry 3). Prepared from **1ba** (0.12 g, 0.40 mmol), *p*-TsOH (75.2 mg, 0.40 mmol), BQ (42.3 mg, 0.40 mmol), and PdCl₂(CH₃CN)₂ (10.3 mg, 0.040 mmol) in dioxane (26.3 mL). The reaction mixture was stirred for 1.5 h at room temperature, and after workup and purification by flash column chromatography (silica gel, petroleum ether/AcOEt 9/1), **3ba** was obtained as an oil (67.3 mg, 58%): ¹H NMR (300 MHz, CDCl₃): δ 1.52 (s, 9H), 3.80 (s, 6H), 4.28 (dd, *J* = 4.3, 1.7 Hz, 2H), 5.82 (dt, *J* = 9.6, 4.3 Hz, 1H), 6.21 (d, *J* = 2.3 Hz, 1H), 6.72–6.79 (m, 1H), 6.82 (d, *J* = 2.3 Hz, 1H) ppm; ¹³C{¹H} NMR (75.5 MHz, CDCl₃): δ 28.4, 42.8, 55.4, 55.6, 81.1, 94.5, 101.1, 111.2, 120.8, 121.0, 138.7, 153.1, 155.5, 159.1 ppm; IR (ATR): 1649 cm⁻¹; MS (ESI) *m/z* (rel intensity): 314.1 (MNa⁺, 12), 292.2 (MH⁺, 5), 236.1 (100); HRMS (ESI-TOF): calcd for C₁₆H₂₁NO₄Na: 314.1368 [MNa⁺]; found: 314.1370. In this reaction, *tert*-butyl 4,6-dimethoxy-2-methyl-1*H*-indole-1-carboxylate (**4ba**) was obtained as a byproduct (oil, 18.9 mg, 16%): ¹H NMR (300 MHz, CDCl₃): δ 1.65 (s, 9H), 2.35 (d, *J* = 1.3 Hz, 3H), 3.86 (s, 3H), 3.87 (s, 3H), 6.30 (d, *J* = 2.0 Hz, 1H), 7.01–7.15 (m, 1H), 7.33–7.43 (m, 1H) ppm; ¹³C{¹H} NMR (75.5 MHz, CDCl₃): δ 12.3, 28.2, 55.3, 55.6, 82.9, 91.4, 94.2, 114.8, 116.7, 120.0, 137.6, 149.9, 154.9, 158.8 ppm; IR (ATR): 1724 cm⁻¹; MS (ESI) *m/z* (rel intensity): 292.2 (MH⁺, 58), 236.1 (100); HRMS (ESI-TOF): calcd for C₁₆H₂₂NO₄: 292.1549 [MH⁺]; found, 292.1557.

Benzyl 5,7-Dimethoxyquinoline-1(2H)-carboxylate (3ca) (Table 1, Entry 8). Prepared from **1ca** (0.11 g, 0.33 mmol), *p*-TsOH (62.8 mg, 0.33 mmol), BQ (35.7 mg, 0.33 mmol), and PdCl₂(CH₃CN)₂ (8.6 mg, 0.033 mmol) in dioxane (22.0 mL). The reaction mixture was stirred for 3 h at room temperature, and after workup and purification by flash column chromatography (silica gel, petroleum ether/AcOEt 9/1), **3ca** was obtained as an oil (71.5 mg, 67%): ¹H NMR (300 MHz, CDCl₃): δ 3.68 (s, 3H), 3.80 (s, 3H), 4.37 (d, *J* = 4.2 Hz, 2H), 5.24 (s, 2H), 5.78–5.89 (m, 1H), 6.23 (d, *J* = 1.9 Hz, 1H), 6.73–6.85 (m, 2H), 7.28–7.44 (m, 5H) ppm; ¹³C{¹H} NMR (75.5 MHz, CDCl₃): δ 43.2, 55.3, 55.6, 67.8, 95.1, 100.7, 111.2, 120.7, 120.8, 128.2, 128.3, 128.6, 136.1, 138.1, 154.0, 155.6, 159.3 ppm; IR (ATR): 1702 cm⁻¹; MS (ESI) *m/z* (rel intensity): 348.1 (MNa⁺, 100), 327.1 (MH⁺ + 1, 9), 326.1 (MH⁺, 54), 282.1 (38); HRMS (ESI-TOF): calcd for C₁₉H₁₉NO₄Na: 348.1212 [MNa⁺]; found: 348.1215.

1-[5,7-Dimethoxyquinolin-1(2H)-yl]ethan-1-one (3da) (Table 1, Entry 10). Prepared from **1da** (93.3 mg, 0.40 mmol), *p*-TsOH (75.4 mg, 0.40 mmol), BQ (42.9 mg, 0.40 mmol), and PdCl₂(CH₃CN)₂ (10.3 mg, 0.040 mmol) in dioxane (26.4 mL). The reaction mixture was stirred for 1 h at 70 °C, and after workup and purification by flash column chromatography (silica gel, petroleum ether/AcOEt 7/3), **3da** was obtained as an oil (78.2 mg, 85%): ¹H NMR (300 MHz, CDCl₃): δ 2.22 (s, 3H), 3.79 (s, 3H), 3.81 (s, 3H), 4.29–4.41 (m, 2H), 5.88 (dt, *J* = 9.5, 4.2 Hz, 1H), 6.28 (d, *J* = 2.2 Hz, 1H), 6.36 (br s, 1H), 6.75 (dt, *J* = 9.5, 1.8 Hz, 1H) ppm; ¹³C{¹H} NMR (75.5 MHz, CDCl₃): δ 22.9, 41.4, 55.5, 55.7, 95.2, 102.0, 112.1, 120.8, 123.1, 138.8, 155.8, 159.2, 170.1 ppm; IR (ATR): 1659 cm⁻¹; MS (ESI) *m/z* (rel intensity): 256.1 (MNa⁺, 83), 234.1 (MH⁺, 100), 192.1 (8); HRMS (ESI-TOF): calcd for C₁₃H₁₆NO₃: 234.1130 [MH⁺]; found: 234.1133. In this reaction, 1-(4,6-dimethoxy-3-methyl-1*H*-indol-1-yl)ethan-1-one (**4da**) was obtained as a byproduct (solid, 9.5 mg, 10%): mp (CH₂Cl₂): 141–143 °C; ¹H NMR (300

MHz, CDCl₃): δ 2.36 (d, J = 1.3 Hz, 3H), 2.55 (s, 3H), 3.86 (s, 3H), 3.87 (s, 3H), 6.35 (d, J = 2.0 Hz, 1H), 6.88 (d, J = 1.3 Hz, 1H), 7.66 (d, J = 2.0 Hz, 1H) ppm; ¹³C{¹H} NMR (75.5 MHz, CDCl₃): δ 12.4, 24.1, 55.3, 55.8, 92.9, 95.2, 114.7, 118.9, 119.5, 137.9, 154.7, 159.5, 168.7 ppm; IR (ATR): 1685 cm⁻¹; MS (ESI) m/z (rel intensity): 234.1 (MH⁺, 100), 192.1 (45); HRMS (ESI-TOF): calcd for C₁₃H₁₆NO₃: 234.1130 [MH⁺]; found: 234.1138.

5,7-Dimethoxy-1-tosyl-1,2-dihydroquinoline (3fa) (Table 4, Entry 1). Prepared from **1fa** (0.11 g, 0.31 mmol), *p*-TsOH (58.4 g, 0.31 mmol), BQ (33.2 mg, 0.31 mmol), and PdCl₂(CH₃CN)₂ (4.0 mg, 0.015 mmol) in dioxane (20.5 mL). The reaction mixture was stirred for 16 h at room temperature, and after workup and purification by flash column chromatography (silica gel, petroleum ether/AcOEt 8/2), **3fa** was obtained as an oil (92.5 mg, 87%): ¹H NMR (300 MHz, CDCl₃): δ 2.33 (s, 3H), 3.74 (s, 3H), 3.85 (s, 3H), 4.37 (dd, J = 4.3, 1.6 Hz, 2H), 5.40 (dt, J = 9.6, 4.3 Hz, 1H), 6.22–6.36 (m, 2H), 6.93 (d, J = 2.3 Hz, 1H), 7.08 (d, J = 8.0 Hz, 2H), 7.37 (d, J = 8.0 Hz, 2H) ppm; ¹³C{¹H} NMR (75.5 MHz, CDCl₃): δ 21.5, 45.2, 55.6, 96.9, 102.9, 112.5, 119.0, 120.4, 127.3, 129.1, 136.6, 136.9, 143.4, 155.7, 159.6 ppm; IR (ATR): 1350 1160 cm⁻¹; MS (ESI) m/z (rel intensity): 368.1 (MNa⁺, 100), 346.1 (MH⁺, 89), 191.1 (33), 190.1 (48); HRMS (ESI-TOF): calcd for C₁₈H₁₉NO₄Sn: 368.0933 [MNa⁺]; found, 368.0934.

5,7-Dimethoxy-4-methyl-1-tosyl-1,2-dihydroquinoline (3fb) (Table 4, Entry 2). Prepared from **1fb** (0.10 g, 0.28 mmol), *p*-TsOH (54.2 g, 0.28 mmol), BQ (30.8 mg, 0.28 mmol), and PdCl₂(CH₃CN)₂ (3.7 mg, 0.014 mmol) in dioxane (19.0 mL). The reaction mixture was stirred for 16 h at room temperature, and after workup and purification by flash column chromatography (silica gel, petroleum ether/AcOEt 9/1), **3fb** was obtained as an oil (65.5 mg, 64%): ¹H NMR (300 MHz, CDCl₃): δ 1.58 (s, 3H), 2.33 (s, 3H), 3.72 (s, 3H), 3.86 (s, 3H), 4.10–4.22 (m, 2H), 5.03–5.14 (m, 1H), 6.33–6.40 (m, 1H), 6.90–6.97 (m, 1H), 7.05–7.14 (m, 2H), 7.30–7.38 (m, 2H) ppm; ¹³C{¹H} NMR (75.5 MHz, CDCl₃): δ 21.0, 21.4, 45.2, 55.5, 55.6, 98.3, 103.6, 115.0, 118.3, 127.5, 128.9, 132.2, 136.7 (C₁), 138.3, 143.1, 157.5, 159.2 ppm; IR (ATR): 1347, 1159 cm⁻¹; MS (ESI) m/z (rel intensity): 382.1 (MNa⁺, 43), 360.1 (MH⁺, 100), 204.1 (10); HRMS (ESI-TOF): calcd for C₁₉H₂₂NO₄S: 360.1270 [MH⁺]; found: 360.1272. In this reaction, 5,7-dimethoxy-4-methyl-1-tosyl-1,4-dihydroquinoline (**5fb**) was obtained as a byproduct (solid, 26.6 mg, 26%): mp (CH₂Cl₂): 106–108 °C; ¹H NMR (300 MHz, CDCl₃): δ 0.39 (d, J = 6.8 Hz, 3H), 2.34 (s, 3H), 3.35 (q, J = 6.8 Hz, 1H), 3.72 (s, 3H), 3.84 (s, 3H), 5.42 (dd, J = 7.5, 6.0 Hz, 1H), 6.29 (d, J = 2.3 Hz, 1H), 6.72 (d, J = 7.5 Hz, 1H), 7.14–7.24 (m, 3H), 7.53 (d, J = 8.3 Hz, 2H) ppm; ¹³C{¹H} NMR (75.5 MHz, CDCl₃): δ 21.5, 22.7, 26.4, 55.4, 55.6, 96.7, 99.3, 115.5, 120.7, 125.1, 127.6, 129.2, 134.3, 135.9, 143.9, 157.1, 158.7 ppm; IR (ATR): 1350, 1164 cm⁻¹; MS (ESI) m/z (rel intensity): 382.1 (MNa⁺, 20), 360.1 (MH⁺, 100), 190.1 (20); HRMS (ESI-TOF): calcd for C₁₉H₂₂NO₄S: 360.1270 [MH⁺]; found, 360.1269.

Synthesis of Indoles 4. General Procedure. To a solution of the corresponding ester **1am–aq**, **1bm** (1 mmol) in 1,4-dioxane (66.7 mL), *p*-TsOH (1 mmol), BQ (1 mmol), and PdCl₂(CH₃CN)₂ (0.1 mmol) were added and the reaction mixture was stirred at 70 °C for 4.5 h. Afterward, water was added to quench the reaction and it was extracted with CH₂Cl₂ (3 × 10 mL). The combined organic extracts were washed with brine (10 mL) and dried (Na₂SO₄). The solvent was evaporated in vacuo, and the residue was purified by flash column chromatography (silica gel, petroleum ether/AcOEt) affording the corresponding 3-substituted indoles **4am–aq**, **4bm**.

Methyl 4,6-Dimethoxy-3-(2-methoxy-2-oxoethyl)-1H-indole-1-carboxylate (4am) (Table 3, Entry 1). Prepared from **1am** (90.7 mg, 0.29 mmol), *p*-TsOH (55.8 mg, 0.29 mmol), BQ (31.7 mg, 0.29 mmol), and PdCl₂(CH₃CN)₂ (7.6 mg, 0.029 mmol) in dioxane (19.4 mL). After workup and purification by flash column chromatography (silica gel, petroleum ether/AcOEt 8/2), **4am** was obtained as a solid (61.1 mg, 68%): mp (CH₂Cl₂): 98–101 °C; ¹H NMR (300 MHz, CDCl₃): δ 3.70 (s, 3H), 3.80 (d, J = 0.9 Hz, 2H), 3.81 (s, 3H), 3.85 (s, 3H), 3.98 (s, 3H), 6.30 (d, J = 2.0, 1H), 7.28 (br s, 1H), 7.37 (s, 1H) ppm; ¹³C{¹H} NMR (75.5 MHz, CDCl₃): δ 32.3, 51.9, 53.6,

55.2, 55.7, 91.6, 94.7, 113.7, 114.1, 121.1, 137.5, 151.4, 154.3, 159.3, 172.2 ppm; IR (ATR): 1728 cm⁻¹; MS (ESI) m/z (rel intensity): 308.1 (MH⁺, 100), 248.1 (2); HRMS (ESI-TOF): calcd for C₁₅H₁₈NO₆: 308.1134 [MH⁺]; found, 308.1136.

tert-Butyl 4,6-Dimethoxy-3-(2-methoxy-2-oxoethyl)-1H-indole-1-carboxylate (4bm) (Table 3, Entry 2). Prepared from **1bm** (0.11 g, 0.33 mmol), *p*-TsOH (62.0 mg, 0.33 mmol), BQ (38.8 mg, 0.33 mmol), and PdCl₂(CH₃CN)₂ (8.5 mg, 0.033 mmol) in dioxane (21.7 mL). After workup and purification by flash column chromatography (silica gel, petroleum ether/AcOEt 9/1), **4bm** was obtained as a solid (46.4 mg, 41%): mp (CH₂Cl₂): 103–105 °C; ¹H NMR (300 MHz, CDCl₃): δ 1.64 (s, 9H), 3.71 (s, 3H), 3.80 (s, 2H), 3.81 (s, 3H), 3.86 (s, 3H), 6.29 (d, J = 1.7, 1H), 7.26 (br s, 1H), 7.35 (s, 1H) ppm; ¹³C{¹H} NMR (75.5 MHz, CDCl₃): δ 28.2, 32.4, 51.9, 55.2, 55.7, 83.3, 91.6, 94.5, 113.2, 113.8, 121.7, 137.4, 149.7, 154.2, 159.1, 172.4 ppm; IR (ATR): 1756, 1720 cm⁻¹; MS (ESI) m/z (rel intensity): 350.2 (MH⁺, 100), 294.1 (72); HRMS (ESI-TOF): calcd for C₁₈H₂₄NO₆: 350.1604 [MH⁺]; found, 350.1606.

Methyl 3-(2-Ethoxy-2-oxoethyl)-4,6-dimethoxy-1H-indole-1-carboxylate (4an) (Table 3, Entry 3). Prepared from **1an** (0.13 g, 0.39 mmol), *p*-TsOH (75.1 mg, 0.39 mmol), BQ (42.7 mg, 0.39 mmol), and PdCl₂(CH₃CN)₂ (10.2 mg, 0.039 mmol) in dioxane (26.3 mL). After workup and purification by flash column chromatography (silica gel, petroleum ether/AcOEt 8/2), **4an** was obtained as a solid (86.4 mg, 68%): mp (CH₂Cl₂): 77–80 °C; ¹H NMR (300 MHz, CDCl₃): δ 1.25 (t, J = 7.1 Hz, 3H), 3.78 (s, 2H), 3.81 (s, 3H), 3.85 (s, 3H), 3.97 (s, 3H), 4.17 (q, J = 7.1 Hz, 2H), 6.30 (d, J = 1.9, 1H), 7.28 (br s, 1H), 7.37 (s, 1H) ppm; ¹³C{¹H} NMR (75.5 MHz, CDCl₃): δ 14.3, 32.6, 53.6, 55.2, 55.7, 60.6, 91.5, 94.6, 113.8, 114.3, 121.1, 137.5, 151.5, 154.3, 159.3, 171.7 ppm; IR (ATR): 1731 cm⁻¹; MS (ESI) m/z (rel intensity): 322.1 (MH⁺, 100), 248.1 (3); HRMS (ESI-TOF): calcd for C₁₆H₂₀NO₆: 322.1291 [MH⁺]; found: 322.1300.

Methyl 3-(2-Butoxy-2-oxoethyl)-4,6-dimethoxy-1H-indole-1-carboxylate (4ao) (Table 3, Entry 4). Prepared from **1ao** (0.11 g, 0.31 mmol), *p*-TsOH (58.6 mg, 0.31 mmol), BQ (33.3 mg, 0.31 mmol), and PdCl₂(CH₃CN)₂ (8.0 mg, 0.031 mmol) in dioxane (20.5 mL). After workup and purification by flash column chromatography (silica gel, petroleum ether/AcOEt 8/2), **4ao** was obtained as a solid (68.0 mg, 63%): mp (CH₂Cl₂): 79–80 °C; ¹H NMR (300 MHz, CDCl₃): δ 0.90 (t, J = 7.3 Hz, 3H), 1.22–1.46 (m, 2H), 1.51–1.69 (m, 2H), 3.79 (s, 2H), 3.81 (s, 3H), 3.86 (s, 3H), 3.99 (s, 3H), 4.17 (t, J = 6.7 Hz, 2H), 6.30 (d, J = 2.0, 1H), 7.29 (br s, 1H), 7.38 (s, 1H) ppm; ¹³C{¹H} NMR (75.5 MHz, CDCl₃): δ 13.7, 19.1, 30.7, 32.6, 53.6, 55.2, 55.7, 64.5, 91.5, 94.6, 113.8, 114.3, 121.1, 137.5, 151.5, 154.3, 159.3, 171.8 ppm; IR (ATR): 1731 cm⁻¹; MS (ESI) m/z (rel intensity): 350.2 (MH⁺, 100), 349.2 (5); HRMS (ESI-TOF): calcd for C₁₈H₂₄NO₆: 350.1604 [MH⁺]; found, 350.1604.

Methyl 3-[2-(tert-Butoxy)-2-oxoethyl]-4,6-dimethoxy-1H-indole-1-carboxylate (4ap) (Table 3, Entry 5). Prepared from **1ap** (0.14 g, 0.40 mmol), *p*-TsOH (75.9 mg, 0.40 mmol), BQ (43.2 mg, 0.40 mmol), and PdCl₂(CH₃CN)₂ (10.4 mg, 0.040 mmol) in dioxane (26.6 mL). After workup and purification by flash column chromatography (silica gel, petroleum ether/AcOEt 9/1), **4ap** was obtained as a solid (75.3 mg, 54%): ¹H NMR (300 MHz, CDCl₃): δ 1.45 (s, 9H), 3.70 (s, 2H), 3.83 (s, 3H), 3.86 (s, 3H), 3.98 (s, 3H), 6.30 (d, J = 2.0, 1H), 7.27 (br s, 1H), 7.37 (s, 1H) ppm; ¹³C{¹H} NMR (75.5 MHz, CDCl₃): δ 28.3, 33.6, 53.6, 55.1, 55.7, 80.3, 91.5, 94.6, 113.9, 114.8, 121.0, 137.5, 151.5, 154.3, 159.2, 171.0 ppm; IR (ATR): 1735 cm⁻¹; MS (ESI) m/z (rel intensity): 350.2 (MH⁺, 31), 294.1 (100); MS (ESI) m/z (rel intensity): calcd for C₁₈H₂₄NO₆: 350.1604 [MH⁺]; found, 350.1608.

Methyl 3-[2-(benzyloxy)-2-oxoethyl]-4,6-dimethoxy-1H-indole-1-carboxylate (4aq) (Table 3, Entry 6). Prepared from **1aq** (0.10 g, 0.27 mmol), *p*-TsOH (51.2 mg, 0.27 mmol), BQ (29.1 mg, 0.27 mmol), and PdCl₂(CH₃CN)₂ (7.0 mg, 0.027 mmol) in dioxane (17.9 mL). After workup and purification by flash column chromatography (silica gel, petroleum ether/AcOEt 8/2), **4aq** was obtained as a solid (80.4 mg, 78%): mp (CH₂Cl₂): 136–138 °C; ¹H NMR (300 MHz, CDCl₃): δ 3.66 (s, 3H), 3.85 (s, 2H), 3.87 (s, 3H), 3.99 (s, 3H), 5.17 (s, 2H), 6.28 (d, J = 1.9, 1H), 7.24–7.45 (m, 7H) ppm; ¹³C{¹H} NMR (75.5 MHz, CDCl₃): δ 32.6, 53.6, 55.0, 55.7, 66.4, 91.5, 94.7, 113.8, 114.1,

121.2, 128.1, 128.3, 128.5, 136.2, 137.5, 151.5, 154.3, 159.3, 171.5 ppm; IR (ATR): 1735 cm⁻¹; MS (ESI) *m/z* (rel intensity): 406.1 (MNa⁺ + 1, 81), 384.1 (MH⁺, 100), 383.1 (17); HRMS (ESI-TOF): calcd for C₂₁H₂₂NO₄: 384.1447 [MH⁺]; found, 384.1452.

Synthesis of 1,4-Dihydroquinolines 5. General Procedure.

To a solution of the corresponding *N*-protected (3,5-dimethoxyphenyl)allyl aniline **1** (1 mmol) in 1,4-dioxane (66.7 mL), *p*-TsOH (1 mmol), BQ (1 mmol), and PdCl₂(CH₃CN)₂ (0.05 mmol) were added and the reaction mixture was stirred at room temperature for 16 h. Afterward, water was added to quench the reaction, and it was extracted with CH₂Cl₂ (3 × 10 mL). The combined organic extracts were washed with brine (10 mL) and dried (Na₂SO₄). The solvent was evaporated in vacuo, and the residue was purified by flash column chromatography (silica gel, petroleum ether/AcOEt), affording the corresponding 1,4-dihydroquinolines **5**.

Methyl 5,7-Dimethoxy-4-methylquinoline-1(4H)-carboxylate (5ab) (Table 2). Prepared from **1ab** (0.11 g, 0.42 mmol), *p*-TsOH (79.8 mg, 0.42 mmol), BQ (45.4 mg, 0.42 mmol), and PdCl₂(CH₃CN)₂ (5.4 mg, 0.021 mmol) in dioxane (28 mL). After workup and purification by flash column chromatography (silica gel, petroleum ether/AcOEt 7/3), **5ab** was obtained as an oil (62.6 mg, 57%): ¹H NMR (300 MHz, CDCl₃): δ 1.14 (d, *J* = 6.8 Hz, 3H), 3.53–3.70 (m, 1H), 3.80 (s, 3H), 3.86 (s, 6H), 5.28–5.44 (m, 1H), 6.30 (d, *J* = 2.2 Hz, 1H), 6.92 (d, *J* = 7.7 Hz, 1H), 7.29 (d, *J* = 2.2 Hz, 1H) ppm; ¹³C{¹H} NMR (75.5 MHz, CDCl₃): δ 22.1, 26.1, 53.2, 55.4, 55.5, 95.5, 98.1, 114.6, 116.0, 125.1, 137.3, 153.2, 156.8, 158.4 ppm; IR (ATR): 1705 cm⁻¹; MS (EI) *m/z* (rel intensity): 263.1 (M⁺, 10), 248.2 (100), 189.1 (64); HRMS (ESI-TOF): calcd for C₁₄H₁₈NO₄: 264.1236 [MH⁺]; found, 264.1251.

Methyl 5,7-Dimethoxy-4-phenylquinoline-1(4H)-carboxylate (5ac) (Table 2). Prepared from **1ac** (98.8 mg, 0.30 mmol), *p*-TsOH (57.4 mg, 0.30 mmol), BQ (32.6 mg, 0.30 mmol), and PdCl₂(CH₃CN)₂ (3.9 mg, 0.015 mmol) in dioxane (20.1 mL). After workup and purification by flash column chromatography (silica gel, petroleum ether/AcOEt 8/2), **5ac** was obtained as a solid (76.0 mg, 77%): mp (CH₂Cl₂) 137–140 °C; ¹H NMR (300 MHz, CDCl₃): δ 3.70 (s, 3H), 3.83 (s, 3H), 3.89 (s, 3H), 4.82 (d, *J* = 6.0 Hz, 1H), 5.42–5.55 (m, 1H), 6.29 (br s, 1H), 7.07 (d, *J* = 7.8 Hz, 1H), 7.11–7.28 (m, 5H), 7.43 (br s, 1H) ppm; ¹³C{¹H} NMR (75.5 MHz, CDCl₃): δ 37.3, 53.4, 55.4, 55.6, 95.8, 97.9, 112.1, 113.9, 125.2, 126.2, 127.4, 128.4, 137.5, 144.8, 153.2, 157.2, 159.0 ppm; IR (ATR): 1727 cm⁻¹; MS (EI) *m/z* (rel intensity): 325.1 (M⁺, 20), 248.1 (100), 189.1 (19); HRMS (ESI-TOF): calcd for C₁₉H₂₀NO₄: 326.1392 [MH⁺]; found: 326.1400.

tert-Butyl 5,7-Dimethoxy-4-phenylquinoline-1(4H)-carboxylate (5bc) (Table 2). Prepared from **1bc** (0.11 g, 0.29 mmol), *p*-TsOH (55.3 mg, 0.29 mmol), BQ (31.4 mg, 0.29 mmol), and PdCl₂(CH₃CN)₂ (3.8 mg, 0.015 mmol) in dioxane (19.3 mL). After workup and purification by flash column chromatography (silica gel, petroleum ether/AcOEt 9/1), **5bc** was obtained as a solid (77.4 mg, 73%): mp (CH₂Cl₂) 110–112 °C; ¹H NMR (300 MHz, CDCl₃): δ 1.61 (s, 9H), 3.71 (s, 3H), 3.84 (s, 3H), 4.83 (d, *J* = 6.2 Hz, 1H), 5.45 (dd, *J* = 7.7, 6.2 Hz, 1H), 6.28 (d, *J* = 2.3 Hz, 1H), 7.06 (d, *J* = 7.7 Hz, 1H), 7.11–7.28 (m, 5H), 7.37 (d, *J* = 2.3 Hz, 1H) ppm; ¹³C{¹H} NMR (75.5 MHz, CDCl₃): δ 28.4, 37.4, 55.4, 55.6, 82.2, 95.5, 98.4, 112.4, 113.2, 126.0, 126.1, 127.5, 128.4, 137.9, 145.1, 151.6, 157.1, 158.9 ppm; IR (ATR): 1727 cm⁻¹; MS (EI) *m/z* (rel intensity): 390.2 (MNa⁺, 27), 312.1 (100); HRMS (ESI-TOF): calcd for C₂₂H₂₅NO₄Na: 390.1681 [MNa⁺]; found: 390.1684.

Methyl 5,7-Dimethoxy-4-(*p*-tolyl)quinoline-1(4H)-carboxylate (5ad) (Table 2). Prepared from **1ad** (0.12 g, 0.36 mmol), *p*-TsOH (67.8 mg, 0.36 mmol), BQ (38.5 mg, 0.36 mmol), and PdCl₂(CH₃CN)₂ (4.6 mg, 0.018 mmol) in dioxane (23.8 mL). After workup and purification by flash column chromatography (silica gel, petroleum ether/AcOEt 8/2), **5ad** was obtained as a solid (98.7 mg, 82%): mp (CH₂Cl₂) 105–106 °C; ¹H NMR (300 MHz, CDCl₃): δ 2.29 (s, 3H), 3.71 (s, 3H), 3.83 (s, 3H), 3.89 (s, 3H), 4.79 (d, *J* = 6.2 Hz, 1H), 5.48 (dd, *J* = 7.7, 6.2 Hz, 1H), 6.29 (d, *J* = 2.3 Hz, 1H), 6.98–7.13 (m, 5H), 7.42 (d, *J* = 2.3 Hz, 1H) ppm; ¹³C{¹H} NMR (75.5 MHz, CDCl₃): δ 21.0, 36.8, 53.3, 55.4, 55.6, 95.8, 97.9, 112.3,

114.1, 125.0, 127.3, 129.1, 135.7, 137.5, 141.9, 153.2, 157.2, 158.9 ppm; IR (ATR): 1727 cm⁻¹; MS (ESI) *m/z* (rel intensity): 340.2 (MH⁺, 100), 248.1 (3); HRMS (ESI-TOF): calcd for C₂₀H₂₂NO₄: 340.1549 [MH⁺]; found: 340.1553.

Methyl 5,7-Dimethoxy-4-(*m*-tolyl)quinoline-1(4H)-carboxylate (5ae) (Table 2). Prepared from **1ae** (0.11 g, 0.31 mmol), *p*-TsOH (59.0 mg, 0.31 mmol), BQ (33.5 mg, 0.31 mmol), and PdCl₂(CH₃CN)₂ (4.0 mg, 0.016 mmol) in dioxane (20.7 mL). After workup and purification by flash column chromatography (silica gel, petroleum ether/AcOEt 8/2), **5ae** was obtained as a solid (96.5 mg, 92%): mp (CH₂Cl₂) 101–102 °C; ¹H NMR (300 MHz, CDCl₃): δ 2.33 (s, 3H), 3.71 (s, 3H), 3.84 (s, 3H), 3.90 (s, 3H), 4.79 (d, *J* = 6.2 Hz, 1H), 5.48 (m, 1H), 6.30 (d, *J* = 2.1 Hz, 1H), 6.91–7.18 (m, 5H), 7.43 (d, *J* = 2.1 Hz, 1H) ppm; ¹³C{¹H} NMR (75.5 MHz, CDCl₃): δ 21.5, 37.2, 53.3, 55.4, 55.6, 95.8, 97.9, 112.1, 114.0, 124.4, 125.0, 127.0, 128.1, 128.3, 137.6, 137.9, 144.8, 153.2, 157.3, 159.0 ppm; IR (ATR): 1727 cm⁻¹; MS (ESI) *m/z* (rel intensity): 340.2 (MH⁺, 100), 248.1 (2); HRMS (ESI-TOF): calcd for C₂₀H₂₂NO₄: 340.1549 [MH⁺]; found: 340.1555.

Methyl 5,7-Dimethoxy-4-(*o*-tolyl)quinoline-1(4H)-carboxylate (5af) (Table 2). Prepared from **1af** (0.11 g, 0.31 mmol), *p*-TsOH (59.6 mg, 0.31 mmol), BQ (33.8 mg, 0.31 mmol), and PdCl₂(CH₃CN)₂ (4.1 mg, 0.016 mmol) in dioxane (20.9 mL). After workup and purification by flash column chromatography (silica gel, petroleum ether/AcOEt 8/2), **5af** was obtained as a solid (87.6 mg, 82%): mp (CH₂Cl₂) 118–121 °C; ¹H NMR (300 MHz, CDCl₃): δ 2.53 (s, 3H), 3.63 (s, 3H), 3.86 (s, 3H), 3.89 (s, 3H), 5.01 (d, *J* = 5.9 Hz, 1H), 5.43 (m, 1H), 6.29 (d, *J* = 2.3 Hz, 1H), 6.77–7.17 (m, 5H), 7.50 (d, *J* = 2.3 Hz, 1H) ppm; ¹³C{¹H} NMR (75.5 MHz, CDCl₃): δ 17.3, 34.0, 53.3, 55.4, 55.7, 95.8, 97.8, 112.1, 112.5, 124.6, 126.0, 126.6, 127.5, 129.9, 134.6, 138.1, 143.6, 153.2, 157.3, 159.0 ppm; IR (ATR): 1724 cm⁻¹; MS (ESI) *m/z* (rel intensity): 340.2 (MH⁺, 100), 248.1 (2); HRMS (ESI-TOF): calcd for C₂₀H₂₂NO₄: 340.1549 [MH⁺]; found, 340.1557.

Methyl 5,7-Dimethoxy-4-(4-methoxyphenyl)quinoline-1(4H)-carboxylate (5ag) (Table 2). Prepared from **1ag** (0.13 g, 0.37 mmol), *p*-TsOH (69.7 mg, 0.37 mmol), BQ (39.6 mg, 0.37 mmol), and PdCl₂(CH₃CN)₂ (4.8 mg, 0.018 mmol) in dioxane (24.4 mL). After workup and purification by flash column chromatography (silica gel, petroleum ether/AcOEt 8/2), **5ag** was obtained as a solid (98.7 mg, 82%): mp (CH₂Cl₂) 109–110 °C; ¹H NMR (300 MHz, CDCl₃): δ 3.71 (s, 3H), 3.75 (s, 3H), 3.82 (s, 3H), 3.89 (s, 3H), 4.77 (d, *J* = 6.2 Hz, 1H), 5.47 (dd, *J* = 7.7, 6.2 Hz, 1H), 6.29 (d, *J* = 2.3 Hz, 1H), 6.78 (d, *J* = 8.7 Hz, 2H), 7.06 (d, *J* = 7.7 Hz, 1H), 7.12 (d, *J* = 8.7 Hz, 2H), 7.41 (d, *J* = 2.3 Hz, 1H) ppm; ¹³C{¹H} NMR (75.5 MHz, CDCl₃): δ 36.4, 53.3, 55.2, 55.4, 55.6, 95.8, 98.0, 112.5, 113.8, 114.2, 125.0, 128.4, 137.1, 137.4, 153.2, 157.1, 158.0, 158.9 ppm; IR (ATR): 1727 cm⁻¹; MS (ESI) *m/z* (rel intensity): 378.1 (MNa⁺, 100), 356.2 (MH⁺, 99), 248.1 (16); HRMS (ESI-TOF): calcd for C₂₀H₂₁NO₅Na: 378.1317 [MNa⁺]; found: 378.1324.

Methyl 5,7-Dimethoxy-4-(3-methoxyphenyl)quinoline-1(4H)-carboxylate (5ah) (Table 2). Prepared from **1ah** (57.6 mg, 0.16 mmol), *p*-TsOH (30.7 mg, 0.16 mmol), BQ (17.4 mg, 0.16 mmol), and PdCl₂(CH₃CN)₂ (2.1 mg, 0.008 mmol) in dioxane (10.8 mL). After workup and purification by flash column chromatography (silica gel, petroleum ether/AcOEt 8/2), **5ah** was obtained as a solid (46.1 mg, 81%): mp (CH₂Cl₂) 101–103 °C; ¹H NMR (300 MHz, CDCl₃): δ 3.71 (s, 3H), 3.74 (s, 3H), 3.82 (s, 3H), 3.88 (s, 3H), 4.80 (d, *J* = 6.2 Hz, 1H), 5.38–5.54 (m, 1H), 6.29 (d, *J* = 1.8 Hz, 1H), 6.65–7.18 (m, 5H), 7.41 (d, *J* = 2.1 Hz, 1H) ppm; ¹³C{¹H} NMR (75.5 MHz, CDCl₃): δ 37.2, 53.3, 55.0, 55.4, 55.6, 95.8, 98.0, 111.3, 112.0, 113.3, 113.8, 119.8, 125.3, 129.3, 137.5, 146.4, 153.1, 157.2, 159.0, 159.6 ppm; IR (ATR): 1720 cm⁻¹; MS (ESI) *m/z* (rel intensity): 356.2 (MH⁺, 100), 248.1 (1); MS (ESI) *m/z* (rel intensity): calcd for C₂₀H₂₂NO₅: 356.1498 [MH⁺]; found, 356.1510.

Methyl 4-[(1,1'-Biphenyl)-4-yl]-5,7-dimethoxyquinoline-1(4H)-carboxylate (5ai) (Table 2). Prepared from **1ai** (0.11 g, 0.28 mmol), *p*-TsOH (53.9 mg, 0.28 mmol), BQ (30.7 mg, 0.28 mmol), and PdCl₂(CH₃CN)₂ (3.7 mg, 0.014 mmol) in dioxane (18.9 mL). After workup and purification by flash column chromatography (silica

gel, petroleum ether/AcOEt 8/2), **Sai** was obtained as a solid (82.6 mg, 73%): mp (CH₂Cl₂) 54–56 °C; ¹H NMR (300 MHz, CDCl₃): δ 3.74 (s, 3H), 3.85 (s, 3H), 3.92 (s, 3H), 4.89 (d, *J* = 6.2 Hz, 1H), 5.53 (dd, *J* = 7.7, 6.2 Hz, 1H), 6.33 (d, *J* = 2.3 Hz, 1H), 7.11 (d, *J* = 7.7 Hz, 1H), 7.20–7.71 (m, 10H) ppm; ¹³C{¹H} NMR (75.5 MHz, CDCl₃): δ 36.9, 53.4, 55.4, 55.6, 95.8, 98.0, 112.0, 113.8, 125.4, 127.0, 127.1, 127.2, 127.8, 128.7, 137.5, 139.1, 141.1, 143.9, 153.2, 157.2, 159.1 ppm; IR (ATR): 1724 cm⁻¹; MS (ESI) *m/z* (rel intensity): 402.2 (MH⁺, 100), 248.1 (1); HRMS (ESI): *m/z* calcd for C₂₅H₂₄NO₄: 402.1705 [MH⁺]; found, 402.1710.

Methyl 4-[4-(*tert*-Butyl)phenyl]-5,7-dimethoxyquinoline-1(4*H*)-carboxylate (5aj**) (Table 2).** Prepared from **1aj** (91.5 mg, 0.24 mmol), *p*-TsOH (45.4 mg, 0.24 mmol), BQ (25.8 mg, 0.24 mmol), and PdCl₂(CH₃CN)₂ (3.1 mg, 0.012 mmol) in dioxane (15.9 mL). After workup and purification by flash column chromatography (silica gel, petroleum ether/AcOEt 9/1), **5aj** was obtained as a solid (79.1 mg, 87%): mp (CH₂Cl₂) 107–109 °C; ¹H NMR (300 MHz, CDCl₃): δ 1.29 (s, 9H), 3.73 (s, 3H), 3.83 (s, 3H), 3.90 (s, 3H), 4.82 (d, *J* = 6.3 Hz, 1H), 5.51 (dd, *J* = 7.6, 6.3 Hz, 1H), 6.30 (d, *J* = 2.3 Hz, 1H), 7.08 (d, *J* = 7.7 Hz, 1H), 7.15 (d, *J* = 8.3 Hz, 2H), 7.26 (d, *J* = 8.3 Hz, 2H), 7.41 (d, *J* = 2.3 Hz, 1H) ppm; ¹³C{¹H} NMR (75.5 MHz, CDCl₃): δ 31.4, 34.3, 36.6, 53.3, 55.4, 55.6, 95.8, 98.0, 112.6, 114.2, 125.3, 127.0, 137.5, 141.6, 148.8, 153.2, 157.1, 158.9 ppm; IR (ATR): 1724 cm⁻¹; MS (ESI) *m/z* (rel intensity): 382.2 (MH⁺, 100), 248.1 (10); HRMS (ESI-TOF): calcd for C₂₃H₂₈NO₄: 382.2018 [MH⁺]; found, 382.2019.

Methyl 5,7-Dimethoxy-4-(4-fluorophenyl)quinoline-1(4*H*)-carboxylate (5ak**) (Table 2).** Prepared from **1ak** (0.11 mg, 0.31 mmol), *p*-TsOH (59.9 mg, 0.31 mmol), *p*-BQ (34.0 mg, 0.31 mmol), and PdCl₂(CH₃CN)₂ (4.1 mg, 0.016 mmol) in dioxane (21.0 mL). After workup and purification by flash column chromatography (silica gel, petroleum ether/AcOEt 8/2), **5ak** was obtained as a solid (77.5 mg, 72%): mp (CH₂Cl₂) 129–131 °C; ¹H NMR (300 MHz, CDCl₃): δ 3.73 (s, 3H), 3.84 (s, 3H), 3.92 (s, 3H), 4.82 (d, *J* = 6.2 Hz, 1H), 5.47 (dd, *J* = 7.7, 6.2 Hz, 1H), 6.31 (d, *J* = 2.3 Hz, 1H), 6.88–6.97 (m, 2H), 7.09 (d, *J* = 7.7 Hz, 1H), 7.14–7.21 (m, 2H), 7.45 (d, *J* = 2.3 Hz, 1H) ppm; ¹³C{¹H} NMR (75.5 MHz, CDCl₃): δ 36.5, 53.4, 55.4, 55.6, 95.8, 98.0, 112.0, 113.6, 115.0 (d, *J* = 21.3 Hz), 125.3, 128.9 (d, *J* = 8.0 Hz), 137.4, 140.6 (d, *J* = 3.1 Hz), 153.1, 157.1, 159.1, 161.4 (d, *J* = 243.9 Hz) ppm; IR (ATR): 1724 cm⁻¹; MS (ESI) *m/z* (rel intensity): 344.1 (MH⁺, 100), 301.1 (1); HRMS (ESI-TOF): calcd for C₁₉H₁₉FNO₄: 344.1298 [MH⁺]; found: 344.1311.

Methyl 5,7-Dimethoxy-4-(naphthalene-1-yl)quinoline-1(4*H*)-carboxylate (5al**) (Table 2).** Prepared from **1al** (72.0 mg, 0.19 mmol), *p*-TsOH (36.3 mg, 0.19 mmol), BQ (20.6 mg, 0.19 mmol), and PdCl₂(CH₃CN)₂ (2.5 mg, 0.010 mmol) in dioxane (12.7 mL). After workup and purification by flash column chromatography (silica gel, petroleum ether/AcOEt 8/2), **5al** was obtained as a solid (58.4 mg, 82%): mp (CH₂Cl₂) 140–142 °C; ¹H NMR (300 MHz, CDCl₃): δ 3.54 (s, 3H), 3.86 (s, 3H), 3.89 (s, 3H), 5.61–5.71 (m, 2H), 6.33 (d, *J* = 2.4 Hz, 1H), 6.92–7.00 (m, 2H), 7.27–7.34 (m, 1H), 7.47–7.55 (m, 2H), 7.56–7.64 (m, 1H), 7.67 (d, *J* = 8.2 Hz, 1H), 7.84–7.91 (m, 1H); 8.34 (d, *J* = 8.4 Hz, 1H) ppm; ¹³C{¹H} NMR (75.5 MHz, CDCl₃): δ 33.3, 53.3, 55.5, 55.6, 95.9, 97.9, 111.5, 113.0, 123.4, 124.1, 125.0, 125.4, 125.9, 126.1, 126.6, 128.9, 130.9, 134.0, 138.7, 141.2, 153.2, 157.3, 159.3 ppm; IR (ATR): 1727 cm⁻¹; MS (ESI) *m/z* (rel intensity): 398.1 (MNa⁺, 53), 376.2 (MH⁺, 100), 248.1 (25); HRMS (ESI-TOF): calcd for C₂₃H₂₂NO₄: 376.1549 [MH⁺]; found: 376.1553.

5,7-Dimethoxy-4-phenyl-1-tosyl-1,4-dihydroquinoline (5fc**) (Table 4, Entry 3).** Prepared from **1fc** (0.10 g, 0.25 mmol), *p*-TsOH (46.6 mg, 0.25 mmol), BQ (26.5 mg, 0.25 mmol), and PdCl₂(CH₃CN)₂ (3.2 mg, 0.012 mmol) in dioxane (16.3 mL). After workup and purification by flash column chromatography (silica gel, petroleum ether/CH₂Cl₂ 4/6), **5fc** was obtained as a solid (43.6 mg, 42%): mp (CH₂Cl₂) 161–163 °C; ¹H NMR (300 MHz, CDCl₃): δ 2.42 (s, 3H), 3.55 (s, 3H), 3.86 (s, 3H), 4.64 (d, *J* = 5.6 Hz, 1H), 5.35–5.50 (m, 1H), 6.24 (br s, 1H), 6.44–6.53 (m, 2H), 6.89–6.98 (m, 3H), 6.99–7.08 (m, 1H), 7.18 (d, *J* = 7.9 Hz, 2H), 7.42 (br s, 1H) 7.63 (d, *J* = 7.9 Hz, 2H) ppm; ¹³C{¹H} NMR (75.5 MHz,

CDCl₃): δ 21.6, 37.7, 55.4, 55.5, 96.5, 97.6, 111.2, 115.7, 124.1, 125.5, 127.2, 127.6, 127.8, 129.7, 134.7, 136.1, 144.2, 144.9, 157.9, 159.4 ppm; IR (ATR): 1350, 1154 cm⁻¹; MS (ESI) *m/z* (rel intensity): 422.1 (MH⁺, 100), 344.1 (3), 267.1 (5), 266.1 (8); HRMS (ESI): *m/z* calcd for C₂₄H₂₄NO₄S: 422.1426 [MH⁺]; found: 422.1431.

4-Benzyl-5,7-dimethoxy-1-tosyl-1,4-dihydroquinoline (5fd**) (Table 4, Entry 4).** Prepared from **1fd** (0.10 g, 0.24 mmol), *p*-TsOH (44.8 mg, 0.24 mmol), BQ (25.4 mg, 0.24 mmol), and PdCl₂(CH₃CN)₂ (3.1 mg, 0.012 mmol) in dioxane (15.7 mL). After workup and purification by flash column chromatography (silica gel, petroleum ether/AcOEt 9/1), **5fd** was obtained as an oil (61.9 mg, 60%): ¹H NMR (300 MHz, CDCl₃): δ 0.97–1.13 (m, 1H), 2.34 (s, 3H), 2.44–2.57 (m, 1H), 3.51–3.61 (m, 1H), 3.71 (s, 3H), 3.87 (s, 3H), 5.24 (t, *J* = 6.7 Hz, 1H), 6.33 (br s, 1H), 6.74 (d, *J* = 7.5 Hz, 1H), 6.90 (d, *J* = 7.5 Hz, 2H), 7.13–7.33 (m, 6H), 7.64 (d, *J* = 7.5 Hz, 2H) ppm; ¹³C{¹H} NMR (75.5 MHz, CDCl₃): δ 21.6, 33.8, 44.7, 55.5, 55.6, 96.7, 99.4, 114.2, 118.8, 125.7, 126.0, 127.7, 128.1, 128.9, 129.5, 134.6, 136.3, 139.7, 144.3, 157.1, 159.0 ppm; IR (ATR): 1358, 1168 cm⁻¹; MS (ESI) *m/z* (rel intensity): 458.1 (MNa⁺, 100), 436.2 (MH⁺, 91), 345.1 (15), 344.1 (96); HRMS (ESI-TOF): *m/z* calcd for C₂₅H₂₅NO₄SNa: 458.1402 [MNa⁺]; found, 458.1406.

(1*R*,2*S*,5*R*)-2-Isopropyl-5-methylcyclohexyl 5,7-dimethoxy-4-methylquinoline-1(4*H*)-carboxylate (5gb**) (Scheme 6).** Prepared from **1gb** (0.11 g, 0.28 mmol), *p*-TsOH (52.5 mg, 0.28 mmol), BQ (29.8 mg, 0.28 mmol), and PdCl₂(CH₃CN)₂ (3.6 mg, 0.014 mmol) in dioxane (18.4 mL). After workup and purification by flash column chromatography (silica gel, petroleum ether/AcOEt 18/1), **5gb** was obtained as a mixture of *C*-4 diastereoisomers in a 58:42 ratio and as an oil (71.3 mg, 67%): [α]_D²⁰ = -57.9 (c 1.13, CH₂Cl₂); ¹H NMR (300 MHz, CDCl₃): δ 0.79–0.97 (m, 10H, both isom), 1.04–1.18 (m, 5H, both isom), 1.44–1.61 (m, 2H, both isom), 1.69–1.76 (m, 2H, both isom), 1.93–2.04 (m, 1H, both isom), 2.14–2.23 (m, 1H, both isom), 3.60–3.68 (m, 1H, both isom), 3.80 (s, 3H, both isom), 3.81 (s, 3H, both isom), 4.68–4.78 (m, 1H, both isom), 5.33–5.38 (m, 1H, both isom), 6.30 (d, *J* = 2.3 Hz, 1H, both isom), 6.93 (d, *J* = 7.3 Hz, 1H, minor isom) 6.95 (d, *J* = 7.3 Hz, 1H, major isom), 7.32 (d, *J* = 2.3 Hz, 1H, minor isom), 7.35 (d, *J* = 2.3 Hz, 1H, major isom); ¹³C{¹H} NMR (75.5 MHz, CDCl₃): δ (major isom.): 16.6, 20.8, 22.0, 22.1, 23.7, 26.1, 26.5, 31.5, 34.3, 41.2, 47.3, 55.4, 55.5, 76.7, 95.5, 98.1, 114.5, 115.5, 125.2, 137.5, 152.5, 156.8, 158.4 ppm (minor isom.): 16.6, 20.8, 22.1, 22.2, 23.7, 26.1, 26.7, 31.5, 34.3, 41.4, 47.3, 55.4, 55.5, 76.5, 95.6, 98.0, 114.8, 115.8, 125.3, 137.6, 152.5, 156.8, 158.4 ppm; IR (ATR): 1716 cm⁻¹; MS (ESI) *m/z* (rel intensity): 410.2 (MNa⁺, 82), 250.1 (9); HRMS (ESI-TOF): calcd for C₂₃H₃₃NO₄Na: 410.2307 [MNa⁺]; found: 410.2316.

(1*R*,2*S*,5*R*)-2-Isopropyl-5-methylcyclohexyl 5,7-dimethoxy-4-phenylquinoline-1(4*H*)-carboxylate (5gc**) (Scheme 6).** Prepared from **1gc** (0.12 g, 0.26 mmol), *p*-TsOH (48.8 mg, 0.26 mmol), BQ (27.7 mg, 0.26 mmol), and PdCl₂(CH₃CN)₂ (3.3 mg, 0.013 mmol) in dioxane (17.1 mL). After workup and purification by flash column chromatography (silica gel, petroleum ether/AcOEt 9/1), **5gc** was obtained as a mixture of diastereoisomers in a 63:37 ratio and as an oil (89.4 mg, 78%): [α]_D²⁰ = -25.3 (c 0.88, CH₂Cl₂); ¹H NMR (300 MHz, CDCl₃): δ 0.72–0.98 (m, 10H, both isom), 1.07–1.18 (m, 2H, both isom), 1.46–1.53 (m, 1H, both isom), 1.53–1.60 (m, 1H, both isom), 1.70–1.76 (m, 2H, both isom), 1.94–2.03 (m, 1H, both isom), 2.18–2.25 (m, 1H, H₂), 3.73 (s, 3H, minor isom), 3.74 (s, 3H, major isom), 3.83 (s, 3H, minor isom), 3.84 (s, 3H, major isom), 4.76–4.89 (m, 2H, both isom), 5.50 (ddd, *J* = 11.1, 7.6, 6.3 Hz, 1H, both isom), 6.28 (d, *J* = 2.2 Hz, 1H, both isom), 7.08 (d, *J* = 7.6 Hz, 1H, minor isom), 7.09 (d, *J* = 7.6 Hz, 1H, major isom), 7.12–7.25 (m, 5H, both isom), 7.38 (d, *J* = 2.2 Hz, 1H) ppm; ¹³C{¹H} NMR (75.5 MHz, CDCl₃): δ (major isom.): 16.6, 20.8, 22.1, 23.7, 26.6, 31.5, 34.3, 37.3, 41.2, 47.4, 55.4, 55.6, 77.0, 95.7, 98.3, 112.5, 113.8, 125.6, 126.2, 127.4, 128.3, 137.7, 145.0, 152.5, 157.1, 158.9 ppm (minor isom.): 16.5, 20.8, 22.1, 23.6, 26.6, 31.5 (C₅), 34.3, 37.3, 41.4, 47.4, 55.4, 55.6, 76.7, 96.0, 98.2, 113.0, 114.2, 125.8, 126.2, 127.5, 128.3, 137.7, 144.8, 152.4, 157.0, 158.9 ppm; IR (ATR): 1716 cm⁻¹; MS (ESI) *m/z* (rel intensity): 474.3 (MNa⁺, 100), 363.2 (5); HRMS (ESI): *m/z* calcd for C₂₈H₃₇NO₄Na: 474.2620 [MNa⁺]; found: 474.2621.

(1*R*,2*S*,5*R*)-2-Isopropyl-5-methylcyclohexyl 5,7-Dimethoxy-4-(naphthalene-1-yl)quinolone-1(4*H*)-carboxylate (**5gl**) (Scheme 6). Prepared from **1gl** (84.8 mg, 0.17 mmol), *p*-TsOH (32.2 mg, 0.17 mmol), BQ (18.3 mg, 0.17 mmol), and PdCl₂(CH₃CN)₂ (2.2 mg, 0.0085 mmol) in dioxane (11.3 mL). After workup and purification by flash column chromatography (silica gel, petroleum ether/AcOEt 9/1), **5gl** was obtained as a mixture of diastereoisomers in a 58:42 ratio and as a solid (66.5 mg, 79%): mp (CH₂Cl₂) 73–75 °C; [α]_D²⁰ = –87.0 (0.71, CH₂Cl₂); ¹H NMR (300 MHz, CDCl₃): δ 0.78–0.99 (m, 10H), 1.03–1.27 (m, 2H), 1.41–1.66 (m, 2H), 1.68–1.79 (m, 2H), 1.80–2.07 (m, 1H), 2.17–2.25 (m, 1H), 3.56 (s, 3H), 3.92 (s, 3H), 4.84 (qd, *J* = 10.7, 4.3 Hz, 1H), 5.61–5.77 (m, 2H), 6.35 (d, *J* = 2.2 Hz, 1H), 6.93–7.11 (m, 2H), 7.32 (t, *J* = 7.7 Hz, 1H), 7.49–7.58 (m, 2H), 7.62 (t, *J* = 7.7 Hz, 1H), 7.70 (d, *J* = 8.1 Hz), 7.90 (d, *J* = 7.7 Hz, 1H); 8.39 (d, *J* = 8.1 Hz, 1H) ppm; ¹³C{¹H} NMR (75.5 MHz, CDCl₃): δ (major isom.): 16.7, 20.8, 22.0, 23.7, 26.6, 31.5, 33.3, 34.3, 41.1, 47.3, 55.5, 55.6, 76.7, 95.8, 98.1, 112.8, 113.4, 123.5, 124.1, 125.3, 125.9, 126.1, 126.6, 128.9, 131.0, 134.0, 138.9, 141.3, 152.5, 157.2, 159.1 ppm (minor isom.): 16.5, 20.7, 22.1, 23.6, 26.4, 31.5, 33.2, 34.3, 41.4, 47.3, 55.5, 55.6, 76.7, 96.0, 98.1, 111.6, 112.1, 123.5, 124.2, 125.3, 125.8, 126.1, 126.5, 128.9, 131.0, 134.0, 138.9, 141.3, 152.6, 157.2, 159.1 ppm; IR (ATR): 1713 cm⁻¹; MS (ESI) *m/z* (rel intensity): 522.3 (MNa⁺, 58), 500.3 (MH⁺, 28), 362.1 (100); HRMS (ESI-TOF): calcd for C₃₂H₃₈NO₄: 500.2801 [MH⁺]; found, 500.2794.

Use of Boc-Val-OH as Ligand. Synthesis of 5ac (1 mmol Scale) (Table 2). To a solution of **1ac** (0.3328 g, 1 mmol) in 1,4-dioxane (68 mL), *p*-TsOH (0.1934 g, 1 mmol), BQ (0.1081 g, 1 mmol), Boc-Val-OH (0.02208 g, 0.1 mmol), and PdCl₂(CH₃CN)₂ (0.019 g, 0.05 mmol) were added and the reaction mixture was stirred at room temperature for 16 h. Afterward, water was added to quench the reaction and it was extracted with CH₂Cl₂ (3 × 10 mL). The combined organic extracts were washed with brine (10 mL) and dried (Na₂SO₄). The solvent was evaporated in vacuo, and the residue was purified by flash column chromatography (silica gel, petroleum ether/AcOEt 8/2) affording **5ac** as a solid (0.2759 g, 85%).

Methyl (2-Allyl-3,5-dimethoxyphenyl)carbamate (6). Over a solution of 2-allyl-3,5-dimethoxyaniline³² (51.1 mg, 0.26 mmol) and pyridine (42.6 μ L, 0.53 mmol) in dry THF (7 mL) under argon atmosphere, methyl chloroformate (22.5 μ L, 0.29 mmol) was added dropwise. The reaction was stirred for 16 h at room temperature, and afterward, the solvent was removed under reduced pressure. The crude reaction was dissolved in CH₂Cl₂ (15 mL) and washed with a 10% aqueous solution of HCl (2 × 15 mL) and with water (15 mL). The combined organic extracts were dried (Na₂SO₄) and concentrated in vacuo. Purification by flash column chromatography (petroleum ether/AcOEt 8/2) afforded **6** as a solid (63.9 mg, 96%): mp (CH₂Cl₂): 83–84 °C; ¹H NMR (300 MHz, CDCl₃): δ 3.36 (dt, *J* = 5.6, 1.6 Hz, 2H), 3.76 (s, 3H), 3.78 (s, 3H), 3.81 (s, 3H), 4.93–5.14 (m, 2H), 5.83–5.97 (m, 1H), 5.26 (d, *J* = 2.4 Hz, 1H), 6.69 (br s, 1H), 7.18 (br s, 1H) ppm; ¹³C{¹H} NMR (75.5 MHz, CDCl₃): δ 27.9, 52.3, 55.4, 55.8, 95.0, 97.8, 109.2, 115.2, 136.1, 137.9, 154.3, 158.1, 159.4 ppm; IR (ATR): 3310, 1695 cm⁻¹; MS (ESI): *m/z* (%): 274.1 (MNa⁺, 100), 252.1 (6); HRMS (ESI-TOF): calcd for C₁₃H₁₇NO₄Na: 274.1055 [MNa⁺]; found: 274.1060.

Methyl 4,6-Dimethoxy-2-methyl-1*H*-indole-1-carboxylate (7). Over a solution of **6** (55.5 mg, 0.22 mmol) in dioxane (14.7 mL), *p*-TsOH (42.0 mg, 0.22 mmol), BQ (23.9 mg, 0.22 mmol), and PdCl₂(CH₃CN)₂ (2.9 mg, 0.011 mmol) were added. The solution was stirred at room temperature for 3 h. Afterward, water was added to quench the reaction and it was extracted with CH₂Cl₂ (3 × 10 mL). The combined organic extracts were washed with brine (10 mL) and dried (Na₂SO₄). The solvent was evaporated in vacuo, and the residue was purified by flash column chromatography (silica gel, petroleum ether/AcOEt 9/1), affording **7** as a solid (42.7 mg, 78%): mp (CH₂Cl₂): 88–90 °C; ¹H NMR (300 MHz, CDCl₃): δ 2.54 (s, 3H), 3.87 (s, 3H), 3.89 (s, 3H), 4.02 (s, 3H), 6.35 (d, *J* = 1.9 Hz, 1H), 6.36 (br s, 1H), 7.36 (d, *J* = 1.9 Hz, 1H) ppm; ¹³C{¹H} NMR (75.5 MHz, CDCl₃): δ 16.8, 53.4, 55.4, 55.8, 92.7, 94.3, 105.1, 113.7, 134.4, 138.0, 152.2, 152.9, 158.2 ppm; IR (ATR): 1720 cm⁻¹; MS

(ESI) *m/z* (rel intensity): 250.1 (MH⁺, 100), 190.1 (4); HRMS (ESI-TOF): calcd for C₁₃H₁₆NO₄: 250.1079 [MH⁺]; found, 250.1079.

■ ASSOCIATED CONTENT

Supporting Information

The Supporting Information is available free of charge at <https://pubs.acs.org/doi/10.1021/acs.joc.9b03174>.

Preparation of substrates **1**; cyclization assays on **1gc**; computational data; ¹H and ¹³C NMR spectra of compounds **1–7** (PDF)

■ AUTHOR INFORMATION

Corresponding Authors

Nuria Sotomayor – Universidad del País Vasco/Euskal Herriko Unibertsitatea UPV/EHU, Bilbao, Spain;

orcid.org/0000-0003-3079-6380;

Email: nuria.sotomayor@ehu.es

Enrique Gómez-Bengoa – Universidad del País Vasco/Euskal Herriko Unibertsitatea UPV/EHU, San Sebastián, Spain; orcid.org/0000-0002-8753-3760;

Email: enrique.gomez@ehu.es

Esther Lete – Universidad del País Vasco/Euskal Herriko Unibertsitatea UPV/EHU, Bilbao, Spain; orcid.org/0000-0001-8624-6842; Email: esther.lete@ehu.es

Other Authors

Asier Carral-Menoyo – Universidad del País Vasco/Euskal Herriko Unibertsitatea UPV/EHU, Bilbao, Spain

Lia Sotorriós – Universidad del País Vasco/Euskal Herriko Unibertsitatea UPV/EHU, San Sebastián, Spain

Verónica Ortiz-de-Elguea – Universidad del País Vasco/Euskal Herriko Unibertsitatea UPV/EHU, Bilbao, Spain

Aitor Diaz-Andrés – Universidad del País Vasco/Euskal Herriko Unibertsitatea UPV/EHU, Bilbao, Spain

Complete contact information is available at: <https://pubs.acs.org/doi/10.1021/acs.joc.9b03174>

Notes

The authors declare no competing financial interest.

■ ACKNOWLEDGMENTS

Ministerio de Economía y Competitividad (CTQ2016-74881-P; CTQ2016-78083-P) and Gobierno Vasco (IT1045-16) are gratefully acknowledged for their financial support. A.C.-M. thanks Gobierno Vasco for a grant. Computational, technical, and human support provided by Servicios Generales de Investigación SGIker (UPV/EHU, MINECO, GV/EJ, ERDF and ESF) is also acknowledged.

■ REFERENCES

- Lei, A.; Shi, W.; Liu, W.; Zhang, H.; He, C. *Oxidative Cross-Coupling Reactions*; Wiley-VCH: Weinheim, Germany, 2017.
- For selected reviews, see: (a) Ferreira, E. M.; Zhang, H.; Stoltz, B. M. *Oxidative Heck-Type Reactions* (Fujiwara–Moritani Reactions). In *The Mizoroki–Heck Reaction*; Oestreich, M. Ed.; Wiley: Chichester, 2009; pp 345–382. (b) Le Bras, J.; Muzart, J. Intermolecular Dehydrogenative Heck Reactions. *Chem. Rev.* **2011**, *111*, 1170–1214. (c) Suna, E.; Shubin, K. Intramolecular Coupling via C(sp²)-H Activation. In *Science of Synthesis. Cross Coupling and Heck-Type Reactions 3. Metal-Catalyzed Heck-Type Reactions and C–H Couplings via C–H Activation*; Larhed, M., Ed.; Georg Thieme Verlag:

Stuttgart, 2013; pp 643–653. (d) Zhou, L.; Lu, W. Towards Ideal Synthesis: Alkenylation of Aryl C–H Bonds by a Fujiwara–Moritani Reaction. *Chem. – Eur. J.* **2014**, *20*, 634–642. (e) Kitamura, T.; Fujiwara, Y. *RSC Green Chemistry Series: From C–H to C–C Bonds: Cross-Dehydrogenative-Coupling*; Li, C.-J., Ed.; Royal Society of Chemistry: London, UK, 2015; Vol. 26, pp 33–54. (f) Topczewski, J. J.; Sanford, M. S. Carbon–Hydrogen (C–H) Bond Activation at PdIV: a Frontier in C–H Functionalization Catalysis. *Chem. Sci.* **2015**, *6*, 70–76. (g) Gensch, T.; Hopkinson, M. N.; Glorius, F.; Wencel-Delord, J. Mild Metal-Catalyzed C–H Activation: Examples and Concepts. *Chem. Soc. Rev.* **2016**, *45*, 2900–2936.

(3) Neufeldt, S. R.; Sanford, M. S. Controlling Site Selectivity in Palladium-Catalyzed C–H Bond Functionalization. *Acc. Chem. Res.* **2012**, *45*, 936–946.

(4) (a) Ferreira, E. M.; Stoltz, B. M. Catalytic C–H Bond Functionalization with Palladium(II): Aerobic Oxidative Annulations of Indoles. *J. Am. Chem. Soc.* **2003**, *125*, 9578–9579. (b) Abbiati, G.; Beccalli, E. M.; Brogini, G.; Zoni, C. Regioselectivity on the Palladium-Catalyzed Intramolecular Cyclization of Indole Derivatives. *J. Org. Chem.* **2003**, *68*, 7625–7628. (c) Garg, N. K.; Stoltz, B. M. A Unified Synthetic Approach to the Pyrazinone Druggable. *Chem. Commun.* **2006**, *21*, 3769–3779. (d) Schiffner, J. A.; Machotta, A. B.; Oestreich, M. A Catalytic Asymmetric Fujiwara–Moritani Cyclization. *Synlett* **2008**, *15*, 2271–2274. (e) Bowie, A. L.; Trauner, D. Total Synthesis of (±)-Rhazinal Using Novel Palladium-Catalyzed Cyclizations. *J. Org. Chem.* **2009**, *74*, 1581–1586. (f) Schiffner, J. A.; Woste, T. H.; Oestreich, M. Enantioselective Fujiwara–Moritani Indole and Pyrrole Annulations Catalyzed by Chiral Palladium(II)–NiOx Complexes. *Eur. J. Org. Chem.* **2010**, *2010*, 174–182. (g) Donets, P. A.; Van der Eycken, E. V. Synthesis of the Azepinoindole Framework via Oxidative Heck (Fujiwara–Moritani) Cyclization. *Synthesis* **2011**, 2147–2153. (h) Kandukuri, S. R.; Jiao, L.-Y.; Machotta, A. B.; Oestreich, M. Diastereotopic Group Selection in Hydroxy-Directed Intramolecular CH Alkenylation of Indole under Oxidative Palladium(II) Catalysis. *Adv. Synth. Catal.* **2014**, *356*, 1597–1609. (i) Abozeid, M. A.; Sairenji, S.; Takizawa, S.; Fujita, M.; Sasai, H. Enantioselective synthesis of tetrahydrocyclopenta(b)indole bearing a chiral quaternary carbon center via Pd(II)–SPRIX-catalyzed C–H activation. *Chem. Commun.* **2017**, *53*, 6887–6890.

(5) (a) Zhang, H.; Ferreira, E. M.; Stoltz, B. M. Direct Oxidative Heck Cyclizations: Intramolecular Fujiwara–Moritani Arylations for the Synthesis of Functionalized Benzofurans and Dihydrobenzofurans. *Angew. Chem., Int. Ed.* **2004**, *43*, 6144–6148. (b) Youn, S. W.; Eom, J. I. Facile Construction of the Benzofuran and Chromene Ring Systems via PdII-Catalyzed Oxidative Cyclization. *Org. Lett.* **2005**, *7*, 3355–3358. (c) Ferreira, E. M.; Zhang, H.; Stoltz, B. M. C–H Bond Functionalizations with Palladium(II): Intramolecular Oxidative Annulations of Arenes. *Tetrahedron* **2008**, *64*, 5987–6001.

(6) (a) Carral-Menoyo, A.; Ortiz-de Elguea, V.; Martínez-Nunes, M.; Sotomayor, N.; Lete, E. Palladium-Catalyzed Dehydrogenative Coupling: An Efficient Synthetic Strategy for the Construction of the Quinoline Core. *Mar. Drugs* **2017**, *15*, 276. (b) Carral-Menoyo, A.; Misol, A.; Gómez-Redondo, M.; Sotomayor, N.; Lete, E. Palladium(II)-catalyzed Intramolecular C–H Alkenylation for the Synthesis of Chromanes. *J. Org. Chem.* **2019**, *84*, 2048–2060.

(7) (a) Kong, A.; Han, X.; Lu, X. Highly Efficient Construction of Benzene Ring in Carbazoles by Palladium-Catalyzed endo-Mode Oxidative Cyclization of 3-(3'-Alkenyl)indoles. *Org. Lett.* **2006**, *8*, 1339–1342. (b) Han, X.; Lu, X. Novel Palladium-Catalyzed Acyloxylation/Cyclization of 2-(3'-Alkenyl)indoles. *Org. Lett.* **2009**, *11*, 2381–2384.

(8) Liu, C.; Widenhoefer, R. A. Palladium-Catalyzed Cyclization/Carboalkoxylation of Alkenyl Indoles. *J. Am. Chem. Soc.* **2004**, *126*, 10250–10251.

(9) Schiffner, J. A.; Oestreich, M. All-Carbon-Substituted Quaternary Carbon Atoms in Oxindoles by an Aerobic Palladium(II)-Catalyzed Ring Closure onto Tri- and Tetrasubstituted Double Bonds. *Eur. J. Org. Chem.* **2011**, *2011*, 1148–1154.

(10) (a) Jaegli, S.; Dufour, J.; Wei, H.-I.; Piou, T.; Duan, X.-H.; Vors, J.-P.; Neuville, L.; Zhu, J. Palladium-Catalyzed Carbo-Heterofunctionalization of Alkenes for the Synthesis of Oxindoles and Spirooxindoles. *Org. Lett.* **2010**, *12*, 4498–4501. (b) Wu, T.; Mu, X.; Liu, G. Palladium-Catalyzed Oxidative Arylalkylation of Activated Alkenes: Dual C–H Bond Cleavage of an Arene and Acetonitrile. *Angew. Chem., Int. Ed.* **2011**, *50*, 12578–12581. (c) Mu, X.; Wu, T.; Wang, H.-Y.; Guo, Y.-I.; Liu, G. Palladium-Catalyzed Oxidative Aryltri-fluoromethylation of Activated Alkenes at Room Temperature. *J. Am. Chem. Soc.* **2012**, *134*, 878–881.

(11) Ortiz-de Elguea, V.; Sotomayor, N.; Lete, E. Two Consecutive Pd(II)-promoted C–H Alkenylation Reactions for the Synthesis of Substituted 3-Alkenylquinolones. *Adv. Synth. Catal.* **2015**, *357*, 463–473.

(12) (a) Würtz, S.; Rakshit, S.; Neumann, J. J.; Dröe, T.; Glorius, F. Palladium-catalyzed oxidative cyclization of N-aryl enamines: from anilines to indoles. *Angew. Chem., Int. Ed.* **2008**, *47*, 7230–7233. (b) Neumann, J. J.; Rakshit, S.; Dröe, T.; Würtz, S.; Glorius, F. Exploring the Oxidative Cyclization of Substituted N-Aryl Enamines: Pd-Catalyzed Formation of Indoles from Anilines. *Chem. Eur. J.* **2011**, *17*, 7298–73033.

(13) Kandukuri, S. R.; Schiffner, J. A.; Oestreich, M. Aerobic Palladium(II)-Catalyzed 5-endo-trig Cyclization: An Entry into the Diastereoselective C-2 Alkenylation of Indoles with Tri- and Tetrasubstituted Double Bonds. *Angew. Chem., Int. Ed.* **2012**, *51*, 1265–1269.

(14) A different mechanism has been proposed for the reaction of N-aryl enamine carboxylates (Scheme 1c), that involves the initial palladation of the nucleophilic enamine. See ref 12.

(15) For selected recent reviews, see: (a) Michael, J. P. Quinoline, Quinazoline and Acridone Alkaloids. *Nat. Prod. Rep.* **2008**, *25*, 166–187. (b) Kaur, K.; Jain, M.; Reddy, R. P.; Jain, R. Quinolines and Structurally Related Heterocycles as Antimalarials. *Eur. J. Med. Chem.* **2010**, *45*, 3245–3264. (c) Garrido Montalbán, A. Quinolines and Isoquinolines. In *Heterocycles in Natural Products Synthesis*; Majumdar, K. C.; Chattopadhyay, S. K. Eds.; Wiley-VCH: Weinheim, Germany, 2011; pp 299–339. (d) Afzal, O.; Kumar, S.; Haider, MdR.; Ali, MdR.; Kumar, R.; Jaggi, M.; Bawa, S. A Review on Anticancer Potential of Bioactive Heterocycle Quinoline. *Eur. J. Med. Chem.* **2015**, *97*, 871–910.

(16) For a review, see: (a) Hilgeroth, A.; Baumert, C.; Coburger, C.; Seifert, M.; Krawczyk, S.; Hempel, C.; Neubauer, F.; Krug, M.; Molnar, J.; Lage, H. Novel Structurally varied N-Alkyl 1,4-Dihydropyridines as ABCB1 Inhibitors: Structure-Activity Relationships, Biological Activity and First Bioanalytical Evaluation. *Med. Chem.* **2013**, *9*, 487–493. For representative examples, see: (b) Hemmer, M.; Krawczyk, S.; Simon, I.; Lage, H.; Hilgeroth, A. Discovery of Substituted 1,4-Dihydroquinolines as Novel Class of ABCB1 Modulators. *Bioorg. Med. Chem.* **2015**, *23*, 5015–5021. (c) Hemmer, M.; Krawczyk, S.; Simon, I.; Hilgeroth, A. Discovery of Substituted 1,4-Dihydroquinolines as Novel Promising Class of P-glycoprotein Inhibitors: First Structure–Activity Relationships and Bioanalytical Studies. *Bioorg. Med. Chem. Lett.* **2015**, *25*, 3005–3008.

(17) (a) Kumar, A.; Kumar, V.; Alegria, A. E.; Malhotra, S. V. Synthetic and Application Perspectives of Azapodophyllotoxins: Alternative Scaffolds of Podophyllotoxin. *Curr. Med. Chem.* **2011**, *18*, 3853–3870. (b) Chernysheva, N. B.; Tsyganov, D. V.; Philchenkov, A. A.; Zavelevich, M. P.; Kiselyov, A. S.; Semenov, R. V.; Semenova, M. N.; Semenov, V. V. Synthesis and Comparative Evaluation of 4-oxa- and 4-aza-podophyllotoxins as Antiproliferative Microtubule Destabilizing Agents. *Bioorg. Med. Chem. Lett.* **2012**, *22*, 2590–2593.

(18) (a) Bodor, N.; Farag, H. H.; Barros, M. D. C.; Wu, W.-M.; Buchwald, P. In Vitro and In Vivo Evaluations of Dihydroquinoline- and Dihydroisoquinoline-based Targetor Moieties for Brain-specific Chemical Delivery Systems. *J. Drug Target.* **2002**, *10*, 63–71. (b) Țintăș, M.-L.; Foucort, L.; Petit, S.; Oudeyer, S.; Gourand, F.; Barré, L.; Papamicaël, C.; Levacher, V. New Developments in Redox Chemical Delivery Systems by Means of 1,4-Dihydroquinoline-based

targetor: Application to galantamine delivery to the brain. *Eur. J. Med. Chem.* **2014**, *81*, 218–226.

(19) Dong, Y.; Dong, L.; Chen, J.; Luo, M.; Fu, X.; Qiao, C. Synthesis and Biological Evaluation of N-Alkyl-1,4-dihydroquinoline Prodrugs of Scutellarin Methyl Ester as Neuroprotective Agents. *Med. Chem. Res.* **2018**, *27*, 1111–1121.

(20) (a) Foucoute, L.; Gourand, F.; Dhilly, M.; Bohn, P.; Dupas, G.; Costentin, J.; Abbas, A.; Marsais, F.; Barré, L.; Levacher, V. Synthesis, Radiosynthesis and Biological Evaluation of 1,4-Dihydroquinoline Derivatives as new Carriers for Specific Brain Delivery. *Org. Biomol. Chem.* **2009**, *7*, 3666–3673. (b) Gourand, F.; Tintás, M.-L.; Henry, A.; Ibazizenè, M.; Dhilly, M.; Fillesoye, F.; Papamicaël, C.; Levacher, V.; Barré, L. Delivering FLT to the Central Nervous System by Means of a Promising Targeting System: Synthesis, (11C)Radiosynthesis, and in Vivo Evaluation. *ACS Chem. Neurosci.* **2017**, *8*, 2457–2467.

(21) Zhang, D.; Llorente, I.; Liebeskind, L. S. Versatile Synthesis of Dihydroquinolines and Quinoline Quinones using Cyclobutenediones. Construction of the Pyridoacridine Ring System. *J. Org. Chem.* **1997**, *62*, 4330–4338.

(22) (a) Skyler, D.; Heathcock, C. H. The Pyridoacridine Family Tree: A Useful Scheme for Designing Synthesis and Predicting Undiscovered Natural Products. *J. Nat. Prod.* **2002**, *65*, 1573–1581. (b) Delfourne, E.; Bastide, J. Marine Pyridoacridine Alkaloids and Synthetic Analogues as Antitumor Agents. *Med. Res. Rev.* **2003**, *23*, 234–252.

(23) (a) Kouznetsov, V.; Vargas Mendez, L. Y.; Melendez Gomez, C. M. Recent Progress in the Synthesis of Quinolines. *Curr. Org. Chem.* **2005**, *9*, 141–161. (b) Barluenga, J.; Rodríguez, F.; Fañanás, F. J. Recent Advances in the Synthesis of Indole and Quinoline Derivatives through Cascade Reactions. *Chem. Asian J.* **2009**, *4*, 1036–1048. (c) Sridharan, V.; Suryavanshi, P. A.; Menéndez, J. C. Advances in the Chemistry of Tetrahydroquinolines. *Chem. Rev.* **2011**, *111*, 7157–7259. (d) Solomon, V. R.; Lee, H. Quinoline as a Privileged Scaffold in Cancer Drug Discovery. *Curr. Med. Chem.* **2011**, *18*, 1488–1508. (e) Alajarin, R.; Burgos, C. Six-membered Heterocycles: Quinoline and Isoquinoline. In *Modern Heterocyclic Chemistry*; Alvarez-Builla, J.; Vaquero, J. J.; Barluenga, J., Eds.; Wiley-VCH: Weinheim, Germany, 2011; Vol. 3, pp 1527–1629.

(24) (a) Wang, D.-H.; Engle, K. M.; Shi, B.-F.; Yu, J.-Q. Ligand-Enabled Reactivity and Selectivity in a Synthetically Versatile Aryl C–H Olefination. *Science* **2010**, *327*, 315–319. (b) Engle, K. M.; Yu, J.-Q. Developing Ligands for Palladium(II)-Catalyzed C–H Functionalization: Intimate Dialogue between Ligand and Substrate. *J. Org. Chem.* **2013**, *78*, 8927–8955. (c) Engle, K. M. The Mechanism of Palladium(II)-mediated C–H Cleavage with Mono-N-protected Amino Acid (MPAA) Ligands: Origins of Rate Acceleration. *Pure Appl. Chem.* **2016**, *88*, 119–138.

(25) Yuan, K.; Soulé, J. F.; Dorcet, V.; Doucet, H. Palladium-Catalyzed Cascade sp² C–H Bond Functionalizations Allowing One-Pot Access to 4-Aryl-1,2,3,4-tetrahydroquinolines from N-Allyl-N-arylsulfonamides. *ACS Catal.* **2016**, *6*, 8121–8126.

(26) DFT Calculations were run with the Gaussian 16 suite of programs. See [Supporting Information](#) for details.

(27) When the computed energies of the structures in Figures 3 and 4 were compared a stabilizing effect of the coordination of the oxygen to palladium by ca. 2 kcal/mol was noted. See [Supporting Information](#) for further details.

(28) The diastereomers could not be separated by chromatographic methods and the ratio was established by integration of representative signals in the ¹H NMR spectrum (for **5gb** and **5gc**) or in the ¹³C NMR (for **5gl**). The diastereoselectivity could not be improved in the presence of MPAA, acids, or changing the palladium precatalyst. See SI for additional assays performed.

(29) Jiang, T.; Huynh, K.; Livinghouse, T. Substrate Structural Effects in Yttrium(III)-Catalyzed Hydroamination/Cyclizations of 1,2-Disubstituted and 1,1,2-Trisubstituted Aminoalkenes Terminated by 2-(Phenyl) and 2-(2-Heteroarenyl) Groups. *Synlett* **2013**, *24*, 193–196.

(30) Race, N.; Bower, J. Palladium Catalyzed Cyclizations of Oxime Esters with 1,2-Disubstituted Alkenes: Synthesis of Dihydropyrroles. *Org. Lett.* **2013**, *15*, 4616–4619.

(31) Watanabe, T.; Oishi, S.; Fujii, N.; Ohno, H. Gold-Catalyzed Hydroarylation of Allenes: A Highly Regioselective Carbon–Carbon Bond Formation Producing Six-Membered Rings. *Org. Lett.* **2007**, *9*, 4821–4824.

(32) Ye, K.-Y.; Dai, L.-X.; You, S.-L. Enantioselective Synthesis of 2,5-Dihydrobenzo[b]azepine Derivatives via Iridium-catalyzed Asymmetric Allylic Amination with 2-Allylanilines and Ring-Closing-Metathesis Reaction. *Org. Biomol. Chem.* **2012**, *10*, 5932–5939.



Cite this: *Org. Biomol. Chem.*, 2019, **17**, 5112

DFT studies on metal-catalyzed cycloisomerization of *trans*-1,5-enynes to cyclopropane sesquiterpenoids†

Lia Sotorriós,^a Vera P. Demertzidou,^b Alexandros L. Zografos^{a*} and Enrique Gómez-Bengoa^{a*}

We have recently described the synthesis of strained carbocyclic sesquiterpenoid motifs through a highly regioselective cycloisomerization of common enyne acetates, in the presence of platinum(II) and gold(I) chlorides as catalysts. In this work, the mechanisms of these cyclization reactions have been studied by means of DFT methods. At the outset of the reactions, the propargyl substrates suffer 1,2- or 1,3-acetate rearrangements, which compete for the formation of a metal–carbene or a vinyl–metal species, respectively. These intermediates are the resting states of the cycles towards the formation of lindenane or myliol core structures. The DFT studies have revealed the energetics of the two migration processes, as well as the reasons for some of the key experimental observations, such as the *syn/anti* preference in the formation of the cyclopropane rings, the different reactivities of substrates containing furan or lactone moieties, and the different outcomes of the reactions when Pt(II) and Au(I) salts are used.

Received 17th April 2019,
Accepted 1st May 2019

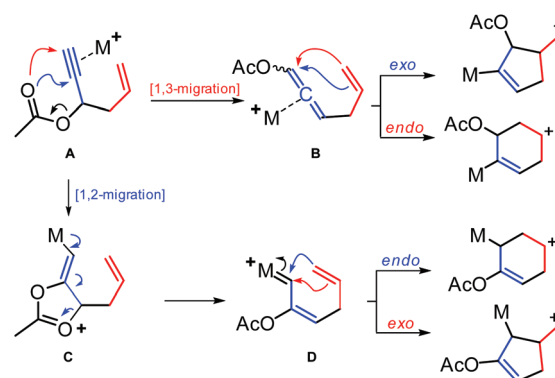
DOI: 10.1039/c9ob00890j

rsc.li/obc

Introduction

Cycloisomerization reactions typically refer to transformations of polyunsaturated acyclic substrates where the reorganization of the electron density results in new cyclized products.¹ The advances in metal-catalyzed processes in the last few decades have led to the evolution of cycloisomerization as one of the most powerful and atom economical methods of modern organic synthesis. Sesquiterpenoids, apart from their intriguing biological properties,² represent a class where the synthetic power of cycloisomerization is well highlighted.³ The resemblance of the cationic nature of metal-catalyzed cycloisomerization reactions to terpenoid biosynthetic pathways and their high efficiency to provide even strained carbocyclic cores counted them, in some cases, as artificial terpene cyclases.⁴ Substrates that are utilized as templates for terpenoid synthesis include mostly flexible 1,6-enynes, propargyl acetates and polyenynes which avoid additional tethers between their unsaturated functionalities.

In metal-catalyzed cycloisomerization reactions, typically enynes are initially activated in the alkyne moiety by a π -metal complex (platinum(II), gold(I and III), rhodium, *etc.*) leading to the formation of a carbocycle from the subsequent addition of the pendant alkene moiety. In the cases where propargylic acetates are involved, the acetate group tends to undergo 1,3-migration to the alkyne to form allenes (**B**, Scheme 1) or 1,2-migration to form metal carbenes (**C**), which are further elaborated to cyclized products through their cycloisomerization by the alkene.^{5,6} Although the high potential of such metal-catalyzed processes is well established, utilization of cycloisomerization reactions with cyclized strained enynes are rather scarce or completely absent from the literature.



Scheme 1 Indicative cycloisomerization pathways for propargyl acetates.

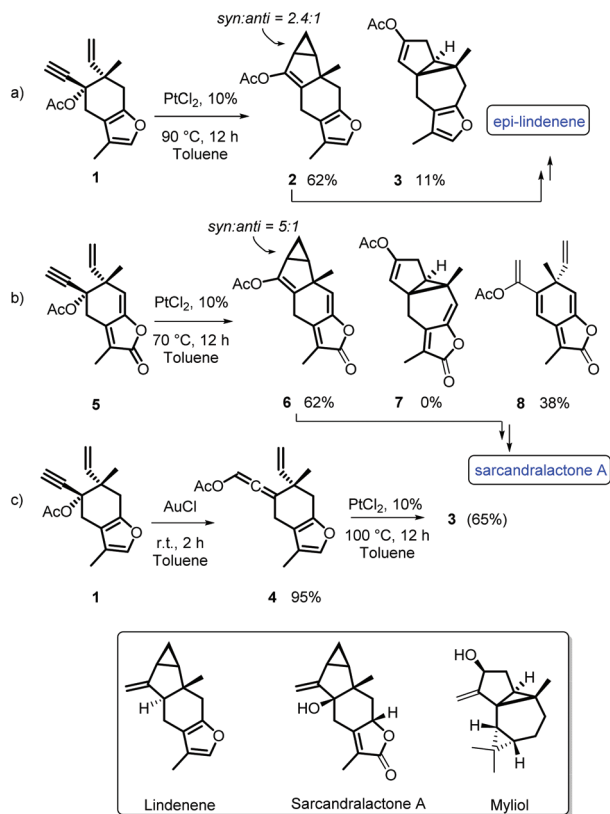
^aDepartment of Organic Chemistry I, Faculty of Chemistry, University of the Basque Country, Manuel Lardizabal 3, 2009 Donostia – San Sebastián, Spain.

E-mail: enrique.gomez@ehu.eus

^bAristotle University of Thessaloniki, University Main Campus, Chemical Department, Laboratory of Organic Chemistry, 54124 Thessaloniki, Greece.

E-mail: alzograf@chem.auth.gr

† Electronic supplementary information (ESI) available: Computational methods, Cartesian coordinates and computed energies of calculated structures. See DOI: 10.1039/c9ob00890j



Scheme 2 Formation of sesquiterpenoid frameworks by Pt(II)- and Au(I)-catalyzed cycloisomerization reactions.

Recently, some of us reported the synthesis of strained carbocyclic sesquiterpene motifs that correspond to lindenene and myliol natural core structures.⁷ Our syntheses relied on the cycloisomerization of *trans*-1,5-enynes **1** and **5** (Scheme 2), which were essentially unexplored under metal-catalyzed conditions.

Apart from the formal synthesis of sarcandra lactone and *epi*-lindenene natural products (Scheme 2),⁸ our strategy brought into light some interesting observations regarding: (a) the experimental preference of platinum(II) chloride towards 1,2- over 1,3-acetate migration, as evidenced by the preferential formation of lindenene over myliol core structures (Scheme 2a); (b) the reaction dependence on the acidity of the propargylic acetate-lactone enyne substrate, which shuts down the 1,3-acetate migration pathway leading only to selective formation of lindenene carbocycles (Scheme 2b); (c) and the crucial role of the metal catalyst on the reaction outcome; experiments showed that gold(I) chloride follows only the 1,3-acetate migration pathway while platinum(II) chloride initiates both 1,2- and 1,3-routes (Scheme 2c). These observations motivated us to study the reaction mechanisms in more detail, with the aid of DFT calculations, aiming at a better understanding of the catalytic cycle and for more efficient design of catalysts and substrates for such cycloisomerization processes.

Discussion

The experimental results, discussed briefly in the introduction, posed some intriguing questions regarding the mechanisms of the key cycloisomerization reactions, and we detail herein the whole mechanistic overview by means of DFT studies. In particular, we were especially interested in interrogating the transition states and intermediates of the catalytic cycles to provide answers to the following specific questions:

(a) What is the reason for the experimentally observed predominance of **2** over **3** in the PtCl₂ catalyzed reaction of elemene-type furan substrate **1**? In a typical experimental procedure, lindenene polycycle **2** is isolated in a *ca.* 2 : 1 ratio over the minor myliol-type product **3** (up to 5 : 1 depending on the conditions, Scheme 2a). What is more, if allene **4** is used as the starting material, only compound **3** is isolated and also observed by NMR, suggesting that allene **4** is an operative intermediate along the route towards **3**.

(b) What is the origin of the different reactivities and selectivities observed between furan **1** and lactone **5** substrates? Both compounds do not have substantial structural differences, and their reactivities should follow probably similar mechanisms, but in contrast to **1**, lactone **5** produces only compounds **6** and **8**,⁸ and not **7** or its derivatives (Scheme 2b). The lack of formation of the latter indicates that, in this case, the selectivity for initial 1,2-acetate migration must be complete. The minor intermediate of this process (**8**) arises from the decoordination of the Pt(II) catalyst at an early stage of the cycle, before the double cyclization with the vinyl moiety takes place, thus highlighting the greater difficulty of this latter step in the case of the lactone.

(c) What are the underlying reasons for the observed diastereoselectivity of product **2**? In general, furan elemene **1** afforded the *syn*-cyclopropane diastereoisomer of **2**, in variable ratios (typically around 2 : 1) over the *anti* isomer (Scheme 2a). A similar *syn* preference was observed for lactone **5**, although in this case with increased selectivity, up to 5 : 1. The identification of the diastereo-differentiating step and a comparison of the activation energies for the *syn* and *anti* pathways would probably allow us to optimize the sequence experimentally to produce cleaner reaction profiles.

(d) How is the divergent reactivity between platinum and gold catalysts explained, which has also been observed by others in related reactions?⁹ Experimentally, in the presence of AuCl, the reaction seems to follow solely the 1,3-migration pathway (Scheme 2c), where it stops at an intermediate stage, after the formation of the allene **4**. Allene **4** is the only product of the reaction, formed in quantitative yield under very mild reaction conditions, occurring typically at room temperature in less than 2 hours. No polycyclized products were ever observed, and more drastic reaction conditions (higher temperatures) led only to decomposition.

In order to shed light on the previous questions, we performed DFT calculations with the Gaussian suite of programs (see the Computational section and ESI† for details).

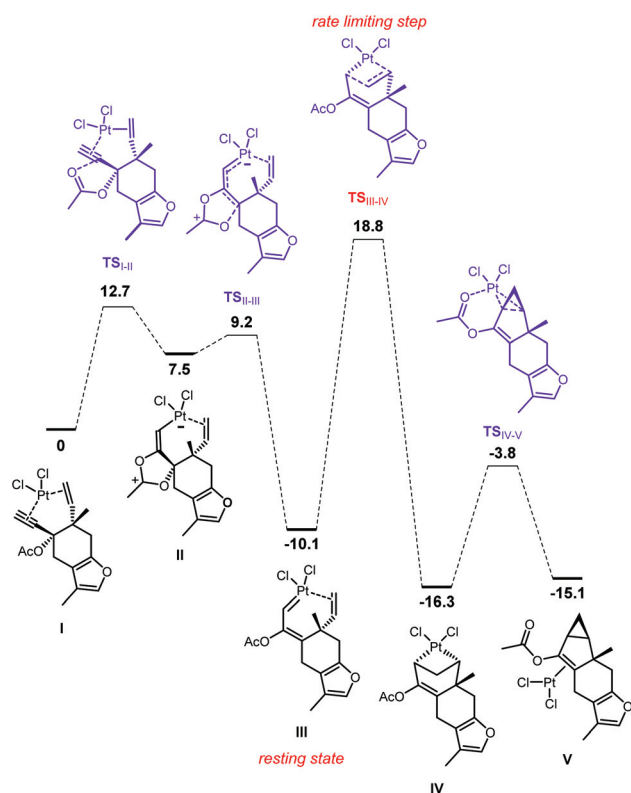
Propargylic acetates typically undergo 1,2- or 1,3-acetate rearrangements in the presence of different metal salts, such as PtCl_2 ¹⁰ or AuCl ,¹¹ and we hypothesized that the main compounds observed in our reactions could arise from these processes, **2** and **6** from 1,2-migration, and **3** and **4** from 1,3-migration (Scheme 2), followed by further evolution of the intermediates and final ring formation.

(a) We initially computed the catalytic cycle that represents the transformation of the furan elemene **1** in the presence of PtCl_2 to the major product, lindenane compound **2** (Scheme 3). The double coordination of the platinum center with the alkene and alkyne of **1** forms a tetracoordinated complex (**I**), which is taken as the starting point for the Gibbs free energy ($G = 0$). After this, the initial 1,2-rearrangement of the acetate group takes place in two steps ($\text{TS}_{\text{I-II}}$ and $\text{TS}_{\text{II-III}}$) of low activation energy, especially the second one (12.7 and 1.7 kcal mol⁻¹, respectively). The cyclic transient intermediate **II** is formed after $\text{TS}_{\text{I-II}}$, and is rapidly transformed into a Pt-carbene complex (**III**).¹² Based on the much lower energy of **III** than that of **I** ($\Delta G = -10.1$ kcal mol⁻¹), we propose that the platinum-carbene **III** is the resting state of the cycle.

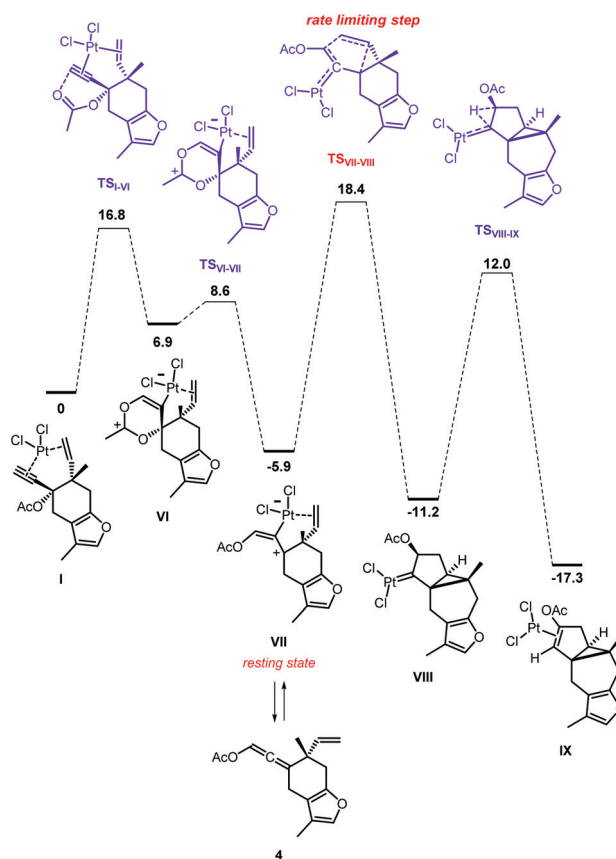
The subsequent cyclometallation through $\text{TS}_{\text{III-IV}}$ leads to the formation of the six-member ring in **IV**. This step must be the rate limiting step as it presents the highest energy within the cycle ($\Delta G^\ddagger = 28.9$ kcal mol⁻¹ from **III**), a value that is in agreement with the experimental temperatures needed, from

60° to 110°. To complete the formation of the final product, complex **IV** suffers a reductive elimination of the low activation energy. The overall process is exergonic by 15.1 kcal mol⁻¹, and is completed with the release of compound **2** from the Pt center in **V**. It is noteworthy that the formation of the intermediate **III** might have some degree of reversibility, caused by the higher activation barrier from **III** to **IV** ($\text{TS}_{\text{III-IV}}$) than the reverse process, from **III** to **I** ($\text{TS}_{\text{I-II}}$).

Next, we could also confirm our previous proposal regarding the formation of the minor product of the reaction (myliol **3** in Scheme 2), which could arise from an initial 1,3-acetate rearrangement, as in Scheme 4. In this case, the attack of the acetate-oxygen on the terminal carbon of the alkyne leads to the formation of a dioxane zwitterionic intermediate (**VI**), which is high in energy ($G = 6.9$ kcal mol⁻¹), and kinetically and thermodynamically unstable, as was **II** shown in Scheme 3. Seemingly, the two steps of the acetate migration are low in energy, especially the second one ($\text{TS}_{\text{I-VI}} = 16.8$ and $\text{TS}_{\text{VI-VII}} = 1.7$ kcal mol⁻¹, respectively). In this case, complex **VII** forms, which is significantly more stable than the starting material **I**, becoming the resting state of the cycle. Complex **VII** corresponds to the coordination of Pt to allene **4**, and its low energy suggests that it can be in equilibrium with the free allene **4**, explaining the experimental isolation of variable



Scheme 3 Energy profile for the transformation of furan elemene **1** into final product **2**, through a 1,2-acetate rearrangement. Gibbs free energy values in kcal mol⁻¹ at the M06/Def2TZVPP level.



Scheme 4 Energy profile for the transformation of furan elemene **1** into final products **3** and **4** through a 1,3-acetate rearrangement. Gibbs free energy values in kcal mol⁻¹ at the M06/Def2TZVPP level.

Table 1 Calculation of the stereo-determining transition states for furan **1** and lactone **5**. The values were obtained using B3PW91-D3 and ω -B97X-D. The final ratios were calculated by kinetic simulation with the COPASI software, to be compared with the experimental values, 65 : 35 (2 : 3) and $\geq 99 : 1$ (6 : 7)

		1,2-Pathway		1,3-Pathway		
Furan 1		TS _{I-II}	TS _{III-IV}	TS _{I-VI}	TS _{VII-VIII}	Ratio 2 : 3
(a)	B3PW91-D3	9.7	15.7	13.7	16.1	65 : 35
(b)	ω -B97X-D	12.0	17.7	16.0	17.2	38 : 62
Lactone 5		TS _{X-XI}	TS _{XII-XIII}	TS _{X-XV}	TS _{XVI-XVII}	Ratio 6 : 7
(c)	B3PW91-D3	9.5	11.5	15.1	9.7	99 : 1
(d)	ω -B97X-D	12.6	16.7	16.9	12.9	58 : 42

amounts of **4** in some of the reaction mixtures. This observation is supported by the fact that allene **4** can serve as a substrate for the formation of the final adduct **3** under the reaction conditions. The subsequent formation of **VIII** through a double cyclization transition state (TS_{VII-VIII}) has the highest activation barrier of the catalytic cycle ($\Delta G^\ddagger = 24.3$ kcal mol⁻¹), becoming the rate limiting step. Carbene **VIII** is then transformed into the final product by a 1,2-hydrogen shift, rendering an overall exergonic cycle by 17.3 kcal mol⁻¹.

As mentioned previously, variable amounts of final products **2** and **3** are formed depending on the experimental reaction conditions, with a slight preference for **2**. The selectivity usually ranges from 2 : 1 to 5.6 : 1, and corresponds to a theoretical energy difference of only 0.4 to 0.9 kcal mol⁻¹. It is worth mentioning that such a small difference can be considered negligible from the computational point of view, given the current level of accuracy of DFT in such large and complex systems, where errors even larger than 1 kcal mol⁻¹ have been reported in some cases.¹³

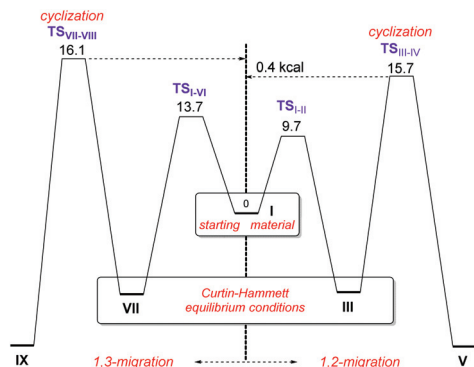
The data shown in Schemes 3 and 4 suggest that the selectivity depends on various factors. First, the initial steps (from **I** to **III** and from **I** to **VII**) are partially reversible, especially for the 1,2 pathway, pointing to the existence of an equilibrium between the starting material (**I**) and the resting states of the two cycles (**III** and **VII**). If pure Curtin-Hammett conditions apply to these systems, the selectivity would be solely dictated by the relative height of the rate limiting steps in each cycle, namely TS_{III-IV} and TS_{VII-VIII} (18.8 vs. 18.4 kcal mol⁻¹), predicting a slight preference for the minor experimental isomer **3** (34 : 66). Meanwhile, the barriers of the initial acetate rearrangement could play some secondary role, especially because of the large energy difference favouring TS_{I-II} over TS_{I-VI} (12.7 vs. 16.8 kcal mol⁻¹). Indeed, in the case of the 1,3-pathway, the initial acetate rearrangement (TS_{I-VI}) becomes energetically significant, compromising the reversibility of the 1,3-migration process. At this point, the reversibility degree of the process is crucial to tip the balance in one direction or the other.

To further clarify this issue, we carried out a simulation of the kinetics of the reaction with the COPASI software.¹⁴ Taking directly the activation DFT energy values from Schemes 3 and 4 as the input for the simulated kinetics,¹⁵ we found that there is an initial accumulation of intermediate **III** (resting state of the cycle) whereas **VII** is not detected, but due to the reversibil-

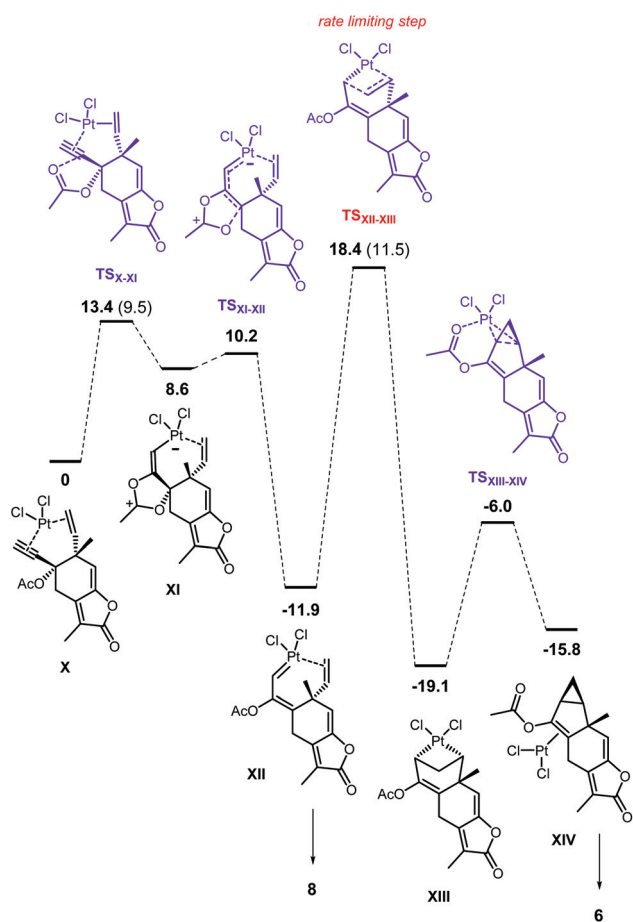
ity of the acetate rearrangement, adduct **3** builds up faster than **2**, and an overall 40 : 60 mixture of the final adducts **2** : **3** was predicted.¹⁶ The value is very similar to the one under Curtin-Hammett conditions mentioned before (34 : 66), indicating that the migration only plays a minor role to determine the selectivity for furan substrate **1**. In any case, the computed preference of **3** is in disagreement with the experimental selectivity, between 65 : 35 and 85 : 15 for the opposite isomer **2**. We have to note here again that this disagreement in the preference of **2** is not so relevant in energetic terms, less than 1 kcal mol⁻¹, from a computed +0.4 kcal mol⁻¹ to an experimental -0.4 kcal mol⁻¹ (values that are within the inherent DFT error).

To further analyze these values, we repeated the calculations with other functionals (B3PW91-D3 and ω B97X-D, Table 1, entries a and b) in toluene and in the gas phase, which confirmed that the cyclization steps (TS_{III-IV} and TS_{VII-VIII}) are rate determining along the 1,2 and 1,3 pathways with furan. Interestingly, using the Grimme's corrected B3PW91-D3 method in toluene, the calculations are able to correctly predict the sense and magnitude of the experimental 2 : 3 selectivity (65 : 35) due to the higher barrier of TS_{VII-VIII} (16.1 kcal mol⁻¹) than that of TS_{III-IV} (15.7, entry a) with this functional. Even more, in the gas phase, the three methods analyzed (M06, B3PW91-D3 and ω B97X-D) predict the right sense of selectivity.¹⁷ The results confirm that the reaction proceeds under Curtin-Hammett equilibrium conditions between intermediates **V** and **IX** (Scheme 5).

(b) A second intriguing question posed by the experimental data referred to the selectivity and reactivity difference between the furan element **1** and its lactone congener **5**. Indeed, the compounds isolated in the reaction of **5** are formed only through the 1,2-acetate rearrangement, with complete selectivity. To understand this observation, the two pathways from lactone **5** were computed, and we found some significant differences in the energy profiles of lactone and furan substrates (Schemes 6-7 vs. 3-4 respectively). For example, the first step of the mechanism suffers from the probable lesser nucleophilicity of the acetate in proximity to the lactone compared to the furan. The computed activation energy values for lactone (TS_{X-XI} in Scheme 6 and TS_{X-XV} in Scheme 7) are higher by 0.7-1.1 kcal mol⁻¹ than the previous ones with furan (TS_{I-II} and TS_{I-VI}, Schemes 3 and 4).

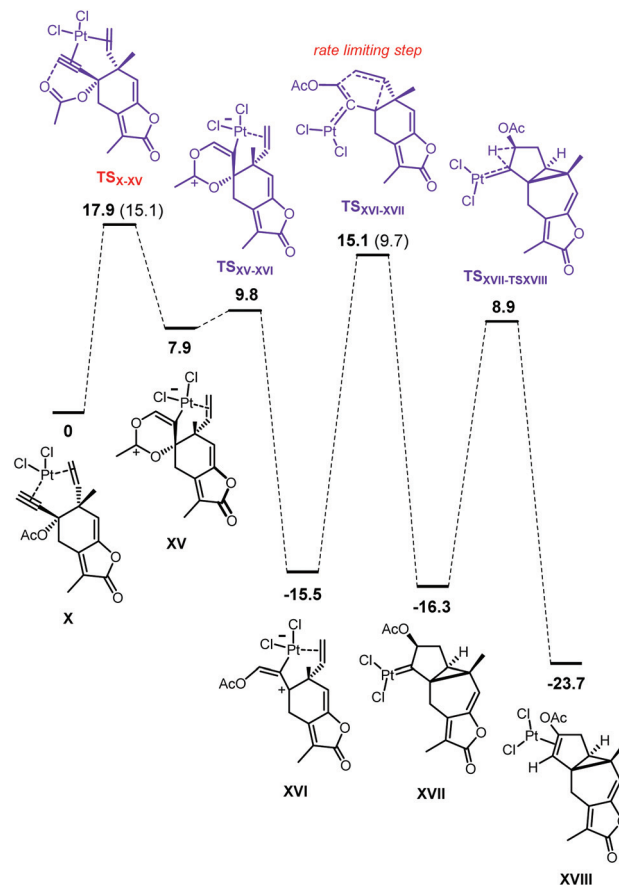


Scheme 5 Analysis of the 2:3 selectivity by a comparison of the 1,2- and 1,3-rearrangement pathways of furan at the B3PW91-D3 level of theory.



Scheme 6 Energy profile for the transformation of lactone elemene 5 into final products 6 and 8 through a 1,2-acetate rearrangement. Gibbs free energy values in kcal mol⁻¹ at the M06/Def2TZVPP level (B3PW91-D3 in parentheses).

As a consequence, the initial acetate migration gains increased significance along the 1,3-pathway, as TS_{X-XV} is higher by 2.8 kcal mol⁻¹ than the cyclization in $TS_{XVI-XVII}$ (17.9



Scheme 7 Energy profile for the transformation of lactone elemene 5 into compound 7 through a 1,3-acetate rearrangement. Gibbs free energy values in kcal mol⁻¹ at the M06/Def2TZVPP level (B3PW91-D3 in parentheses).

vs. 15.1 kcal mol⁻¹, Scheme 7), and it even approaches the activation energy of the 1,2-pathway (18.4 kcal mol⁻¹ in the rate limiting step, $TS_{XII-XIII}$, Scheme 6). This finding suggests that the acetate migration could become the selectivity-determining step in the case of lactones. According to the values in Scheme 7, the migration is also an irreversible process, cancelling out the possibility of Curtin-Hammett equilibration of the intermediates, as was the case for the furan substrate.

In this regard, while M06 probably overestimates the energy barrier of the cyclization in $TS_{XII-XIII}$, leading to a computed 34:66 ratio for 6:7, the other functionals in Table 1 (entries c and d) highlight the key role of the initial 1,3-migration barrier (TS_{X-XV}) along the reaction pathway. B3PW91-D3 and ω B97X-D afford the highest absolute barriers for the lactone formation for that step (TS_{X-XV} ; 15.1 and 16.9 kcal mol⁻¹, bold figures in Table 1), becoming higher than the cyclization in $TS_{XVI-XVII}$ in both cases (15.1 vs. 9.7, 16.9 vs. 12.9). These data also confirm the irreversibility of the 1,3-migration in Scheme 7 and its role in determining the selectivity. Indeed, B3PW91-D3 (entry c) predicts a 6:7 ratio of 99:1, in agreement with the experimental data.

In summary, we believe that the difference in the behaviour of furan and lactone arises from the combination of the follow-

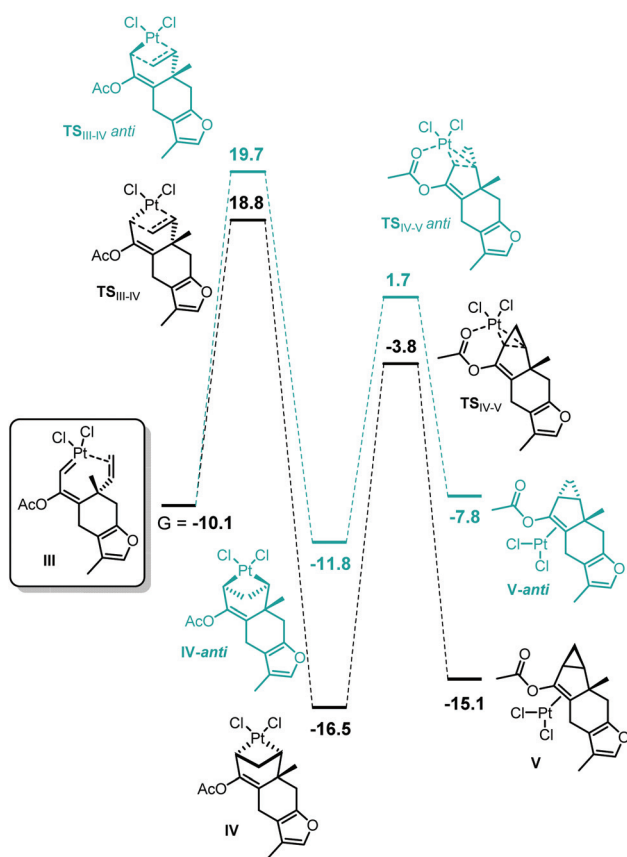
ing effects: (1) the low selectivity found in furan relates to the fact that the acetate migration is reversible, the rearranged intermediates are in equilibrium, and the cyclization is the rate determining step, presenting similar activation energies for the formation of **2** and **3**. (2) The complete selectivity in lactones is a consequence of the increased irreversibility of the 1,3-migration step, which becomes selectivity determining, and the large energy difference between the barriers for 1,3- and 1,2-migration.

Another important feature of the reaction with the lactone substrate is the formation of significant amounts of compound **8** (Scheme 2), arising from the early decooordination of platinum from intermediate **XII** (Scheme 6), before cyclization. Interestingly, the energy values provide an explanation, noting that the activation energy for the cyclometallation step $TS_{XII-XIII}$ is higher for lactone (30.3 kcal mol⁻¹ from **XII**) than that for furan (28.9 kcal mol⁻¹ from **III** to TS_{III-IV} in Scheme 3). At the same time the relative stability of the corresponding resting states is higher for **XII** than that for **III** (-11.9 vs. -10.1 kcal mol⁻¹). Thus, the cyclization step is not efficient enough in the case of the lactone substrate, inducing the formation of **8** by decooordination of the metal center.

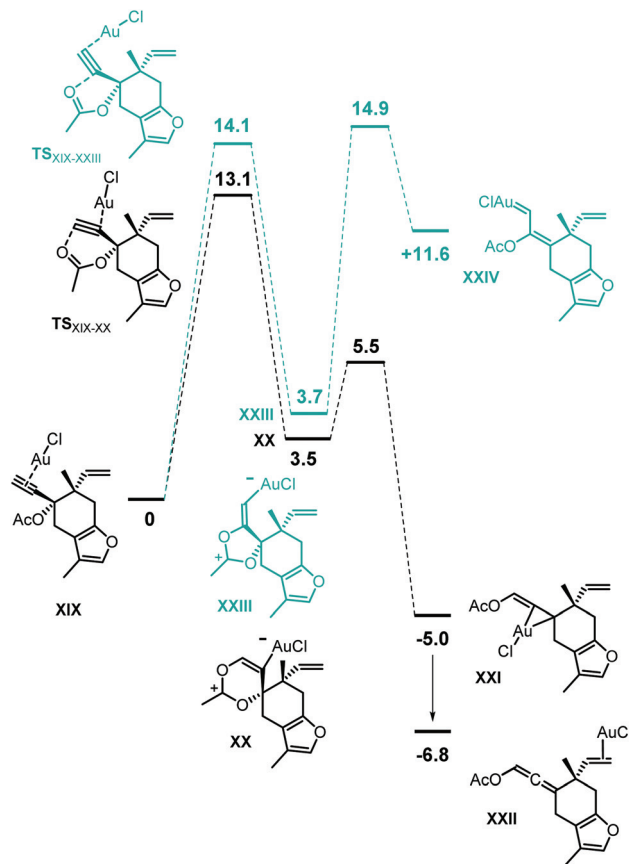
(c) The third point of interest was the *syn/anti* selectivity observed in the formation of product **2**. In Scheme 3, we only

show one of the possible diastereoisomers during transition state TS_{III-IV} , the one actually leading to the major final *syn* isomer. In fact, a second isomeric transition state exists, leading to the *anti*-cyclopropane derivative. As outlined in Scheme 8, the energy difference between both transition states TS_{III-IV} and $TS_{III-IV-anti}$ (ca. 0.9 kcal mol⁻¹) is able to explain the preferential formation of the *syn* product and the low selectivity.

(d) Finally, we had previously described that the reaction in the presence of AuCl as the catalyst leads to a completely different outcome, since we only observed the quantitative formation of allene acetate **4**. This fact means that the reaction is completely selective towards the initial 1,3-acetate migration, since no compound related to tetracycle **2** was observed, and also that the reaction prematurely stops at an intermediate stage of the process, after the formation of allene-Au(i) complex **XXII** (Scheme 9). To understand these observations, we recomputed the 1,2- and 1,3-migration pathways in the presence of gold(i) chloride. It must be taken into consideration here that Au(i) is a dicoordinating species, and it does not form a complex with the alkene fragment in **XIX** at the outset of the reaction. Initially, in contrast to the Pt(II) salt, Au(i) seems to facilitate the 1,3-acetate migration (TS_{XIX-XX} , $\Delta G^\ddagger = 13.1$ kcal mol⁻¹) over the 1,2-process ($TS_{XIX-XXIII}$, $\Delta G^\ddagger = 14.1$ kcal mol⁻¹).



Scheme 8 Formation of *syn* and *anti* isomers of **V**, by diastereomeric cyclometallation pathways. Gibbs free energy values in kcal mol⁻¹.



Scheme 9 1,2- and 1,3-acetate migration pathways in the presence of an AuCl catalyst. Gibbs free energy values in kcal mol⁻¹.

However, although being important, the low energy difference ($\Delta\Delta G^\ddagger = 1.0 \text{ kcal mol}^{-1}$) alone does not suffice to explain the sole formation of **4**. A detailed inspection of the subsequent steps after the 1,2-migration is more informative, since the endergonic formation of **XXIII** ($G = +3.7 \text{ kcal mol}^{-1}$) is followed by the appearance of a highly unstable intermediate (**XXIV**, $G = +11.6 \text{ kcal mol}^{-1}$). The 1,2-migration process must be, thus, very disfavored and reversible. In contrast, the formation of the allene–Au(I) complex **XXI** is exergonic at $5.0 \text{ kcal mol}^{-1}$, and therefore fairly irreversible. The reaction is then under thermodynamic control, driven by the much lower energy of **XXII** than that of **XXIV**. Also, the significant stability difference between the gold carbene **XXIV** and the platinum carbene counterpart (**III**, Scheme 3) nicely explains the diverse reactivity patterns of platinum and gold.

On the other hand, we have experimentally proved that allene **4** does not further evolve in the presence of Au(I). To account for this behavior, we have compared the coordination ability of allene and alkene moieties towards Au(I), finding that alkene-complex **XXII** is preferred by almost 2 kcal mol^{-1} , corresponding to the 30 : 1 preference over the allene complex **XXI**. The alkene can divert in this way the Au atom from the catalytic cycle, stopping the reaction at this stage. Also the alkene **XXII**/alkyne **XIX** ligand exchange would direct gold towards a new molecule of the substrate, re-entering a new catalytic cycle for the formation of allene **4**, as experimentally found.

Conclusions

DFT studies have been applied to shed light on the mechanisms of the cyclization reactions of complex enyne acetates, with the aim of understanding the reactivity and selectivity features of our experimental systems. The formation of the lindane core fragments arises from an initial 1,2-acetate rearrangement, whereas the competing 1,3-migration leads to the formation of the myliol core structures. In the case of the furan substrates, the computed selectivity of the initial migration and the fine balance between the energies of migration and cyclization offer a qualitative explanation of the low selectivity of the formation of lindane/myliol derivatives. In the case of the lactone substrates, their higher electron withdrawing character increases the energy of the 1,3-acetate rearrangement and its irreversibility, inducing a higher selectivity, and leading exclusively to lindane-type of products. Finally, we were also able to explain the large differences in reactivities between PtCl_2 and AuCl salts as catalysts. In the case of gold, the exclusive formation of allene **4** could be initially attributed to a selective 1,3-rearrangement. Surprisingly, the initial 1,2- and 1,3-acetate migration processes present comparable energies (14.1 and $13.1 \text{ kcal mol}^{-1}$), but the former leads to the endergonic formation of a highly unstable gold carbene, making the acetate transfer completely reversible, and triggering the formation of allene **4** through a more favorable, downhill mechanism.

Computational details

DFT calculations were carried out with the M06¹⁸ functional as implemented in the Gaussian 09 suite of programs.¹⁹ Optimization was performed in a solvent model (IEFPCM, solvent = toluene), using the 6-311G(d,p) basis set for non-metallic atoms and the SDD²⁰ basis set for platinum and gold. Final energies were obtained by performing single point energy calculations on the optimized structures with the basis set Def2TZVPP²¹ and the functionals M06, ω B97X-D²² and B3PW91,²³ adding the D3 version of Grimme's dispersion²⁴ for the latter. Some zwitterionic intermediates and charged species are proposed to participate in the catalytic cycles, and therefore an implicit solvation model was also incorporated into the calculations (IEFPCM, solvent = toluene).²⁵ The stationary points were characterized by vibrational frequency calculations in order to verify that they have the right number of imaginary frequencies. Connectivity of the transition states with the corresponding associated minima were established by IRC.²⁶

Conflicts of interest

There are no conflicts to declare.

Acknowledgements

We thank the Spanish Ministerio de Ciencia e Innovación (CTQ2016-78083-P) and IZO-SGI SGIker of UPV/EHU for financial and human support. Also we would like to acknowledge support of this work by the project "OPENSREEN-GR" (MIS 5002691) which is implemented under the Action "Reinforcement of the Research and Innovation Infrastructure", funded by the Operational Programme "Competitiveness, Entrepreneurship and Innovation" (NSRF 2014–2020) and co-financed by Greece and the European Union (European Regional Development Fund). Finally, the project was inspired by helpful discussions within CHAOS-COST Action CA15106. Part of this research has been financially supported by the General Secretariat for Research and Technology (GSRT) and the Hellenic Foundation for Research and Innovation (HFRI) (Scholarship Code: 995).

Notes and references

- For general reviews on metal-catalysis in synthesis please refer to: (a) R. Ardkhean, D. J. F. Caputo, S. M. Morrow, H. Shi, Y. Xiong and E. A. Anderson, *Chem. Soc. Rev.*, 2016, **45**, 1557; (b) X.-W. Li and B. Nay, *Nat. Prod. Rep.*, 2014, **31**, 533; (c) K. C. Nicolaou and J. S. Chen, *Chem. Soc. Rev.*, 2009, **38**, 2993. For the Diels–Alder reaction in total synthesis please refer to: (d) K. C. Nicolaou, S. A. Snyder, T. Montagnon and G. Vassilikogiannakis, *Angew. Chem., Int. Ed.*, 2002, **41**, 1668. For some excellent reviews on transition metal catalyzed cycloisomerization reactions please

- refer to: (e) C. Aubert, O. Buisine and M. Malacria, *Chem. Rev.*, 2002, **102**, 813; (f) V. Michelet, P. Y. Toullec and J.-P. Genet, *Angew. Chem., Int. Ed.*, 2008, **47**, 4268; (g) A. Furstner, *Chem. Soc. Rev.*, 2009, **38**, 3208; (h) Y. Yamamoto, *Chem. Rev.*, 2012, **112**, 4736; (i) I. D. G. Watson and F. D. Toste, *Chem. Sci.*, 2012, **3**, 2899; (j) R. Dorel and A. M. Echavarren, *Chem. Rev.*, 2015, **115**, 9028; (k) Y. Wang, M. E. Muratore and A. M. Echavarren, *Chem. – Eur. J.*, 2015, **21**, 7332.
- 2 For selected references for clinical trials of sesquiterpenoids as anticancer agents please refer to: (a) A. Ghantous, H. Gali-Muhtasib, H. Vuorela, N. A. Saliba and N. Darwiche, *Drug Discovery Today*, 2010, **15**, 668; (b) M. H. Amorim, R. M. Gil da Costa, C. Lopes and M. M. Bastos, *Crit. Rev. Toxicol.*, 2013, **43**, 559; (c) M. R. Orono Kreuger, S. Grootjans, M. W. Biavatti, P. Vandenabeele and K. D'Herde, *Anti-Cancer Drugs*, 2012, **23**, 883.
 - 3 C. I. Stathakis, P. L. Gkizis and A. L. Zografos, *Nat. Prod. Rep.*, 2016, **33**, 1093.
 - 4 (a) M. Willot and M. Christmann, *Nat. Chem.*, 2010, **2**, 519; (b) Q. Zhou, X. Chen and D. Ma, *Angew. Chem., Int. Ed.*, 2010, **49**, 3513; (c) K. Molawi, N. Delpont and A. M. Echavarren, *Angew. Chem., Int. Ed.*, 2010, **49**, 3517.
 - 5 Acyloxy migration in Pt catalysis: (a) E. Mainetti, V. Mouriés, L. Fensterbank, M. Malacria and J. Marco-Contelles, *Angew. Chem., Int. Ed.*, 2002, **41**, 2132; (b) E. Soriano, P. Ballesteros and J. Marco-Contelles, *Organometallics*, 2005, **24**, 3182.
 - 6 Acyloxy migration in Au catalysis: (a) V. Rautenstrauch, *J. Org. Chem.*, 1984, **49**, 950; (b) V. Rautenstrauch, U. Burger and P. Wirthner, *Chimia*, 1985, **39**, 225.
 - 7 V. P. Demertzidou and A. L. Zografos, *Org. Biomol. Chem.*, 2016, **14**, 6942.
 - 8 Total synthesis of sarcandralactone: (a) J. A. Eagan, M. Hori, J. Wu, K. S. Nanyi-va and S. A. Snyder, *Angew. Chem., Int. Ed.*, 2015, **54**, 7842; (b) T. W. Fenlon, M. W. Jones, R. M. Adlington and V. Lee, *Org. Biomol. Chem.*, 2013, **11**, 8026; (c) T. W. Fenlon, D. Schwaebisch, A. V. W. Mayweg, V. Lee, R. M. Adlington and J. E. Baldwin, *Synlett*, 2007, 2679.
 - 9 (a) A. S. K. Hashmi, E. Kurpejović, W. Frey and J. W. Bats, *Tetrahedron*, 2007, **63**, 5879; (b) G. Zhang, V. J. Catalano and L. Zhang, *J. Am. Chem. Soc.*, 2007, **129**, 11358; (c) E. Soriano and J. M. Marco-Contelles, *Computational Mechanisms of Au and Pt Catalyzed Reactions in Topics in Current Chemistry*, Spriger, Heidelberg Dordrecht London New York, 2011, p. 302, ISSN: 0340-1022; (d) M. Pernpointner and A. S. K. Hashmi, *J. Chem. Theory Comput.*, 2009, **5**, 2717; (e) R. Zriba, V. Gandon, C. Aubert, L. Fensterbank and M. Malacria, *Chem. – Eur. J.*, 2008, **14**, 1482.
 - 10 Y. Harrak, C. Blaszczakowski, M. Bernard, K. Cariou, E. Mainetti, V. Mouriés, A. L. Dhimane, L. Fensterbank and M. Malacria, *J. Am. Chem. Soc.*, 2004, **126**, 8656.
 - 11 (a) O. Nieto Faza, C. Silva López, R. Álvarez and A. R. de Lera, *J. Am. Chem. Soc.*, 2006, **128**, 2434; (b) T. de Haro, E. Gómez-Bengoia, R. Cribiú, X. Huang and C. Nevado, *Chem. – Eur. J.*, 2012, **18**, 6811.
 - 12 An alternative mechanism, consisting of an initial cyclopropanation of the enyne system, catalyzed by PtCl₂ has been previously proposed for simpler acyclic models: E. Soriano and J. Marco-Contelles, *Acc. Chem. Res.*, 2009, **42**, 1026. We have verified that this mechanism cannot compete with initial acetate migration in our polycyclic substrate systems. See the ESI† for further details.
 - 13 Y. Zhao and D. G. Truhlar, *Theor. Chem. Acc.*, 2008, **120**, 215.
 - 14 COPASI; a COMplex PATHway SIMulator, S. Hoops, S. Sahle, R. Gauges, C. Lee, J. Pahle, N. Simus, M. Singhal, L. Xu, P. Mendes and U. Kummer, *Bioinformatics*, 2006, **22**, 3067.
 - 15 The combination of DFT methods and kinetic simulations with the COPASI software has been recently shown to be a powerful approach to reproduce the reaction rates of different experimental systems. For examples of organometallic reactions, see: (a) J. Jover, *Phys. Chem. Chem. Phys.*, 2017, **19**, 29344; (b) D. Wei, O. Sadek, V. Dorcet, T. Roisnel, C. Darcel, E. Gras, E. Clot and J.-B. Sortais, *J. Catal.*, 2018, 300; (c) G. Aullón, M. Crespo, J. Jover and M. Martínez, *Adv. Inorg. Chem.*, 2017, **70**, 195–242; (d) L. Artús Suárez, Z. Culakova, D. Balcels, W. H. Bernskoetter, O. Eisenstein, K. I. Goldberg, N. Hazari, M. Tilset and A. Nova, *ACS Catal.*, 2018, **8**, 8751; (e) A. Eibel, D. E. Fast and G. Gescheidt, *Polym. Chem.*, 2018, **9**, 5107; (f) M. Griesser, R. Shah, A. T. Van Kessel, O. Zilka, E. A. Haidasz and D. A. Pratt, *J. Am. Chem. Soc.*, 2018, **140**, 3798; (g) D. E. Hill, Q.-I. Pei, E.-X. Zhang, J. R. Gage, J.-Q. Yu and D. G. Blackmond, *ACS Catal.*, 2018, **8**, 1528; (h) Q. Liang, A. Salmon, P. J. Kim, L. Yan and D. Song, *J. Am. Chem. Soc.*, 2018, **140**, 1263; (i) H. H.-M. Yeung, A. F. Sapnik, F. Massingberd-Mundy, M. W. Gaultois, Y. Wu, D. A. X. Fraser, S. Henke, R. Pallach, N. Heidenrich, O. V. Magdysyuk, N. T. Vo and A. L. Goodwin, *Angew. Chem., Int. Ed.*, 2018, **58**, 566.
 - 16 The complete data and graphics of the simulated kinetics are collected in the ESI.†
 - 17 When the calculations were run in the gas phase, the three methods, M06 (5.2 : 1), B3PW91-D3 (3.8 : 1) and ωB97X-D (29.3 : 1), show the correct sense of 2 : 3 selectivity. See the ESI† for more details.
 - 18 Y. Zhao and D. G. Truhlar, The M06 suite of density functionals for main group thermochemistry, thermochemical kinetics, noncovalent interactions, excited states, and transition elements: two new functionals and systematic testing of four M06-class functionals and 12 other functional, *Theor. Chem. Acc.*, 2008, **120**, 215.
 - 19 M. J. Frisch, G. W. Trucks, H. B. Schlegel, G. E. Scuseria, M. A. Robb, J. R. Cheeseman, G. Scalmani, V. Barone, B. Mennucci, G. A. Petersson, H. Nakatsuji, M. Caricato, X. Li, H. P. Hratchian, A. F. Izmaylov, J. Bloino, G. Zheng, J. L. Sonnenberg, M. Hada, M. Ehara, K. Toyota, R. Fukuda, J. Hasegawa, M. Ishida, T. Nakajima, Y. Honda, O. Kitao, H. Nakai, T. Vreven, J. A. Montgomery Jr., J. E. Peralta, F. Ogliaro, M. Bearpark, J. J. Heyd, E. Brothers, K. N. Kudin, V. N. Staroverov, T. Keith, R. Kobayashi,

- J. Normand, K. Raghavachari, A. Rendell, J. C. Burant, S. S. Iyengar, J. Tomasi, M. Cossi, N. Rega, J. M. Millam, M. Klene, J. E. Knox, J. B. Cross, V. Bakken, C. Adamo, J. Jaramillo, R. Gomperts, R. E. Stratmann, O. Yazyev, A. J. Austin, R. Cammi, C. Pomelli, J. W. Ochterski, R. L. Martin, K. Morokuma, V. G. Zakrzewski, G. A. Voth, P. Salvador, J. J. Dannenberg, S. Dapprich, A. D. Daniels, O. Farkas, J. B. Foresman, J. V. Ortiz, J. Cioslowski and D. J. Fox, *Gaussian 09, Revision D.01*, Gaussian, Inc., Wallingford CT, 2013.
- 20 (a) M. Dolg, U. Wedig, H. Stoll and H. Preuss, *J. Chem. Phys.*, 1987, **86**, 866; (b) D. Andrae, U. Haussermann, M. Dolg, H. Stoll and H. Preuss, *Theor. Chim. Acta*, 1990, **77**, 123.
- 21 (a) F. Furche and R. Ahlrichs, *J. Chem. Phys.*, 2003, **119**, 12753; (b) F. Weigend and R. Ahlrichs, *Phys. Chem. Chem. Phys.*, 2005, **7**, 3297.
- 22 J.-D. Chai and H. Head-Gordon, *Phys. Chem. Chem. Phys.*, 2008, **10**, 6615.
- 23 J. P. Perdew, in *Electronic Structure of Solids '91*, ed. P. Ziesche and H. Eschig, Academic Verlag, Berlin, 1991, p. 11.
- 24 S. Grimme, J. Antony, S. Ehrlich and H. Krieg, *J. Chem. Phys.*, 2010, **132**, 154104.
- 25 (a) E. Cancès, B. Mennucci and J. Tomasi, *J. Chem. Phys.*, 1997, **107**, 3032; (b) M. Cossi, V. Barone, B. Mennucci and J. Tomasi, *Chem. Phys. Lett.*, 1998, **286**, 253; (c) J. Tomasi, B. Mennucci and E. Cancès, *J. Mol. Struct.: THEOCHEM*, 1999, **464**, 211.
- 26 (a) K. Fukui, *Acc. Chem. Res.*, 1981, **14**, 363; (b) H. P. Hratchian and H. B. Schlegel, in *Theory and Applications of Computational Chemistry: The First 40 Years*, ed. C. Dykstra, G. Frenking, S. Kim and G. Scuseria, Elsevier Science, 2005.